INFORMATION TO USERS

This manuscript has been reproduced from the microfilm master. UMI films the text directly from the original or copy submitted. Thus, some thesis and dissertation copies are in typewriter face, while others may be from any type of computer printer.

The quality of this reproduction is dependent upon the quality of the copy submitted. Broken or indistinct print, colored or poor quality illustrations and photographs, print bleedthrough, substandard margins, and improper alignment can adversely affect reproduction.

In the unlikely event that the author did not send UMI a complete manuscript and there are missing pages, these will be noted. Also, if unauthorized copyright material had to be removed, a note will indicate the deletion.

Oversize materials (e.g., maps, drawings, charts) are reproduced by sectioning the original, beginning at the upper left-hand corner and continuing from left to right in equal sections with small overlaps.

Photographs included in the original manuscript have been reproduced xerographically in this copy. Higher quality 6" x 9" black and white photographic prints are available for any photographs or illustrations appearing in this copy for an additional charge. Contact UMI directly to order.

ProQuest Information and Learning
300 North Zeeb Road, Ann Arbor, MI 48106-1346 USA
800-521-0600

UMI®

DISSERTATION

QUANTITATIVE ANALYSIS OF THE UNCOMPAHGRE NATIONAL FOREST SOIL AND ITS EXTRACTS BY ^{13}C DP- AND CP-MAS SOLID STATE NMR METHODS

Submitted by

Camille Keeler

Department of Chemistry

In partial fulfillment of the requirements

for the Degree of Doctor of Philosophy

Colorado State University

Fort Collins, Colorado

Summer 2001

COLORADO STATE UNIVERSITY

11th of June, 2001

WE HEREBY RECOMMEND THAT THE DISSERTATION PREPARED UNDER OUR SUPERVISION BY CAMILLE KEELER ENTITLED QUANTITATIVE ANALYSIS OF THE UNCOMPAHGRE NATIONAL FOREST SOIL AND ITS EXTRACTS BY ^{13}C DP- AND CP-MAS SOLID STATE NMR METHODS BE ACCEPTED AS FULFILLING IN PART REQUIREMENTS FOR THE DEGREE OF DOCTOR OF PHILOSOPHY.

Committee on Graduate Work

Adviser

Department Head

ABSTRACT OF DISSERTATION

QUANTITATIVE ANALYSIS OF THE UNCOMPAHGRE NATIONAL FOREST SOIL AND ITS EXTRACTS BY ^{13}C DP- AND CP-MAS SOLID STATE NMR METHODS

We have carried out the first absolutely quantitative solid-state ^{13}C NMR study on a soil and its separated components. The Uncompahgre National Forest soil was collected and separated into a humin fraction, humic acid, and fulvic acid using a classic soil separation method. The soil separation was performed in a quantitative manner such that all the organic carbon in the soil and its separated fractions was accounted for by elemental analysis. Compared to the carbon detected by elemental analysis, ^{1}H-to-^{13}C CP-MAS and ^{13}C DP-MAS spin-counting accounted for substantially less than 100 percent of the carbon, from a low of 48 percent of the carbon, to a high of about 86 percent of the carbon, depending on the method and particular soil fraction. The peak areas for spin counting spectra generated by DP- and CP-MAS were corrected to account for relaxation and cross-polarization processes to yield NMR peak integrals that are directly proportional to the amount of carbon in a particular functional group that the peak represents. The DP-MAS generated spectra, following the aforementioned peak area corrections, were found to have greater relative intensity in the aromatic region

compared to the corresponding CP-MAS spectra for the same soil components. The quantitative ^{13}C MAS NMR analysis was accompanied by an extensive error analysis of the regressions, calibrations, and deconvolution procedures used in this thesis.

The percent of the carbon detected by NMR compared to that detected by elemental analysis for the whole soil increased dramatically following a de-ashing treatment that employed the use of hydrofluoric acid. This treatment was found to greatly reduce the iron content, as detected by elemental analysis, while preserving the integrity of the organic content of the soil. Vibrating sample magnetometer (VSM) measurements were taken on all the soil and soil extracts, along with the HF-treated soil, to better understand the nature of the iron in these samples. These VSM measurements qualitatively confirmed the iron elemental analysis results for these samples and indicated that ferrimagnetic particles were retained in the whole soil, HF-treated whole soil, and humin fraction. Calculations using the Curie law of paramagnetism confirmed the susceptibility measurements on these samples and showed that paramagnetic iron was the dominate form of iron in the soil and soil fractions.

A second method for estimating the carbon content by NMR, the empirical relationship method, utilizes peak areas and their organic carbon functionality assignments. This method more closely predicted some of the carbon contents, but is based on many subjective functionality assignments and the more error prone individual peak areas. For this reason this second method, while gaining popularity in some soil research areas, was evaluated but not a major focus in this thesis.

Large systematic errors associated with the external reference calibration for DP- and CP-MAS spin counting spurred investigation into B_1 RF-field homogeneity and its

relationship to quantitative spin counting in NMR. The B_1 field for the spinner and coil configuration was measured and found to be in rough agreement with B_1 fields simulated by using the law of Biot-Savart. A CP- and DP-MAS peak area study for a mixture of three different ^{13}C labeled L-alanine compounds, as a function of sample position, showed greater deviation in signal intensities for CP-MAS generated peak areas. The methodology used to create coil shapes and predict their B_1 field profile was employed in creating two types of coil designs, of which the simulations predict that the variable pitch and radius coil produced a nearly homogeneous B_1 field throughout the sample volume.

Camille Keeler
Department of Chemistry
Colorado State University
Fort Collins, CO 80523
Summer 2001

ACKNOWLEDGMENTS

I would like to thank Dr. Herman Lock for providing both scientific and emotional support during the dark years in the laboratory. I sincerely appreciate the scientific opportunities and financial support that my advisor, Dr. Gary E. Maciel, provided during my stay at Colorado State University. I would also like to thank my family members and friends who gave helpful advice and remained supportive throughout my dramatic personal changes over the past seven years.

TABLE OF CONTENTS

Chapter 1

INTRODUCTION TO THE ABSOLUTE QUANTITATIVE DETERMINATION OF CARBON IN SOIL AND ITS SEPARATED SOIL COMPONENTS BY SOLID STATE ^{13}C MAS SPIN-COUNTING NMR METHODS.

1.1 Introduction

1.1.1 Historical Perspective

The first extractions of soil organic material were performed by F. Achard in 1786. In that study, a dark brown solution was obtained when soil was allowed to react with an alkaline solution[1]. This was followed by treatment with sulfuric acid, which caused the precipitation of a dark material that would later be named humic acid. The primary interest in soil chemistry in the 18th and 19th century was agricultural. Since then, many new instrumental and wet chemical methods have been developed to better understand the nature of the organic and other phases of soil. In addition, the focus of soil research has changed. Soil research is no longer focussed entirely on agricultural applications; the role of soil in our environment, in all of its interactions, spurs much of the modern research in this area.

Soil is considered to be a complex heterogeneous mixture of organic and inorganic components, of which some parts are relatively non-reactive chemically due to small surface areas (rocks and undecomposed organic matter), physically distributed in a layered structure, otherwise known as horizons[2]. The organic, physical and inorganic properties of a soil are dependent on a number of factors, some of those factors being local weather, temperature, geological origin, and local plant and animal life (including human activity). Based on these factors, soil structure and chemistry are unique to a particular location. A complex living assembly of bacteria, plant life, and other living creatures overshadow the chemical and physical properties of soil, all of which play a critical role in the cycle of life on earth.

Initiated over two thousand years ago, soil science has a very rich history. The focus of the present brief historical introduction is to highlight some of the more famous scientists who would be of interest to most modern chemists. This introduction should by no means be used as a complete guide to soil science. For a much more complete overview of soil science history, readers are encouraged to examine the published works of Kononova[3] and Orlov[1].

J. G. Wallerius, in his book, Fundamentals of Agricultural Chemistry (1761), proposed that the primary nutrient for plants was humus. The term "humus" describes the fraction of soil organic matter that has no visually recognizable origin. Soil organic matter includes non-decomposed litter, along with humus. Wallerius had first proposed, as did Lomonosov at this time, that the formation of soil is related to the decomposition of plant and animal matter[3]. Justus von Liebig (1803-1873), famous for his contributions to the field of organic chemistry, proposed that a major nutrition component of plants was

of mineral origin and later challenged Wallerius' theory of plant nutrition. His contributions to soil chemistry include a more precise definition of nutritional needs for plant life and a prepared synthetic fertilizer (albeit an ineffective fertilizer) from fused mineral carbonates[1]. It was these debates about the nutritional needs for plants that fueled a desire to know the composition of soil, both the inorganic and organic composition, as it was well known that soil types had an effect on crop quality and yield. It should be noted that in the early 19th century there was no knowledge of the relationship between soil microorganisms and soil decomposition. Organic matter decomposition was believed to be entirely due to abiotic reactions.

Johans Jacob Berzelius (1779-1848) was well known in the field of chemistry for his contributions to understanding metal oxide compositions, electrochemical theory, naming conventions, the discovery of several new elements and the precise determination of nearly 50 atomic weights. In addition to his contributions to the field of chemistry, including the proposed compositions of several minerals found in soils, his contributions to soil science included the isolation of two new classes of organic compounds from natural waters, crenic and apocrenic acids[3]. He examined the process of humification through organic extractions from decomposed wood and plant matter. In addition to the isolation of humus acids, he had described the properties of many of these compounds and many of the corresponding metal-acid complexes. In the 1830's, Berzelius classified humic substances into three major components: Humic acid, the alkaline soluble fraction; humin, the inert and insoluble fraction; and the aforementioned crenic and apocrenic acids. From 1912 to 1919 S. Oden would associate crenic and apocrenic acids with the modern term "fulvic acids."[3] This classification scheme, in which soil can be chemically

separated into three main fractions (humic acid, humin, and fulvic acid), has become the foundation for much of the modern research of humus substances. It is the quantitative determination of carbon in these soil fractions, beyond what can be provided from elemental analysis and wet-chemical techniques, that is the focus of the research presented in this thesis.

In the second half of the 19th century interest grew in the chemical composition of soils; however, V. V. Dokuchaev took the approach that soil composition alone was not enough to determine the genesis and properties of a soil[1]. Dokuchaev presented a more detailed correlation between the ecology of a soil and its genesis, i.e. the humification process. His ability to relate both the chemical composition and ecology of a soil to the formation of soil organics represented a shift from simply pursuing organic molecular structures to understanding soil structure and its relationship to soil composition. Dokuchaev, from his soil genesis research, fathered the concept that humus is organically heterogeneous and best described as a mixture of organic products of decomposition and other reactions. Until that time, it was generally accepted that humus was composed of a mixture of discrete organic compounds that could eventually be extracted, separated and assigned structures. This is overshadowed by the fact that there are an enormous number of chemically unique organic compounds that cannot be isolated individually from humic materials and purified. Thus, the terms "humic acid" and "fulvic acid" refer to the products of specific isolation procedures (i.e., "humic acid" is the alkaline soluble fraction of whole soil humus) rather than to a precise chemical structure.

It wasn't until the second half of the 19th century, following the revolutionary work of Pasteur, that biological organisms were believed to be involved in the

decomposition process. It was the later work of Von Post (1862), Darwin (1882), Kostychev (1886, 1889), Mueller (1887) and Ramann (1888) that established the link between soil life and decomposition[1]. Many biological experiments of the late 19th century focussed on the formation of humic materials from pure, isolated plant materials through biological degradation. Many of these experiments were open to criticism because they were performed on isolated materials, rather than whole soils. For the studies presented in this thesis, continuing biological activity in the Uncompahgre forest soil was minimized. A biological study of the Uncompahgre soil sample was beyond the scope of this thesis project. Drying and heating the soil before extractions eliminated the bulk of the biological activity in the Uncompahgre soil.

Another key aspect of a soil, the inorganic composition, is critical in evaluating the nature and physical properties of a soil. The inorganic fraction of soil, such as clay minerals and quartz particles, is the fraction that does not contain any organic carbon. This fraction plays a part in the physical properties of a soil, such as soil texture and aggregate formation, pH, soil swelling properties and cation-exchange capacity. It was the pioneering work of Dokuchaev that demonstrated that there was a strong correlation between the inorganic portion of soil and the formation of soil humus[1]. It was discovered that humus played a role in the dissolution and mobility of minerals in soil, which in turn would become part of the nutritional needs for plants. Moreover, the complex oxidation/reduction processes that occur in soil were believed to occur between the organic and inorganic parts of soil, rather than only being confined to either the inorganic or organic phase. It was the work of soil scientists of the first half of the 20th century (Tyurin and Gutkina, Kahn, Zyrin, Naidenova) that put focus on the humin, the base

insoluble and acid insoluble fraction in soil. This soil fraction contains most of the clay particles, which were known to be involved in soil particle formation. Some of those investigations focussed on the separation of strongly held organics from inorganic particles – the so-called "clay-humic" complexes[4,5]. Modern studies have revealed that these organomineral complexes in soil play a role in the formation of soil aggregates and may protect small inorganic particles from further degradation, a process in competition with the earlier mentioned process of mineral degradation from soil[6].

The inorganic fraction of the Uncompahgre soil was not directly probed in the present study for structural information beyond what is provided by elemental analysis. Direct and quantitative NMR approaches into the inorganic fraction, albeit suggested as further studies, are beyond the scope of this thesis. However understanding the role of certain inorganic materials in quantitative ^{13}C NMR measurements of soil and soil extracts is well within the scope of this thesis and is examined in later chapters. In the present study, the inorganic fraction of soil was left unchanged from its natural state in the Uncompahgre forest soil beyond the effects of the chemical extractions.

1.1.2 Wet Chemical Analysis and Total Carbon Determination in Soils

Up until the late 1800's, soil research depended entirely on empirical observations, simple inorganic acid/base tests and extractions, and the corresponding gravimetric analyses. This changed when the first chemical methods were developed for determining organic carbon content. In the early 1900's, the first wet chemical methods for quantifying total carbon in soil were developed. These wet chemical methods were based on the chemical oxidation of soil carbon to CO_2, and either quantifying the change

in oxidation state of the reagent or directly determining CO_2. In order to quantify an amount of carbon oxidized based on the change in oxidation states of the reagent, such as dichromate, a molar relationship between the oxidation of a *humic substance* and product, Cr^{3+}, must be established. Since humic materials have carbon in various oxidative states, it is impossible to know that exact relationship; consequently, an estimate has typically been used. In addition, any competing oxidation process, such as the oxidation of metal ions or incomplete oxidation of the organic carbon, will also complicate this process of relating the reduction of a reagent to the amount of oxidized carbon. Nonetheless, over the years the general procedure has been improved and many recent comparisons between wet chemical and the more accepted dry combustion methods have shown results generally within 10 percent on a variety of soils[6,7,8]. Wet chemical methods remain attractive due to their relative low-cost.

In addition to carbon elemental analysis, a number of chemical methods exist for the determination of specific functional groups in humic materials. Standard methods exist for phenolic hydroxyl, carboxylic acid, quinones, carbonyl groups and methoxyl functionality[9]. Recent comparisons between these wet-chemical methods and spectroscopic methods show inconsistencies[10,11], possibly owing to the fact that quantitative wet chemical analysis is strongly dependent on the skill of the scientist. Nonetheless, these methods provide a qualitative measure for some types of organic functionality in soil, and are still in use today.

1.1.3 Instrumental Analysis of Soil and Soil Components

Instrumental approaches to soil chemistry are associated with the second half of the 20th century. Much like the case of wet-chemical methods developed years before, a new set of analytical techniques and measurements could be applied to soil to determine soil composition and structure. The low detection limits and selectivity of some of the new instrumental methods allowed scientists to probe the behavior and fate of pollutants in soil, thus making soil chemistry an important aspect in environmental chemistry. With these advancements, much of soil science was now spurred by a whole series of environment-related applications. The methods presented below are accepted as being the most successfully employed in this area. It is beyond the scope of this thesis to discuss every instrumental application to soil science. Rather, the most commonly employed techniques will be presented for their significance to the historical development of soil science and their value as quantitative analysis techniques.

Instrument based elemental analysis provided a new method to quantitatively measure most elements in soil. These and other methods gave scientists the power to detect trace elements that would have been nearly impossible to determine eariler. This was yet another useful tool not only for agricultural applications, but also for detecting trace amounts of toxic species such as lead and mercury. Elemental analysis benefits from its quantitative nature and simple data interpretation, but it suffers in that it is oblivious to physical and chemical structural information. Some elemental analysis methods for soil have been found to be unreliable for some common elements in soil (such as oxygen in a clay mineral lattice) and research continues in this area. Some excellent reviews have been produced in this area[12,13]. Elemental analysis data on the

Uncompahgre National Forest soil form the foundation from which all quantitative comparisons will be drawn in this thesis.

The total quantitative analysis of carbon in soil by classic methods will play a most critical role in this research. The results from the total carbon determination by oxidation/CO_2 quantification methods will be used to judge the quantitative capabilities of the applied NMR methods. There are some excellent reviews on the carbon analysis of soils that are suggested for the interested reader[6,7,14,15]. Of the two basic approaches that have been used in the past to determine the total carbon content of soil, modern dry combustion methods are accepted as the most accurate for total carbon determination[6,7,14,15]. The other methods for carbon determination were popular in the past because of their experimental ease and low-cost.

Dry combustion methods involve burning the soil sample in an oxygen environment and quantitatively determining the CO_2 that is evolved. The sample is typically heated by a conducting graphite furnace or through induction with high power radio-frequency energy. Iron particles or similar conducting materials are often mixed in with the sample in the induction method to provide a means for the sample to heat up. The CO_2 that is evolved is then measured either gravimetrically, coulometrically, titrimetrically or by gas chromatography (flame ionization detection or thermal conductivity) methods[6,7,14,15]. The total organic carbon determination for the Uncompahgre Forest soil and soil components was provided by Huffman Laboratories (Golden, CO), which employs a home-built graphite-furnace/dry-combustion method and coulometric detection of CO_2.

Optical absorption methods of soil analysis, such as UV/VIS, IR and near-IR, have generally been limited to soil and clay mineral uses. It was found that "younger" humic acids had a smaller optical density in UV/VIS spectroscopy compared to older humic acids[16]. This was later correlated to the greater concentration of aromatic carbon in the older and to the predominance of side chains in the young humic acid[9,17,18]. UV/VIS techniques have also been used to establish a degree of aromaticity in humic materials. Humus materials typically show a broad, featureless absorption spectrum in the visible region, smoothly sloping downward from 200 nm to 700 nm.

The extremely broad, overlapping absorption lines from UV/VIS spectra have made quantitative relationships between organic species/functionality within the same sample nearly impossible to determine by that approach. Moreover, UV/VIS absorption behaves non-linearly with relation to different functionalities within soil; i.e. there will be no visible absorption for certain functionalities, such as methyl groups. In addition, since soil and soil components contain a distribution of different chemical species of unknown structure, no universal absorption coefficients can be used to relate absorption of light to a specific humic species, and thus be correlated to a concentration of a particular species. This fundamental issue keeps optical absorption measurements on the organic portion of soil from being absolutely quantitative. However, this does not rule out potentially useful UV/VIS measurements, where one soil or soil component can be semi-quantitatively compared to that of another soil through a reproducible method.

The absorption of light for humic substances increases with the degree of condensation of aromatic rings, the ratio of aromatic to aliphatic carbons, the concentration of organic matter and with increasing molecular weight[9,17,18]. Scheffer

(1954) and Welte (1955) showed that the ratio of extinction coefficients (ϵ) at 465 nm and 665 nm was independent of the total carbon content of the soil[9,17,18]. This ratio is often referred to as the E4:E6 ratio, or the chromacity coefficient Q, and gives a relative measure from which to compare different humus extracts from different soils.

IR absorption of soils, like UV/VIS absorption spectra of soils, may be used to track the existence of specific pollutant molecules or, in a more general sense, track a particular chemical feature of soil. IR absorption can be used to generate *relative* quantitative comparisons between soil components, with some advantages over UV/VIS absorption. IR absorption is inherently more selective to particular organic functional groups and may be used to obtain information otherwise invisible by UV/VIS methods. These *relative quantitative* optical methods have proven valuable in soil science, providing another method for classifying types of soil and following changes in soil and soil components.

Initially, IR experiments were utilized to confirm the chemically heterogeneous nature of humus materials and implied that humic extracts from different soils have the same principal structure. Typical absorption bands for soil in the 1230 to 1250 cm^{-1} range are associated with hydroxyl and =C-O- groups; a 1150 to 1050 cm^{-1} band is due to deformation of alcohol OH groups; 1720 to 1700 cm^{-1} is due to carbonyl groups. The absorption frequencies of carboxyl groups are sensitive to the extent of de-protonation and interactions with metal cations. Minor differences between the carboxylate absorption frequency for metal-humate complexes and the non-complexed form have constituted the basis for many studies on the ion-absorption properties of soil components[19-21]. IR analysis has also been used to identify chemically modified (i.e.,

methylated[22], etc.) humic materials and to help characterize a wide variety of humic materials[11,23-31] in various stages of decomposition[32-36].

Although dispersive IR instruments are still widely employed for soil analysis, there have been improvements in this area through the use of Fourier Transform IR (FTIR), Diffuse-Reflectance Infrared Spectroscopy (DRIFTS), and Attenuated Total Reflectance (ATR) IR techniques. DRIFTS has become more popular for soil analysis, as it does not suffer from some of the scattering that is often seen at higher wavenumbers from pellet analysis[37,38]. DRIFTS also benefits from greater absorption and fewer baseline problems compared to pellet analysis methods. FTIR, DRIFTS, and ATR methods have all been successfully applied to soil science research[37,38]. Of these three methods, FTIR is used far more often than DRIFTS, which has been used far more often than ATR, to gain information about soil samples. DRIFTS and ATR are often employed as complementary techniques, giving small improvements in spectral resolution and intensity in regions that may suffer in conventional dispersive and FTIR methods. Neither technique provides any additional insight into the challenge of making absolute quantitative measurements of all organic functionality in soil and soil components by IR methods. It may be possible to perform quantitative IR measurements on *specific* organic functionalities in soils, if care is taken with calibrating the response of the IR with respect to specific functional groups found in the soil sample[11]. It is not surprising that such a *relative* or *absolute* quantitative study has not been initiated on all the major IR absorption bands, owing to the difficulty of such a study. Such a study would not extend to all the organic functionalities in soil and would, therefore, not be able to provide a total quantitative carbon analysis.

1.1.4 Relevant NMR theory

NMR has become well established for the structural characterization of liquids or compounds in solution and plays a critical role in research projects of many disciplines. Over the past 25 years, nuclear magnetic resonance spectroscopy has been successfully employed in the characterization of solid samples of organic-geochemical origin[39-42]. The introduction of ^{1}H decoupling, cross-polarization (CP) and magic angle spinning (MAS) have made it possible to obtain high-resolution ^{13}C NMR spectra on solid samples in a relatively short time. This contrasts with a solution-state NMR analysis that would normally be very difficult or inappropriate for such samples, as a significant part of soil cannot be dissolved under conditions that would preserve the very chemical structures we wish to investigate. Although long understood to be capable of quantitative measurements, NMR has mostly been used in a qualitative manner for the analysis of organic-geochemical samples. In this section, the basic NMR theory[43,44] that relates to quantitative CP- and DP-MAS experiments will be reviewed.

1.1.4.1 NMR Basics

Nuclear magnetic resonance is based on the interaction between a nucleus with a magnetic moment and an applied external magnetic field. The potential energy for the interaction between a spin magnetic moment $\boldsymbol{\mu}$ and an externally applied field $\mathbf{B_0}$ is given by the dot product between the external field and the magnetic moment:

$$E = -\boldsymbol{\mu} \bullet \mathbf{B_0} \qquad (1.1)$$

Expressing μ in terms of the nuclear spin angular momentum and assuming that B_o is the magnitude of an external magnetic field directed along the z axis gives the energy as

$$E = -hm\gamma B_o/2\pi \quad (1.2)$$

where m ($m = I, I-1, I-2, \ldots -I$) is the magnetic quantum number and γ is the magnetogyric ratio, a proportionality constant between the magnetic moment and angular momentum. The parameter γ is unique to every distinct nuclide. It can be seen that, when $I \neq 0$ and $\mathbf{B}_o > 0$, more than one energy level exists and an energy transition is possible. For the case where the nucleus involved has $I = ½$, such as with ^{13}C, then $m = \pm ½$ and the transition energy can be written as:

$$\Delta E = h\gamma B_o/2\pi \quad (1.3)$$

The Larmor precession frequency f_o in Hz is given by

$$\omega_o = f_o 2\pi = \gamma B_o \quad (1.4)$$

where f_o is also the frequency of radiation needed to excite the E_{-+} transition. ^1H and ^{13}C resonate at 100.5 and 25.25 MHz at an external field strength of 2.35 T, the field strength employed in the solid phase soil experiments detailed in this thesis. For simplification, equations in the following section will be for the $I = ½$ case.

There will be a net absorption of energy at frequency f_o because there are unequal populations of spins in the two levels, with slightly more being in the lower energy level at thermal equilibrium. The ratio of the number of nuclei in the lower energy level (N_1) to that of the higher energy level (N_2) is predicted by the Boltzman distribution law to be

$$N_2/N_1 = e^{-\Delta E/kT} \quad (1.5)$$

at an absolute temperature T, with Boltzman constant k. Expanding the exponential and making the approximation $h\omega_o/2\pi << kT$ (a good approximation at normal temperatures) allows the above ratio to be expressed as:

$$N_2/N_1 = 1 - h\omega_o/2\pi kT \qquad (1.6)$$

For the ^1H nucleus at 2.35 T, that ratio is approximately 0.999984, which corresponds to roughly 0.0008 % of the ^1H in the sample contributing to the NMR signal. This is the main reason why NMR is considered a 'low sensitivity' experiment. Perhaps the most important consequence of the above relationships is that a net absorption of energy is possible for every NMR active nucleus and that the intensity of such an NMR signal is directly proportional (in a predictable manner) to the number of nuclei involved in the transition. It can be concluded at this point that, although based on an inherently low-sensitivity phenomenon, it is possible to do quantitative NMR experiments on complex organic samples.

1.1.4.2 The Chemical Shift

The circulation of electrons around nuclei induced by the strong external field $\mathbf{B}_o$ creates induced magnetic fields (opposing the strong external magnetic field) that ultimately modify (shield) the local magnetic field $\mathbf{B}_{loc}$ at the nearby nucleus. Nuclei in different chemical environments will experience different $\mathbf{B}_{loc}$ fields and will therefore resonate at slightly different frequencies. This shielding is different for each unique bonding situation and forms the basis by which different chemical structures are identified by NMR. This shielding effect of local electrons about a nucleus is described

by a chemical shielding parameter σ that can be related to the external and local magnetic field through the following equation:

$$B_{loc} = B_o(1 - \sigma) \quad (1.7)$$

The resonance frequency f of a nucleus in a particular chemical situation is related to the resonance frequency of an unshielded nucleus (f_o) through the shielding parameter such that:

$$f = f_o(1 - \sigma) \quad (1.8)$$

The chemical shift of the peak of interest can then be defined by δ, and can be referenced relative to the resonance frequency of a standard compound f_{ref} (such as tetramethylsilane—a chemical shift standard for ^{13}C or ^{1}H or ^{29}Si NMR) such that:

$$\delta = 10^6(f - f_{ref})/ f_o \quad (1.9)$$

In this manner, the chemical shift is given in units of parts per million (ppm), a scale that is independent of the external field strength under which the experiment was conducted. For diamagnetic samples, protons typically have a chemical shift range of 0 to 12 ppm, while ^{13}C has a chemical shift range of roughly 0 to 220 ppm. The ^{13}C NMR spectra of soils and soil extracts are complex and typically fill this entire chemical shift range with numerous peaks representing a wide range of compounds and organic functionality.

Liquid and solid-state samples demonstrate very different chemical shift behavior in NMR. In samples where the molecules of interest are rapidly tumbling in a random fashion, the nuclear shielding results in a single isotropic chemical shift resonance for each nucleus in a chemically unique environment. In this particular situation, σ is a scalar that characterizes the chemical shift.

Chemical shielding is very sensitive to both the local electronic environment and the orientation of the molecule with respect to the external magnetic field. For most solid samples, where relatively little molecular motion exists, the orientation of the molecule relative to the external field has to be considered when evaluating B_{loc} and the chemical shift parameter is best characterized by a second rank tensor. The relationship between the local and external field is written as

$$\mathbf{B}_{loc} = (\mathbf{1}-\boldsymbol{\sigma}) \cdot \mathbf{B}_0 \tag{1.10}$$

where $\boldsymbol{\sigma}$ is the second rank chemical shift tensor. The reference frame that diagonalizes the nine components of the chemical shift tensor is known as the principle axis system, in which only the diagonal elements (σ_{11}, σ_{22}, σ_{33}) are nonzero. The laboratory frame component (σ_{zz}) is the only component of the chemical shift tensor that commutes with the Zeeman Hamiltonian and contributes to the NMR spectrum in the first order. The resulting secular term of the chemical shielding Hamiltonian reads as follows:

$$H_C = -\gamma\hbar\sigma_{zz}I_zB_0 \tag{1.11}$$

The principal axis system is related to the laboratory axis system through a series of rotations described by the polar angles θ_{11}, θ_{22}, and θ_{33}. Assuming $\boldsymbol{\sigma}$ has principal values σ_{11}, σ_{22}, and σ_{33} along its principal axes and is related to the direction of B_0 through the three corresponding angles θ_{11}, θ_{22}, and θ_{33}, then[47]

$$\sigma_{zz} = \sigma_{11}\cos^2\theta_{11} + \sigma_{22}\cos^2\theta_{22} + \sigma_{33}\cos^2\theta_{33} \tag{1.12}$$

Under liquid-like rapid isotropic tumbling, each polar angle in the above equation varies randomly such that each $\cos^2$ term is equal to 1/3. Under this rapid tumbling situation,

the above anisotropic interaction time averages to the isotropic value for the chemical shift:

$$\sigma_{zz} = 1/3(\sigma_{11} + \sigma_{22} + \sigma_{33}) = (1/3)\mathbf{Tr}\boldsymbol{\sigma} = \boldsymbol{\sigma}_{iso} \quad (1.13)$$

1.1.4.3 Chemical Shift Anisotropy

For a solid, each different nuclear site will generally have unique values for θ_{11}, θ_{22}, θ_{33} and a different value for σ_{zz}. It should be noted that for a random powder of crystallites, a distribution of chemical shifts would be expected, reflecting the chemical shift and statistical probability of each crystallite orientation. The resulting "powder pattern" would be spread over a frequency range of $f_0|\sigma_{11} - \sigma_{33}|$ and is described as the chemical shift anisotropy (CSA). Without a method to reduce the CSA powder pattern to its isotropic value, it would be very difficult, if not impossible, to relate chemical structure to peak areas of complex organic solids. Although this suggests NMR signals from a solid sample would be spread over the entire isotropic chemical shift range and quite possibly beyond, the direct relationship between signal area and nuclei involved in the transition would still hold true. The only way CSA's hinder our ability to do quantitative NMR experiments is by reducing signal-to-noise ratios and spectral resolution.

1.1.4.4 Magic Angle Spinning

The anisotropic chemical shift found in solid samples can be averaged to the isotropic value by rapid mechanical rotation of the sample about an axis tilted from the

direction of the external field B_0. If the solid sample is rotated with angular frequency ω_r about an axis at angle θ_m with respect to B_0, we have[47],

$$\cos\theta_p = \cos\theta_m \cos\chi_p + \sin\theta_m \sin\chi_p \cos(\omega_r t + \psi_p) \qquad (1.14)$$

with χ_p describing the angular relationship between one of three principal axes (p) of the sample and the axis of rotation and ψ_p being the initial azimuthal angle. Equation 1.14 describes the angular behavior of the principal axis when under rapid rotation at an angle θ_m relative to the direction of B_0. Substitution of relationship 1.14 into equation 1.13 and averaging over rotation results in

$$\overline{\sigma_{zz}} = \tfrac{1}{2}(\sigma_{11} + \sigma_{22} + \sigma_{33})\sin^2\theta_m + \tfrac{1}{2}(3\cos^2\theta_m - 1)(\sigma_{11}\cos^2\chi_1 + \sigma_{22}\cos^2\chi_2 + \sigma_{33}\cos^2\chi_3) \qquad (1.15)$$

When θ_m is equal to 54.74 degrees, called the "magic angle", the above relationship reduces to equation 1.13, where the chemical shift is averaged to the isotropic value. Rapid sample rotation about the magic angle is called magic angle spinning[45,46] (MAS) and is used extensively in solid state NMR to improve spectral resolution by collapsing CSA powder patterns to the average, and typically more narrow, isotropic value of their chemical shifts.

1.1.4.5 Chemical Shift Dispersion

The dispersion of isotropic chemical shifts over a range of the spectrum for a given class of carbon atoms is mainly responsible for the broad, overlapping peaks in the ^{13}C MAS spectra of soil and soil components. The isotropic chemical shifts for particular functional groups in a molecule can vary depending on conformations and on inter- and intra- molecular interactions and subtle variations in local chemical structure. For a mixture of non-crystalline and complex organic compounds, such as those found in soils,

a class of functional group will experience a large ^{13}C chemical shift dispersion. For example, the dispersion of chemical shifts for methyl groups in solid ^{13}C MAS spectra of soil or soil extracts is often on the order of 10 ppm or more, as can be seen in the many spectra presented in this thesis.

1.1.4.6 The Dipolar Interaction

Spin 1/2 nuclei produce localized magnetic fields that slightly alter the magnetic field experienced by other nuclei that are nearby. In a solid sample in which there are neighboring nuclei, the nuclei of interest will experience a distribution of different magnetic fields. This effect is referred to as the dipole-dipole interaction and results in a broadening of the resonance. The fast tumbling motion of molecules in liquids normally average out the dipolar interaction, which results in much narrower lines in liquid samples than is normally observed in solid samples. The dipolar interaction can exist between heteronuclear or homonuclear spin pair(s) or a combination of both. It is the heteronuclear dipolar interaction that exists between ^{1}H and ^{13}C in soils and soil components (and most other organic compounds) that makes certain useful experiments, namely cross-polarization (Chapter 3) and spectral editing (Chapter 4) experiments, possible.

The ^{13}C-^{13}C homonuclear dipolar interaction is of little concern for soil samples, as the natural abundance of ^{13}C nuclei is small enough (1.1 percent) to make the occurrence of ^{13}C-^{13}C dipolar spin pairs rare. The ubiquitous ^{1}H-^{1}H homonuclear dipolar spin pairs, having strong dipolar couplings, make it necessary to employ additional instrumental techniques to obtain high-resolution ^{1}H NMR spectra of soils and soil

components. This homonuclear coupling plays a less dramatic role in our ability to obtain high-resolution ^{13}C NMR spectra. It is the ^{1}H-^{13}C heteronuclear spin interaction, being common due to the abundance of ^{1}H in organic solids and a relatively strong interaction, which could add additional line broadening in organic solids that is not normally observed in solution state ^{13}C NMR spectra.

The truncated Hamiltonian representing the secular part of a heteronuclear dipolar interaction reads as follows[47]:

$$H_D \approx \hbar\omega_D\left(1-3\cos^2\theta\right)I_Z S_Z \tag{1.16}$$

where $\omega_D = \hbar\gamma_I\gamma_S r^3$, r is the internuclear distance and θ is the angle between the vector joining the two nuclear spins and $\mathbf{B_o}$. If the solid sample is spun about an axis at an angle β with respect to the external field at a frequency of ω_r, the angle θ becomes time dependent and follows the relationship:

$$\cos\theta(t) = \cos\beta\cos\beta' + \sin\beta\sin\beta'\cos(\omega_r t + \phi) \tag{1.17}$$

where β' is the angle between the time dependent internuclear vector and spinning axis and ϕ is the initial azimuthal angle. Squaring the above relationship and taking the average over time yields:

$$\overline{\cos^2\theta} = (1/6)\left(3\cos^2\beta - 1\right)\left(3\cos^2\beta' - 1\right) + (1/3) \tag{1.18}$$

Substitution of equation 1.18 into 1.16 yields the time-averaged, truncated heteronuclear dipolar Hamiltonian. The term $3\cos^2\beta$-1 vanishes when β is equal to 54.74 degrees, the magic angle, and the consequence of that is that the heteronuclear dipolar interaction gets averaged to zero. Unlike the chemical shift interaction, the energy of this interaction is independent of the externally applied magnetic field and is often in the 10's of kHz

energy range. For many chemical situations, the ^{1}H-^{13}C heteronuclear dipolar interaction is too large to be averaged by MAS at practicable rotation frequencies. This necessitates the addition of strong proton decoupling during the data acquisition phase of the experiment. This is achieved by irradiating the sample at the proton resonance frequency with ample power during acquisition[48-50]. It is the combination of both MAS and strong ^{1}H decoupling which yields the narrowest possible peaks in ^{13}C NMR of soils and soil components.

1.1.4.7 DP-MAS

A common NMR experiment used for the analysis of organic compounds is the direct polarization (DP) experiment, which is also known as the single pulse or Bloch decay experiment. In this experiment, the net magnetization of nuclei to be observed is tilted from the direction of $\mathbf{B}_0$ with a short, powerful RF pulse. Following the short pulse (denoted a $\pi/2$ or 90° pulse, which indicates a rotation of the magnetization 90° from the direction of $\mathbf{B}_0$), the decaying magnetization in the x-y plane is detected and digitized, a process also known as the data acquisition. In practice, the acquisition is accompanied by strong ^{1}H decoupling to reduce $^{13}C/^{1}H$ heteronuclear dipolar couplings and hence the spectral linewidths. Following a delay period, the experiment is repeated and the signal added to the previous experiment. Magic angle spinning is maintained throughout the entire experiment. Figure 1.1(a) shows the pulse schematic for the DP-MAS NMR experiment.

1.1.4.8 CP-MAS

Another very common experiment used to analyze samples of organic-geochemical origin is the cross-polarization (CP) experiment. In this experiment, polarization is typically transferred from a more abundant, higher-γ nucleus (such as ^{1}H in organic solids) to an insensitive nucleus such as ^{13}C. ^{1}H nuclei, being much more abundant and having a higher γ than carbon, represents a large spin angular-momentum reservoir or "spin bath". The less abundant, lower γ ^{13}C nuclei represent a much smaller (i.e., smaller heat capacity) spin bath. The ^{13}C and ^{1}H spin baths are normally in contact through their heteronuclear dipolar interaction. Thermal contact between the ^{13}C and ^{1}H spin reservoirs is made more efficient when the Hartmann-Hahn condition is met, a condition in which two long RF pulses at the ^{1}H and ^{13}C Larmor frequencies are applied with relative intensities given by $\gamma_H B_{1H} = \gamma_C B_{1C}$. When the Hartman-Hahn match is reached, the Zeeman energies of both spin reservoirs are equal in a double rotating frame and mutual $^{13}C/^{1}H$ spin "flip-flops" become a very efficient way to transfer energy between spin baths. In this way the spin temperature is equalized between the two spin reservoirs. The ^{13}C spin bath lowers in temperature much more than the ^{1}H spin bath temperature is raised during the cross-polarization period, owing to the difference in spin bath sizes. During cross polarization, the ^{13}C nuclei experience a change in polarization that is less than or equal to the ratio of the γ values (γ_H/γ_C) or roughly a factor of four.

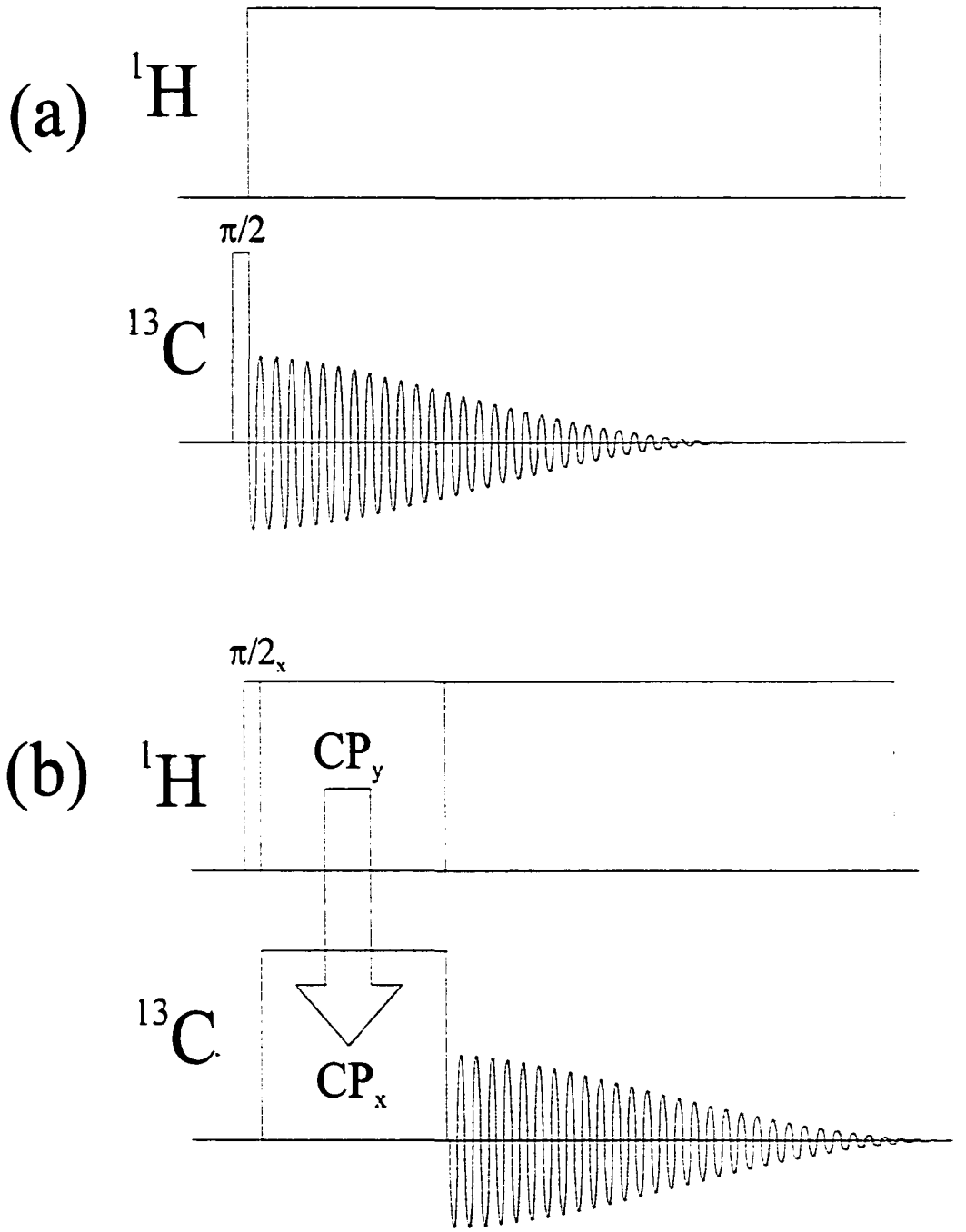

Figure 1.1 Radio-frequency pulse schematics for the (a) ^{13}C DP-MAS NMR experiment and (b) the ^{1}H-to-^{13}C CP-MAS experiment.

The ^{13}C nuclei experience cross-polarization enhancements that depend on the duration of the contact period with protons. Figure 1.1(b) shows the pulse schematic for a typical CP experiment. The initial proton $\pi/2$ pulse brings the ^{1}H magnetization into the x-y plane where it is subsequently "spin-locked" along the direction of the cross-polarization RF pulse. The proton magnetization is essentially cooled when spin-locked in the direction of the cross-polarization pulse. The spin-lock condition is not an equilibrium condition for the protons, so the spin-locked magnetization decays, with a rate determined by $T_{1\rho}$, the longitudinal relaxation constant for protons spin-locked in the rotating frame. While the spin-locked proton magnetization is decaying, the ^{13}C magnetization is growing with a rate constant T_{CH}^{-1}, which is a reflection of the strength of the heteronuclear ^{13}C-^{1}H dipolar interaction. The balance between the loss of proton magnetization and growth of ^{13}C magnetization dictates which contact period will generate the greatest CP signal enhancement. In addition to the CP enhancement, the CP-MAS experiment benefits from the fact that the cross-polarization generated ^{13}C magnetization is dependent on the state of the ^{1}H spin-reservoir before contact is established; the repetition delay between experiments is then chosen to compensate for the longitudinal relaxation of the protons in the laboratory frame, rather than the typically longer ^{13}C T_1 relaxation times.

1.1.5 Solution State NMR Analysis of Soils and Soil Components

Solution state ^{13}C and ^{1}H NMR has been successfully applied to the study of the solvent-soluble fractions of soil. The narrow peaks that are found in liquid state NMR spectra of soil extracts have proved to be valuable for organic structural determinations

and have contributed to many of the chemical-shift assignments[24,51-53] used in this thesis. A typical solid-state humic acid ^{13}C CP-MAS NMR spectrum is shown in Figure 1.2 with tentative chemical-shift assignments in place to show which functional groups correspond to each major NMR peak in the spectrum. These shift assignments are confirmed by NMR spectroscopy and further elaborated in Chapter 4 of this thesis. Additional chemical treatments, such as acid hydrolysis and methylation, on humic and fulvic acids have been used to aid in making spectral assignments[54-58]. Liquid state NMR was used to discover the effects of acid on common structures in humic materials; acid hydrolysis with 6 M HCl was found to reduce the concentrations of carbohydrates and proteinaceous materials[57,58]. Many derivatization studies were followed with liquid-state NMR[54-59]. Derivatization by ^{13}C-labeled methylation is a chemical method used to improve spectral assignments and signal-to-noise ratios by reaction with –OH functionality to create methoxy groups[57]. The chemical shift of the ^{13}C-labeled methoxy group depends on the origin of the hydroxy functionality, be it phenolic, carboxylic, carbohydrate, enolic, or aliphatic hydroxyls. Derivatization selectivity depends on the methylating reagent (e.g., CH_3I, diazomethane) and reaction conditions[59].

An advantage of liquid-state NMR over solid state analysis of soils or soil extracts is the ability to take advantage of *scalar* couplings. This makes it possible to use experiments such as DEPT[60] to separate spectra into CH_3-only, CH_2-only, CH-only and CH_0 only subspectra. Recently, DEPT/QUAT experiments were employed on a soil fulvic acid, the data from which was used to propose an "average" structure for fulvic acid[61]. The solid state analog of such an experiment, based on the *dipolar* interaction, was recently employed on humic acid and is presented in Chapter 4 of this thesis.

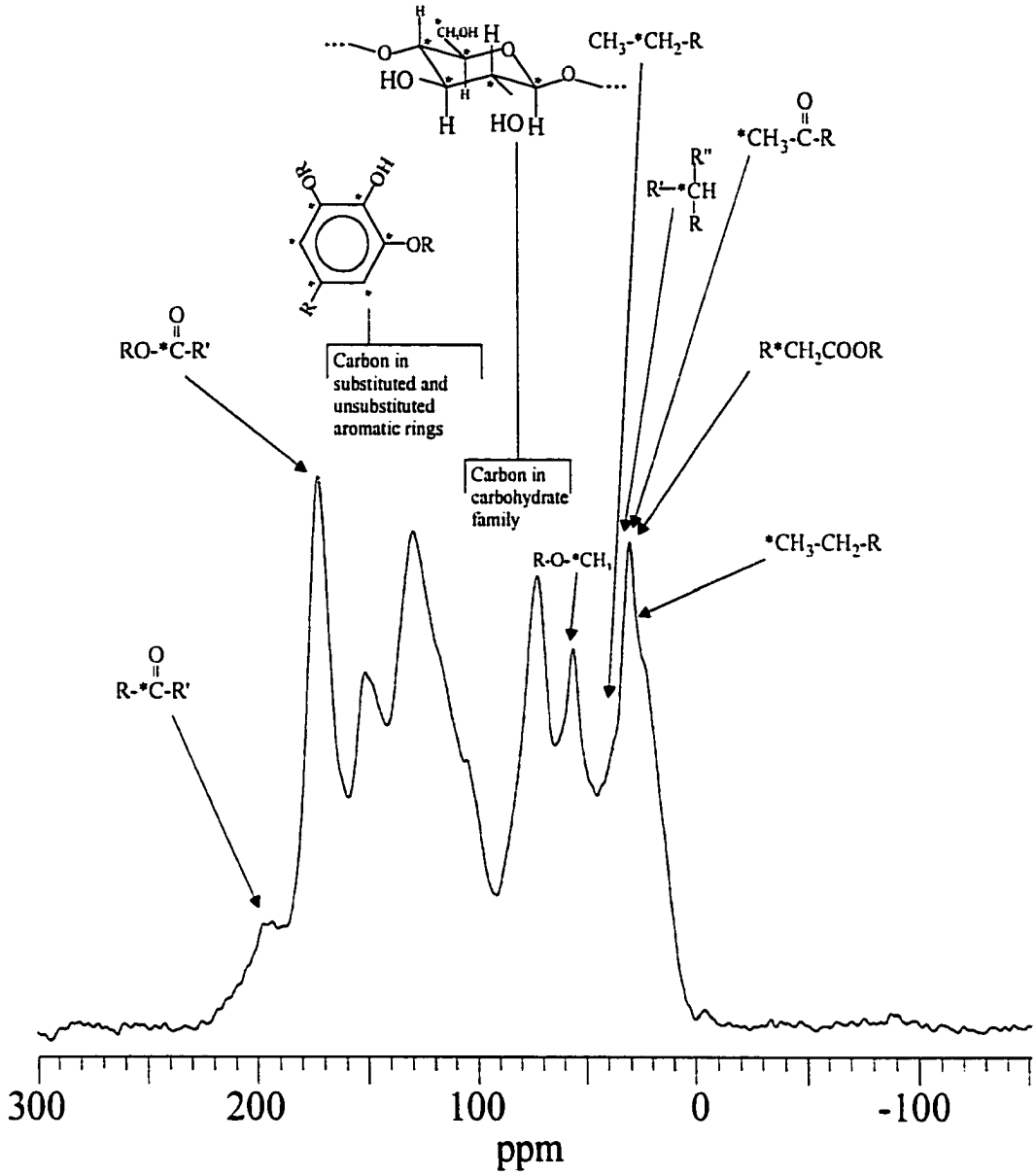

Figure 1.2 A typical ^{13}C CP-MAS spectrum of humic acid extracted from the Uncompahgre National Forest soil. Tentative chemical shift assignments for this humic acid are shown with arrows pointing to the peak corresponding to its representative major organic component and/or functional group. These shift assignments are explained in detail in Chapter 4 of this thesis.

The majority of the solution state NMR studies on soil extracts have focussed on identifying key organic components from an extract of a soil of particular importance. Few of those solution-state NMR spectra have been acquired in a relatively quantitative manner,[62,63] with none to date (to the author's best knowledge) having been acquired in an absolutely quantitative manner. Variations of NOE factors among the different functional groups in such samples make it necessary to use inverse gated decoupling and long relaxation delays between scans to achieve a uniform relationship between signal intensity and number of ^{13}C nuclei[64]. Meeting these requirements further reduces sensitivity by a significant factor due to the loss of the NOE and by using longer repetition delays.

1.1.6 NMR as an Analytical Tool for Soil Analysis

1.1.6.1 Relative and Absolute Quantification

Soil scientists have few analytical tools with which to make *absolute* quantitative measurements on soil and humic components, i.e., measurements in which a signal response can be quantitatively related to an amount of matter. *Relative* quantitative measurements are made to compare amounts of material, either within the same sample or between samples, without necessarily knowing the absolute amount of matter involved in the comparison. Both relative and absolute quantitative measurements require a measuring method that consistently relates signal to an absolute amount of material; an absolute quantitative measurement has the further requirement of quantifying that

relationship. The direct relationship between signal response and number of nuclei inherent in NMR allows for both absolute and relative quantitative measurements to be made. The aforementioned problems associated with the quantitative spectroscopic analysis of soil and soil components by IR and UV/VIS make it difficult, if not impossible, to establish a quantitative relationship between a signal intensity and amount of carbon in a complex organic material. Solid state NMR has been widely used in the past in a relative quantitative manner to compare the concentrations of different functionalities found in soils and soil extracts[62,65] or simply in a non-quantitative manner to compare structural trends. It is the goal of the research reported in this thesis to determine the extent to which solid-state NMR can be used to make absolute quantitative measurements, also known as spin-counting, on soil samples in their native state, and to provide the methodology for achieving quantitative solid-state NMR spectra on soils and soil extracts.

There are two general approaches that can be used in solid state NMR to obtain absolutely quantitative (spin-counting) results, direct polarization with magic angle spinning (DP-MAS) and cross polarization with magic angle spinning (CP-MAS). DP-MAS spin counting has the benefit of being a relatively straight-forward method and requires fewer experiments than the comparable spin-counting experiment by CP-MAS. The benefit of simplicity is often overshadowed by the poorer quality spectra (i.e., worse baseline roll and signal-to-noise ratios) obtained by DP-MAS relative to CP-MAS. For this latter reason, CP-MAS has been the experiment of choice for examining soil and soil extracts by solid state NMR. Both methods have their merits and drawbacks and will be examined in detail in the forthcoming chapters of this thesis.

Relatively quantitative (99.9 percent or greater accuracy, not considering signal-to-noise factors) DP-MAS solid-state NMR experiments are realized when the repetition delay between experiments is at least five times greater than the longest longitudinal relaxation time of any peak in the sample. Under these experimental conditions, the peak area for each peak in the NMR spectrum can be directly related to the number of nuclei being observed. The same result can be achieved with shorter repetition delays when the T_1 relaxation times are known for each chemically unique species and a correction factor, based its T_1 relaxation time and repetition delay, can be applied to each peak area in the spectrum.

Similar results in CP-MAS spin-counting NMR experiments are achieved when signal intensities are corrected for both the ^1H T_1 relaxation time(s) and for the cross-polarization behavior (typically described by rotating frame time constants $T_{1\rho}$ and T_{CH}). The cross-polarization signal enhancement, in conjunction with generally shorter repetition delays due to short ^1H T_1 relaxation times, contribute to the enhanced signal-to-noise ratios and signal quality typical of CP-MAS results on these materials. The ^1H T_1 relaxation times are often short enough that CP-MAS experiments are simply run with a repetition delay greater than or equal to fives times the ^1H T_1, so no T_1 correction is necessary. The cross-polarization time constants, T_{CH} and $T_{1\rho}$, must be accurately quantified, which often requires 20 to 30 data points (20 to 30 spectra) and adequate signal-to-noise so that accurate correction factors can be applied to the spin-counting CP-MAS spectrum. It is the determination of these correction factors that consumes the most time of the CP-MAS spin-counting procedure and actually makes the entire procedure of

spin-counting by CP-MAS roughly as time consuming as the entire DP-MAS spin-counting procedure.

Relative quantification is a prerequisite for *absolute* quantitative measurements by NMR. A requirement for successful spin-counting is that a quantifiable peak area in the DP-MAS or CP-MAS sample spectrum can accurately be related, either empirically or directly, to an absolute number of NMR active spins. Spin counting in this manner has been achieved in solid state NMR by acquiring a spectrum of the unknown with some well-characterized external reference in the sample area. These reference materials are often added to the MAS rotor sealed in a small capillary tube[66,67], or are physically mixed throughout the sample of interest, or may actually be the MAS rotor material[68]. External references are often chosen for their robust signals, chemical inertness, chemical stability, NMR relaxation characteristics, ease of handling and chemical shift. The overall methodology behind spin counting in solid-state NMR has been well characterized and successfully applied to a number of samples of geochemical origin such as coals[69].

1.1.6.2 Requirements for Spin-Counting

Solid state CP-MAS and DP-MAS NMR experiments can be made absolutely quantitative when a few sample and instrumental conditions are met. The NMR signal must be proportional to the number of observable NMR nuclei in the sample (with the appropriate signal intensity corrections), must be measurable (e.g., not broadened to the point where the signal cannot be measured), and must be significantly greater than the noise in the spectrum. DP-MAS has not been the solid-state NMR experiment of choice for the ^{13}C analysis of soil samples for several reasons. ^{13}C DP-MAS experiments often

do not yield acceptable signal-to-noise ratios for soil and soil extracts. This is due to the breadth of peaks commonly found in the spectra of these types of samples and the typically low carbon content of whole soils and their extracts. Chemical shift anisotropy, chemical shift dispersion, insufficient proton decoupling, paramagnetism, and ferromagnetism can all contribute to the broadening of an NMR resonance compared to what would be found in the liquid state. CP-MAS experiments will suffer from the same broadening mechanisms, but generally produces signals of greater intensity over a given experimental time than those from DP-MAS experiments.

Broadening due to chemical shift anisotropy (CSA) is overcome by employing magic angle spinning (MAS). A typical consequence of MAS is the presence of spinning-side bands, peaks that are centered about the isotropic peak and at frequency intervals equal to integer multiples of the spinning speed and continuing throughout the breadth of the CSA. MAS at a speed near or greater than the chemical shift range for ^{13}C, which is necessary to bring the spinning side bands out of the chemical shift range, is ideal for quantitative work. This greatly simplifies the procedure to quantify the contribution to the total peak area from a particular functional group. The necessity for employing a minimum MAS speed at a particular external field strength (we chose 4.5 kHz at an external field strength of 2.35 T) puts restrictions on which commercially available MAS systems can appropriately be applied to NMR experiments on soil at a particular field. The optimum combination of field and commercial MAS system will provide adequate spinning speed with the largest sample volume possible, as the signal intensity is proportional to the amount of sample. Fortunately, there are sufficient quantities of soil and soil extracts available from the extraction procedure to fill the 2.1

ml sample volume of the large volume spinner employed in this study (*vide infra*). Because of the relationships and trade-offs among sample size, CSA, MAS speed, B_0, etc., as it has been found with many organic geochemical samples that signal-to-noise ratios are not simply optimized by moving to higher external field strengths.

Line broadening in solid state NMR does not interfere with quantitative measurements until, for whatever reason, the peak representing the particular functional group is so broad that it cannot be integrated or deconvoluted accurately and/or precisely. All of the broadening mechanisms mentioned thus far do not directly conflict with a total spin-counting measurement on a soil. However it is necessary to minimize linewidths to allow for the best possible assignments of peak-position to chemical-functionality, which is why MAS and decoupling powers of 50 kHz or greater are so critical in making these measurements. Computer-assisted peak deconvolutions (determination of peak areas) are generally more successful with smaller line widths, as narrow peaks are less likely to overlap.

1.1.6.3 Paramagnetism and Ferrimagnetism in Soil Components

Paramagnetic and ferrimagnetic impurities in soils, primarily in the form of ionic Fe^{3+} and iron-containing minerals, have long been identified as potentially damaging to making quantitative NMR measurements[70,71]. Iron is rarely encountered in nature in its pure metallic form; rather it is most often encountered in an oxidized state. Iron oxides and minerals can be ferrimagnetic, as in the mixed oxidation state material Fe_3O_4 (magnetite), paramagnetic (Fe^{3+} ions), or even anti-ferromagnetic as found with $FeTiO_4$ (ilmenite) and certain Fe-containing aluminosilicates (nontronite)[72]. Working with iron

in soils in general, and treating soils for these materials to obtain better NMR results in particular, is complicated by the poorly understood chemical nature of iron in soils.

The presence of paramagnetic and/or ferrimagnetic materials in a sample can broaden NMR peaks to immeasurable, and hence non-quantifiable, proportions. Soils and soil extracts, in particular, may contain large amounts of both ferrimagnetic and paramagnetic compounds. These are both particularly troublesome as they are often intimately a part of soil structure and difficult, if not impossible, to remove without disturbing either the carbon content or the organic structure of that which is being studied.

Ferrimagnetic and paramagnetic species have classically been removed from materials of organic-geochemical origin through the use of powerful magnets, high gradient magnetic separators, and chemical treatments[70,73,74]. Post-treated soil samples and mineral sand samples have shown dramatic improvements in resolution and sensitivity by solid-state NMR analysis[70,74]; however, none of the published results were analyzed in an *absolute* quantitative manner, with the exception of the research by Vassallo et al.[73]. Each of these methods may help by selectively removing either ferrimagnetic or paramagnetic species from soil, but rarely without affecting the organic portion of soil, be it by chemical modification (i.e., chemical reduction or degradation) or through altering the physical coupling between organics and ferrimagnetic or paramagnetic species. The existence of the aforementioned "clay-humic" complex greatly complicates the complete separation of the ferrimagnetic or paramagnetic component from organic materials based on magnetic susceptibilities or ferrimagnetism. Some of these classic procedures, modified to accommodate a quantitative separation,

can be applied to soils and soil components to narrow the linewidths of otherwise immeasurable peaks without affecting the organic fraction of soils.

The chemical treatments applied in previous NMR studies on soils and/or soil components to remove the effect of iron on the NMR spectra were designed to either reduce paramagnetic Fe^{3+} to the diamagnetic Fe^{2+} ion or form a Fe^{3+} complex that can be removed selectively. Treatments with reducing agents, such as sodium dithionite, in conjunction with complexing agents such as citrate, have had limited success in producing better quality NMR spectra[70]. While the treatments do reduce Fe^{3+} to Fe^{2+} in solution, paramagnetic iron resists reduction in soils[75], possibly owing to its inaccessibility. This makes this iron removal method strongly dependent on the form of iron, whether it is in mineral or complexed ionic form, and hence varies with the soil type. Such a chemical treatment could effectively reduce and remove free iron in ionic form; ferrimagnetic iron would remain relatively undisturbed using this method. The ditionite/citrate method for iron reduction and removal generally uses very large amounts of citrate salts, which may be difficult to remove from treated soil and/or extracts.

A popular method for de-ashing soil and soil extracts uses hydrofluoric acid (HF) as a reagent. HF treatments have been used to help concentrate the organic fraction of soil, but have also been shown to significantly improve NMR spectra of soil and its fractions[70,76]. HF can dissolve many mineral compounds and likely has a greater accessibility for iron in oxides and other minerals. Because of this, HF treatments generally remove ferrimagnetic iron better than reductive treatments with sodium dithionite followed by citrate complexation[70,76]. A possible drawback of using HF on soils is the other chemistry that may occur, particularly the potential hydrolysis of

carbohydrates. The effects of chemical treatments on the quality of NMR spectra and spin counting of the Uncompahgre whole soil and its extracts will be reviewed in the following chapters.

1.2 Experimental

1.2.1 Soil Collection and Separation

1.2.1.1 Site Selection

A site was chosen for soil collection based on its characteristically high organic matter content and low iron content. In addition, this site was chosen for the type, concentration, and variety of organic functionalities in its organic matter. A site with all these qualitative characteristics was located in southern Colorado in the Uncompahgre National Forest (based on the suggestions of Dr. E. F. Kelly of CSU's Soil and Crop Sciences Department). Soil was collected from the upper 8" horizon about the base of an Aspen stand. Approximately 10 lbs. of soil was collected and placed into plastic buckets, where the soil was stored under ambient conditions. The separation of this soil is shown diagrammatically in Figure 1.3 and explained in detail in the following sub-sections.

1.2.1.2 Removal of Leaf-Litter

The leaf-litter, stones, and partly decomposed litter were removed from the bulk soil by physical separation. This was accomplished by first sifting the soil with a 1/4" mesh galvanized wire screen. A second pass through a smaller mesh (24 holes/inch)

aluminum screen further removed partly decomposed organic matter and stones. The remaining fine-particulate soil was stored at –20 °C in sealed containers until it was to be chemically separated.

1.2.1.3 Base Extraction Uncompahgre Forest Soil

The soil was separated using the classic procedure outlined by M. Schnitzer[77]. An amount of the physically separated Uncompahgre National Forest soil was collected in a crystallizing dish and dried at 50 °C until a constant weight of 140.43 g was obtained. To this was added 1.4 L of HPLC grade distilled water followed by stirring with a magnetic stir bar/plate combination. The pH of the whole slurry was measured at 5.1, utilizing a calibrated Aldrich pH meter. To this was added 5.69 g of fresh NaOH pellets to make a 0.1 M NaOH solution. The slurry was quantitatively transferred to a large Erlenmeyer flask under flowing argon. This was stirred overnight with a large magnetic stir bar and stir plate combination. The pH of the soil slurry/base mixture was measured at 11.8 the following day.

1.2.1.4 Humin Isolation

The base treated soil was filtered through coarse filter paper using a large filter-flask, Büchner funnel and water aspirator. The collected solids were mixed with 400 ml of HPLC grade water and centrifuged at 6000 rpm for 20 minutes to separate out any remaining soil solution. This procedure was repeated two more times. The consolidated 1.2 L of soil washings was added to the deep-brown soil extract from the first filtration step. The remaining solids (now to be referred to as the humin fraction) were

qualitatively transferred to a crystallizing dish and dried under ambient conditions. The humin fraction was further dried at 50 °C until a constant weight of 122.77 g was obtained. This weight includes the clay and fine particulate that remained in the filter paper from the first filtration step.

1.2.1.5 Humic Acid

The soil extract was acidified using 1 M HCl until the pH measured 2.0, as measured by the calibrated pH meter. The acidified soil extract was stirred for 10 minutes and then allowed to sit undisturbed and sealed for 30 hours. At the end of the 30 hour period, the pH was again measured and found to be 2.1. The humic acid was separated from the fulvic acid solution by centrifugation at 8000 rpm for 30 minutes, followed by decanting the supernatant (fulvic acid solution) into a large 20 L round bottom flask. The humic acid fraction was quantitatively collected into a 2 L round bottom flask and dried to a dark powder using rotary evaporation at 45 °C under reduced pressure of 15 Torr, using a water aspirator, until a constant weight of 12.52 g was reached.

1.2.1.6 Fulvic Acid

The remaining fulvic acid solution was rotary-evaporated at 45 °C and 15 Torr until a volume of 710 ml was reached. This concentrated fulvic acid solution was divided into several parts for further analysis and separation. The pH of this solution was 2.2. To 350 ml of the concentrated fulvic acid solution was added 5.0 g of 20-50 mesh Biorad AG 50W-8X proton-form cation exchange resin beads. This was occasionally stirred

over a 5 hour period. The pH was measured at 1.5 after the first hour of stirring and found to be 1.5 after 5 hours of occasional stirring. The supernatant solution was decanted from the resin beads and collected. To the supernatant was added three washings of the resin beads with 50 ml HPLC grade water. The fulvic acid solution was rotary evaporated to near dryness at 40 °C and 15 Torr pressure. The remaining slurry was dried under flowing dry nitrogen at room temperature until 7.93 g of dry ion-exchanged fulvic acid remained. The resin beads were dried and weighed 3.01 g. A second collection of fresh resin beads (5.0 g) was dried under room conditions and weighed 2.944 g after drying, for comparison to the weight loss of the ion-exchange resin used in the fulvic acid treatment. The remaining fulvic acid solution was dried by rotary evaporation at 40 °C and 15 Torr until a thick solution of about 100 ml was obtained. This was further dried under flowing dry N_2 until a constant dry weight of 9.84 g of solid fulvic acid was reached.

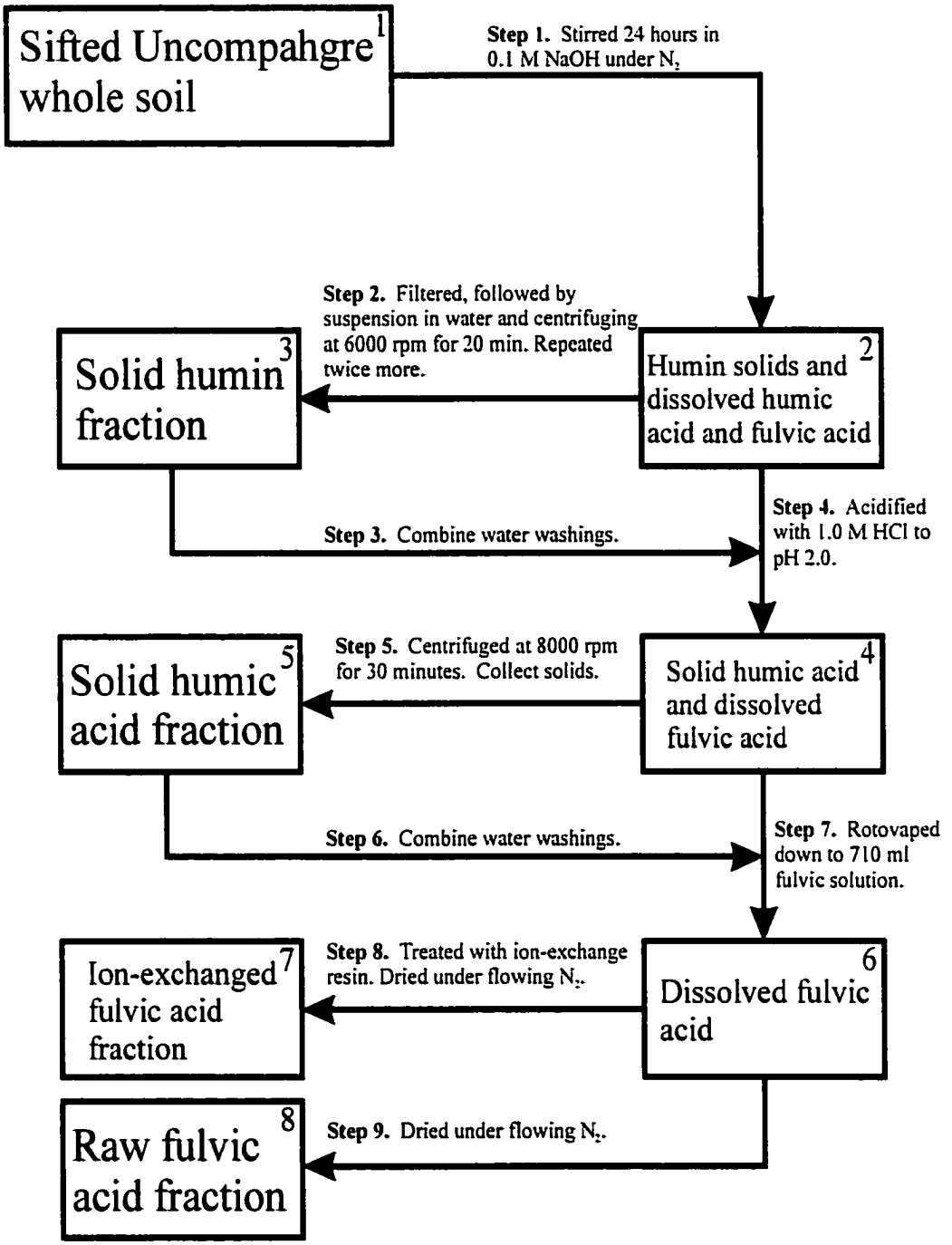

Figure 1.3 The soil separation scheme used for Uncompahgre whole soil. Products of the separation procedure are depicted in boxes. Steps are written with the step numbers in bold text.

1.2.2 Spin-Counting Standard and Calibration

1.2.2.1 DP-MAS

The silicone rubber used in the DP-MAS spin-counting experiments was from a tube of Dow Corning 732 multi-purpose sealant (pure silicone rubber). The silicone rubber sealant (Figure 1.4(b)) was spread onto a piece of glass and allowed to cure under room conditions for more than two months. The silicone rubber was then carefully peeled from the glass and cut into small blocks (1 to 2 mm edge). The external reference tube was prepared by cutting 3 mm NMR (liquids) tubes to approximately 2.92 cm and packed with a weighed amount (typically 70-90 mg) of silicone rubber pieces. The silicon rubber was tightly packed at to the bottom of the cut 3 mm NMR tube, sealed with a torch and placed in the center of the spinner with Kel-F mounts (as shown in Figure 1.5(e)) and a hole drilled in the rotor cap. The silicone rubber spin counting reference was empirically calibrated against a series of organic compounds as outlined in Chapter 2 of this thesis.

1.2.2.2 CP-MAS

A previously prepared and purified [3.2.1] bicyclo-4-pyrrolidino-N-methyl-octan-8-one triflate compound, ^{13}C labeled at the carbonyl position, was used as the external reference for CP-MAS experiments[66]. The structure of the ^{13}C labeled [3.2.1] bicyclo-4-pyrrolidino-N-methyl-octan-8-one triflate is shown in Figure 1.4(a). This external reference was packed into a melting point capillary tube (roughly 1.8 mm outer diameter

and 3.0 cm in length) and placed in the center of the spinner with Kel-F mounts (as shown in Figure 1.6(e)) and a hole drilled in the rotor cap. The capillary tube was used to hold between 3 and 20 mg of reference material, which was calibrated against a series of organic compounds as outlined in Chapter 3 of this thesis.

(a)

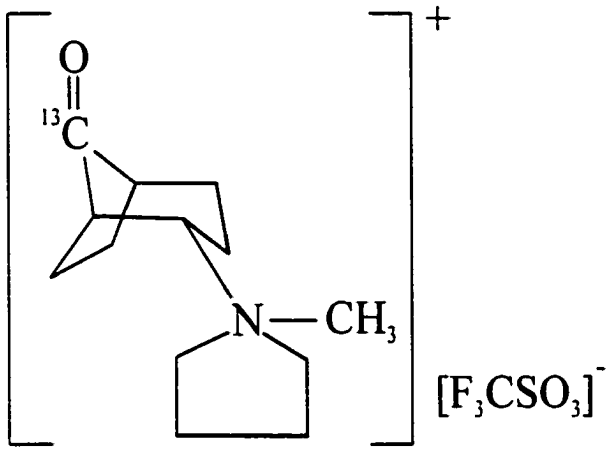

(b)

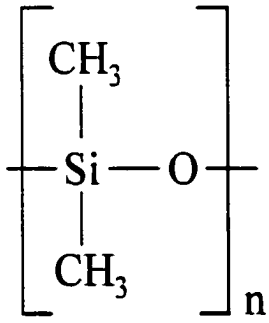

Figure 1.4 The chemical structure of the (a) ^{13}C-labeled CP-MAS spin reference compound [3.2.1] bicyclo-4-pyrrolidino-N-methyl-octan-8-one triflate and (b) the idealized chemical structure for the DP-MAS spin-reference compound, silicone rubber.

1.2.3 MAS Set-up

Magic-angle spinning (MAS) at 4.4 to 4.6 kHz was achieved with a home-built version of a Chemagnetics-style large volume MAS stator. This design used torlon air bearings and brass stators normally employed in the commercially available Chemagnetics large-volume MAS system. The remainder of the stator was made from Kel-F plastic rod to minimize CP-MAS background signals, while providing good structural properties. Spinning speed was monitored though the use of optical detection of opposing light/dark areas on the outside of the MAS sample rotor. An exploded detailed view of the MAS rotor assembly is shown in Figure 1.5(a)-(d) (DP-MAS assembly) and Figure 1.6(a)-(d) (CP-MAS assembly). This rotor assembly typically held between 1.3 and 2.2 g of soil or soil extract.

Commercially available Chemagnetics-style thick-wall 14 mm pencil rotors were modified to accommodate both the soil sample and the silicone rubber sealed external reference. A thin disk of Kel-F was machined to fit in the base of the zirconia sleeve (Figures 1.5(c), 1.6(c). At the center of this disk a hole was drilled to accommodate the tip of the glass tube containing the reference material. A hole was drilled in the center of the underside of the Kel-F drive tip (Figure 1.5(a), 1.6(a)) to accommodate the opposite end of the sealed spin-reference containing tube.

Spinning speeds of 4.4 to 4.6 KHz were achieved with roughly 50 psi drive air and 12 psi bearing air. A high capacity air line (10-15 scfm at room temperature and 70 psi) was needed to provide the necessary air flow to the drive portion of the MAS system. In addition, two high capacity commercial air-drying systems (Wilkerson model WRA 0015) were employed to drop the dew point of the air to roughly –70 °C.

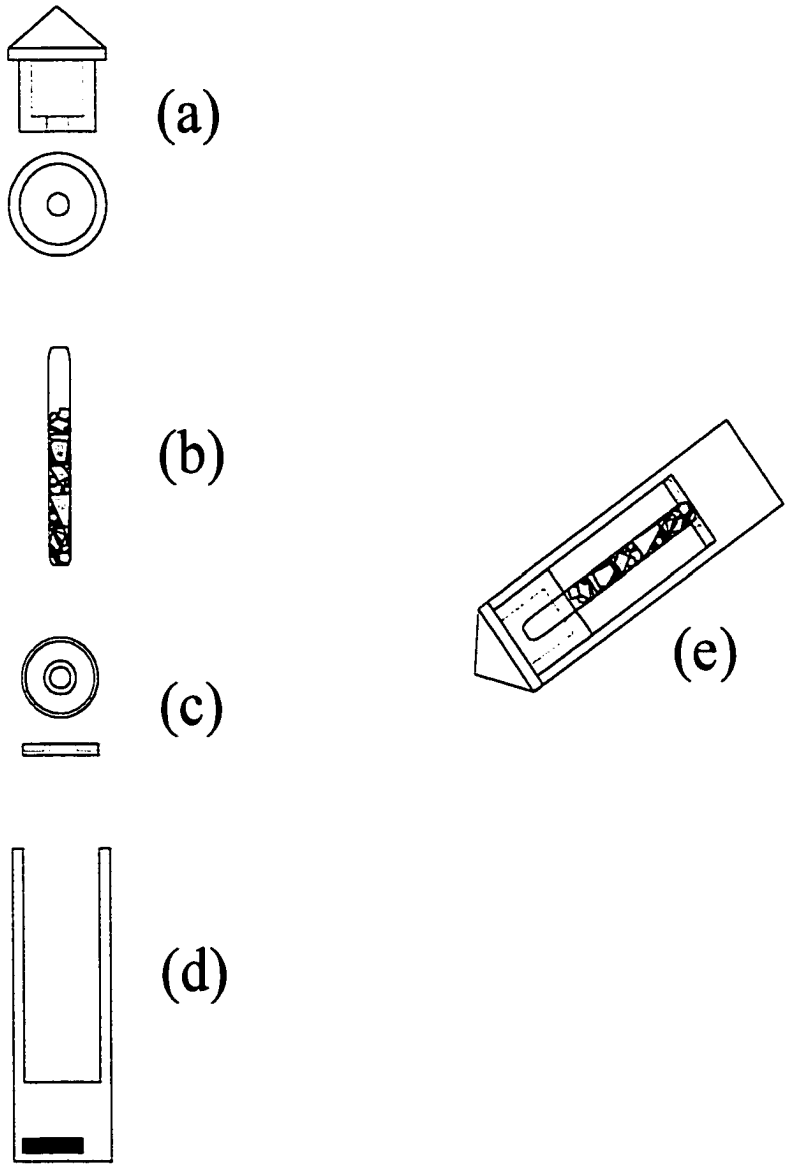

Figure 1.5 An exploded view of a modified Chemagnetics-style large volume spinning system with sealed insert containing silicone rubber for spin counting. Diagram of a (a) Kel-F rotor cap drilled to accommodate 3 mm sealed insert; (b) sealed insert made from 3 mm glass NMR tube with silicone rubber reference; (c) lower stabilizing Kel-F insert; (d) ceramic rotor body; and (e) assembled view. Diagram is to scale.

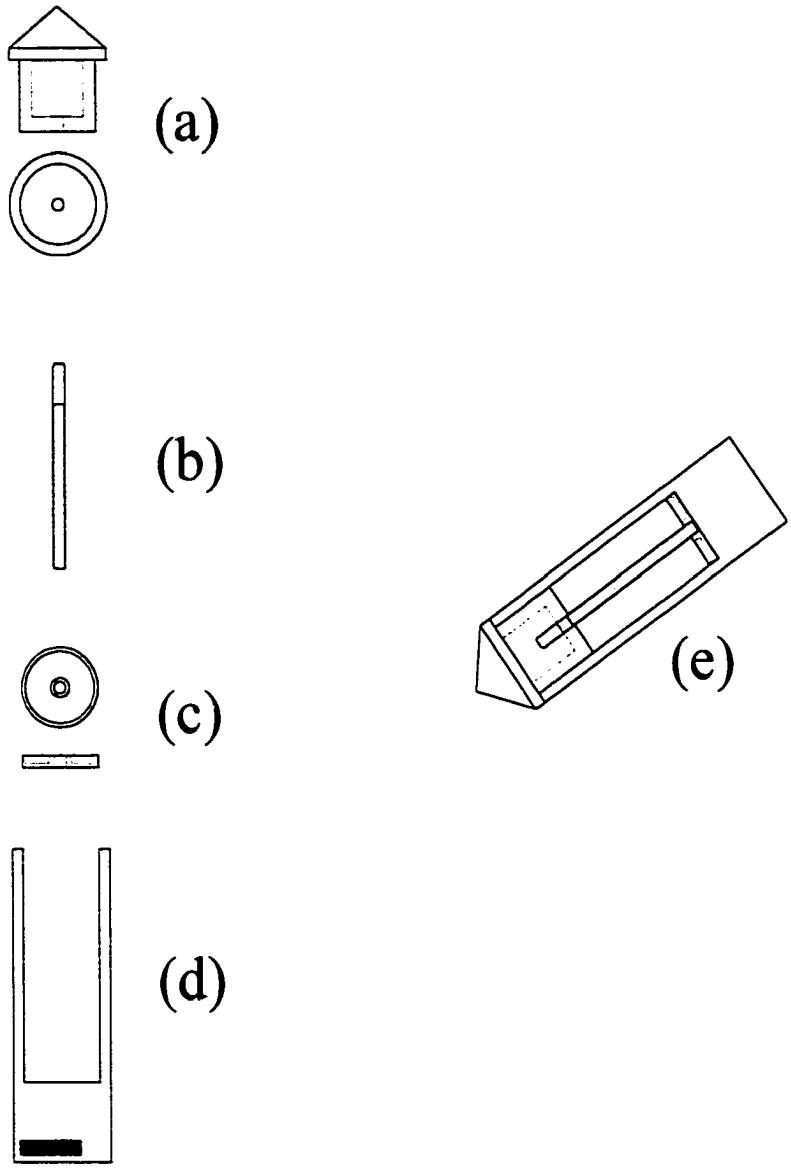

Figure 1.6 An exploded view of a modified Chemagnetics-style large volume spinning system with sealed insert containing [3.2.1] spin reference compound for spin counting by CP-MAS. Diagram of a (a) Kel-F rotor cap drilled to accommodate capillary tube sealed insert; (b) sealed insert made from 1.8 mm OD capillary tube with [3.2.1] spin reference compound; (c) lower stabilizing Kel-F insert; (d) ceramic rotor body; and (e) assembled view. Diagram is to scale.

Flexible hose and connectors with inner diameter of 1/4" to 3/8" were needed to maintain a high airflow to the MAS system and stable spinning speeds.

1.2.4 The NMR Console and NMR Experiments

All DP- and CP-MAS experiments on soil materials were carried out on a wide-bore superconducting magnet at a ^{13}C resonant frequency of 25.27 MHz and a ^{1}H resonance frequency of 100.49 MHz. The two-channel, home-built console was upgraded with a Chemagnetics Phoenix data station, pulse-programmer and receiver. Home-built power amplifiers routinely capable of 300 watts were employed for all experiments. A probe with an eight-turn double-tuned coil for ^{1}H and ^{13}C was constructed for the large volume MAS system described earlier. In each experiment, RF-field strengths in both channels were 50 kHz or greater. All data acquisitions, data processing and peak deconvolutions were performed on a Sun Microsystems Sparc 5, running Spinsight Version 3.5.2.

Background signals were obtained by simply re-running each experiment without the corresponding sample loaded (but with the spin-counting reference in place) in the spinner under the exact same conditions as for the spin-counting experiments. Background signals were deconvoluted using the Spinsight software to create a noise-free version of the background signal. The noise-free background signal was digitally subtracted from the original soil spectrum to create a background, ^{13}C-signal-free spectrum. Background corrections were not necessary for every experiment, because some MAS/experimental configurations generated no significant background signal.

1.2.5 Chemical Treatments

1.2.5.1 Dithonite Reduction

Reduction of the Fe^{3+} in ball-milled humic acid extracted from the Uncompahgre National Forest soil was attempted by stirring the extract in a sodium dithionite solution at pH 5.0. A typical treatment used 250 milligrams of sodium dithionite (roughly a four-times molar excess to the iron content of the humic acid) in 10 milliliters of distilled water for 2.0 grams of the humic acid, stirred in an Erlenmeyer flask. Following the overnight treatment, the excess water was removed using a lyophilizer and the sample kept under N_2 gas to prevent any re-oxidation of Fe^{2+} to Fe^{3+}.

1.2.5.2 Hydrofluoric Acid De-Ashing

Soil and soil extracts were slurried with 2 percent HF solutions and stirred. Samples were centrifuged in sealed polyethylene containers between HF treatments. A typical HF treatment was as follows: 4 g of soil was mixed with five aliquots (80 ml each) of HF solution, stirred for three hours and centrifuged, mixed with two aliquots, stirred for 24 hours and centrifuged, and finally mixed with one 80 ml aliquot and allowed to stir for 48 hours. The supernatant solution was collected after each centrifugation step and the final de-ashed soil was rinsed three times with distilled water and dried at 60 °C.

1.2.5.3 Ion Exchange

A cation exchange resin with a strong affinity for Fe^{3+} ions, supported on 1 mm diameter glass beads, was used to selectively collect Fe^{3+} from soil and soil extracts. Bio-rad AG 50W-X8 resin in the hydrogen form was stirred with the ball-milled soil component for several hours and removed using a mesh screen. The post-treatment ion exchange beads were then rinsed with water and the supernatant was combined with the treated soil fraction. The soil fraction was then dried either with a lyophilizer or under vacuum (1 Torr) at room temperature.

1.2.6 Elemental Analysis

Elemental analyses for total carbon and iron were provided by Huffman Laboratories in Golden, CO. All samples submitted for analysis were finely ground to sub-50 μm diameter particles in a ball mill. Huffman Laboratories established the total carbon content by combustion under flowing oxygen at 1000 °C, followed by the coulometric detection of CO_2 on a custom built analyzer. Total iron was determined by digestion in a mixture of nitric, hydrochloric and perchloric acid, followed by quantification by ICP. Ash contents were determined by the Water, Soil, and Plant Testing Laboratory at Colorado State University by burning at 550 °C in a furnace, followed by the gravimetric determination of ash.

References

1. Orlov, D. S. Soil Chemistry Russian Translation Series 92 A. A. Balkema Publishers. Brookfield, VT 1992; pp 1-28.

2. Tan, K. H. Principals of Soil Chemistry, 3rd Ed., M. Dekker, New York, 1998.

3. Kononova, M. M. Soil Organic Matter, 2nd Ed., Pergamon Press, Oxford, 1966; pp 13-45.

4. Tan, K. H. The Release of Silicon, Aluminum, and Potassium During Decomposition of Soil Minerals by Humic Acid. *Soil Sci.* **1980**, *129*, 5-12.

5. Orlov, D. S. Soil Chemistry Russian Translation Series 92 A. A. Balkema Publishers. Brookfield, VT 1992; Chaper 12.

6. Metson, A. J.; Blakemore, L. C.; Rhoades, D. A. Methods for the determination of soil organic carbon: a review, and application to New Zealand soils. *New Zealand J. Sci.* **1979**, *22*, 205-28.

7. Tabatabai, M. A. Soil Organic Matter Testing: An Overview. In *Soil Organic Matter: Analysis and Interpretation.* SSSA Special Publication no. 46; Soil Science Society of America: Madison, WI, 1996, 1-9.

8. Charles, J. M.; Simmons, S. Methods for the determination of carbon in soils and sediments. A review. *Analyst* **1986**, *111*, 385-390.

9. Schnitzer, M.; Kahn, S. U. Characterization of humic substances by chemical methods. In *Humic Substances in the Environment*; McLaren, D. A., Ed.; Marcel Dekker, Inc., New York, 1972; pp 29-54

10. Beyer, L.; Schulten, H.-R.; Frund, R. Properties and composition of soil organic matter in forest and arable soils of Schleswig-Holstein: 1. Comparison of morphology and results of wet chemistry, CPMAS ^{13}C-NMR spectroscopy and pyrolysis-field ionization mass spectrometry. *Z. Pflanzenernahr. Bodenk.* **1992,** *155*, 345-354.

11. Celi, L.; Schnitzer, M.; Negre, M. Analysis of carboxyl groups in soil humic acids by a wet chemical method, fourier-transform infrared spectrophotometry, and solution-state carbon-13 nuclear magnetic resonance. A comparative study. *Soil Sci.* **1997**, *162*, 189-197.

12. Wilson, M. A.; Burt, R.; Lynn, W. C.; Klameth, L. C. Total elemental analysis digestion method evaluation on soils and clays. *Commun. Soil Sci. Plant Anal.* **1997,** *28*, 407-426.

13. Kawasaki, A.; Arai, S. Evaluation of digestion methods for multi-elemental analysis of organic wastes by inductively coupled plasma mass spectometry. *Soil Sci. Plant Nutr.* **1996,** *42*, 251-260.

14. Jimenez, R. R.; Ladha, J. K.; Automated Elemental Analysis: A rapid and reliable but expensive measurement of total carbon and nitrogen in plant and soil samples. *Commun. Soil Sci. Plant Anal.* **1993,** *24*, 1897-1924.

15. Matejovic, I. Determination of carbon, hydrogen, and nitrogen in soils by automated elemental analysis (dry combustion method). *Commun. Soil Sci. Plant Anal.* **1993,** *24*, 2213-2222.

16. Campbell, C. A.; Paul, E. A.; Rennie, D. A.; McCallum, K. J. Applicability of the carbon-dating method of analysis to soil humus studies. *Soil Sci.* **1967**, *104*, 217-227.

17. Kononova, M. M. Soil Organic Matter, 2nd Ed., Pergamon Press, Oxford, 1966; pp 101, 104.

18. Choudhry, G. Photophysical and photochemical properties of soil and aquatic humic materials. In *Residue Reviews*, Spinger-Verlag, New York, 1984; pp. 59-73.

19. Senesi, N.; Sposito, G.; Martin, J. P. Copper(II) and Iron(III) Complexation by Soil Humic Acids: An IR and ESR Study. *Sci. Tot. Environ.* **1986**, *55*, 351-362.

20. Adhikari, M.; Chakrabarti, K. K.; Chakrabarti, G. Infra-red studies on humic and fulvic acid complexes with metal salts and their sols. **1978**, *44*, 287-8.

21. Byler, D. M.; Gerasimowicz, W. V.; Susi, H.; Schnitzer, M. FT-IR spectra of soil constituents: Fulvic acid and fulvic acid complex with ferric ions. *Appl. Spectosc.* **1987**, *41*, 1428-30.

22. Ruggiero, P.; Sciacovelli, O.; Testini, C.; Interesse, F. S. Spectroscopic studies on soil organic fractions-II. IR and ^{1}H-NMR spectra of methylated and unmethylated fulvic acids. *Geochim. Cosmochim. Acta.* **1978,** *42*, 411-416.

23. Zech, W.; Hempfling, R.; Haumaier, L.; Schulten, H.-R.; Haider, K. Humification in subalpine Rendzinas: Chemical analyses, IR and ^{13}C NMR spectroscopy and pyrolysis-field ionization mass spectrometry. *Geoderma*, **1990,** *47*, 123-138.

24. Ricca, G.; Severini, F. Structural investigations of humic substances by IR-FT, ^{13}C-NMR spectroscopy and comparison with a maleic oligomer of known structure. *Geoderma* **1993,** *58*, 233-244.

25. Yang, Y-H.; Sheng, F-L.; Tao, Z-Y. Transmission FT-IR difference spectroscopic characterization of a fulvic acid from weathered coal in water. *Toxicol. Environ. Chem.* **1995**, *51*, 135-144.

26. Francioso, O.; Sanchez-cortes, S.; Tugnoli, V.; Ciavatta, C.; Gessa, C. Characterization of peat fulvic acid fractions by means of FT-IR, SERS, and ^{1}H, ^{13}C NMR spectroscopy. *Appl. Spectosc.* **1998**, *52*, 270-277.

27. Kawahigashi, M.; Fujitake, N.; Takahashi, T. Structural information obtained from spectral analysis (UV-VIS, IR, ^{1}H NMR) of particle size fractions in two humic acids. *Soil Sci. Plant Nutr.* **1996**, *42*, 355-360.

28. Frund, R.; Ludemann, H.-D.; Gonzalez-Vila, F. J.; Almendros, G.; del Rio, J. C.; Martin, F. Structural differences between humic fractions from different soil types as determined by FT-IR and ^{13}C-NMR studies. *Sci. Tot. Environ.* **1989**, *81/82*, 187-194.

29. Gessa, C.; Cabras, M. A.; Micera, G.; Polemio, M.; Testini, C. Spectroscopic characterization of extracts from humic and fulvic fractions: IR and ^{1}H NMR spectra. *Plant Soil* **1983**, *75*, 169-177.

30. Lobartini, J. C.; Tan, K. H. Differences in humic acid characteristics as determined by carbon-13 nuclear magnetic resonance, scanning electron microscopy, and infrared analysis. *Soil Sci. Soc. Am. J.* **1988**, *52*, 125-130.

31. Dereppe, J.-M.; Moreaux, C.; Debyser, Y. Investigation of marine and terrestrial humic substances by ^{1}H and ^{13}C, nuclear magnetic resonance and infrared spectroscopy. *Org. Geochem.* **1980**, *2*, 117-124.

32. Yonebayashi, K.; Hattori, T. Chemical and biological studies on environmental humic acids II. ^{1}H-NMR and IR spectra of humic acids. *Soil Sci. Plant Nutr.* **1989**, *35*, 383-392.

33. Wershaw, R. L.; Leenheer, J. A.; Kennedy, K. R.; Noyes, T. I. Use of 13C NMR and FTIR for elucidation of degradation pathways during natural litter decomposition and composting. I. Early stage leaf degradation. *Soil Sci.* **1996**, *161*, 667-679.

34. Zech, W.; Johansson, M.-B.; Haumaier, L.; Malcom, R. L. CPMAS ^{13}C NMR and IR spectra of spruce and pine litter and of the Klason lignin fraction at different stages of decomposition. *Z. Pflanzenernahr. Bodenk.* **1987**, *150*, 262-265.

35. Hempfling, R.; Ziegler, F.; Zech, W.; Schulten, H.-R. Litter decomposition and humification in acidic forest soils studied by chemical degradation, IR and NMR spectroscopy and pyrolysis field ionization mass spectrometry. *Z. Pflanzenernahr. Bodenk.* **1987**, *150*, 179-186.

36. Inbar, Y.; Chen, Y.; Hadar, Y. Solid-state carbon-13 nuclear magnetic resonance and infrared spectroscopy of composted organic matter. *Soil Sci. Soc. Am. J.* **1989**, *53*, 1695-1701.

37. Piccolo, A. Advanced infrared techniques (FT-IR, DRIFT, and ATR) applied to organic and inorganic soil materials. In transactions of the 15th World Congress of Soil Science, Acapulco, Mexico July 10-16, 1994; International Society of Soil Science and The Mexican Society of Soil Science: Mexico, 1994; Volume 3a, 3-22.

38. Piccolo, A.; Conte, P. Advances in Nuclear Magnetic Resonance and Infrared Spectroscopies of Soil Organic Particles. In Structure and Surface Reactions of Soil Particles, P. M. Huang, N. Senesi, J. Buffle, Eds.; John Wiley and Sons Ltd.: New York, 1998; pp 183-250.

39. D. E. Axelson "Solid State Nuclear Magnetic Resonance of Fossil Fuels: An Experimental Approach." Multiscience Publications, Montreal, Can, 1985.

40. Magnetic Resonance of Carbonaceous Solids, R. E. Botto, Y. Sanada, eds., Advances in Chemistry Series 229, American Chemical Society, Washington, DC, 1993, pp. 175-419.

41. NMR of Humic Substances and Coal: Techniques, Problems, and Solutions. Wershaw, R. L.; M. A. Mikita; eds., Lewis Publishers, Inc., Chelsea, MI, 1987, p 236.

42. Maciel, G. E.; Erbatur, O. NMR Characterization of Solid Fossil Fuels. Coal and Oil Shale, in *Nuclear Magnetic Resonance in Modern Technology*, Maciel, G. E., ed., NATO ASI Series, Kluwer, Dordrecht, Netherlands, 1994, pp. 165-224.

43. Stejskal, E. O.; Memory, J. D. High Resolution NMR in the Solid State, Oxford Press, New York, 1994, pp. 3-60.

44. Fukushima, E.; Roeder, S. B. W. Experimental Pulse NMR: A Nuts and Bolts Approach, Addison-Wesley Publishing Co., Inc., London, 1981, Chapters 1, 2.

45. Andrew, E. R. Magic angle spinning in solid state NMR spectroscopy. *Philos. Trans. R. Soc. London, Ser. A* **1981**, *299*, 505-20.

46. Kessemeier, H.; Norberg, R. E. Pulsed nuclear magnetic resonance in solids. *Phys. Rev.* **1967**, *155*, 321-337.

47. Stejskal, E. O.; Memory, J. D. High Resolution NMR in the Solid State, Oxford Press, New York, 1994, Chapters 3,4.

48. Pines, A.; Gibby, M. G.; Waugh, J. A. Proton-enhanced nuclear induction spectroscopy. Method for high-resolution NMR of dilute spins in solids. *J. Chem. Phys.* **1972**, *56*, 1776-7.

49. Pines, A.; Gibby, M. G.; Waugh, J. A Proton-enhance NMR of dilute spins in solids. *J. Chem. Phys.* **1973**, *59*, 569-90.

50. Andrew, E. R.; Bradbury, A.; Eades, R. G. Nuclear magnetic resonance spectra from a crystal rotated at high speed. *Nature* **1958**, *182*, 1659.

51. Jokic, A.; Srejic, R.; Pfendt, P. A.; Zakrzewska, J. Characterization of lake sediment humic acids from the Celije lake system near Krusevac (central Serbia) by ^{13}C and ^{1}H solution NMR and ^{13}C CPMAS NMR. *Water, Air Soil Pollut.* **1995**, *84*, 159-173.

52. Skjemstad, J. O.; Frost, R. L.; Barron, P. J. Structural units in humic acids from South-eastern Queensland soils as determined by ^{13}C NMR spectroscopy. *Aust. J. Soil Res.* **1983**, *21*, 539-547.

53. Watanabe, A.; Tsutsuki, K.; Kuwatsuka, S.; Kuwatsuka, K. ^{13}C-NMR investigation of humic acid and fulvic acids obtained from some typical japanese soils. *Sci. Tot. Environ.* **1989**, *81-82*, 195-200.

54. Ogner, G. The ^{13}C nuclear magnetic resonance spectrum of a methylated humic acid. *Soil Biol. Biochem.* **1979**, *11*, 105-108.

55. Preston, C. M.; Ripmeester, J. A. Application of solution and solid-state ^{13}C NMR to four organic soils, their humic acids, fulvic acids, humins and hydrolysis residues. *Can. J. Spectrosc.* **1982**, *27*, 99-105.

56. Gonzalez-vila, F. J.; Ludemann, H.-D.; Martin, F. ^{13}C-NMR Strucural features of soil humic acids and their methylated, hydrolyzed and extracted derivatives. *Geoderma* **1983**, *31*, 3-15.

57. Schnitzer, M.; Preston, C. M. Effects of acid hydrolysis on the ^{13}C NMR spectra of humic substances. *Plant Soil* **1983**, *75*, 201-211.

58. Preston, C. M.; Schnitzer, M. Effects of chemical modifications and extractants on the carbon-13 NMR spectra of humic materials. *Soil Sci. Soc. Am. J.* **1984**, *48*, 305-311.

59. Thorn, K. A.; Steelink, C.; Wershaw, R. L. Methylation patterns of aquatic humic substances determined by ^{13}C NMR spectroscopy. *Org. Geochem.* **1987**, *11*, 123-137.

60. Bendall, M. B.; Pegg, D. T. Complete accurate editing of decoupled 13C spectra using DEPT and a Quaternary-oly sequence, *J. Magn. Reson.* **1983**, *53*, 272-296.

61. Shin, H. S.; Moon, H. An "Average" structure proposed for soil fulvic acid aided by DEPT/QUAT 13C NMR pulse techniques. *J. Soil Sci.* **1996**, *161*, 250-256.

62. Frund, R.; Ludemann, H.-D. The quantitative analysis of solution- and CPMAS-C-13 NMR spectra of humic material. *Sci. Tot. Environ.* **1989**, *81/82*, 157-168.

63. Conte, P.; Piccolo, A.; van Lagen, B.; Buurman, P.; de Jager, P. A. Quantitative differences in evaluating soil humic substances by liquid- and solid-state ^{13}C-NMR spectroscopy. *Geoderma* **1997**, *80*, 339-352.

64. Piccolo, A.; Conte, P. Advances in Nuclear Magnetic Resonance and Infrared Spectroscopies of Soil Organic Particles. In Structure and Surface Reactions of Soil Particles, P. M. Huang, N. Senesi, J. Buffle, Eds.; John Wiley and Sons Ltd.: New York, 1998; pp 197-201.

65. Mao, J-D.; Hu, W-G.; Schmidt-Rohr, K.; Davies, G.; Ghabbour, E. A.; Xing, B. Quantitative characterization of humic substances by solid-state Carbon-13 nuclear magnetic resonance. *Soil Sci. Soc. Am. J.* **2000**, *64*, 873-884.

66. Hall, R. A.; Jurkiewicz, A.; Maciel, G. E. A Bicyclic Ketone as a Solid-State ^{13}C NMR Intensity Reference. *Anal. Chem.* **1993**, *65*, 534-538.

67. Jurkiewicz, A.; Maciel, G. E. Spin Dynamics and Spin Counting in the ^{13}C CP-MAS Analysis of Argonne Premium Coals. *Fuel* **1994**, *73*, 828-835.

68. Zhang, M.; Maciel, G. E. Large-sample ^{13}C MAS n.m.r. spectroscopy of coal: relaxation and spin counting. *Fuel* **1990**, *69*, 557-563.

69. Pan, V. H.; Maciel, G. E. The analysis of three representative premium coals by ^{13}C nuclear magnetic resonance. *Fuel* **1993**, *72*, 451-468.

70. Skjemstad, J. O.; Clarke, P.; Taylor, J. A.; Oades, J. M; Newman, R. H. The Removal of Magnetic Materials from Surface Soils. A Solid State ^{13}C CP/MAS n.m.r. Study. *Aust. J. Soil Res.* **1994**, *32*, 1215-1229.

71. Pfeffer, P. E.; Gerasimowicz, W. V.; Piotrowski, E. G. Effect of paramagnetic iron on quantitation in carbon-13 cross polarization magic angle spinning nuclear magnetic resonance spectrometry of heterogeneous environmental matrices. *Anal. Chem.* **1984**, *56*, 734-741.

72. Dunlop, D. J. Rock magnetism : fundamentals and frontiers. Cambridge University Press: New York, 1997.

73. Vassallo, A. M.; Wilson, M. A.; Collin, P. J.; Oades, J. M.; Waters, A. G.; Malcolm, R. L. Structural analysis of geochemical samples by solid-state nuclear magnetic resonance spectometry. Role of paramagnetic material. *Anal. Chem.* **1987**, *59*, 558-562.

74. Arshad, M. A.; Ripmeester, J. A.; Schnitzer, M. Attempts to improve solid state ^{13}C NMR spectra of whole mineral soils. *Can. J. Soil Sci.* **1988,** *68*, 593-602.

75. Senesi, N.; Griffith, S. M.; Schnitzer, M. Binding of Fe^{3+} by humic materials. *Geochim. Cosmochim. Acta* **1977**, *41*, 969-976.

76. Preston, C. M.; Schnitzer, M.; Ripmeester, J. A. A Spectroscopic and Chemical Investigation on the De-ashing of a Humin. *Soil Soc. Am. J.* **1989**, *53*, 1442-1447.

77. Schnitzer, M. Organic Matter Characterization. *In Methods of soil analysis, part 2. Chemical and microbiological properties*, second edition; Page, A. L., Ed.; Agronomy series number 9 (part 2); American Society of Agronomy and Soil Science Society of America: Madison, WI, 1982; pp. 581-594.

Chapter 2

SOLID STATE ^{13}C NMR STUDIES OF UNCOMPAHGRE FOREST SOIL AND ITS SEPARATED SOIL COMPONENTS BY ^{13}C DP-MAS SPIN-COUNTING METHODS

2.1 Introduction to Spin-Counting by ^{13}C DP-MAS NMR

The characteristically long T_1 relaxation times (some in excess of 10 s) of ^{13}C found in solid soil samples makes direct polarization experiments less appealing for most purposes than cross-polarization experiments due to sensitivity constraints. With the exception of a few cases, all solid-state ^{13}C NMR spectra of soil samples reported in the literature were acquired with the significantly more sensitive ^{1}H-to-^{13}C CP-MAS technique (the pulse schematic for ^{13}C CP-MAS is shown in Figure 1.1(b)). The baseline distortions that can plague ^{13}C DP-MAS experiments on soils also make the CP-MAS approach more attractive. Acoustic ringing and pulse breakthrough[1], along with other phenomenon which distort the amplitude of the first few points of the acquired signal (FID), can cause severe baseline distortions in the typically broad ^{13}C NMR spectra of soil components. It is the implementation of spin-temperature alternation[2] in the ^{13}C CP-MAS experiment which essentially separates the phase dependence of the signal from that of the distortion, making it possible to employ phase-cycling to significantly reduce

the aforementioned distortions[1]. The ^{13}C DP-MAS experiment does not employ an equivalent to spin-temperature alternation and hence often yields ^{13}C NMR spectra with undesirable baseline distortions.

It is the inherent simplicity of ^{13}C DP-MAS experiments that make them attractive for use in spin-counting or quantitative NMR experiments. An extensive literature search yielded no studies on the absolute quantitative analysis of soil/soil components by DP-MAS NMR methods, probably owing to the aforementioned difficulties. One of our goals was to explore the possibility of using a large-volume sample spinner with ^{13}C DP-MAS to quantify the amount of carbon in the Uncompahgre Forest soil and its extracts.

Experimental ^{13}C DP-MAS and ^{13}C solution-state NMR experiments have been shown to produce similar spectra[3]. The RF pulse sequence of the solution-state inverse-gated decoupling ^{13}C solution state experiment and DP-MAS experiment, shown in Figure 1.1(a), are practically identical; the DP-MAS experiment utilizes magic angle spinning to average CSA's to zero and requires stronger ^{1}H decoupling than that typically employed in solution-state experiments. Solution-state analysis of these samples were not utilized for quantitative analysis owing to the insolubility of soil and soil extracts in most solvents. The results from an absolute quantitative ^{13}C DP-MAS analysis of the Uncompahgre whole soil and its soil components are presented in this chapter. Tables and figures for this chapter are collected at the end of the chapter for clarity.

2.2 Results

2.2.1 Gravimetric and Elemental Analysis of the Uncompahgre National Forest Soil Components

The elemental carbon and iron analysis for the whole soil, the hydrofluoric acid treated whole soil (HF-treated soil) and each soil extract, along with ash contents, are reported in Table 2.1. The data in Table 2.1 represents the same soil, soil treatments, and extraction procedure used throughout this thesis. The HF-treatment was not part of the extraction and should be considered separate from the gravimetric analysis of the separation procedure. The whole soil (140.43 grams) is 16.07 percent carbon by elemental analysis, corresponding to a total of 22.57 grams of carbon. The humin fraction, humic acid, and both fulvic acid fractions each contain 14.56, 5.50, and 3.35 grams of carbon, respectively, for a total of 23.41 grams of carbon detected by elemental analysis in the extracts and humin fraction. Analogous data for the iron in each sample is given in Table 2.1. When not elaborated in the text of this thesis, the fulvic acid fraction is the ion-exchanged fulvic acid, upon which the majority of ^{13}C DP-MAS experiments were run.

2.2.2 Calibration of the External Reference

A silicone rubber reference was empirically calibrated against a series of pure carbon-containing compounds of known structure with favorable ^{13}C DP-MAS NMR properties. With the results of the calibration, the T_1-corrected area (A_{corr}^{DP}) of the silicone rubber peak at 0 ppm of the ^{13}C DP-MAS spin-counting spectrum can be assigned a

number that corresponds to an absolute amount of natural-abundance carbon. Once the relationship between peak area and amount of carbon is established, the peak areas from the soil or soil component can be related to this empirically determined absolute amount of carbon.

The calibration value associated with the silicone rubber external reference is somewhat dependent on the particular coil and spinner configuration. The DP-MAS ^{13}C spectrum of the HF-treated soil was run under a different coil and spinner configuration than the other spin-counting spectra. Calibration trials were run under both hardware configurations; this difference is reflected in the number of milligrams of carbon associated with the external reference in the HF-treated soil versus the other samples, as shown in Tables 2.3-2.7.

The calibration experiments on the silicone rubber are summarized in Table 2.2. The correction terms (C_{T_1}) for each pure organic compound are based on Eqs. 2.2-2.3 and ^{13}C T_1 values determined on these compounds (also in Table 2.2) and are presented along with the pulse delay (t_d) used for each calibration experiment in Table 2.2. The calculated number of milligrams of carbon is reported for the 79.5 milligram silicone rubber external reference for each calibration compound (as a function of the peak position for the compound). The average of these calibration values was used to determine the percent carbon and milligrams of carbon in each deconvoluted peak by ^{13}C DP-MAS spin-counting for the HF-treated soil; the results are summarized in Table 2.4. A second capillary, containing 85.9 mg of silicone rubber, was not directly calibrated against each compound; rather it was assigned a value based on its weight relative to the 79.5 mg silicone rubber containing capillary. The whole soil, humin fraction, humic acid,

and fulvic acid DP-MAS spin-counting spectra were run using a different spinner/coil assembly than used for the HF-treated soil (a rotor crash destroyed the original assembly). For that particular coil/spinner assembly, the 79.5 mg silicone rubber external reference capillary showed a 10.4 percent greater value in the calibration with hexamethylbenzene relative to the calibration trial with the original spinner/coil assembly. This value was incorporated into the calculations for DP-MAS spin-counting and is shown in Tables 2.3, 2.5-2.7.

2.2.3 ^{13}C T_1 Relaxation Times for the Uncompahgre Forest Soil Components

The ^{13}C T_1 relaxation times were determined for the soil and each soil component using a Torchia style pulse program[4], as shown in Figure 2.1. The spectra from the ^{13}C T_1 experiments are shown in Figure 2.2(a) (whole soil), 2.3(a) (HF-treated soil), 2.4(a) (humin fraction), 2.5(a) (humic acid), and 2.6(a) (fulvic acid). Each ^{13}C spectrum of the ^{13}C T_1 experiments was deconvoluted into individual peaks as shown in Figures A2-2 (whole soil), A2-3 (HF-treated soil), A2-4 (humin fraction), A2-5 (humic acid), and A2-6 (fulvic acid) of the appendix section in this thesis. Each experimental spectrum plotted in Figures 2.2(a)-2.6(a) is again shown in Figures A2-2-A2-6 of the appendix, along with the "synthetic" spectrum, the individual deconvoluted peaks used to generate the "synthetic" spectrum, and the difference spectrum. The difference spectrum was generated by subtracting the synthetic spectrum from the experimental spectrum and gives an indication as to how successful a particular deconvolution is. The peak areas of the deconvoluted peaks of Figures A2-2-A2-6 were then used to obtain ^{13}C T_1 relaxation times, as shown in the plots of Figures 2.2(b)-2.6(b), and tabulated in Tables 2.3-2.7.

The peak areas of each deconvoluted peak are shown plotted versus the τ delay period for the Torchia style experiment in Figures 2.2(b) (whole soil), 2.3(b) (HF-treated soil), 2.4(b) (humin fraction), 2.5(b) (humic acid), and 2.6(b) (fulvic acid). Each plot was created to illustrate the ^{13}C relaxation behavior for a particular peak, with the chemical shift of that particular peak written within the plot diagram. These plots were fitted with either single or double component exponential factors using the SigmaPlot 5.0 program. A solid line represents the calculated fit and solid black circles represent the experimental data points in each plot.

2.2.4 Spin Counting of the Uncompahgre Forest Soil Components by ^{13}C DP-MAS NMR

Figure 2.7 shows each DP-MAS spin counting spectrum on a relative intensity scale for each of the soil components. The spectra of Figure 2.7 and that of the HF-treated soil are shown deconvoluted (with (a) the experimental, (b) "synthetic", (c) deconvoluted, and (d) difference spectrum) in Figures 2.8 (whole soil), 2.9 (HF-treated soil), 2.10 (humin fraction), 2.11 (humic acid), and 2.12 (fulvic acid). The ^{13}C T_1 relaxation times for all the deconvoluted peaks of each of the spin-counting spectra and of the silicone rubber were derived from the results in Figures 2.2(b)-2.6(b) and are summarized in table format in Tables 2.3-2.7, along with the T_1 "corrected" peak areas (A_{corr}^{DP}) for each peak represented in Figures 2.8-2.12. The corresponding amount of carbon for each peak, reported in mg of carbon out of the total sample weight and as a percentage of the total detected carbon by DP-MAS spin counting are reported in the columns marked "mg of carbon" and "percent of total" respectively, in Tables 2.3-2.7.

To the right of the cells marked "Total (not including reference at 0 ppm)" in Tables 2.3-2.7 is the sum of the corresponding peak integrals in columns titled A_{exp}^{DP} and A_{corr}^{DP}, not including the peak integral from the external reference. These values represent the total integral of the corresponding ^{13}C DP-MAS spin-counting spectrum and that of the T_1 corrected spectrum, respectively. The cell to the right of this A_{corr}^{DP} cell gives the total number of milligrams of carbon detected in this experiment. The error associated with each total integral was determined from the propagated error of the sum of the corresponding individual deconvoluted peaks.

To the right of the cell labeled "total percent carbon by DP-MAS spin-counting" is the calculated percent carbon in the sample based on the total T_1 corrected ^{13}C DP-MAS spin-counting integral relative to the external reference peak area. An estimated relative error for this value is reported in the same cell in parenthesis. This error estimate was generated by propagating the error associated with the deconvolution of the reference peak at 0 ppm, the error associated with the total T_1 corrected ^{13}C DP-MAS spin-counting integral, and that from the empirical calibration of the external reference (8.70 percent).

Table 2.8 summarizes the elemental, gravimetric, and DP-MAS spin counting data for each soil and soil extract. The percent carbon detected by DP-MAS spin counting is presented along with the percent carbon detected by elemental analysis. The ratio of the percent carbon detected by DP-MAS to that detected by elemental analysis is provided in the column titled "(amount of carbon detected by DP-MAS) / (amount of carbon detected by elemental)".

The spectra of Figure 2.13 are computer generated much like the synthetic spectra shown in Figures 2.8(b)-2.12(b), but have been adjusted to reflect the ^{13}C T_1 amplitude

corrected peak areas (A_{corr}^{DP}) of Tables 2.3-2.7. Each computer generated spectrum was created by applying the appropriate T_1 correction term (C_{T_1}) to each of the deconvoluted peaks for each spectrum. The humin (Fig. 2.13(b)), humic acid (Fig. 2.13(d)), and fulvic acid (Fig. 2.13(e)) spectra were added, in ratios to represent their weight contribution to the whole soil and their sample weight, to generate a synthetic whole soil spectrum (Fig. 2.13(f)). The overlaid spectrum, plotted with a dotted line, in Figure 2.13(f) is the whole soil spectrum of Figure 2.13(a). This illustrates the difference between the T_1-corrected whole soil spectrum and the synthetic whole soil spectrum generated by adding the appropriate ratios of the humin, humic acid, and fulvic acid spectra. The largest discrepancy between the synthetic whole soil spectrum and the T_1-corrected whole soil spectrum occurs in the 160-190 ppm region, where the synthetic spectrum shows significantly greater intensity.

2.2.5 Estimated Error Associated with Spin Counting by ^{13}C DP-MAS NMR

Error associated with the dependent variable in the ^{13}C T_1 plots of Figures 2.2-2.6(b) was propagated to the correction factor (C_{DP}) and presented as a relative deviation in Tables 2.3-2.7. This error was calculated from the standard error of the estimate (SEE) on each ^{13}C T_1 regression analysis, and was determined using the SigmaPlot 5.0 program. The standard error of the estimate is an example of a root mean square error estimate, and is a measure of the accuracy of a regression analysis.

The relative standard deviation (standard deviation as a percentage) associated with each deconvoluted peak area of each of the ^{13}C DP-MAS spin-counting experiments was estimated by finding the relative standard deviation for each peak of interest in 20

non-sequential deconvolutions on each of the DP-MAS spin-counting spectra shown in Figures 2.8-2.12. These values are reported in the column with heading "ERE" (Estimated Relative Error) of Tables 2.3-2.7. This estimated error reflects the large uncertainty in peak areas typically encountered when deconvoluting broad, superimposed peaks.

The total of the peak integrals ($A_{\exp}^{DP}$) before being multiplied by the correction term (C_{T_1}) is shown at the bottom of the column. The error for this total, and for that of the ^{13}C T_1 corrected peaks (A_{corr}^{DP}) total area, is propagated from the sum of the values printed in that particular column. The error associated with the number of milligrams of carbon for the reference material peak at 0 ppm is that from the relative standard deviation of the calibration trials, as presented in Table 2.2. Finally, the error associated with the total percent carbon was determined by propagating the error of the total corrected peak area, the error associated with calibrating the external reference, and the error of the corrected peak area for the external reference.

2.2.6 Iron Removal and Reductive Treatments on Soil Components

Spin-counting DP-MAS spectra obtained before-and-after the iron removal treatments on fulvic acid and whole soil are shown in Figure 2.14. The fulvic acid was treated with ion exchange resin (Figure 2.14(a)) and the whole soil with an HF solution (Figure 2.14(b)), as described in the Experimental sections 1.2.5.2-3 of Chapter 1. The spectra for each treated component are scaled relative to that of the untreated soil component using scaling factors to correct for unequal number of signal acquisitions.

Shown to the right of each set of spectra are sets of smaller, superimposed spectra, arbitrarily scaled to show spectral changes (or lack thereof) caused by the treatments.

Figure 2.15 shows two spectra of humic acids. The uppermost spectrum (Fig. 2.15(a)) is the ^{13}C DP-MAS spectrum of a humic acid after being treated in a water slurry under hydrogenation conditions (80 psi H_2 gas) for four days. The corresponding untreated humic acid spectrum is shown below the spectrum of the H_2-treated humic. Spectrum (c) represents the difference between spectrum (a) and (b). Both spectra were acquired under conditions (16 s repetition delay) so as to yield quantitative spectra that do not require corrections based on the ^{13}C relaxation times of the samples. There are no significant differences between the spectra of the H_2-treated and untreated samples.

2.3 Discussion

2.3.1 ^{13}C DP-MAS Spin-counting Calculations

To provide quantitative results in which peak areas can be directly correlated directly to a specific number of spins (relative to that of an external standard), the direct polarization (DP) spin-counting experiments must be either a) run with a sufficiently long repetition delay (t_d) for all (99.9%) the magnetization to return to its equilibrium state ($t_d \geq 5T_1$) before the next data acquisition, or b) be "corrected" to account for the situation in which when $t_d < 5T_1$. To obtain the corrected peak area (A_{corr}^{DP}) when $t_d < 5T_1$, the experimental peak area is simply multiplied by a T_1 correction factor (C_{T_1}) as shown in equation 2.1.

$$A_{corr}^{DP} = (A_{exp}^{DP})(C_{T_1}) \qquad (2.1)$$

where

$$C_{T_1} = \frac{1}{\left(1 - e^{-t_d / T_1}\right)} \qquad (2.2)$$

Equation 2.2 is used for situations where a single exponential factor can describe the relaxation behavior of the peak of interest. Equation 2.3 is used to correct peak areas in situations where the relaxation behavior can be described satisfactorily only if two exponential factors are used. In Equation 2.3, β is the fraction of the relaxation component represented by $T_{1(1)}$ and $(1-\beta)$ is the contribution from the second relaxation component, represented by $T_{1(2)}$.

$$C_{T_1} = \frac{1}{\beta\left(1 - e^{-t_d / T_{1(1)}}\right) + (1-\beta)\left(1 - e^{-t_d / T_{1(2)}}\right)} \qquad (2.3)$$

T_1 "corrected" peak areas (A_{corr}^{DP}) are then proportionally related to the T_1 "corrected" peak area of the silicone reference (in the DP-MAS spin counting spectra), which has been calibrated against a series of ^{13}C NMR solid standards. The individual peaks of the deconvoluted spectrum can then reported in absolute quantities of carbon.

2.3.2 ^{13}C T_1 Relaxation and Organic Structure in the Uncompahgre Forest Soil Components

Many of the ^{13}C T_1 plots of Figures 2.2(b)-2.6(b) show (quite dramatically) data that are described by multiple exponential decay functions. Most of the ^{13}C T_1 relaxation data of these soil components are best described by two component exponential functions; no single soil component demonstrates this behavior more dramatically than the whole soil peaks at 172, 150, 130, 104, 84 and 72 ppm (Figure 2.2(b)). This may indicate a two-domain system, one giving a very short ^{13}C T_1 relaxation time (such as

would be expected from a domain containing paramagnetic centers) and the other much longer. Upon close visual inspection with the naked eye, the whole soil (before ball-mill grinding) appears to be composed of a relatively undecomposed domain, comprised of leaf litter with dimensions on the order of a millimeter (able to pass through the fine mesh screen used in the soil collection process), and domain of no visually recognizable origin. Presumably, the undecomposed organic material would have longer ^{13}C T_1's as the cellulose and lignin of these materials are more likely to be free of paramagnetic centers and are likely to be more crystalline.

The ^{13}C NMR spin-lattice relaxation times of peaks in the chemical shift range of 0 to 40 ppm show the least change when being compared between the different soil components. These peaks, typically assigned to paraffinic components and lipids, generally show two-component ^{13}C T_1 behavior, with a fairly dramatic difference between the two relaxation times. The peaks centered at 172, 150, 130, 104, 84 and 72 ppm show much greater differences in ^{13}C T_1 behavior between the different soil fractions. The HF-treated soil and remaining soil fractions show two-component ^{13}C T_1 behavior for these peaks, with the faster component being significantly slower than the fast T_1 component of the whole soil. These trends indicate that the aqueous chemical treatments on the whole soil somehow affect the carbon that displays faster ^{13}C T_1 relaxation behavior and may re-organize the paramagnetic and/or ferrimagnetic iron domains in these samples. The wax-like organic domain, being hydrophobic, may be somewhat insulated from the effects of the aqueous treatments and hence, show the least change in ^{13}C T_1 behavior from the extractions.

The fulvic acid shows two-component ^{13}C T_1 behavior similar to that of the whole soil, but with slow ^{13}C T_1 components being significantly faster than most ^{13}C T_1's found in the other soil fractions. The fulvic acid has the lowest concentration of iron compared to the other soil components, but due to a low carbon content, has an atomic carbon-to-iron ratio (C/Fe) similar to that of the humic acid. Paramagnetic centers can play a key role in spin-lattice relaxation[5] and, due to the concentration of paramagnetic iron impurities in the fulvic acid, is likely involved in the ^{13}C relaxation behavior of the fulvic acid. Fulvic acid samples tend to have the lowest molecular weight distribution of the separated components[6]. The smaller molecular weights and, hence, smaller molecular size(s) may be related to an increase in molecular mobility (i.e., a shortened correlation time of the molecular motions) and increase the spectral density at the Larmor precession frequency for ^{13}C (25 MHz). An increase in the spectral density at the Larmor precession frequency for ^{13}C will act to lower ^{13}C spin-lattice relaxation times[5].

The ^{13}C spin-lattice relaxation times for cellulose, having ^{13}C NMR chemical shifts occurring in the range of 60 to 80 ppm, and at 104 ppm, are sensitive to cellulose's local molecular order[7-9]. Crystalline cellulose typically shows much longer ^{13}C T_1 behavior than non-crystalline cellulose. Studies involving the use of ball-mills to alter the crystallinity of cellulose samples have shown that dramatic changes occur in the ^{13}C MAS NMR peak widths of such samples upon physical pulverization[9,10]. The ^{13}C T_1 data on the whole soil were taken following pulverization with a ball-mill grinder. This grinding preparation likely altered the natural structure of the cellulose in these samples and may have altered the ^{13}C T_1's from that which would have been measured on the un-ground soil.

Some of the ^{13}C T_1 data presented in Figures 2.2(b)-2.6(b) are incomplete due to poorly resolved peaks and/or insufficient intensity from the CP-based Torchia-style ^{13}C T_1 measurements. In cases where a particular peak was deconvoluted in the ^{13}C DP-MAS spin-counting spectrum but, for the aforementioned reasons, no ^{13}C T_1 value could be determined confidently for it from the corresponding Torchia-style experiment, the ^{13}C T_1 value from the same peak of another spectrum was used in its place. The peak at 197 ppm in the humin fraction was very poorly resolved from the peak at 172 ppm; the ^{13}C T_1 from the peak at 197 ppm of the whole soil was used in its place. The fulvic acid peaks at 56, 115, and 197 ppm were not adequately resolved in the Torchia-type ^{13}C T_1 experiments; these values were estimated/approximated by the corresponding values determined for humic acid.

2.3.3 Quantitative Carbon Elemental Analysis of the Uncompahgre Forest Soil Components

The total carbon contents by elemental analysis reported in Table 2.1 are semiquantitatively consistent, to within 4 percent of the gravimetric soil separation data in the sense that the total number of grams of carbon in the whole soil (22.51 grams) is 3.8 percent lower than the total carbon content of the humin (14.56 grams), humic (5.50 grams) and fulvic (3.34 grams) fractions combined. The furnace/coulometric method for total carbon content is generally accurate within two percent of the total carbon content for whole soil/soil components[11-14]. The soil and soil extracts may not hold the same amount of moisture under the mild drying conditions used during the storage of these materials. Both of these factors could account for the minor discrepancy (4 percent) in

the gravimetric/percent elemental carbon data. It was found that the most consistent elemental data were obtained when the samples were sent for analysis after being pulverized to an extremely fine powder in a ball mill grinder. Samples ground to a coarse powder with a regular ceramic mortar and pestle were found to give less consistent elemental results. The total iron content of 140.43 grams of whole soil was 1.47 grams, which is in close agreement to the total iron content of the humic, humin, and fulvic fractions put together (1.46 grams).

2.3.4 Inconsistencies Between Carbon Elemental Analysis and Spin-Counting

The results summarized in Table 2.8 show major inconsistencies between the total percent carbon detected by DP-MAS spin counting (versus elemental analysis) and soil fraction. We were able to account for 68.7, 71.3, 71.7, 85.9 and 59.1 percent of the carbon by DP-MAS spin counting compared to the carbon elemental analysis for fulvic acid, humic acid, humin, HF-treated soil, and whole soil, respectively. If one compares these results with the iron contents shown in Table 2.1, there does not appear to be a predictable relationship between iron content and the percent carbon detected by ^{13}C DP-MAS. However this does not necessarily exclude iron from the possible causes of our inability to quantitatively spin-count carbon in soil and soil components by NMR. The HF-treated soil, however, has the lowest percent iron and gave the most satisfactory results regarding the quantitative analysis by DP-MAS spin counting. It is possible that ferrimagnetic forms of iron are proportionally much more damaging to our ability to quantitatively spin-count ^{13}C by NMR than paramagnetic forms of iron. The iron contents reported in Table 2.1 provide no indication as to which form of iron is predominate in a

particular soil fraction. Elemental analysis on these soil fractions show very low concentrations of copper and manganese, indicating that iron is likely the dominant element responsible for complications (in this particular NMR study of soil components) due to paramagnetic materials.

2.3.5. Iron Removal and ^{13}C DP-MAS Signal Loss

2.3.5.1 Ion-exchanged Fulvic Acid

Upon inspection, the spectra of Figure 2.14(a) would lead one to believe that the ion-exchange treatment improves the percent carbon observed by DP-MAS spin counting for fulvic acid, but not nearly enough to account for the 31.3 percent discrepancy. In fact, while the quality of the spectrum, in terms of overall signal-to-noise and resolution, did improve, the percent carbon observed by DP-MAS spin counting actually slightly decreased. The total integrals of the spectra in Figure 2.14(a) (normalized and acquired in a quantitative manner), when corrected for sample weight are 1.00 and 1.07 for untreated and ion-exchanged fulvic acid, respectively. These total normalized integrals are not proportional to the percent carbon determined by elemental analysis (16.41 and 21.84 percent carbon for untreated and treated fulvic acid, respectively), and in fact suggest that less of the carbon in the ion-exchanged fulvic acid is detected by NMR. This combination of spectral and elemental analysis data correspond to a *decrease* in percent carbon observed by NMR of roughly 18 percent upon ion exchange treatment.

This reduction in the percent carbon observed upon ion-exhange treatement of the fulvic acid could be due in part to the fact that broadened spectra are much more difficult

to quantify accurately in terms of their signal areas. The small, overlaid spectra above and to the right in Figure 2.14(a) show the two spectra on an arbitrary scale in order to demonstrate spectral differences; the pre-treated fulvic acid appears to have signal distortions in the form of trailing peaks near higher frequency (higher ppm). The data in Table 2.1 suggest that the ion-exchange treatment effectively removed a portion of the iron from the fulvic acid; the spectra of Figure 2.14(a) suggest that removing iron in fulvic acid did little more than slightly improve the resolution of the spectrum. The fulvic acid, since it was in solution during the last stage of the separation procedure, likely contains iron in its predominately paramagnetic (Fe (III)) form, either hydrated or complexed with the organic fraction. The ion-exchange resin displays a greater selectivity to Fe^{3+} than to Na^{+} or H^{+} and successfully removed about 33 percent of the Fe^{3+} from the fulvic acid. Gravimetric analysis of the resin beads before and after being used in the fulvic acid treatment suggests that the resin beads retained very little organic material (roughly 4 percent of the raw fulvic acid).

2.3.5.2 Hydrofluoric Acid Treated Soil

The hydrofluoric acid treatments of the whole soil show a more dramatic change in the before and after DP-MAS spectra than did those of the ion-exchanged fulvic acid. The whole soil sample lost 46 percent of its weight from the HF treatments, which suggests that the percent carbon in the post-treated sample would be approximately 29.9 percent carbon *or less* ([4.0 g of whole soil x 16.07 percent carbon in the whole soil]/2.15 g of post-treated soil), if no carbon were lost due to the treatments. Elemental analysis of the HF-treated material showed 29.88 percent carbon. This indicates that the HF-

treatment washed away very little of the organics, an encouraging result from the aspect of our ability to employ treatments that do not alter the organic content. The overall changes in the spectrum are very subtle (as shown by the overlaid spectra in Figure 2.14(b)), suggesting that the HF-treatment was responsible for very few chemical changes, if any, to the organic portion of the soil. The most dramatic compositional change for this sample was the change in percent iron, which was reduced to less than 25 percent of that of the untreated soil. This treatment produced a sample that responded more favorably to spin counting by ^{13}C DP-MAS NMR, with 85.7 percent of the carbon accounted for (see Table 2.4), compared to the results of elemental analysis.

2.3.6 Carbohydrate and Lignin Content of the Uncompahgre Forest Soil Components

Carbohydrates in the form of cellulose, hemi-cellulose and complex sugars in soils and soil extracts typically show strong resonances around 72 and 104 ppm, with smaller peaks at about 62 and 82 ppm. The structural unit for cellulose is shown in Figure 2.16(a). Carbons at position 2, 3, and 5 of sugars typically have ^{13}C NMR chemical shifts in the range of 65-75 ppm; the higher frequency shoulder of the major peak at 72 ppm is primarily due to C-4 carbons. The peaks centered at 104 and 62 ppm are most often due to anomeric (C-1) and C-6 carbons of carbohydrates. In soils, the peak at 72 ppm is often very broad and encompasses all the peaks from 82 to 62 ppm. The ^{13}C chemical shifts associated with cellulose and complex sugars of soil samples in ^{13}C MAS spectra are not typically resolved, making the distinction of different classes of carbohydrates by solid state NMR difficult at best and beyond the scope of this study.

The peak centered at 104 ppm has contributions from both the anomeric carbon of carbohydrates and unsubstituted aromatic carbons C-2 and C-6 of syringyl lignin structures. Based on that ^{13}C chemical shift assignment, it would be incorrect to simply use the sum of the peak areas at 104 and 72 ppm to determine the carbohydrate contribution to the soil component spectrum. The percent contribution of carbon from carbohydrates is calculated by assuming that the peak at 72 ppm would contribute 83.3 percent (or 5 out of every 6 carbons in the carbohydrate structure which contribute to the ^{13}C NMR peak at 72 ppm) of carbon in such structures. This would indicate that 38.1, 15.8, 24.8, 19.8, and 24.9 percent of the carbon in fulvic acid, humic acid, humin, HF-treated soil, and whole soil, respectively, is due to carbohydrates. The extraction procedure used 140.43 g of whole soil, which is 16.07 percent carbon by elemental analysis, of which 24.9 percent is carbohydrate based, which corresponds to 5.62 grams of carbohydrates. Similar analysis on the humin (122.77 grams), humic acid (12.52 grams) and fulvic acid fractions (7.93 grams for ion-exchanged and 9.84 grams for un-treated) show that they contain 3.61, 0.868, 1.27 grams of sugar-like materials, respectively. More of the carbohydrate material that is extracted winds up concentrated in the fulvic acid fraction, as indicated by the significantly higher carbohydrate content in fulvic acid.

These carbohydrate contents are presumably subject to the same error found in our ability to spin-count all the carbon in these samples by ^{13}C DP-MAS NMR. Nevertheless, the sum of the estimated weights of carbohydrate carbon in the humin, humic, and fulvic acid fractions (5.75 grams) is roughly equal to that in the 140.43 grams of whole soil (5.61 grams). A greater percentage of the carbon in the HF-treated soil is

NMR "visible," which suggests that the lower percent carbon in sugar structures in the HF-treated soil more likely represents the true content of sugar structures in the Uncompahgre whole soil. In addition, there was no evidence, based on carbon elemental analysis and the corresponding gravimetric analysis that any significant amount of carbon was washed out during the treatment.

The aromatic carbon in soil fractions can be estimated from the peak intensities at 150, 130, 115, and 104 ppm, assuming lignin to be the primary source of aromatic carbon in the soil component. The peak intensity at 104 ppm is due to both the unsubstituted aromatic carbons of structures similar to syringyl lignin units and the anomeric carbon of carbohydrates. The contribution to this peak area from the sugar-like structures can be subtracted out on the basis of sugar-like structural content of the soil (as estimated above), leaving a peak area that better represents the aromatic carbon content. The sum of these peak areas and that of the aromatic portion of the peak area at 104 ppm then gives 38.8, 35.7, 37.0, 41.3, and 27.7 percent of the carbon in aromatic rings for the whole soil, HF-treated soil, humin, humic, and fulvic acid, respectively. For 140.43 grams of whole soil, which is 16.07 percent carbon, this corresponds to 8.76 grams of carbon in six-member aromatic rings. Similar calculations for the humin (122.77 grams), humic acid (12.52 grams), and fulvic acid (7.93 grams for ion-exchanged and 9.84 grams for untreated) yield 5.39, 2.27, and 0.925 grams of aromatic carbon. These estimates are presumably subject to the same error found in our ability to spin-count all the carbon in these samples by ^{13}C DP-MAS NMR; however, the sum of the weights of aromatic carbon in the humin, humic, and fulvic acid fractions (8.59 grams) estimated in the manner indicated above is roughly equal to that in the 140.43 grams of whole soil (8.76

grams). These results indicate that the lignin-like material that is extracted tends to concentrate in the humic acid fraction. There is more aromatic carbon in the whole soil, HF-treated soil, humin, and humic acid than carbohydrate carbon. The fulvic acid displays the opposite pattern, with more carbohydrate carbon than aromatic carbon. Overall, the whole soil has significantly more aromatic carbon than carbohydrate carbon.

The two main types of lignin, syringyl and guaiacyl-based, can be distinguished based on the ratios of the methoxy peak areas and that of the aromatic region. A ratio of 6:1 for aromatic carbon to methoxy carbon would suggest a guaiacyl-based lignin, and a ratio of 6:2 would suggest a syringyl-based lignin. Estimates of the lignin composition based on this method are made assuming that *all* the methoxy functionality is lignin based, and is subject to the rather large estimated relative errors noted in Tables 2.3-2.7. The whole soil shows a ratio of aromatic carbons to methoxy carbons of 6.00 to 1.00. The HF-treated soil shows a ratio of 6.00 to 1.29. Similarly, the humin, humic acid, and fulvic acid fractions show ratios of 6.00:0.910, 6.00:1.05, and 6.00:1.08, respectively. These ratios indicate that the bulk of the lignin is guaiacyl-based. The forest from which this soil was collected was mainly comprised of soft wood trees, such as spruce and aspen trees. Soft wood lignin typically contains higher amounts of guaiacyl building units, which is consistent with our findings here.

2.3.7 The Empirical Relationship Method for Organic Content Determination in Soil Components

2.3.7.1 Introduction to the Empirical Relationship Method

A second NMR-based method for estimating the percent carbon, oxygen, and hydrogen in a solid organic sample is an empirical one found in the recent literature. The empirical relationship method has been used to obtain estimates of the carbon, oxygen, and hydrogen contents from *relatively* quantitative ^{13}C MAS NMR data when *absolute* quantitative (spin-counting) data on the soil component are not available. Although we question the value of this approach on fundamental scientific/philosophical grounds, this method was included in this study for completeness. One should note that apparent agreement between the results obtained by this method and by classical elemental analysis does not mean that one has quantitatively accounted for all the organic carbon in the sample; it simply implies (at best) that one has a self-consistent structural model of the organic matter in terms of structure and elemental composition.

The empirical relationship method is based on the corrected peak areas (A_{corr}^{DP}) of Tables 2.3-2.7 and the chemical assignment for each peak. Each individual deconvoluted peak illustrated in Figures 2.8-2.12 corresponds to a particular functional group or a set of functional groups. Based on carefully chosen functional group assignments, "elemental numbers" can be associated with each peak. These "elemental numbers" reflect the atomic ratios of carbon, hydrogen, and oxygen in that particular functionality assignment. The elemental numbers are normalized to make carbon contribute one elemental number to the numbers describing a particular organic functional group. The elemental number assignments for each peak of each soil fraction are elaborated in the following sections. The combination of the corrected peak areas with the elemental compositions for each peak makes it possible to generate an elemental ratio of carbon to oxygen to hydrogen for the entire organic content of the soil. From this elemental ratio, the percent carbon,

oxygen, and hydrogen can be estimated for the organic soil component. Table 2.9 shows the results of applying this method to the soil and soil components. The percent carbon, hydrogen, and oxygen for each soil component is presented along with the percent carbon on an ash-free basis from elemental analysis.

The percent carbon, oxygen, and hydrogen were derived from the aforementioned elemental numbers for each peak and their relative percentages of the "T_1 corrected" total peak area for the ^{13}C DP-MAS spin-counting spectrum of each soil component. Equations 2.4-2.6 (below) show the mathematical relationships used to generate the percent carbon, hydrogen, and oxygen for each of the soil components from the aforementioned *relative* quantitative peak information.

$$\%C = \frac{1200}{16\sum_i n_i^O p_i + 1200 + \sum_i n_i^H p_i} \tag{2.4}$$

$$\%H = \frac{\sum_i n_i^H p_i}{16\sum_i n_i^O p_i + 1200 + \sum_i n_i^H p_i} \tag{2.5}$$

$$\%O = \frac{16\sum_i n_i^O p_i}{16\sum_i n_i^O p_i + 1200 + \sum_i n_i^H p_i} \tag{2.6}$$

In these equations, n_i^X represents the elemental number for element X for a peak at position i and p_i represents the percentage contribution of peak i to the total signal area. The number 1200 occurring in each of the denominators represents the sum of carbon p_i values (100) multiplied by the atomic weight of carbon.

2.3.7.2 C, H, O Elemental Relationships in Soil Component Organic Functionality

The assumed elemental relationship for each peak is elaborated in the following paragraphs. Except in cases for which the spectral editing results in Chapter 4 indicate that different C, H, O elemental relationships should be employed for particular peaks. elemental relationships provided in the literature were used for the calculations by this method. The elemental relationships derived by Malcolm[15], and Mao et al.[16,17] were shown in their work to yield percent carbon contents (on an ash-free basis) in good agreement with elemental analysis results for a range of humic materials.

Peaks in the ^{13}C NMR chemical shift range of 190 ppm to 200 ppm in soil samples are likely due to carbonyl groups in ketones. Aldehydes will also show intensity in this region; however, there was no C(O)-H intensity detected by spectral-editing experiments for this peak in humic acid (see Chapter 4 of this thesis). We extend this assignment to the remaining soil-derived samples. With this functional group assignment, we assign an "elemental number" of one to carbon and oxygen, but none to hydrogen ($C_1O_1H_0$). Peaks in the chemical shift range from 160 to 190 ppm are typically assigned to carboxylic acid, carbonyls in ester groups, and the carboxylate anion functionality. Because the spectral editing results for humic acid in Chapter 4 of this thesis do not differentiate the spectral contribution from these three different functional groups, the elemental composition values from the recent literature are used to describe these functional groups. Assuming a 75 percent contribution from –COOH and 25 percent from R-O-C*OR' (ester), this peak would have the elemental numbers shown in the subscripts of the empirical formula, $C_1O_{1.875}H_{0.75}$.

The peaks in the range from 140 to 160 ppm are typically assigned to carbons in the aromatic rings of syringyl and guaiacyl, as shown in Figure 2.16(b, c), that are bonded to oxygen-containing functional groups such as –OH and $-OCH_3$. Assuming that the aromatic structures in the Uncompahgre soil are primarily guaiacyl based, typical of the soft-wood trees found at the sampling site, and we assign $C_1O_1H_1$ for each phenolic functional group and $C_1O_{0.5}$ for each methoxy-bound aromatic carbon (the oxygen is shared in this case and therefore contributes 0.5 to the elemental number), then our elemental numbers are $C_1O_{0.75}H_{0.5}$, using the ratios of methoxy to phenolic groups on guaiacyl structures. Assuming the peaks in the ^{13}C chemical shift range from 120 to 140 ppm are represented by C_1 due to quaternary carbons (from C-1 of guaiacyl groups), the elemental representation becomes $C_1O_0H_0$. The peaks in the chemical shift range from 110 to 120 ppm are generally assigned to unsubstituted carbons of aromatic rings, such as C-2, C-5, C-6 of guaiacyl structures[18,19], and are assigned elemental numbers $C_1O_0H_1$. The peak centered at 105 ppm has typically been assigned to the unsubstituted carbons of syringyl structures and to the anomeric carbon of cellulose[20-22]. From the data in section 2.3.6, we estimate a 25 percent contribution from aromatic structures of syringyl units ($C_1O_0H_1$) and the remaining due to C-1 of cellulose ($C_1O_1H_1$); the elemental relationship becomes $C_1O_{0.75}H_1$. The peaks in the range from 60 to 95 ppm are assigned to C-2,3,4,5,6 carbons of cellulose-type structures. Based on the cellulose structure, shown in Figure 2.16(a), we assign an elemental ratio of $C_1O_{0.66}H_{1.5}$.

The peak centered at 56 ppm is typically associated with methoxy functional groups and is assigned an elemental ratio of $C_1O_{0.5}H_3$. Finally, for the peaks centered at 39, 30, and 20 ppm, we assign elemental ratios of $C_1O_0H_2$, $C_1O_0H_2$, and $C_1O_0H_3$,

respectively. These correspond to aliphatic carbons, with the peak at 30 ppm being from a combination of 50 percent CH and 50 percent CH_3 functionality, the peak at 20 ppm being due to CH_3 functionality, and the peak at 39 ppm being due to CH_2 functional groups (as suggested by the spectral-editing data in Chapter 4 of this thesis).

2.3.7.3 Carbon Content of the Uncompahgre Forest Soil Components by the ^{13}C DP-MAS Based C, H, O Empirical Relationships (CHOER) Method

The second method for determining total percent carbon did predict carbon contents that are closer to the elemental carbon values obtained by classical (non-NMR) methods than those determined by DP-MAS spin counting. As mentioned above, this is not surprising, since the CHOER method is not an *a priori* approach, but merely confirms a self-consistent structural model. The values reported by this CHOER method were made under a number of assumptions, one of those being that the samples contain only C, H, O based organic material. Thus, the values reported using this method should be compared to the percent carbon on an ash-free basis. A criticism of this method of NMR data analysis for soil is that the results are very dependent on a number of rather broad assumptions regarding the ultimate structure of soil. The C, H, and O empirical relationship is established on the basis of three assumptions: 1) the contribution from other elements found in the organic structures of soil (e.g. N, P) is relatively small, 2) each peak can be assigned a known elemental relationship between C, H, and O, and 3a) all of the carbon is "NMR visible," or 3b) at least that organic carbon which is "NMR visible" is consistent with the C, H, and O elemental ratios of all of the organic carbon in the sample. From the NMR spin counting results of this project we know that assumption

3a is certainly not valid, so the most we can hope for is that assumption 3b holds. Thus, perhaps the most important assumption made when applying this method is that the "NMR invisible" ^{13}C signal (41, 14, 28, 29, and 31 percent "NMR invisible" ^{13}C signal in whole soil, HF-treated soil, humin, humic, and fulvic acid respectively) has the same C, H, O empirical relationship as the "NMR visible" ^{13}C signal, i.e., what has been already accounted for by ^{13}C DP-MAS NMR. As seen in Table 2.9, the percent carbon by elemental analysis on an ash-free basis for the fulvic acid was 7.5 percent lower than the value determined using the C, H, O DP-MAS empirical relationship method. For the whole soil, HF-treated whole soil, humin and humic acid fractions, results of classical elemental carbon analysis are within three percent of the values by the CHOER method. While the CHOER method produced values closer to the elemental analysis values for percent carbon, the number of assumptions made during the calculations make the results much more subjective (and less significant) than those from the aforementioned spin counting method. Moreover, these values are strongly dependent on the large estimated relative errors (the total error for each peak are reported in Tables 2.3-2.7) found for each deconvoluted peak and greatly affect the error associated with the percent carbon determined by the method of C, H, and O empirical relationships.

2.3.8 Estimates of Ferrimagnetic and Paramagnetic Content of Soil Components by Means of the Vibrating Sample Magnetometer Method

2.3.8.1 Ferrimagnetic and Paramagnetic Iron in Soils Components and their Relationship to Spin Counting

There have been a number of soil NMR studies in the past that have qualitatively established a link between ^{13}C NMR signal loss and iron content[23-25]. High-gradient magnetic separators have been used to help separate the strongly ferrimagnetic components from soils and dramatically improve spectral quality[25]. Many attempts at the reduction or extraction of paramagnetic iron by the means of chemical treatments, such as the sodium dithionite reduction, have also been reported[24-27]. Other chemical treatments, such as the de-ashing of soil or soil components by hydrofluoric acid, have been used to improve the quality of ^{13}C MAS NMR spectra[27,28]. All but the study by Vassallo et al.[24] have failed to establish any quantitative link between iron content in soil components and signal loss. In the research by Vassallo et al., it was found that in low-ash and low-iron fulvic acid, nearly quantitative spin-counting results by ^{13}C CP-MAS were obtained. Indeed, the form of iron in soils (e.g. ferrimagnetic or paramagnetic) has not been quantified in the aforementioned studies as there are few well-understood methods for establishing the iron type in soils.

The vibrating sample magnetometer (VSM), in conjunction with classic iron elemental analysis, can be used to aid in the identification of the iron type in soils by giving an indication of the ferrimagnetic/ferromagnetic and paramagnetic contents. The VSM can be used to measure the saturation magnetization of a sample, i.e. the magnetization of a sample at which a field-independent behavior is shown, which is directly related to the ferrimagnetic and/or ferromagnetic content of a material. While paramagnetic iron does not show a saturation magnetization at the magnetic fields and temperatures used in this study, the paramagnetic content of a material can be estimated from the magnetic susceptibility of the material. The magnetization curve resulting from

the vibrating sample magnetometer measurement on our soil shows a positive slope superimposed upon a saturation or "S-shaped" curve, as is seen in Figure 2.17(a). The ferrimagnetic/ferromagnetic impurities in the sample contribute only to the saturation or "S-shaped" part of the magnetization curve. The positive slope of the magnetization curve can be related to the magnetic susceptibility while in the presence of ferromagnetic/ferrimagnetic components. This makes the VSM method more attractive than a simple Gouy balance for investigating the form of iron in soils; the Gouy balance cannot provide an accurate susceptibility measurement if ferrimagnetic components are present.

Soil is known to contain magnetite as the most common form of ferrimagnetic material in soil. Ferrimagnetic materials display a large spontaneous magnetization resulting from the incomplete cancellation of anti-parallel magnetic moments within magnetic domains. This is different from ferromagnetism, where the magnetic moments act in parallel within the magnetic domains and display a cooperative magnetization. Elemental iron displays ferromagnetic behavior, but rarely exists in soils as it is readily oxidized. The Uncompahgre National Forest soil contains very little manganese, and therefore very little paramagnetic Mn^{2+}, and roughly one percent iron by weight. Under the assumption that the iron in our soil is either paramagnetic Fe^{3+} or ferrimagnetic magnetite, the results from the VSM were used to determine the quantities of each of these two forms of iron in our soil components. Susceptibility measurements by VSM cannot be used to quantify the iron type when large amounts of anti-ferromagnetic iron (e.g., such as that in Fe_2O_3 minerals) are present; the diamagnetic material gives a much weaker signal response which would be occluded by the dominant

paramagnetic/ferrimagnetic response of the other forms of iron. The lack of a distinguishable VSM signal response from anti-ferromagnetic forms of iron is a potential drawback of using VSM to quantify the form of iron in soil components.

2.3.8.2 Calculations for Estimating Paramagnetic and Ferrimagnetic Content

The magnetization of N paramagnets in an externally applied field H is predicted by Langevin theory to start at 0 magnetization at 0 field and saturate at extremely high magnetic fields. At moderately low external fields and at room temperature, Langevin theory predicts nearly linear behavior for the response of magnetization with changing field[29]. Under the assumption that this response is linear, the volume magnetic susceptibility (in cgs units) for N particles, each having magnetic moment M, is

$$\chi = \frac{J}{H} = \frac{NM^2}{3kT} \qquad (2.7)$$

where J is the magnetization, k is the Boltzmann constant and T is the Kelvin temperature. This relationship is also known as the Curie law of paramagnetic susceptibility. The susceptibility measured from the plots in Figure 2.17 was taken as the positive slope of the magnetization curve at 10 kOe, where the magnetization behaves nearly linearly as a function of the external field. The theoretical susceptibility of each of the soil components was also estimated using Equation 2.7 and assuming all the iron (as N paramagnets) in each sample was in the form of Fe^{3+}, with each Fe^{3+} having a magnetic moment (M) of 5.92 Bohr magnetons. The measured and calculated susceptibilities are presented in Table 2.10.

Pure magnetite has a saturation magnetization of about 480 G at room temperature[30]. The saturation magnetization is directly proportional to the amount of

ferrimagnetic/ferromagnetic material in the sample; and for magnetite particles dispersed in a medium, the saturation magnetization can be calculated from the simple volume proportion of magnetite in the sample. The saturation magnetization was measured for each of our soil-component samples from the magnetization curves (Figure 2.17) by simply determining the magnetization at 10 kOe, and subtracting out the positive-slope contribution ($J/H > 0$ and constant) from paramagnetism. The limiting saturation magnetization for the soil components was calculated assuming all the iron was in the form of magnetite. The limiting saturation magnetization and that measured from the plots in Figure 2.17 are presented in Table 2.10.

2.3.8.3 Magnetic Saturation and Susceptibilities from the Vibrating Sample Magnetometer

The results from the experimental trials on the vibrating sample magnetometer (VSM)[31] in the Department of Physics (laboratory of Dr. Carl Patton) at Colorado State University are shown in Figure 2.17. Each plot is scaled in units of magnetic moment (emu), also known as the magnetization, per gram of material to simplify direct visual comparisons between samples. Each plot has both a forward scan magnetization curve from –10 kOe to 10 kOe, and a reverse scan magnetization curve from 10 kOe back to –10 kOe. A hysteresis results when the forward and reverse magnetization curves display different behavior in response to the changing magnetic field. The hysteresis indicates that a material is retaining magnetization after being at a high external magnetic field, and is indicative of the presence of a ferromagnetic or ferrimagnetic material[32]. This retained magnetization, or "magnetized" material will display a non-zero magnetization

when the applied field is at 0 kOe. Paramagnets and diamagnets do not retain their magnetization after being at high magnetic field and hence do not display hysteresis. The whole soil and humin plots show a strong saturation magnetization with a hysteresis, while the HF-treated soil shows a smaller magnetization with hysteresis, indicating that these samples contain ferrimagnetic and/or ferromagnetic materials.

The other *J*-vs-*H* traces, for the fulvic acid and humic acid, show no hysteresis; however the humic acid did not yield reproducible results and only the forward scan is shown. The magnetization curves for fulvic acid and HF-treated whole soil are too weak to accurately measure their susceptibility, indicating that they have little paramagnetic and ferrimagnetic/ferromagnetic content. The measured saturation magnetization, along with the measured susceptibilities for selected VSM plots, are shown in Table 2.10. Table 2.10 also shows theoretical values for saturation and susceptibility, calculated under a set of assumptions regarding the state of the iron in the sample.

2.3.8.4 Quantification of Iron in Soil Components by the VSM method

The vibrating sample magnetometer results show responses that are in rough agreement with the iron contents reported in Table 2.10 for each of the samples in the sense that larger magnetic moments are reported for samples with greater concentrations of iron. We can also qualitatively recognize the samples that contain ferrimagnetic particles by recognizing a hysteresis in the VSM plots for the whole soil, humin and HF-treated soil. These results are in agreement with the qualitative observation that the whole soil contains magnetite, a ferrimagnetic ore[29], which can be lifted from the soil with a simple bar magnet. A small amount of magnetite was removed from the whole

soil with a bar magnet soon after it was collected and before the analyses in this thesis study. The humin fraction of the soil is comprised of the inorganic and base insoluble remains of the soil that remain after the base extractions; this is where magnetite would be expected to accumulate. The VSM results on humin confirm our suspicion that the bulk of the ferrimagnetic particles remain in the humin fraction following the extraction procedure.

The theoretical saturation magnetization corresponding to the percent iron shown in Table 2.10 (in the column titled "% Fe by weight"), assuming all the iron is in the form of magnetite, is reported in the far right column. These calculated values are much higher (by roughly two orders of magnitude) than the measured values, indicating that very little of the iron content in these samples is in the form of magnetite. This result is consistent with the elemental analysis of these samples, in that a soil that contained iron only in the form of magnetite would be expected to have little or no iron extracted into the humic and fulvic acid fractions. The ferrimagnetic content, in milligrams of magnetite, are given in Table 2.11. These values were determined from the measured saturation magnetization and are reported in Table 2.10.

The measured volume magnetic susceptibilities for the whole soil, humin, and humic acid are slightly smaller than the volume magnetic susceptibilities calculated on the basis that the only paramagnetic substance in each sample was in the form of isolated Fe^{3+} ions in the concentrations reported for that sample by elemental analysis. Based on the saturation magnetization measurements, the iron in the whole soil, HF-treated whole soil, and the humin is only 2.8, 0.67, and 3.2 percent magnetite, and the remaining iron is either in paramagnetic or diamagnetic forms. The near agreement between the estimated

and measured susceptibilities for the whole soil, humin, and humic acid indicate that little of the iron in these samples is in diamagnetic form. The fulvic acid and humic acid show no hysteresis in their VSM plots, which is an indication that very little or no magnetite exists in these fractions. The fulvic acid and HF-treated whole soil showed such weak responses to the magnetic field that a part of their paramagnetic response would be masked by the diamagnetic response (which would contibute a negative component to the slope of the VSM plot) of the soil component itself. The magnetic susceptibilities for the fulvic acid and HF-treated soil were not measured from the plots in Figure 2.17 due to their weak response to the magnetic field.

2.3.9 Unpaired Electrons in Humic Acid and Sodium Dithionite Treated Humic Acid

2.3.9.1 Electron Spin Resonance Analysis of a Dithionite Treated and Untreated Humic Acid

Humic acid from the bulk extraction of the Uncompahgre Forest soil was examined by EPR before and after treatment with sodium dithionite. Sodium dithionite was added to the bulk humic acid as described in section 1.2.5.1, and the post treated humic samples were sealed in 5 mm EPR tubes under nitrogen. Equal amounts of humic material were analyzed in each sample tube. The ESR spectra of the untreated bulk humic acid (Fig. 2.18(a)) and the sodium dithionite treated humic acid (Fig. 2.18(b)) are each shown with two different amplitude scaling factors to ease visual comparisons among the spectra. The treated and untreated humic acids both have a broad, asymmetric

resonance with g-value 4.35, and a much narrower resonance with g-value 2.00. The line width for the narrow peak with g-value 2.00 is approximately 5 G in both the treated and untreated humic EPR spectra, while the resonance with g-value 4.35 covers approximately 1000 G in both the dithionite treated and untreated humic spectra.

2.3.9.2 Paramagnetic Content of a Humic Acid by ESR

Absolute measurements of paramagnetic spin concentration require a rather involved analysis of many ESR factors[33], and were not attempted as part of this research study. While both the dithionite-treated and untreated samples contained the same amount of humic material and great care was taken in positioning the sample within the ESR cavity, the ESR spectra presented in Figure 2.18 are best analyzed on a qualitative level. Factors that affect quantitation in ESR, such as the unpaired electron spin-lattice relaxation time and microwave-power saturation[33], would also need to be investigated for more quantitative comparisons between spectra.

The double integral of the signal with g-value 4.35 is identical, within the noise level, between the treated and untreated humic acid samples. Signals with this g-value in humic materials are typically associated with Fe^{3+} bound to carboxylate and phenolic functionalities in humic materials, as suggested by the many IR and Mössbauer spectroscopy studies found in the literature[34-37]. In the study by Senesi et al.[37], the paramagnetic iron in humic acid was partially reduced to Fe^{2+} by hydrazine and was largely removed upon hydrolysis with 6 M HCl. While these studies showed promise in removing and/or reducing Fe^{3+} to Fe^{2+}, they did not investigate any of the chemical changes that may have occurred during the harsh treatment with concentrated HCl.

Figure 2.18 shows, by the unchanged ESR signal with g-value of 4.35 that the sodium dithionite treatment did not chemically reduce the Fe^{3+} in the humic material.

There is a marked increase in the intensity of the resonance with g-value 2.00 in the sodium dithionite treated humic acid. This increase was not accompanied by a change in the line width of the resonance. Sharp resonances with g-value near 2.00 in ESR spectra of humic substances are typically associated with, but not limited to, the free radical of semiquinone units[33,38]. Radicals of methoxybenzene and many nitrogen-associated radicals resonate with the same g-value in humic materials. With a few exceptions[39,40], the organic free-radical resonance in ESR spectra of humic materials found in the literature is typically free of any hyperfine spitting. The lack of hyperfine spitting observed in literature spectra is consistent with our findings here and unfortunately renders impossible any further description of the local chemical environment about the organic radical.

The increase in intensity of the organic free radical has been observed in ESR spectra in the literature of humic and fulvic materials treated with hydrazine[37]. This effect has been attributed to an increase in free-radical concentrations by the chemical reduction of quinone structural units to the semiquinone radical[37,38]. While this assignment is generally accepted in literature reviews as the predominant source of organic free radicals in humic materials, there is no additional evidence to support such an assignment here. The ^{13}C DP-MAS spectrum of the Uncompahgre humic acid does not provide any additional information, such as distinguishable ^{13}C NMR peaks at 187 and 137 ppm for the carbonyl carbon and protonated aromatic carbon of quinone,

respectively, to support the aforementioned assignment for the ESR peak with g-value 2.00.

The presence of Fe^{3+} in it's oxidized state and stability of the semiquinone radical in soil or soil components is strongly dependent on a number of environmental factors such as pH, soil redox potential, and temperature[33]. The competition of numerous redox reactions occurring in soil, in conjunction with the aforementioned environmental factors, may hinder the effectiveness of chemical reductions in soil components. The general resistance to chemical reduction of key species in humic acid extracts, as indicated by our own chemical treatments and those reported in the literature, may indicate that significantly stronger reducing agents than sodium dithionite are needed to reduce both Fe^{3+} and quinone structural units. It would be desirable, from the standpoint of spin counting by NMR, to reduce the total free-electron concentration by reducing Fe^{3+} while leaving the concentration of semiquinone radicals relatively low or unchanged.

Yet another factor which may lessen the effectiveness of chemical reductions in humic acid is related to the simple chemical accessibility of the component we wish to reduce. In the study by Senesi et al.[37], Fe^{3+} was found to reside in humic acid in as many as three different binding sites, with each site responding slightly differently to chemical reductions. In that study, which employed ESR and Mössbauer spectroscopy to follow the oxidation state and binding environment of Fe^{3+} in humic acid, some of the different responses of the bound Fe^{3+} to reduction were attributed to the physical accessibility of that particular binding site to chemical treatments.

2.3.10 Error Analysis of Spin Counting by ^{13}C DP-MAS NMR

Each ^{13}C DP-MAS NMR experiment on a soil or a soil component was carried out only once, making it impossible to assign a standard deviation based on results from a number of trials. For this reason, the error associated with spin-counting of soils by ^{13}C DP-MAS NMR was estimated based on repetitions of the empirical calibration of the silicone rubber external reference and repetitions of deconvolutions of the soil component spectra, and based on the error associated with the regression analysis of the ^{13}C T_1 relaxation data. We focused on these three specific aspects of spin counting, as we believe they play the greatest roles in the total error of spin counting by ^{13}C DP-MAS NMR.

In order to assess the *random* error associated with the deconvolution procedure, a relative standard deviation was assigned to the integral of each individual deconvoluted peak based on a trial of 20 deconvolutions for the spin counting DP-MAS spectrum of each soil component. Each trial was accompanied by a re-phasing of the spectrum and each deconvolution was made with peak widths and heights as variables. It was found that, while the *total* integral for the *entire* ^{13}C DP-MAS spectrum of soil components remained relatively consistent (± 1.2, 1.3, 2.3, 1.2, 1.6 percent for the whole soil, HF-treated soil, humin, humic acid, and fulvic acid, respectively), the deconvolution of each individual peak was not nearly so reproducible. This is due to the fact that most of these peaks are broad and partially overlapping. The estimated error of each individual peak area by deconvolution is shown in Tables 2.3-2.7 in the column labeled "A_{exp}^{DP} (±ERE %)". "ERE" meaning "estimated relative error". The error of the total integral (i.e., the sum of each deconvoluted peak area rather than the integral taken of the *entire* spectrum) was ± 4.4, 4.5, 5.8, 4.9, 3.8 percent for the whole soil, HF-treated soil, humin, humic acid, and

fulvic acid, respectively. This error, which is based on the propagated error of the *sum* of each deconvoluted peak, is reported in Tables 2.3-2.7, rather than the smaller error associated with the repetitive integration of the *entire* spectrum.

As seen in Tables 2.3-2.7, the deconvolution procedure for soil and soil extracts introduced the largest *random* error, based on repetitions of deconvoluion/integration of a specific spectrum. The second source of random error, originating from the regression analysis of the ^{13}C T_1 data and propagated to the T_1 correction term (C_{T_1}) shown in Tables 2.3-2.7, was significantly smaller than the error associated with deconvolutions. As expected, the larger, more isolated peaks, such as the peaks at 72 and 172 ppm, typically display a smaller relative standard deviation than those of the broad, overlapping peaks. The smaller peaks that overlap considerably with neighboring peaks, such as peaks at 197, 115, and 39 ppm, typically show much greater ERE. The ERE for each individual peak will greatly affect our ability to quantitatively assign amounts of cellulose and lignin for a particular fraction. The broad and featureless peaks centered around 150, 130, and 115 ppm prevent us from being able to quantitatively assign amounts of lignin-like materials in each fraction.

A relative standard deviation of ± 8.7 percent was found for the ^{13}C DP-MAS calibration trials of the silicone rubber with standard compounds. One can see from the deviations reported in Tables 2.3-2.7 that this was found to be the single largest source of identifiable *systematic* error for spin-counting the total carbon content of soil and/or soil components in this study. The estimated relative error from deconvolutions was the largest source of *random* error for spin-counting the total carbon content of soil and/or soil components, and the single largest identifiable source of error for the individual

deconvoluted peak areas of the soil component spectra. The error associated with the ^{13}C T_1 correction term contributed much less to the error of the spin counting of the total carbon content and to the individual deconvoluted peak errors.

2.4 Conclusions

We have demonstrated that the percent carbon observed in the Uncompahgre Forest soil and soil extracts by ^{13}C DP-MAS NMR is significantly lower than that reported by the more quantitative elemental analysis method. The large volume spinning system, used at an external field strength of 2.35 T, provides adequate sensitivity and magic-angle spinning speeds for the ^{13}C DP-MAS analysis of soil and soil components. The sensitivity provided by the large volume spinning system keeps adequate the total experimental time for ^{13}C DP-MAS spin counting on soil components by providing spectra with good signal-to-noise ratios (i.e., signal-to-noise ratios that do not significantly contribute to the large error associated with spin-counting of soil components) in a few hours. Treating the whole soil with a dilute HF solution removed the bulk of the iron from the sample and resulted in ^{13}C DP-MAS spin-counting results that nearly agreed, within the experimental uncertainty, with the more quantitative carbon elemental data for the same sample. Moreover, the HF-treatment appears to have left the carbon content of the soil undisturbed, in both chemical structure and physical carbon content. Ion-exchange treatments on fulvic acid were found to reduce the iron content, but did little to improve the DP-MAS spin-counting results. The ^{13}C DP-MAS spin-counting results were used to aid in the estimation of cellulose and lignin-like organic contents in the soil and its extracts.

The percent carbon obtained by the method of C, H, and O empirical relationships is based on much more subjective judgements regarding the ultimate structure of the organic portion of soil than the ^{13}C DP-MAS spin-counting method outlined in this chapter. This makes the percent carbon reported by the method of C, H, and O empirical relationships less appealing as a quantitative analysis method. Using this empirical relationship method, we were able to predict the total percent carbon for the soil components to within three percent of the ash-free carbon contents determined by elemental analysis, with the exception of the fulvic acid.

Magnetic measurements made on soil components with a vibrating sample magnetometer aid in the identification of the iron content in soils, and can be used to distinguish ferrimagnetic from paramagnetic iron. The whole soil, HF-treated soil, and humin were found to contain less than four percent of their iron content as ferrimagnetic constituents, while the bulk of the iron in these fractions was found to be primarily paramagnetic iron. For reasons beyond the understanding of the author, the humic acid did not yield reproducible VSM results. The ability to accurately spin-count the carbon in soil samples by DP-MAS methods improves as the iron content is reduced; however, a quantitative link between iron content and spin counting in soil components has not been firmly established. Utilizing the Curie law of paramagnetism and assuming that all of the iron detected by elemental analysis is present as isolated Fe^{3+} ions, the predicted volumetric susceptibilities of the samples were slightly higher than the measured values. These challenges notwithstanding, the VSM method may play a key role in establishing a link between ^{13}C DP-MAS spin counting and iron content.

Table 2.1 Elemental analysis and ash content summary.

Soil Component	weight of fraction (g)	% Carbon from elemental analysis	% Ash[g]	% Carbon on ash-free basis	%Fe from elemental analysis	Total Fe in fraction from elemental analysis (g)	Total Carbon in fraction from elemental analysis (g)
Whole Soil	140.43	16.07	70.30	54.12	1.05	1.47	22.51
HF-treated soil	2.15[f]	29.88	43.60	52.88	0.25	0.0054	0.642
Humin	122.77	11.86	76.80	51.12	1.07	1.31	14.56
Humic Acid	12.52	43.91	15.80	52.15	0.90	0.11	5.50
Fulvic Acid A[a] (ion exchange treated)	7.93	21.84	47.40	41.52	0.14	0.011	3.34
Fulvic Acid B[b]	9.84	16.41	56.30	37.55	0.21	0.020	
Ion Exchange Resin[c]	3.00	N/A			0.002	0.000	
Ion Exchange Resin[d] (after fulvic acid treatment)	3.00	N/A			0.11	0.0033	
Total for Humic, Humin, Fulvic Acid[e] (A, B, resin)						1.46	23.40

[a] Fraction of fulvic acid which was treated with Biorad AG 50W-8X proton-form cation exchange resin beads.

[b] Raw fulvic acid fraction, untreated with ion exchange resin beads.

[c] Biorad AG 50W-8X proton-form cation exchange resin beads, dried and ground for analysis, as received from Biorad.

[d] Biorad AG 50W-8X cation exchange resin beads post fulvic acid treatment, dried and ground for elemental analysis.

[e] Total Fe in fraction, equal to Humin + Humic Acid + Fulvic Acid A + Fulvic Acid B + Ion Exchange Resin (post treatment) – Ion Exchange Resin (as received from Biorad).

[f] Remaining material from HF-treatments on 4.00 g of Uncompahgre whole soil.

[g] Ash contents provided by Water, Soil, and Plant Testing Laboratory at Colorado State University.

Table 2.2. Calibration[a] of a capillary containing silicone rubber.

compound	peak position (ppm)	t_d (s)[b]	Carbon-13 T_1 (s)[c]	C_{T_1} [d]	Calibration of capillary containing 79.5 mg silicone rubber.[e] (mg of natural abundance carbon)
hexamethylbenzene	131	20.00	1.50	1.00	19.52
hexamethylbenzene	16.9	20.00	1.44 (20%), 0.37 (80%)	1.00	20.01
glycine	175	20.00	5.19	1.02	20.01
glycine	46	20.00	1.82	1.00	26.44
L-alanine	20.40	36.00	0.05	1.00	22.12
L-alanine	49.70	36.00	1.83	1.00	23.40
L-alanine	177.90	36.00	7.20	1.01	21.41
Syringic Acid	169.30	450.00	146	1.05	22.62
Syringic Acid	147.10	450.00	146	1.05	21.09
Syringic Acid	138.36	450.00	146	1.05	20.80
Syringic Acid	120.70	450.00	146	1.05	21.35
Syringic Acid	105.00	450.00	146	1.05	23.92
Syringic Acid	56.00	450.00	3.00	1.00	21.16
average					21.83
standard deviation					1.90
relative deviation					8.70 %

[a] All calibrations were run with the same radio-frequency field intensities used for the spin-counting experiments on the individual soil samples. Magic angle spinning speeds of 3.0 kHz were used for these calibrations.

[b] The ^{13}C DP-MAS delay period used in the calibration of the silicone rubber external reference.

[c] ^{13}C T_1's reported as single or multiple component values with the percentage contribution from each relaxation component reported in parenthesis. ^{13}C T_1's were determined by the Torchia[4] experiment, as shown in Figure 2.1.

[d] The ^{13}C T_1 correction term for the peak of the compound used to calibrate the external reference, as described in equations 2.1-2.3.

[e] The calibration value empirically assigned to the reference material. The values reported here are based on peak integrals that have been corrected to account for ^{13}C T_1 relaxation (A_{corr}^{DP}).

Table 2.3 ^{13}C T_1, DP-MAS spin-counting results for Uncompahgre whole soil (1.705 g).

ppm	Carbon-13 T_1 (s)[a]	C_{T_1} [b] (±SEE %)	A_{exp}^{DP} [c] (±ERE %)	A_{curr}^{DP} [d] (±Total % Error)	mg of carbon[e]	% of total[f] (p_i)
197	0.006 (67.0%), 0.676(33.0%)	1.00 (± 2.19 %)	184.23 (± 27.01 %)	184.4 (± 27.10 %)	4.52	2.79
172	0.055 (54.5%), 3.041(45.5%)	1.14 (± 4.24 %)	925.9 (± 6.99 %)	1054.86 (± 8.18 %)	25.82	15.97
150	0.049 (42.9%), 4.417(57.1%)	1.30 (± 4.82 %)	518.92 (± 11.34 %)	674.82 (± 12.32 %)	16.52	10.21
130	0.096 (54.6%), 5.133(45.4%)	1.26 (± 4.64 %)	1177.27 (± 14.14 %)	1486.68 (± 14.88 %)	36.39	22.50
115	0.079 (40.8%), 2.083(59.2%)	1.09 (± 8.49 %)	301.93 (± 30.21 %)	330.6 (± 31.38 %)	8.10	5.00
104	0.056 (34.3%), 4.05(65.7%)	1.32 (± 4.76 %)	263.21 (± 21.05 %)	348.55 (± 21.58 %)	8.53	5.28
72	0.498 (50.5%), 6.369(49.5%)	1.36 (± 3.21 %)	1007.08 (± 8.14 %)	1369.28 (± 8.75 %)	33.52	20.72
56	0.062 (47.0%), 2.175(53.0%)	1.09 (± 4.06 %)	390.64 (± 14.83 %)	426.56 (± 15.38 %)	10.44	6.46
39	0.035 (42.1%), 1.431(57.9%)	1.04 (± 6.08 %)	91.08 (± 30.44 %)	94.42 (± 31.05 %)	2.31	1.43
30	0.107 (68.0%), 1.705(32.0%)	1.03 (± 2.76 %)	365.84 (± 13.65 %)	377.4 (± 13.93 %)	9.23	5.71
20	0.075 (52.6%), 1.542(47.4%)	1.04 (± 5.16 %)	250.51 (± 14.86 %)	259.72 (± 15.73 %)	6.36	3.93
0[h]	2.703 (100%)	1.29 (± 0.47 %)	760.86 (± 4.19 %)	985.10 (± 5.93 %)	24.11[g] (± 8.70 %)	
	Total (not including reference at 0 ppm)		5476.6 (± 4.35 %)[i]	6607.29 (± 4.67 %)[i]	161.74	100 %
	total percent carbon by DP-MAS spin counting				9.5 (± 10.7 %)[j]	

[a] ^{13}C T_1's reported as single or multiple component values with the percentage contribution from each relaxation component reported in parenthesis.

[b] ^{13}C T_1 correction term as shown in equations 2.1-2.3, with error estimated from the standard error of the estimate (SEE).

[c] The experimental peak areas with the estimated relative error given in parenthesis (based on 20 independent deconvolutions as described in section 2.2.5).

[d] Raw peak areas for each deconvoluted peak multiplied by the relaxation correction factor (C_{T_1}). The total relative error is given as a percent error in parenthesis and is propagated from the error of the ^{13}C T_1 correction term and that of the experimental peak area.

[e] Amount of carbon in milligrams per deconvoluted peak in the whole spinner sample (1.705 g).

[f] Percent carbon of the DP-MAS detected carbon, p_i = 100*(mg C for peak i)/(sum of mg C for all peaks).

[g] Result and percent relative error from calibration of capillary containing 79.5 mg of silicone rubber with standard materials.

[h] Peak due to silicone rubber external reference.

[i] Sum of the individual peak integrals in the same column, excluding the integral due to the reference material at 0 ppm. The error for this total is the propagated error of the sum of the aforementioned integrals.

[j] The total percent carbon with relative error given in parenthesis. Error for this total is the propagated error of the total corrected peak integral, and the errors associated with the external reference.

Table 2.4 ^{13}C T_1, DP-MAS spin-counting results for the HF-treated Uncompahgre whole soil (1.630 g).

ppm	Carbon-13 T_1 (s)[a]	C_{T_1} [b] (±SEE %)	A_{exp}^{DP} [c] (±ERE %)	A_{corr}^{DP} [d] (±Total % Error)	mg of carbon[e]	% of total[f] (p_i)
197	0.327 (48.1%), 11.696(51.9%)	1.58 (± 4.55 %)	79.05 (± 20.21 %)	125.25 (± 20.72 %)	39.65	9.17
172	0.566 (53.3%), 7.479(46.7%)	1.38 (± 1.93 %)	114.34 (± 7.18 %)	157.45 (± 7.44 %)	49.84	11.53
150	0.697 (40.4%), 13.141(59.6%)	1.79 (± 3.33 %)	76.35 (± 6.25 %)	136.56 (± 7.08 %)	43.23	10.00
130	0.508 (47.3%), 9.132(52.7%)	1.52 (± 2.53 %)	170.17 (± 5.41 %)	258.06 (± 5.98 %)	81.70	18.89
115	0.412 (36.2%), 5.688(63.8%)	1.46 (± 2.1 %)	28.82 (± 17.3 %)	42.11 (± 17.43 %)	13.33	3.08
104	0.487 (36.8%), 6.775(63.2%)	1.54 (± 1.77 %)	62.5 (± 9.16 %)	96.23 (± 9.33 %)	30.46	7.04
72	0.58 (39.3%), 6.035(60.7%)	1.46 (± 2.11 %)	154.8 (± 11.04 %)	225.42 (± 11.24 %)	71.36	16.50
56	0.19 (51.3%), 2.352(48.7%)	1.10 (± 2.23 %)	95.53 (± 25.76 %)	104.85 (± 25.85 %)	33.19	7.68
39	0.228 (42%), 3.797(58%)	1.25 (± 2.82 %)	47.35 (± 13.82 %)	59.35 (± 14.1 %)	18.79	8.77
30	0.182 (74.9%), 3.097(25.1%)	1.07 (± 1.74 %)	49.17 (± 29.98 %)	52.81 (± 30.03 %)	16.72	3.72
20	0.219 (69.4%), 2.006(30.6%)	1.04 (± 1.52 %)	59.86 (± 19.9 %)	62.46 (± 19.96 %)	19.77	3.62
0[h]	2.703 (100%)	1.29 (± 0.47 %)	53.27 (± 5.04 %)	68.97 (± 5.06 %)	21.83[g] (± 8.70 %)	
	Total (not including reference at 0 ppm)		937.94 (± 4.51 %)[i]	1320.55 (± 4.24 %)[i]	418.00	100 %
	total percent carbon by DP-MAS spin counting				25.6 (± 10.9 %)[j]	

[a] ^{13}C T_1's reported as single or multiple component values with the percentage contribution from each relaxation component reported in parenthesis.

[b] ^{13}C T_1 correction term as shown in equations 2.1-2.3, with error estimated from the standard error of the estimate (SEE).

[c] The experimental peak areas with the estimated relative error given in parenthesis (based on 20 independent deconvolutions as described in section 2.2.5).

[d] Raw peak areas for each deconvoluted peak multiplied by the relaxation correction factor (C_{T_1}). The total relative error is given as a percent error in parenthesis and is propagated from the error of the ^{13}C T_1 correction term and that of the experimental peak area.

[e] Amount of carbon in milligrams per deconvoluted peak in the whole spinner sample (1.630 g).

[f] Percent carbon of the DP-MAS detected carbon, p_i = 100*(mg C for peak i)/(sum of mg C for all peaks).

[g] Result and percent relative error from calibration of capillary containing 79.5 mg of silicone rubber with standard materials.

[h] Peak due to silicone rubber external reference.

[i] Sum of the individual peak integrals in the same column, excluding the integral due to the reference material at 0 ppm. The error for this total is the propagated error of the sum of the aforementioned integrals.

[j] The total percent carbon with relative error given in parenthesis. Error for this total is the propagated error of the total corrected peak integral, and the errors associated with the external reference.

Table 2.5 ^{13}C T_1, DP-MAS spin-counting results for humin fraction (1.907 g).

ppm	Carbon-13 T_1 (s)[a]	C_{T_1} [b] (±SEE %)	A_{exp}^{DP} [c] (±ERE %)	A_{corr}^{DP} [d] (±Total % Error)	mg of carbon[e]	% of total[f] (p_i)
197[g]	0.006 (67.0%), 0.676(33.0%)	1.00 (± 2.19 %)	291.49 (± 22.72 %)	291.75 (± 22.83 %)	6.90	4.27
172	0.15 (47.9%), 3.169(52.1%)	1.17 (± 3.7 %)	1031.09 (± 6.45 %)	1209.38 (± 7.44 %)	28.60	17.70
150	0.135 (35.4%), 2.761(64.6%)	1.18 (± 5.63 %)	473.03 (± 17.99 %)	557.59 (± 18.85 %)	13.19	8.16
130	0.193 (53.3%), 3.935(46.7%)	1.20 (± 3.12 %)	1268.9 (± 20.52 %)	1527.24 (± 20.76 %)	36.12	22.35
115	0.095 (41.2%), 1.68(58.8%)	1.06 (± 4.53 %)	421.12 (± 30.11 %)	445.34 (± 30.45 %)	10.54	6.52
104	0.374 (100%)	1.00 (± 5.28 %)	282.29 (± 30.21 %)	282.3 (± 30.67 %)	6.67	4.13
72	0.199 (39.7%), 2.733(60.3%)	1.16 (± 1.96 %)	1214.01 (± 7.67 %)	1410.86 (± 7.92 %)	33.37	20.65
56	0.123 (55.4%), 1.783(44.6%)	1.05 (± 3.76 %)	365.38 (± 13.03 %)	383.55 (± 13.56 %)	9.07	5.61
39	0.035 (42.1%), 1.431(57.9%)	1.04 (± 0 %)	80.10 (± 31.52 %)	83.04 (± 31.52 %)	1.97	1.22
30	0.156 (71.2%), 1.673(28.8%)	1.03 (± 2.06 %)	408.59 (± 11.99 %)	419.66 (± 12.16 %)	9.93	6.14
20	0.203 (100%)	1.00 (± 9.04 %)	221.25 (± 16.01 %)	221.25 (± 18.39 %)	5.24	3.24
0[i]	2.703 (100%)	1.29 (± 0.47 %)	787.60 (± 3.67 %)	1019.73 (± 3.7 %)	24.11[h] (± 8.70 %)	
	Total (not including reference at 0 ppm)		6057.26 (± 5.78 %)[j]	6831.97 (± 6.04 %)[j]	161.5	100 %
	total percent carbon by DP-MAS spin counting				8.5 (± 11.2 %)[k]	

[a] ^{13}C T_1's reported as single or multiple component values with the percentage contribution from each relaxation component reported in parenthesis.

[b] ^{13}C T_1 correction term as shown in equations 2.1-2.3, with error estimated from the standard error of the estimate (SEE).

[c] The experimental peak areas with the estimated relative error given in parenthesis (based on 20 independent deconvolutions as described in section 2.2.5).

[d] Raw peak areas for each deconvoluted peak multiplied by the relaxation correction factor (C_{T_1}). The total relative error is given as a percent error in parenthesis and is propagated from the error of the ^{13}C T_1 correction term and that of the experimental peak area.

[e] Amount of carbon in milligrams per deconvoluted peak in the whole spinner sample (1.907 g).

[f] Percent carbon of the DP-MAS detected carbon, p_i = 100*(mg C for peak i)/(sum of mg C for all peaks).

[g] ^{13}C T_1 data taken from whole soil spectra.

[h] Result and percent relative error from calibration of capillary containing 79.5 mg of silicone rubber with standard materials.

[i] Peak due to silicone rubber external reference.

[j] Sum of the individual peak integrals in the same column, excluding the integral due to the reference material at 0 ppm. The error for this total is the propagated error of the sum of the aforementioned integrals.

[k] The total percent carbon with relative error given in parenthesis. Error for this total is the propagated error of the total corrected peak integral, and the errors associated with the external reference.

Table 2.6 ^{13}C T_1, DP-MAS spin-counting results for humic acid (1.637 g).

ppm	Carbon-13 T_1 (s)[a]	C_{T_1} [b] (±SEE %)	A_{exp}^{DP} [c] (±ERE %)	A_{corr}^{DP} [d] (±Total % Error)	mg of carbon[e]	% of total[f] (p_i)
197	0.207 (100%)	1.00 (± 3.48 %)	77.50 (± 33.00 %)	77.50 (± 33.18 %)	14.90	2.91
172	0.07 (42.6%), 0.63(57.4%)	1.00 (± 1.37 %)	452.71 (± 6.39 %)	453.16 (± 6.53 %)	87.15	17.02
150	0.102 (52.1%), 0.774(47.9%)	1.00 (± 3.08 %)	299.06 (± 10.81 %)	299.88 (± 11.24 %)	57.67	11.26
130	0.068 (43%), 0.607(57%)	1.00 (± 1.20 %)	544.29 (± 15.76 %)	544.72 (± 15.81 %)	104.75	20.46
115	0.121 (54.7%), 0.914(45.3%)	1.01 (± 2.26 %)	192.57 (± 22.17 %)	193.68 (± 22.28 %)	37.24	7.27
104	0.044 (37.6%), 0.448(62.4%)	1.00 (± 3.26 %)	131.69 (± 29.73 %)	131.70 (± 29.91 %)	25.33	4.95
72	0.092 (46.1%), 0.896(53.9%)	1.01 (± 2.5 %)	349.22 (± 6.05 %)	351.41 (± 6.55 %)	67.57	13.20
56	0.056 (39.9%), 0.45(60.1%)	1.00 (± 1.27 %)	193.28 (± 12.06 %)	193.29 (± 12.13 %)	37.17	7.26
39	0.044 (27.8%), 0.801(72.2%)	1.00 (± 2.29 %)	69.23 (± 23.95 %)	69.57 (± 24.06 %)	13.38	2.61
30	0.115 (60.5%), 1.012(39.5%)	1.01 (± 2.29 %)	199.89 (± 17.97 %)	201.42 (± 18.12 %)	38.73	7.56
20	0.08 (58.1%), 0.545(41.9%)	1.00 (± 4.02 %)	146.51 (± 20.19 %)	146.55 (± 20.58 %)	28.19	5.50
0[h]	2.703 (100%)	1.29 (± 0.47 %)	103.43 (± 4.87 %)	133.92 (± 4.89 %)	25.75[g] (± 8.70 %)	
	Total (not including reference at 0 ppm)		2655.96 (± 4.86 %)[i]	2662.88 (± 4.91 %)[i]	512.03	100 %
	total percent carbon by DP-MAS spin counting				31.3 (± 11.1 %)[j]	

[a] ^{13}C T_1's reported as single or multiple component values with the percentage contribution from each relaxation component reported in parenthesis.

[b] ^{13}C T_1 correction term as shown in equations 2.1-2.3, with error estimated from the standard error of the estimate (SEE).

[c] The experimental peak areas with the estimated relative error given in parenthesis (based on 20 independent deconvolutions as described in section 2.2.5).

[d] Raw peak areas for each deconvoluted peak multiplied by the relaxation correction factor (C_{T_1}). The total relative error is given as a percent error in parenthesis and is propagated from the error of the ^{13}C T_1 correction term and that of the experimental peak area.

[e] Amount of carbon in milligrams per deconvoluted peak in the whole spinner sample (1.637 g).

[f] Percent carbon of the DP-MAS detected carbon, p_i = 100*(mg C for peak i)/(sum of mg C for all peaks).

[g] Result and percent relative error from calibration of capillary containing 79.5 mg of silicone rubber with standard materials.

[h] Peak due to silicone rubber external reference.

[i] Sum of the individual peak integrals in the same column, excluding the integral due to the reference material at 0 ppm. The error for this total is the propagated error of the sum of the aforementioned integrals.

[j] The total percent carbon with relative error given in parenthesis. Error for this total is the propagated error of the total corrected peak integral, and the errors associated with the external reference.

Table 2.7 ^{13}C T_1, DP-MAS spin-counting results for fulvic acid (1.381 g).

ppm	Carbon-13 T_1 (s)[a]	C_{T_1}[b] (±SEE %)	A_{exp}^{DP}[c] (±ERE %)	A_{corr}^{DP}[d] (±Total % Error)	mg of carbon[e]	% of total[f] (p_i)
197[g]	0.207 (100%)	1.00 (± 3.48 %)	24.48 (± 43.20 %)	24.48 (± 43.34 %)	4.52	2.10
172	0.074 (61.2%), 0.749(38.8%)	1.00 (± 1.91 %)	189.74 (± 9.67 %)	190.09 (± 9.85 %)	35.05	16.28
160	0.062 (67.5%), 0.506(32.5%)	1.00 (± 2.61 %)	36.04 (± 25.09 %)	36.04 (± 25.23 %)	6.65	3.09
150	0.012 (50.2%), 0.363(49.8%)	1.00 (± 2.72 %)	94.93 (± 18.73 %)	94.94 (± 18.93 %)	17.51	8.13
130	0.073 (59.1%), 0.71(40.9%)	1.00 (± 0.92 %)	131.31 (± 13.78 %)	131.50 (± 13.81 %)	24.24	11.26
115[g]	0.121 (54.7%), 0.914(45.3%)	1.01 (± 2.26 %)	45.29 (± 19.49 %)	45.55 (± 19.62 %)	8.39	3.90
104	0.064 (53.8%), 0.634(46.2%)	1.00 (± 2.11 %)	75.41 (± 11.49 %)	75.48 (± 11.69 %)	13.92	6.47
72	0.085 (57.2%), 0.67(42.8%)	1.00 (± 1.2 %)	370.07 (± 5.38 %)	370.47 (± 5.51 %)	68.30	31.73
56[g]	0.056 (39.9%), 0.45(60.1%)	1.00 (± 1.27 %)	58.37 (± 21.00 %)	58.37 (± 21.04 %)	10.76	5.00
39	0.101 (66.1%), 0.956(33.9%)	1.01 (± 1.33 %)	52.1 (± 16.83 %)	52.37 (± 16.88 %)	9.65	4.49
30	0.067 (73.1%), 0.438(26.9%)	1.00 (± 2.45 %)	52.17 (± 17.44 %)	52.17 (± 17.61 %)	9.62	4.47
20	0.062 (72.7%), 0.379(27.3%)	1.00 (± 2.57 %)	35.94 (± 22.18 %)	35.94 (± 22.33 %)	6.63	3.08
0[i]	2.703 (100%)	1.29 (± 0.47 %)	105.03 (± 3.82 %)	135.99 (± 3.85 %)	24.11[h] (± 8.70 %)	
	Total (not including reference at 0 ppm)		1165.85 (± 3.82 %)[j]	1167.4 (± 3.87 %)[j]	206.98	100 %
	total percent carbon by DP-MAS spin counting				15.0 (± 10.3 %)[k]	

[a] ^{13}C T_1's reported as single or multiple component values with the percentage contribution from each relaxation component reported in parenthesis.

[b] ^{13}C T_1 correction term as shown in equations 2.1-2.3, with error estimated from the standard error of the estimate (SEE).

[c] The experimental peak areas with the estimated relative error given in parenthesis (based on 20 independent deconvolutions as described in section 2.2.5).

[d] Raw peak areas for each deconvoluted peak multiplied by the relaxation correction factor (C_{T_1}). The total relative error is given as a percent error in parenthesis and is propagated from the error of the ^{13}C T_1 correction term and that of the experimental peak area.

[e] Amount of carbon in milligrams per deconvoluted peak in the whole spinner sample (1.381 g).

[f] Percent carbon of the DP-MAS detected carbon, p_i = 100*(mg C for peak i)/(sum of mg C for all peaks).

[g] ^{13}C T_1 data taken from humic acid spectra.

[h] Result and percent relative error from calibration of capillary containing 79.5 mg of silicone rubber with standard materials.

[i] Peak due to silicone rubber external reference.

[j] Sum of the individual peak integrals in the same column, excluding the integral due to the reference material at 0 ppm. The error for this total is the propagated error of the sum of the aforementioned integrals.

[k] The total percent carbon with relative error given in parenthesis. Error for this total is the propagated error of the total corrected peak integral, and the errors associated with the external reference.

Table 2.8. Summary of results from ^{13}C DP-MAS spin counting.

Soil component	weight percent of soil	% C by DP-MAS spin counting	% C by elemental analysis	(amount of carbon detected by DP-MAS) / (amount of carbon detected by elemental) x 100%
Fulvic Acid[a]	3.66	15.0	21.84	68.7
Humic Acid	8.92	31.3	43.91	71.3
Humin	87.42	8.5	11.86	71.7
HF-treated soil	N/A	25.6	29.88	85.7
Whole soil	100	9.5	16.07	59.1

[a] Elemental and DP-MAS data is that of the ion-exchange treated fulvic acid.

Table 2.9 Summary of elemental percentages by the empirical relationship method.

Sample	Empirical Relationship Method[a]			% C by elemental on an ash-free basis[c]
	% Carbon	% Hydrogen	% Oxygen	
Fulvic Acid	49.0	4.30	46.7	41.5
Humic Acid	54.3	4.35	41.4	52.1
Humin	53.1	3.85	43.1	51.1
HF-treated soil	54.3	4.47	41.2	52.9
Whole soil	53.6	4.10	42.3	54.1

[a] Calculations based on the relationships established in section 2.3.7.

Table 2.10 Summary of vibrating sample magnetometer data and corresponding calculations.

Soil component	% Fe by weight[a]	sample size (g)[b]	measured volume magnetic susceptiblity[c] (cgs)	calculated volume magnetic susceptibility[d] assuming all iron as Fe^{3+} (cgs)	measured saturation magnetization[e] (Gauss)	calculated saturation magnetization[f] assuming all iron in form of pure magnetite (Gauss)
whole soil	1.05	0.178	1.6E-06	3.3E-06	4.3E-02	1.51
HF-treated soil	0.25	0.119	N/A	5.2E-07	1.6E-03	0.24
humin	1.07	0.129	1.4E-06	2.4E-06	3.6E-02	1.11
humic acid	0.90	0.128	1.2E-06	2.0E-06	6.1E-02	N/A
fulvic acid	0.14	0.111	N/A	2.7E-07	8.1E-04	N/A

[a] Percent iron from elemental analysis provided by Huffman Laboratories.
[b] Actual sample size used in VSM analysis. The sample holder was constructed of Kel-F and had a sample volume of 0.15 cm^3.
[c] Volume magnetic susceptibility in cgs units (emu cm^{-3} Oe^{-1}) from the slope at 10 kOe of the experimental data in Figure 2.17 and corrected for sample density.
[d] Calculated volume magnetic susceptibility (in cgs units) using the Curie law of paramagnetic susceptibility (Eq. 2.7), assuming each iron atom to be in the form of Fe^{3+} and having a magnetic moment of 5.92 Bohr magnetons (9.27E-21 G cm^3).
[e] The measured saturation magnetization in gauss (emu/cm^3) from the experimental data in Figure 2.17 (extrapolated to 0 Oe) and corrected for sample density.
[f] The calculated saturation magnetization assuming all of the iron in the sample is in the form of pure magnetite (Fe_3O_4), with a density of 5.5 g/cm^3 and a room temperature saturation magnetization of 480 G for pure magnetite.

Table 2.11 Magnetite content in Uncompahgre Forest soil and soil components from saturation magnetization.

Soil component	fraction weight (g)	% Fe by weight from elemental analysis	Total Fe in fraction from elemental analysis (g)	Total magnetite in fraction from saturation magnetization (mg)
whole soil	140.43	1.05	1.47	58.4
HF-treated soil	2.15[a]	0.25	0.0054	0.050
humin	122.77	1.07	1.31	58.8
humic acid	12.52	0.90	0.11	N/A
fulvic acid (ion-x)	7.93	0.14	0.011	N/A

[a] Remaining material from HF-treatments on 4.00 g of Uncompahgre whole soil.

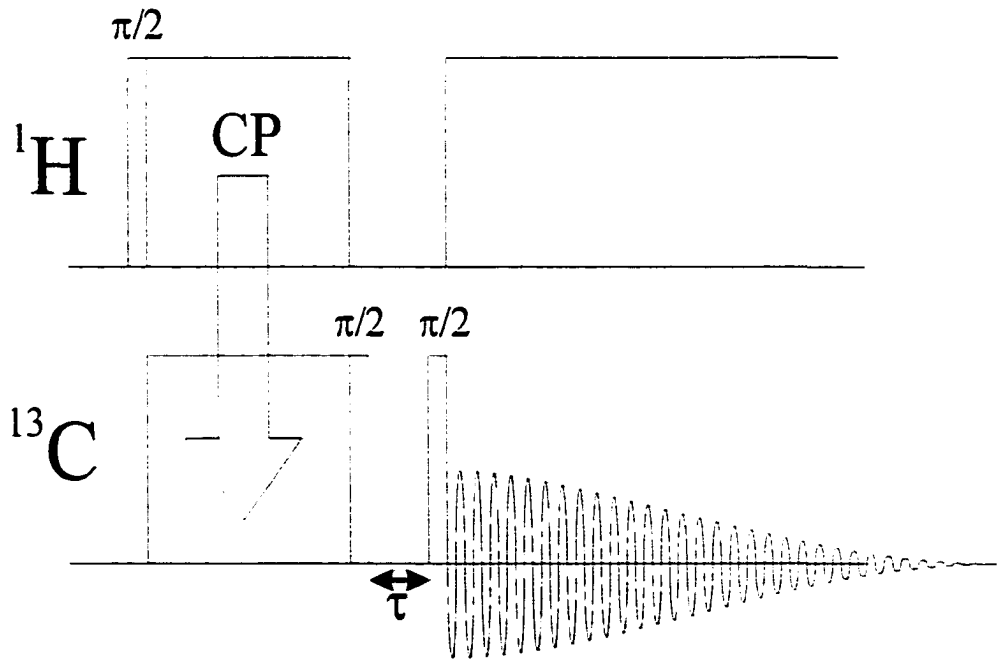

Figure 2.1 Radio-frequency pulse schematics for the Torchia-style ^{13}C T_1 experiment. Pulse widths are given in radians ($\pi/2$ is equal to a 90° pulse). The cross polarization period is indicated by "CP".

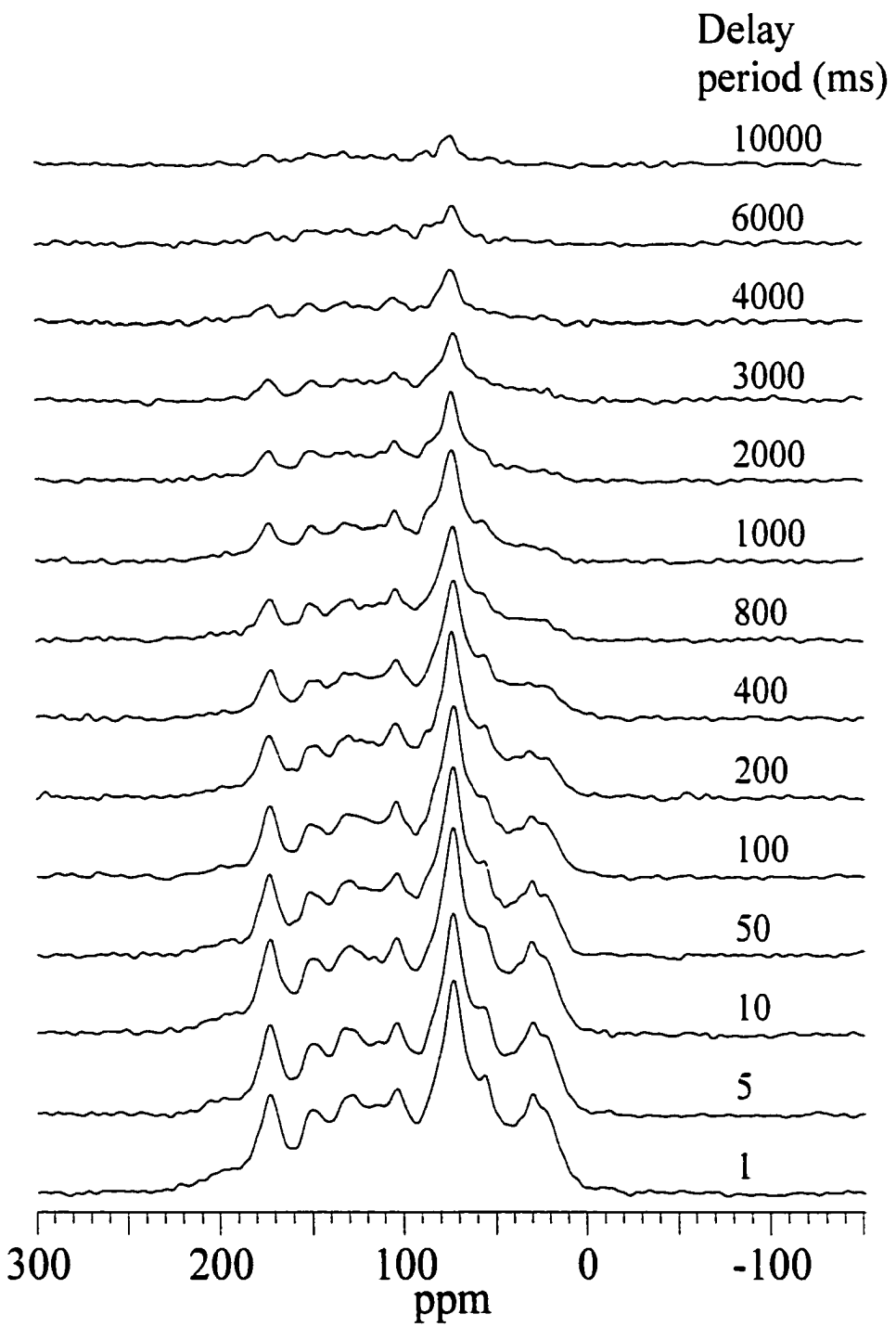

Figure 2.2(a) Carbon-13 T_1 measurement of Uncompahgre whole soil. The τ delay period is given to the right of each spectrum.

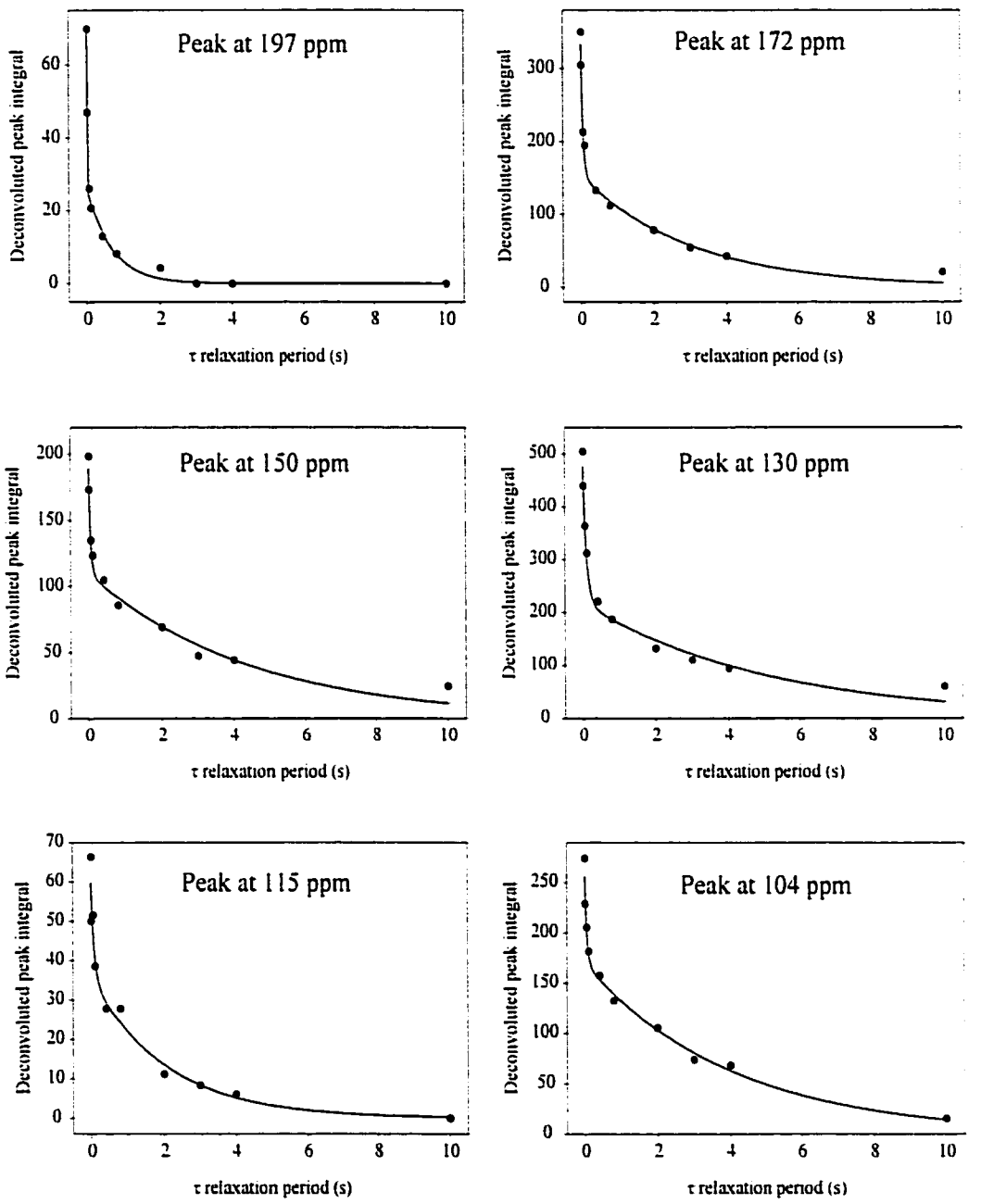

Figure 2.2(b) Experimental ^{13}C T_1 relaxation data for Uncompahgre whole soil and corresponding curve fits for the data of Figure 2.2. Each graph was generated by plotting the peak area of each deconvoluted peak of Figure 2.2A (featured in detail in the appendix of this thesis) versus the τ relaxation period. Graphical data are sorted by peak region in ppm. Curve fits using either a single or double component exponential decay are presented by a solid black line in each plot and overlay the experimental data, presented as solid black dots.

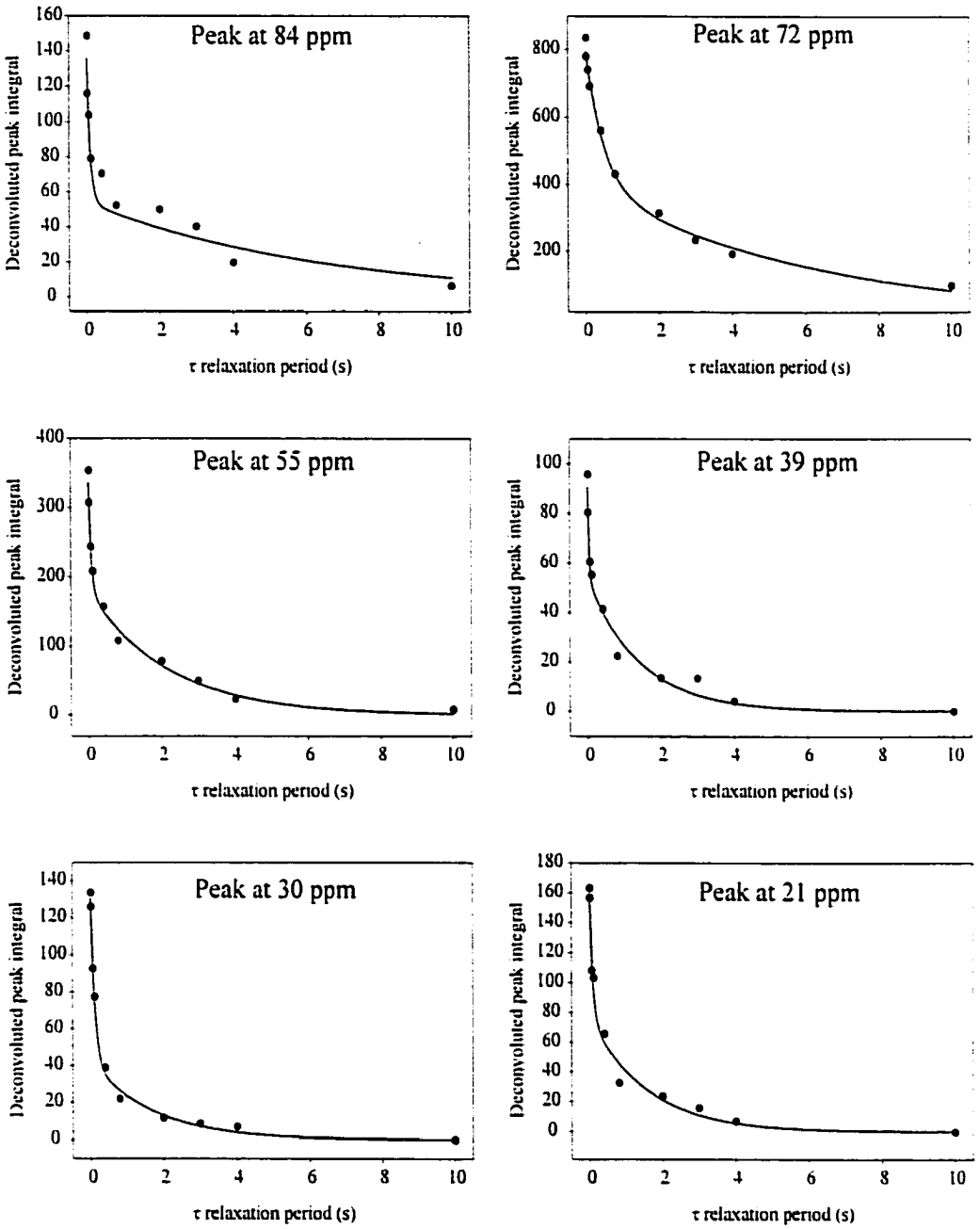

Figure 2.2(b) (continued).

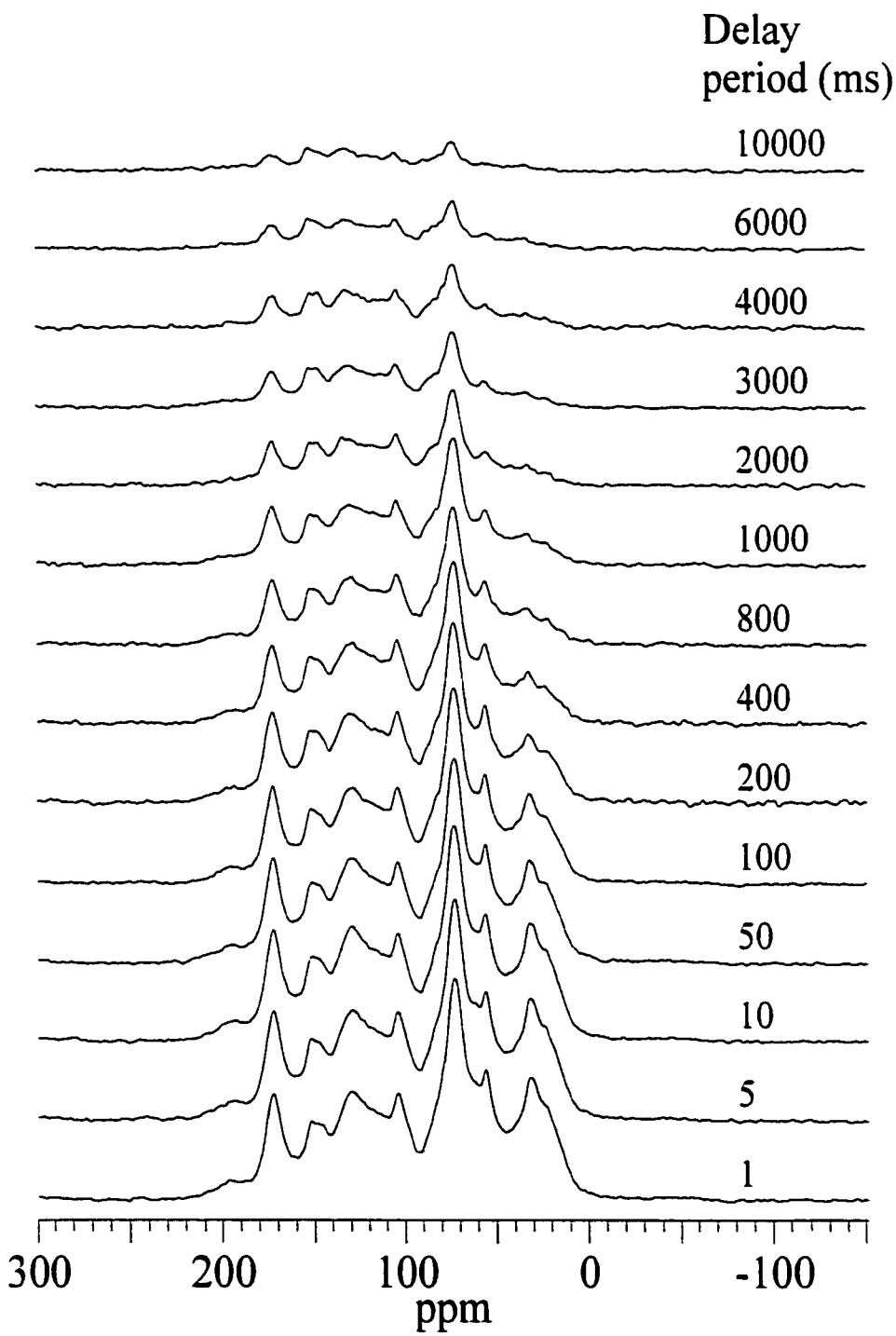

Figure 2.3(a) Carbon T_1 measurement of HF-treated Uncompahgre whole soil. The τ delay period is given to the right of each spectrum.

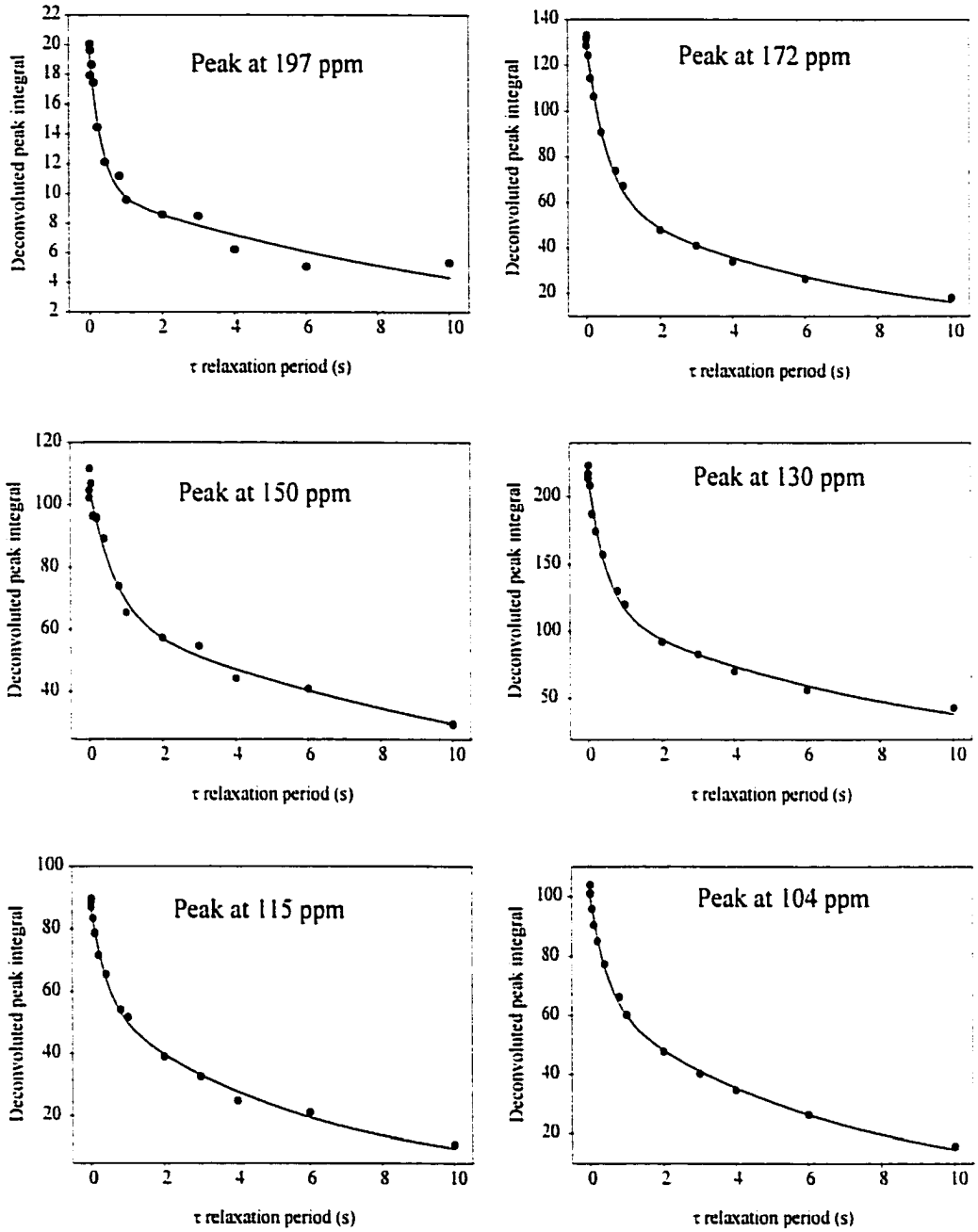

Figure 2.3(b) Experimental ^{13}C T_1 relaxation data for HF-treated Uncompahgre soil and corresponding curve fits for the data of Figure 2.3. Each graph was generated by plotting the peak area of each deconvoluted peak of Figure 2.3A (featured in detail in the appendix of this thesis) versus the τ relaxation period. Graphical data are sorted by peak region in ppm. Curve fits using either a single or double component exponential decay are presented by a solid black line in each plot and overlay the experimental data, presented as solid black dots.

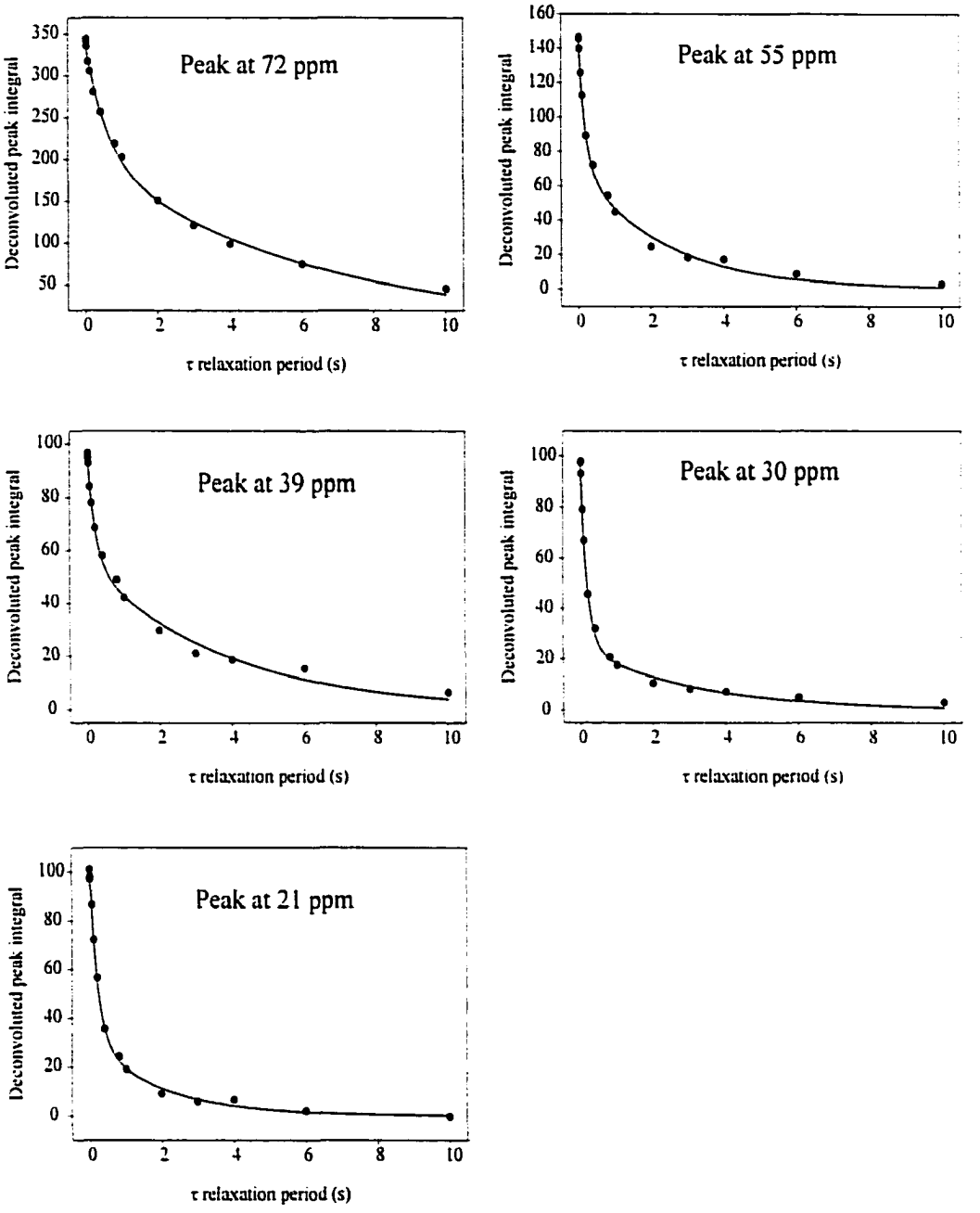

Figure 2.3(b) (continued).

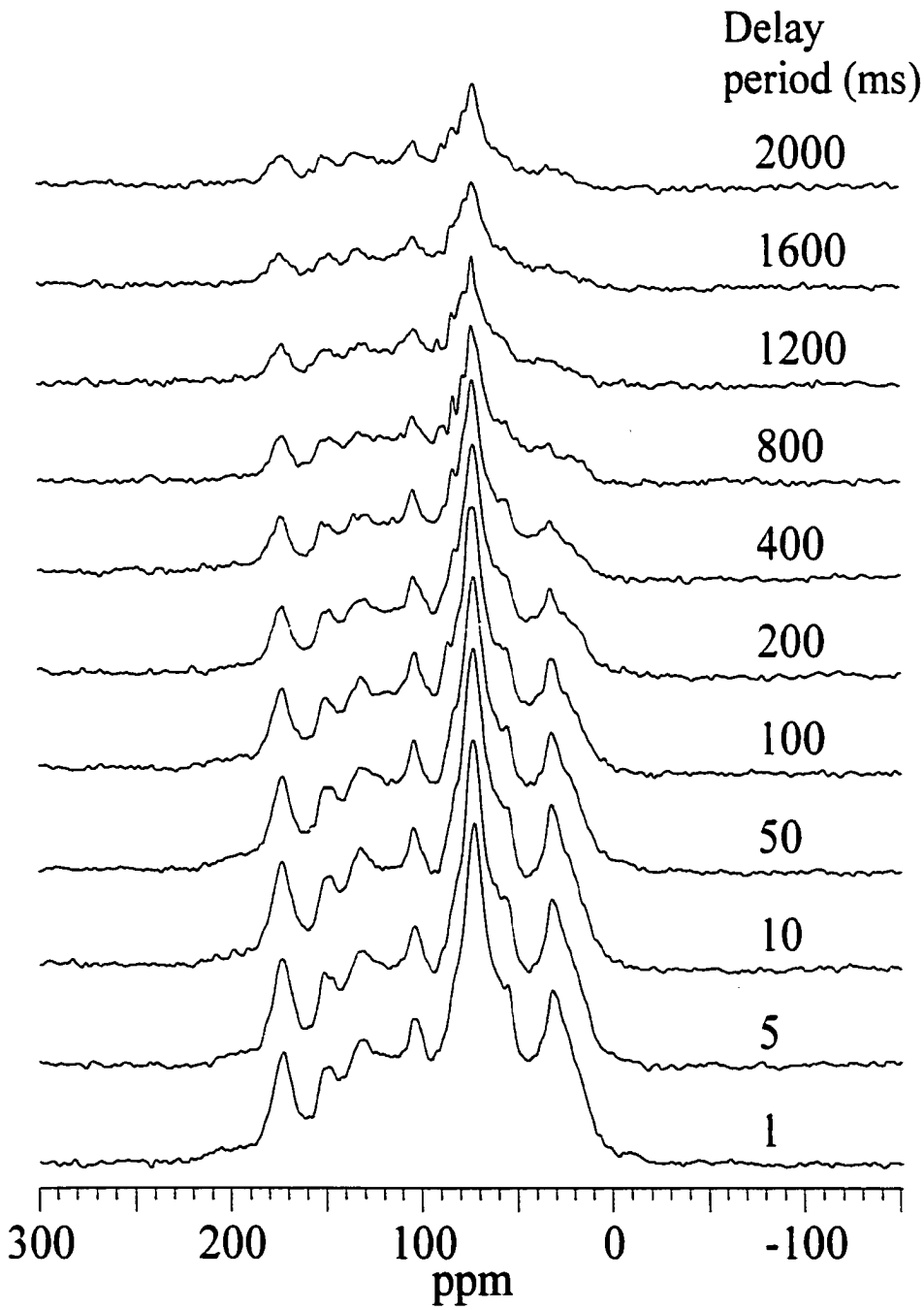

Figure 2.4(a) Carbon-13 T_1 measurement of Uncompahgre soil humin fraction. The τ delay period is given to the right of each spectrum.

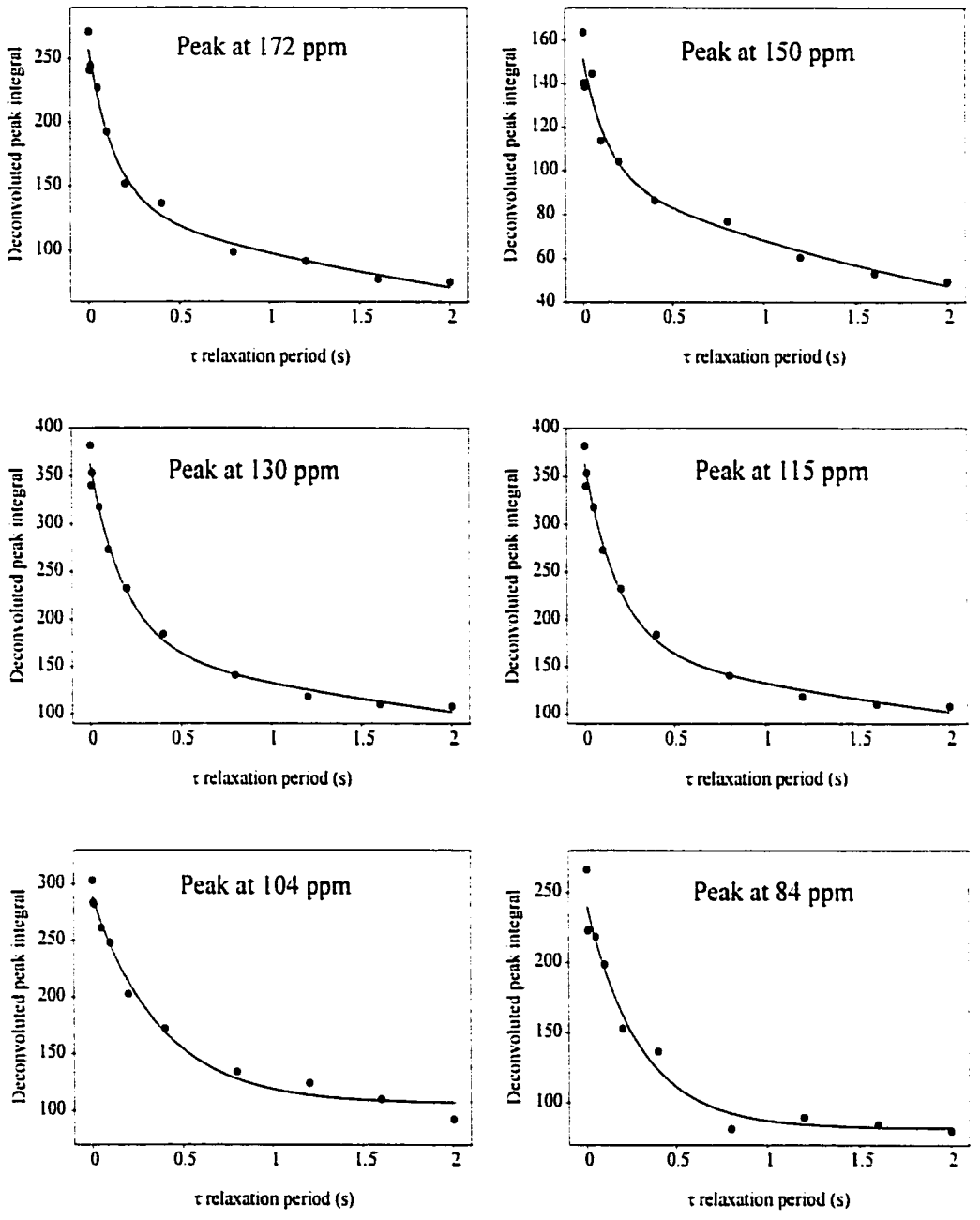

Figure 2.4(b) Experimental ^{13}C T_1 relaxation data for the humin fraction of the Uncompahgre soil and corresponding curve fits for the data of Figure 2.4. Each graph was generated by plotting the peak area of each deconvoluted peak of Figure 2.4A (featured in detail in the appendix of this thesis) versus the τ relaxation period. Graphical data are sorted by peak region in ppm. Curve fits using either a single or double component exponential decay are presented by a solid black line in each plot and overlay the experimental data, presented as solid black dots.

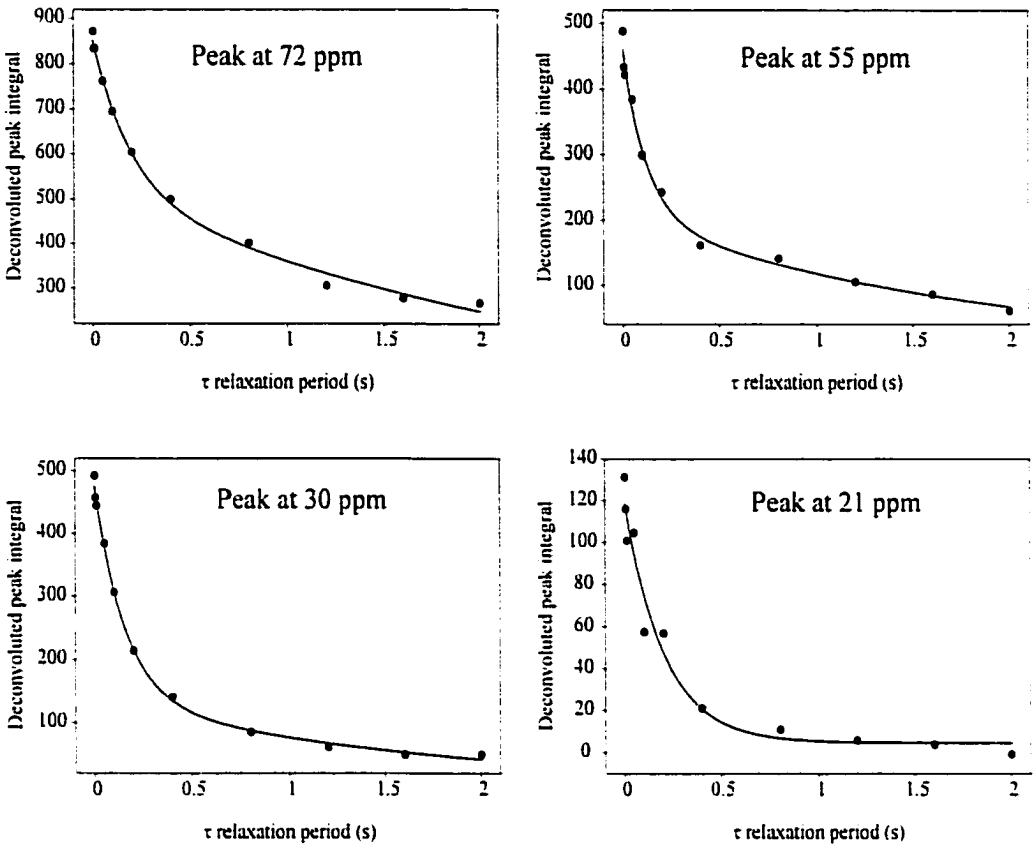

Figure 2.4(b) (continued).

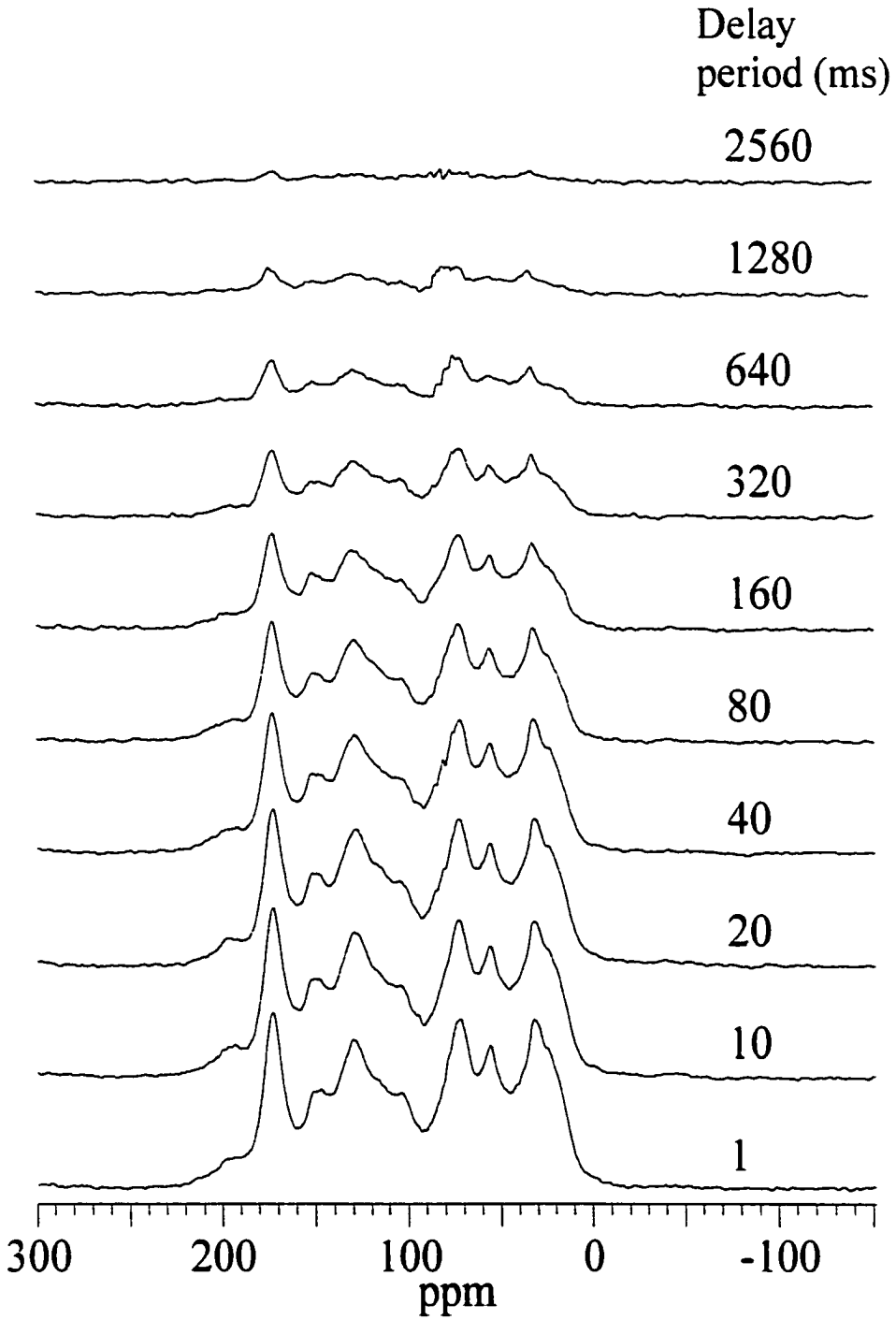

Figure 2.5(a) Carbon-13 T_1 measurement of Uncompahgre soil humic acid. The τ delay period is given to the right of each spectrum.

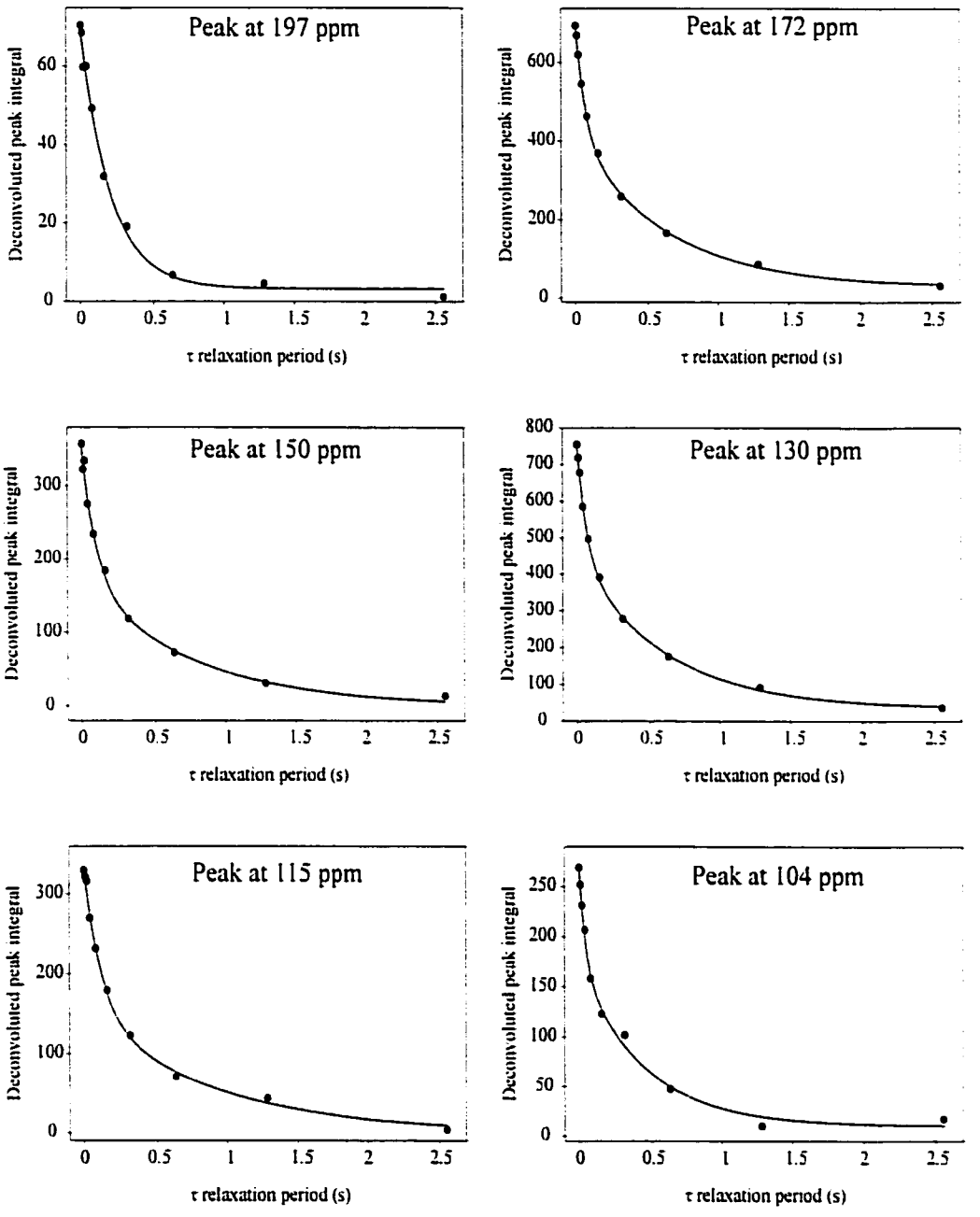

Figure 2.5(b) Experimental ^{13}C T_1 relaxation data for the humic acid fraction of the Uncompahgre soil and corresponding curve fits for the data of Figure 2.5. Each graph was generated by plotting the peak area of each deconvoluted peak of Figure 2.5A (featured in detail in the appendix of this thesis) versus the τ relaxation period. Graphical data are sorted by peak region in ppm. Curve fits using either a single or double component exponential decay are presented by a solid black line in each plot and overlay the experimental data, presented as solid black dots.

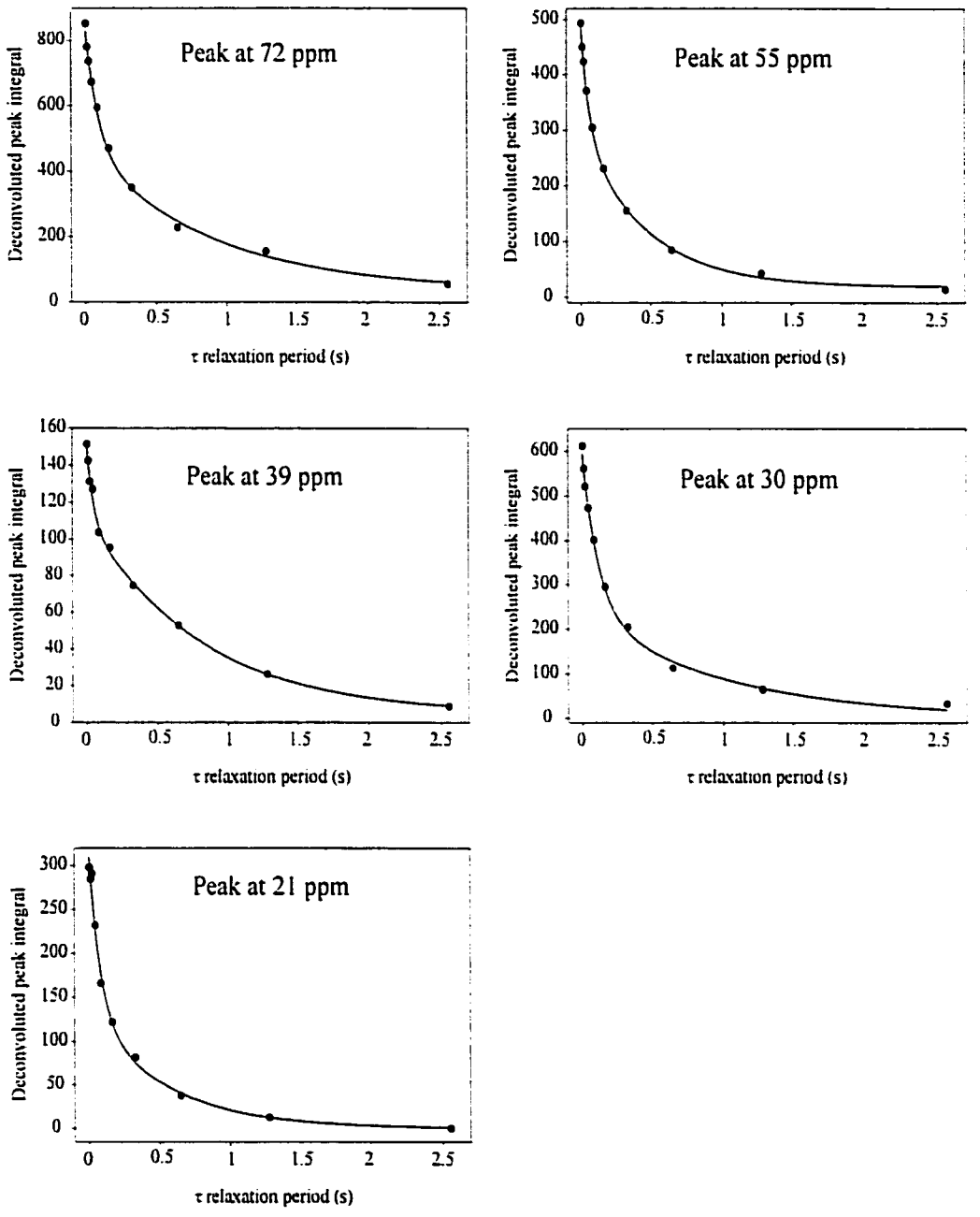

Figure 2.5(b) (continued).

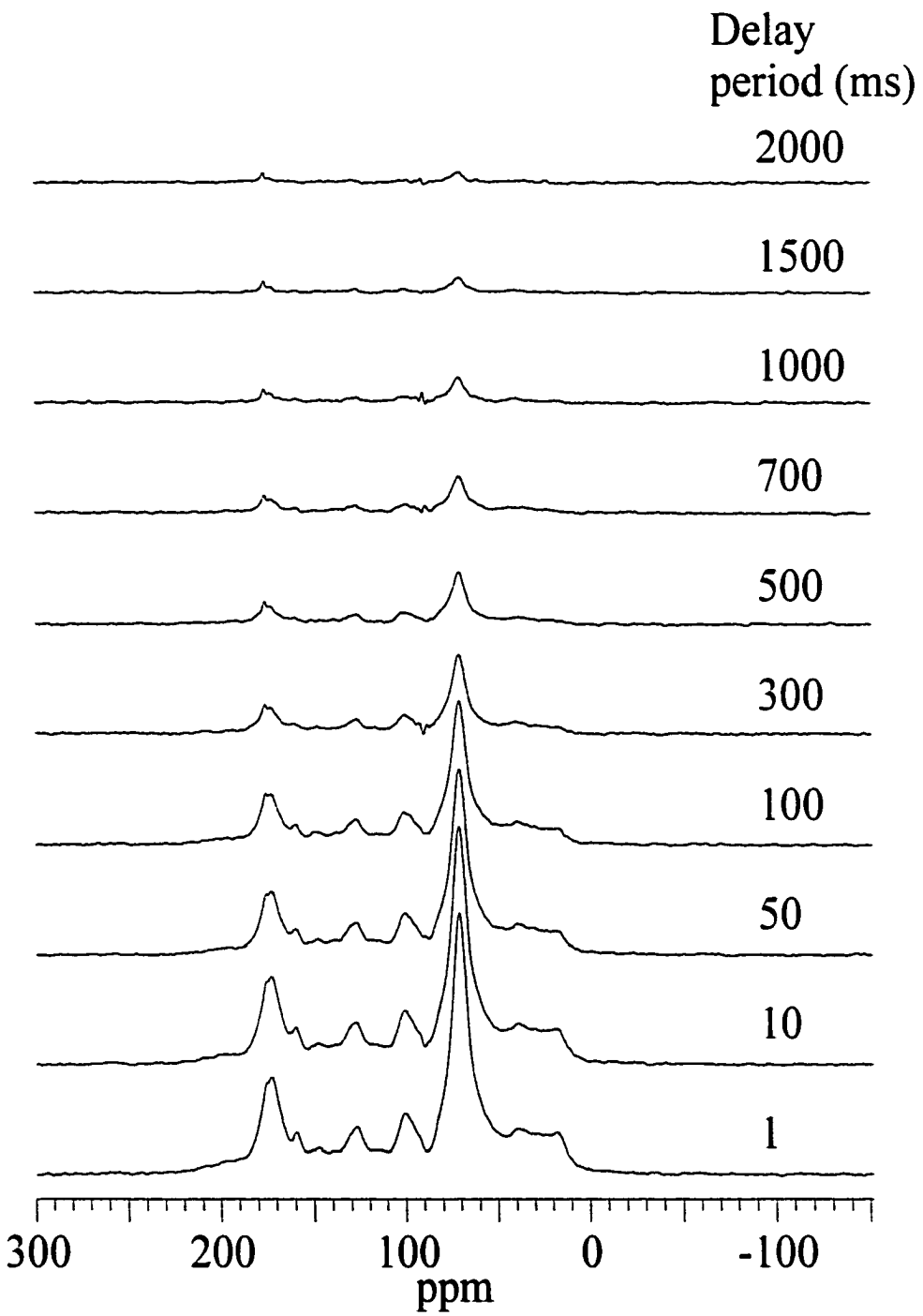

Figure 2.6(a) Carbon-13 T_1 measurement of Uncompahgre soil fulvic acid. The τ delay period is given to the right of each spectrum.

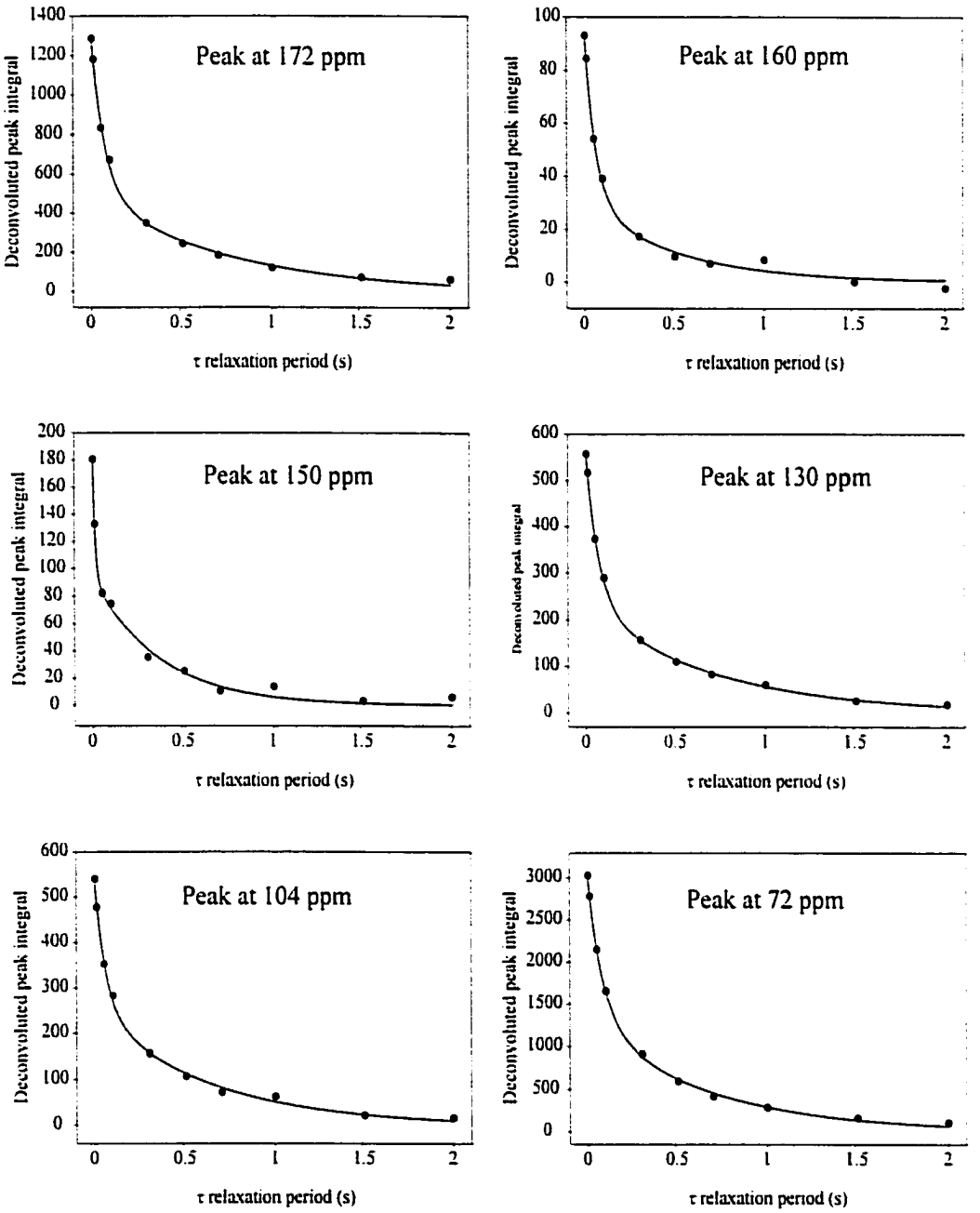

Figure 2.6(b) Experimental ^{13}C T_1 relaxation data for the fulvic acid fraction of the Uncompahgre soil and corresponding curve fits for the data of Figure 2.6. Each graph was generated by plotting the peak area of each deconvoluted peak of Figure 2.6A (featured in detail in the appendix of this thesis) versus the τ relaxation period. Graphical data are sorted by peak region in ppm. Curve fits using either a single or double component exponential decay are presented by a solid black line in each plot and overlay the experimental data, presented as solid black dots.

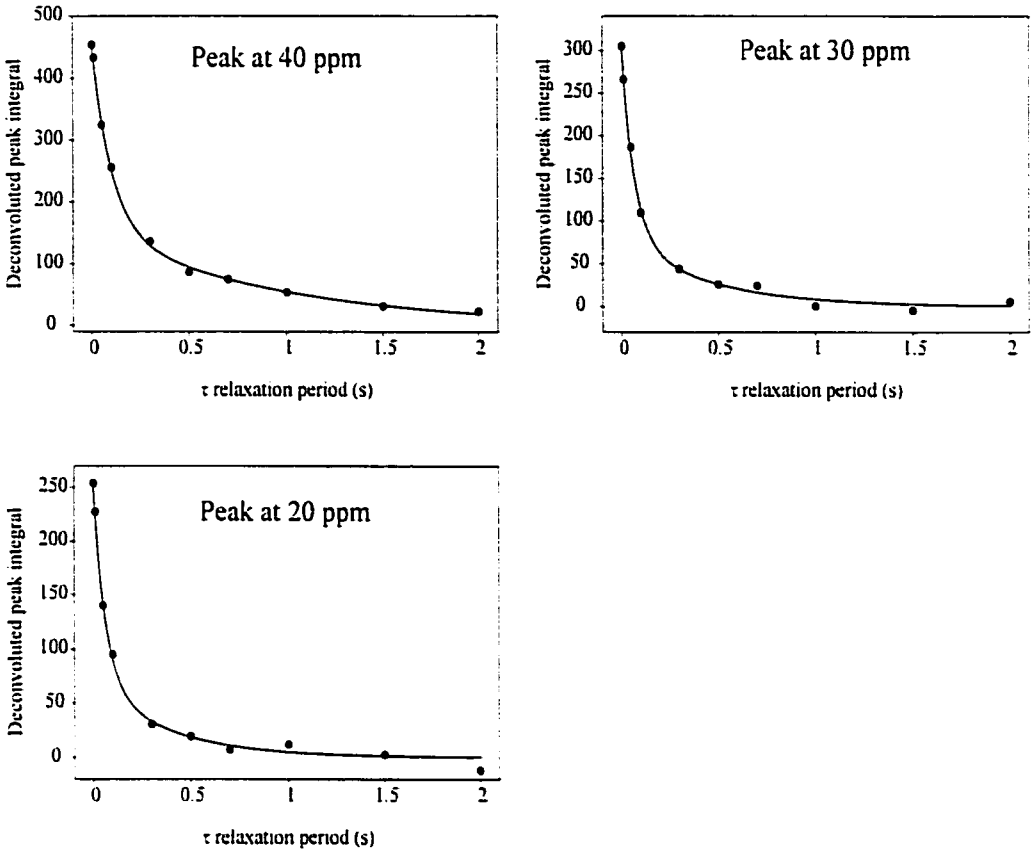

Figure 2.6(b) (continued).

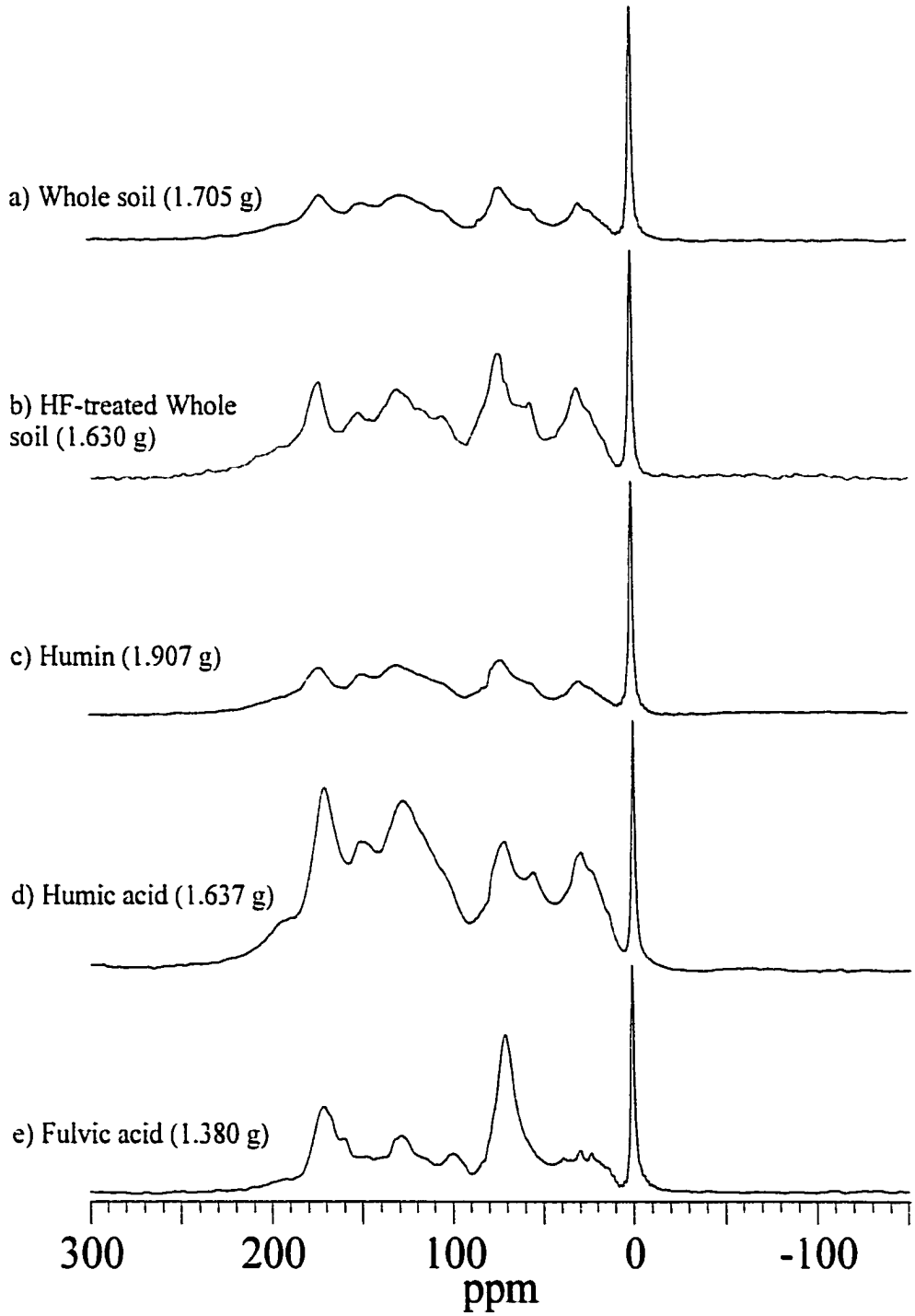

Figure 2.7 Carbon-13 DP-MAS spectra of Uncompahgre whole soil, HF-treated soil, and soil components. Each soil fraction has 79.5 mg silicone rubber (except the humic acid spectrum which was acquired with 85.9 mg silicone rubber) as an external reference and is referenced at 0 ppm. Each spectrum is scaled to an equal number of acquisitions.

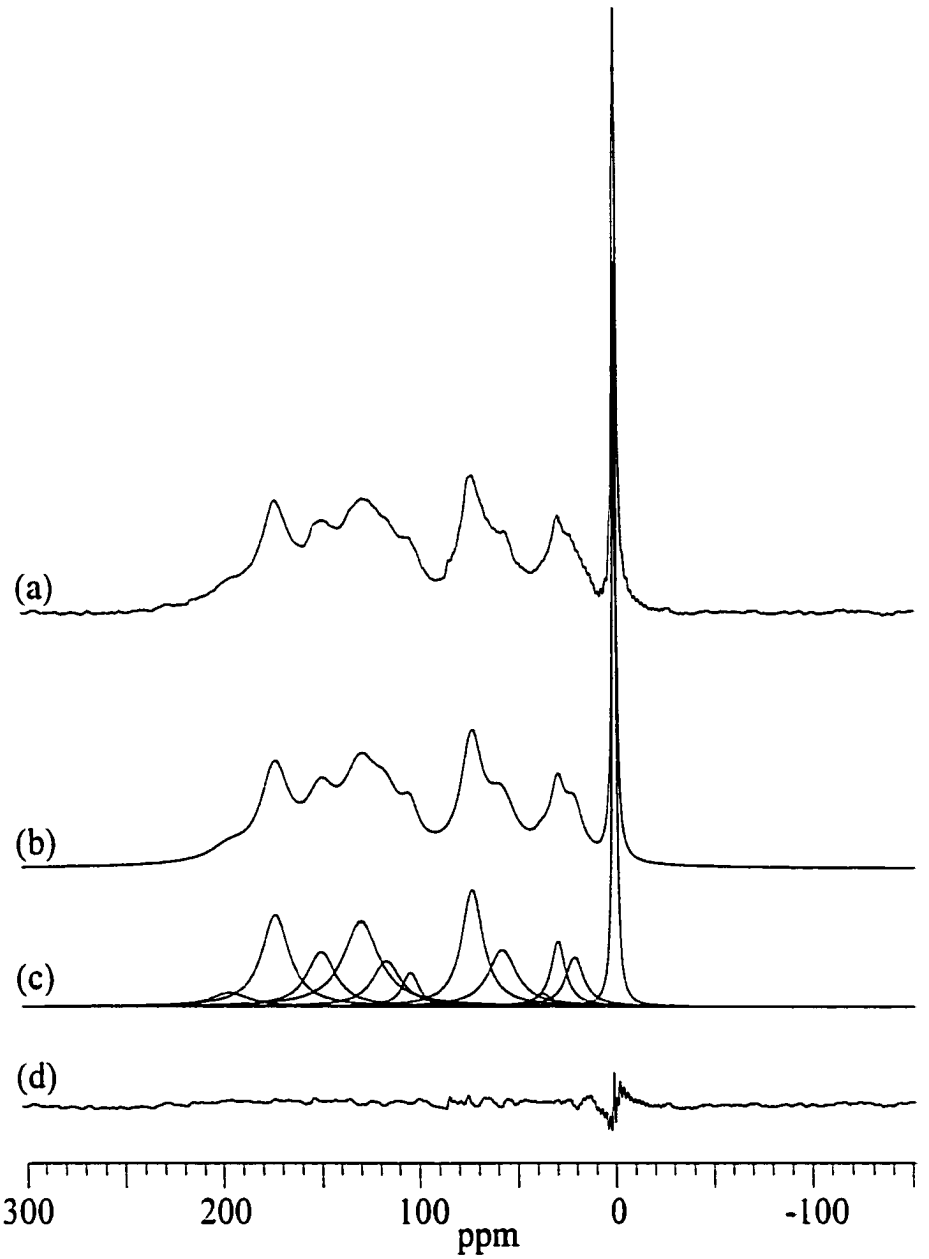

Figure 2.8 Carbon-13 DP-MAS spectrum of Uncompahgre whole soil (1.705 g) and 79.5 mg of silicone rubber external reference. The uppermost spectrum (a) represents the experimental spectrum. The result from the deconvolution of spectrum (a) is shown in (c) as individual peaks. The "synthetic" spectrum (b) is the sum of the peaks of (c). Spectrum (d) is the difference of spectrum (a) minus spectrum (b).

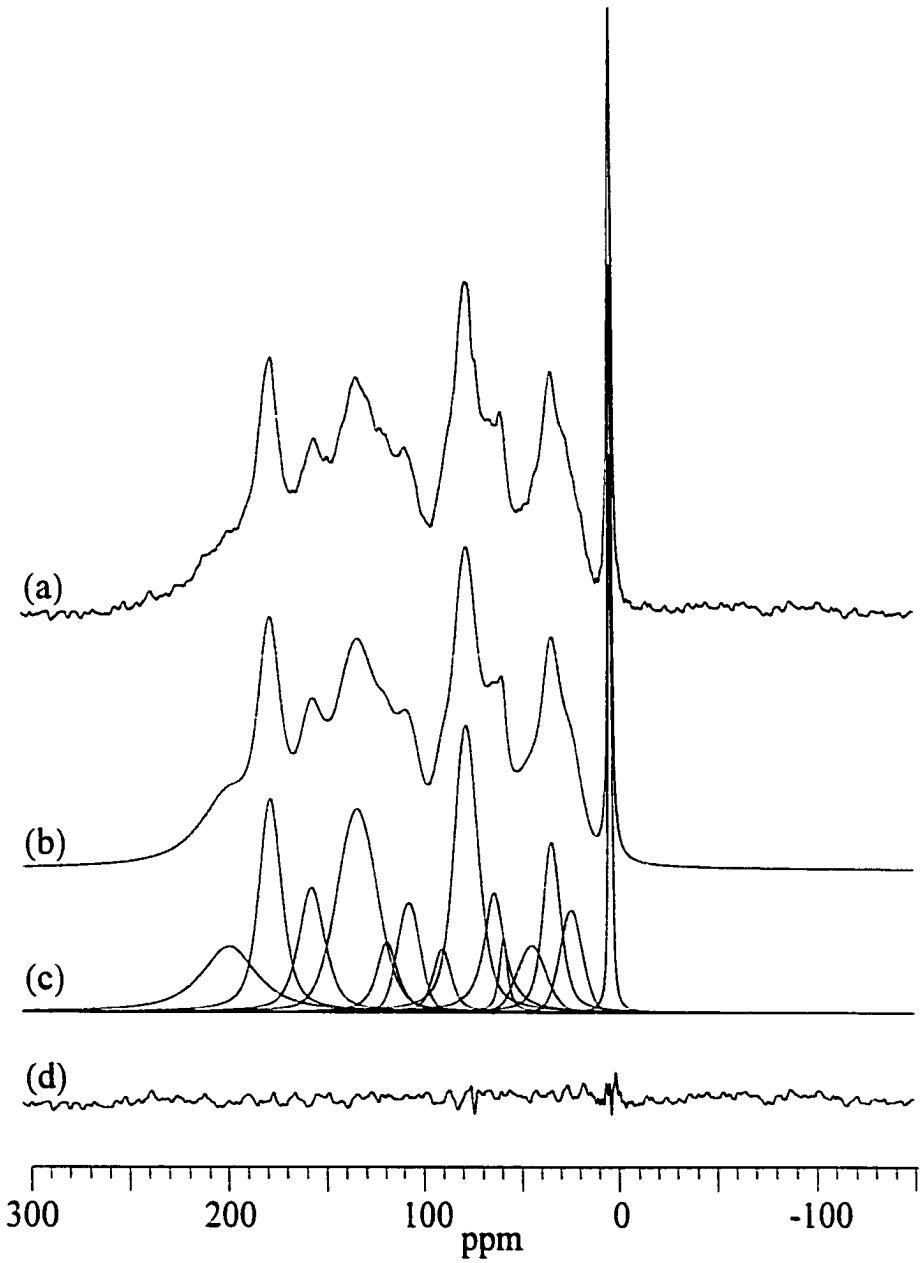

Figure 2.9 Carbon-13 DP-MAS spectrum of HF-treated Uncompahgre whole soil (1.630 g) and 79.5 mg of silicone rubber external reference. The uppermost spectrum (a) represents the experimental spectrum. The result from the deconvolution of spectrum (a) is shown in (c) as individual peaks. The "synthetic" spectrum (b) is the sum of the peaks of (c). Spectrum (d) is the difference of spectrum (a) minus spectrum (b).

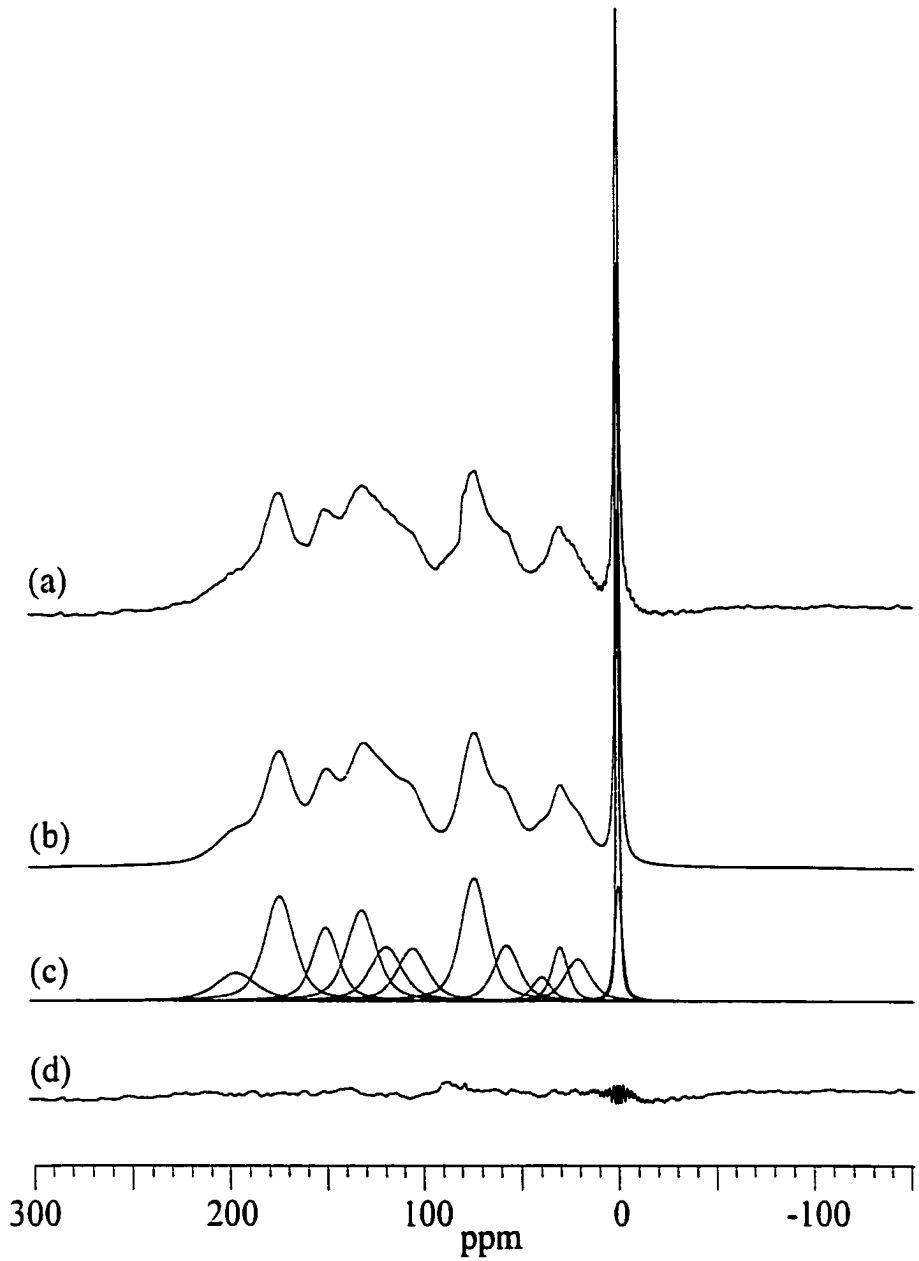

Figure 2.10 Carbon-13 DP-MAS spectrum of Uncompahgre humin (1.907 g) and 79.5 mg of silicone rubber external reference. The uppermost spectrum (a) represents the experimental spectrum. The result from the deconvolution of spectrum (a) is shown in (c) as individual peaks. The "synthetic" spectrum (b) is the sum of the peaks of (c). Spectrum (d) is the difference of spectrum a minus spectrum (b).

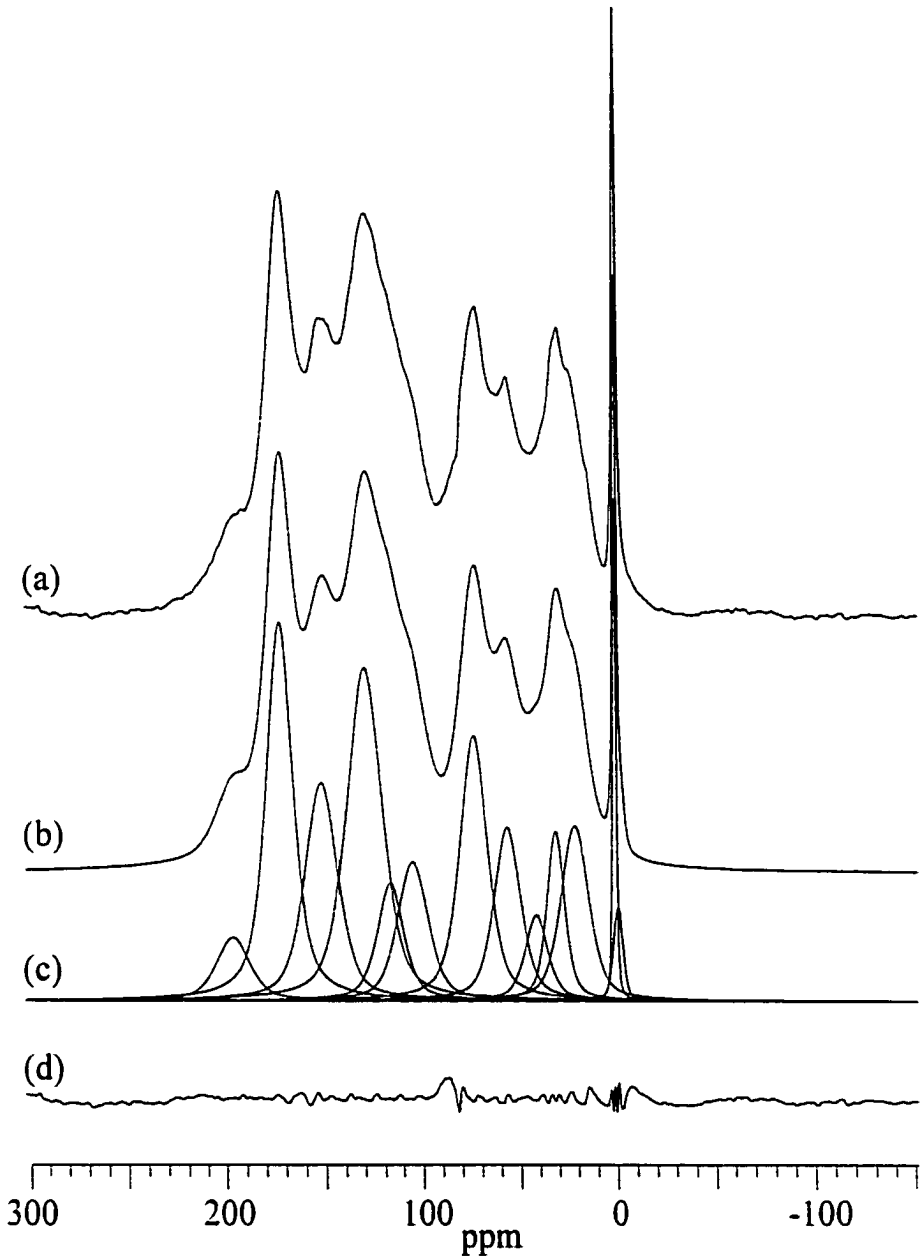

Figure 2.11 Carbon-13 DP-MAS spectrum of Uncompahgre humic acid (1.637 g) and 84.9 mg of silicone rubber external reference. The uppermost spectrum (a) represents the experimental spectrum. The result from the deconvolution of spectrum (a) is shown in (c) as individual peaks. The "synthetic" spectrum (b) is the sum of the peaks of (c). Spectrum (d) is the difference of spectrum a minus spectrum (b).

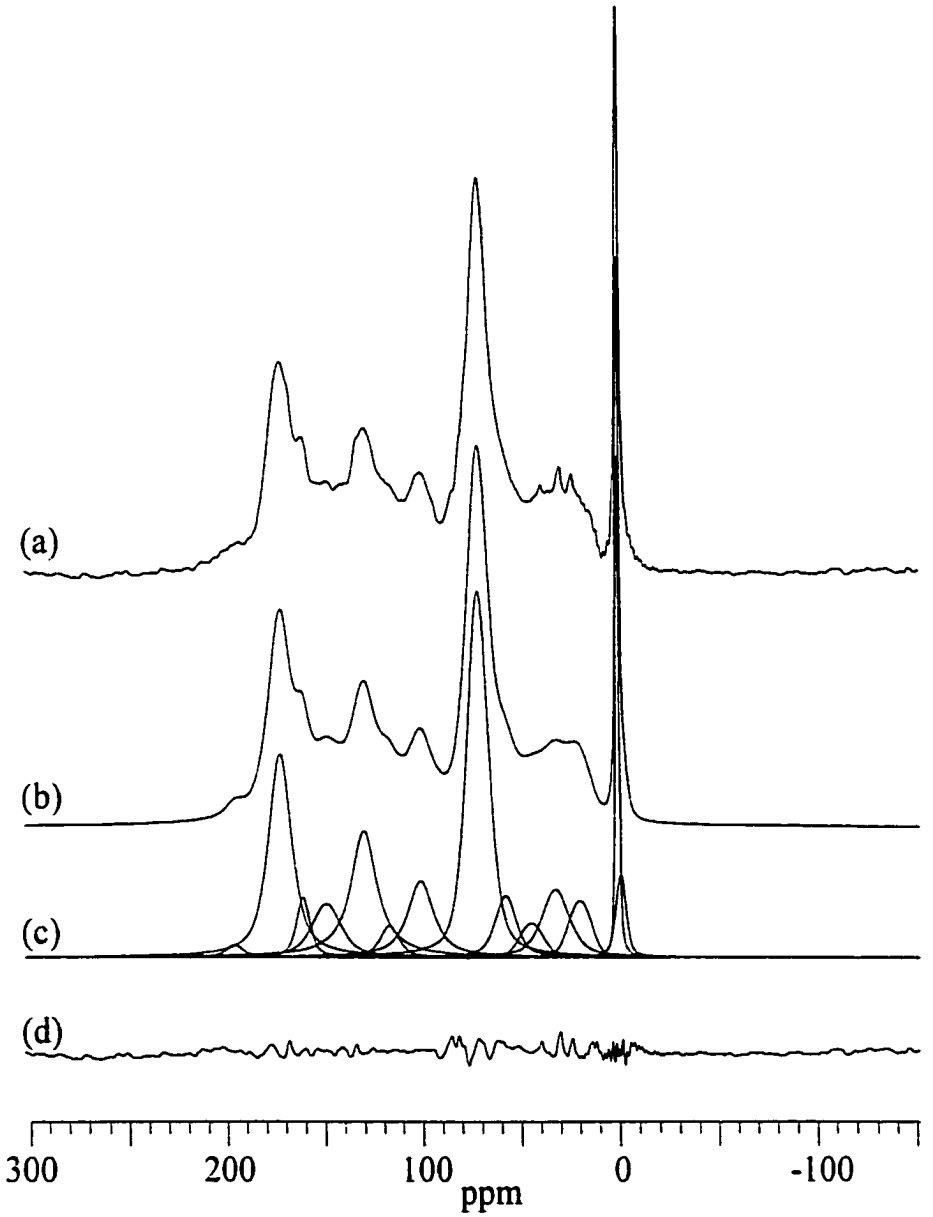

Figure 2.12 Carbon-13 DP-MAS spectrum of Uncompahgre fulvic acid (1.381 g) and 79.5 mg of silicone rubber external reference. The uppermost spectrum (a) represents the experimental spectrum. The result from the deconvolution of spectrum (a) is shown in (c) as individual peaks. The "synthetic" spectrum (b) is the sum of the peaks of (c). Spectrum (d) is the difference of spectrum (a) minus spectrum (b).

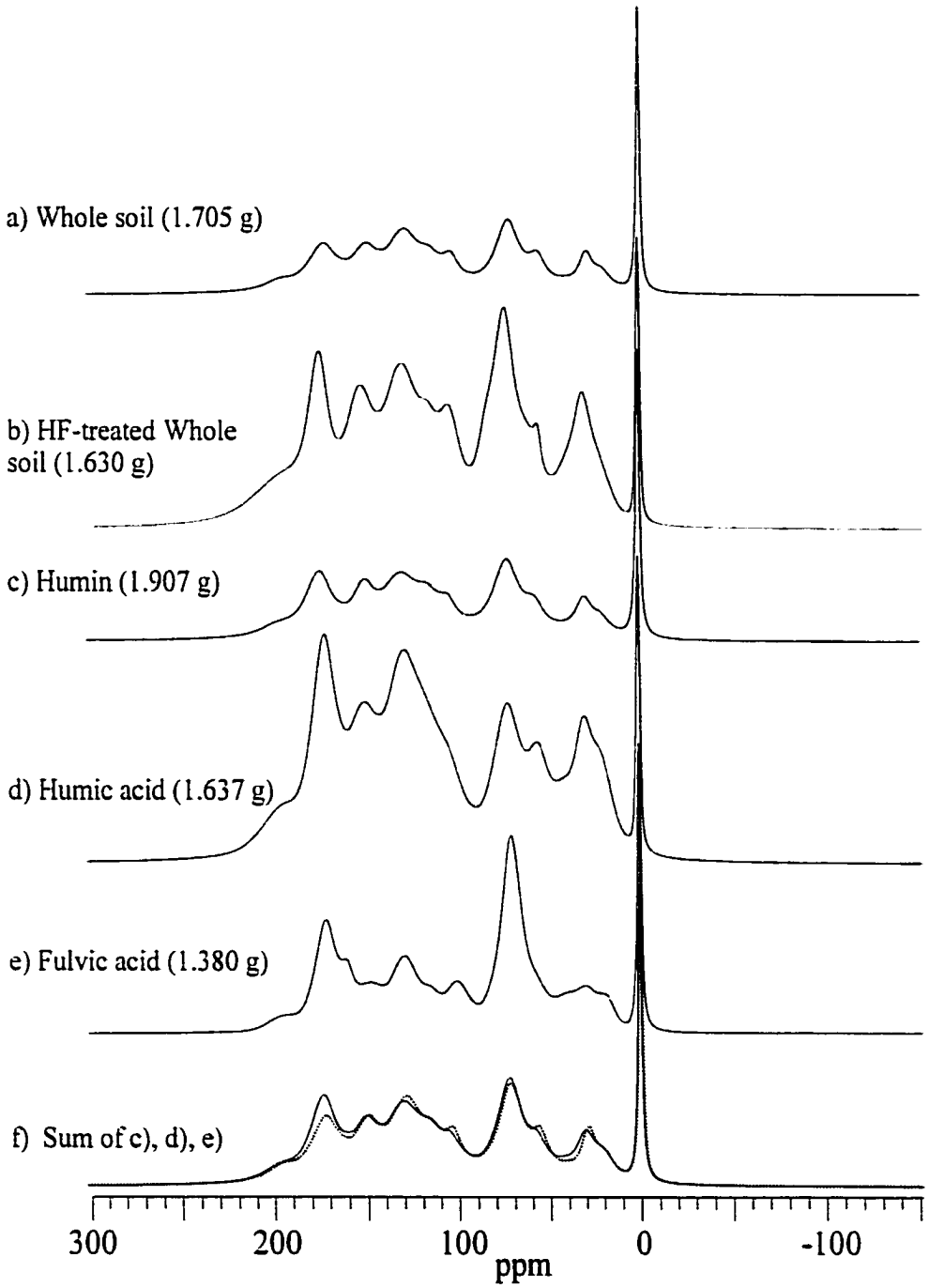

Figure 2.13 Computer generated "T_1 corrected" spectra of a) 1.705 g whole soil, b) 1.630 g HF-treated soil, c) 1.907 g humin fraction, d) 1.637 g humic acid, e) 1.380 g fulvic acid. Spectra a) through e) were created by taking the synthetic spectra of Figures 2.8 (b) through 2.12 (b) and applying the appropriate T_1 correction factors (C_{T_1}) to each deconvoluted peak needed to generate the total synthetic spectrum. Spectrum f) is a computer generated whole soil spectrum, created by summing the humin, humic, and fulvic spectra with amplitude corrections as demonstrated in the following relationship: ((0.782 x spectrum c) + (0.0929 x spectrum d) + (0.157 x spectrum e)). These amplitude corrections were made to reflect the actual amount of each fraction extracted from the whole soil and to correct for the different sample sizes. Spectrum f) also shows the spectrum of the whole soil (Fig. 2.13(a)) overlaid and plotted with a dotted line.

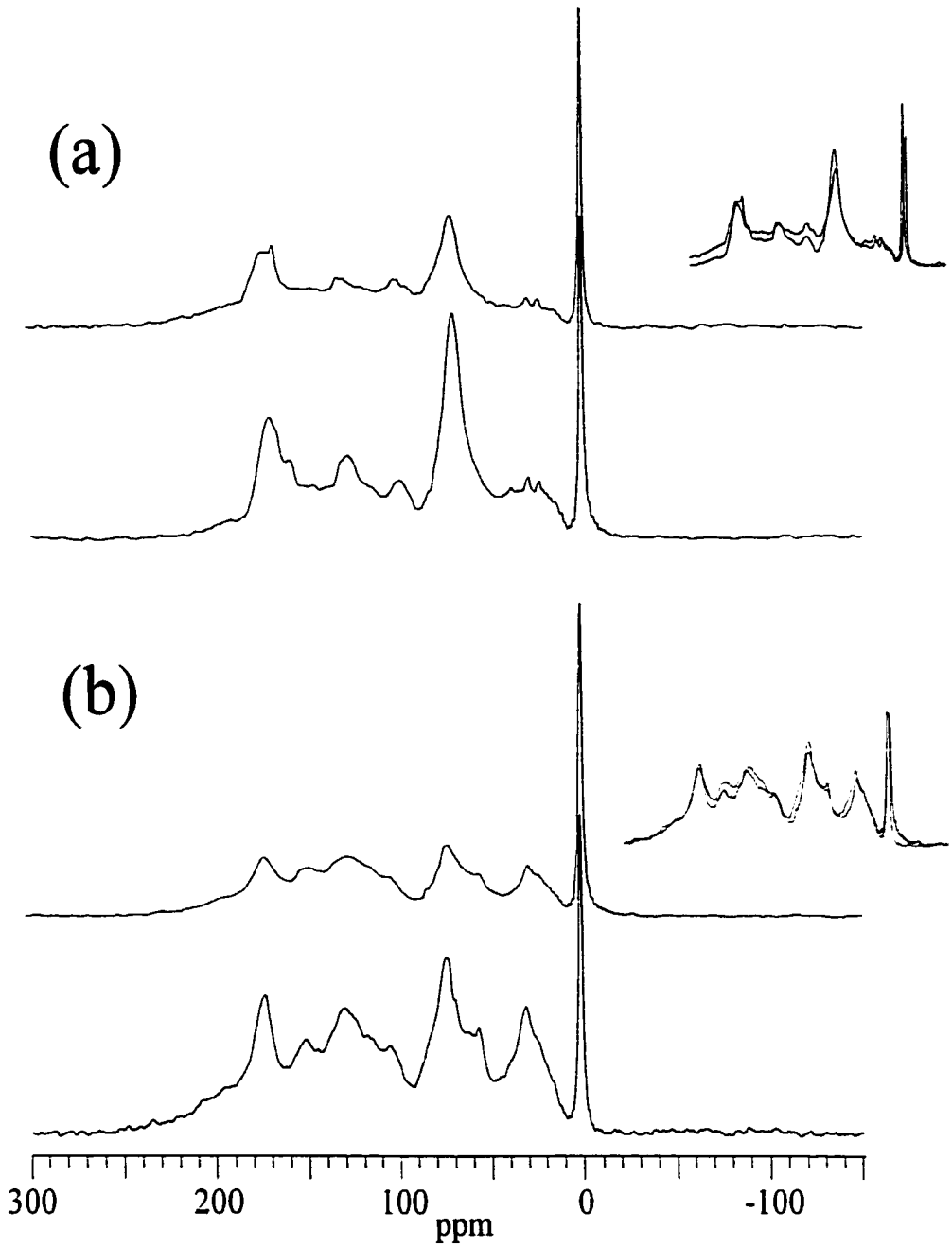

Figure 2.14 (a) Upper DP-MAS spectrum is of 1.287 g untreated fulvic acid with 79.5 mg silicone rubber; lower spectrum is of 1.381 g ion-exchange resin treated fulvic acid with 79.5 mg silicone rubber. Both fulvic acid spectra were scaled relative to the number of signal acquisitions. (b) Upper DP-MAS spectrum is of untreated Uncompahgre whole soil with 79.5 mg silicone rubber, 1.705 g sample size and the lower spectrum is of 1.63 g of hydrofluoric acid treated whole soil with 79.5 mg of silicone rubber as an external reference. Both spectra were scaled relative to the number of signal acquisitions. Floating above and to the right of each set of spectra are the two spectra overlaid (with arbitrary scaling) to show changes in spectral detail with the treatments.

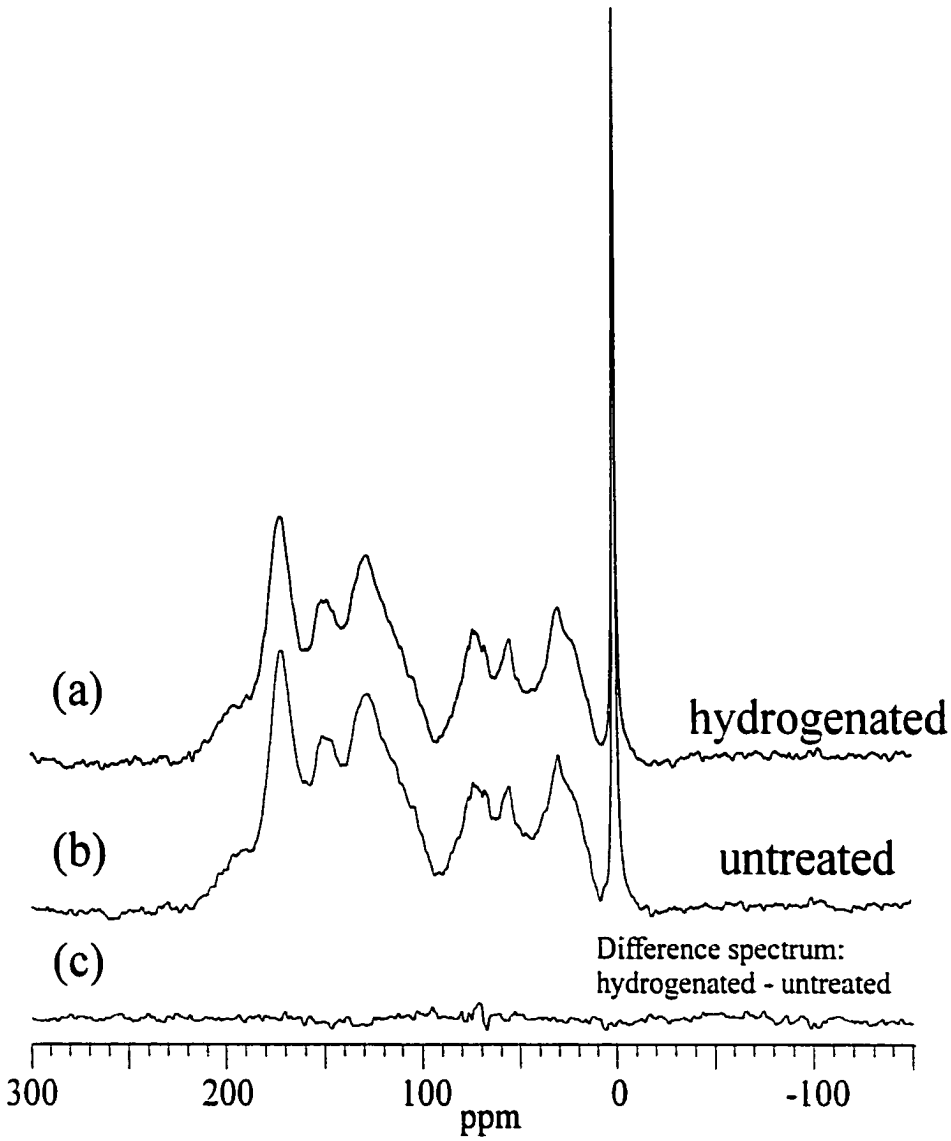

Figure 2.15 ^{13}C DP-MAS spectra of Humic acid (extracted in bulk from the Uncompahgre forest soil) (a) after a 3-day, 80 psi hydrogen treatment, (b) untreated, and (c) the difference of spectrum (a) - spectrum (b). Each experimental spectrum is of 1.142 g of dried sample with 79.5 mg of silicone rubber as an external reference. Each spectrum was obtained in a quantitative manner with a 16 s. pulse delay and 2400 acquisitions.

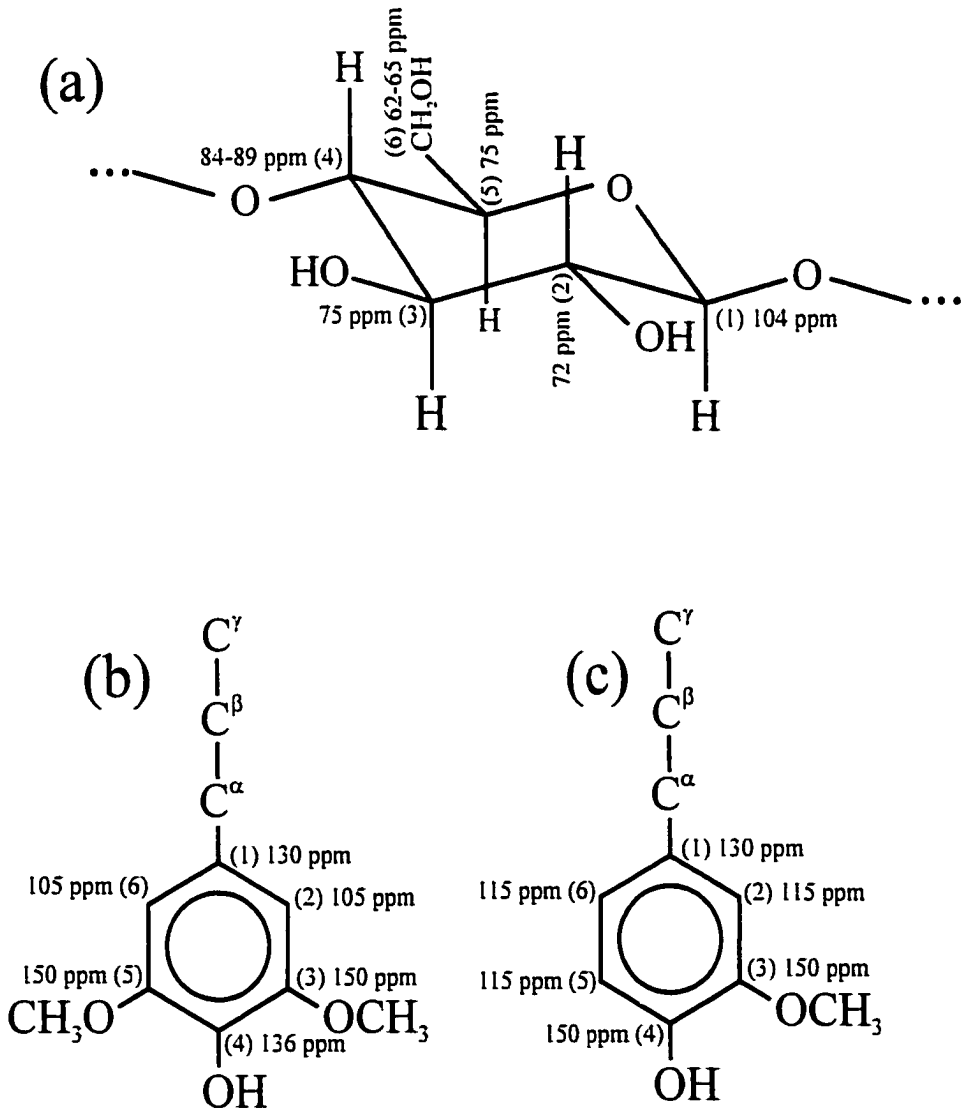

Figure 2.16 The basic structural units for (a) cellulose, (b) syringyl and (c) guaiacyl lignin building blocks. The structures have carbon positions labeled with numbers in parenthesis for reference within the text. Approximate ^{13}C NMR chemical shifts are given next to each corresponding carbon number.

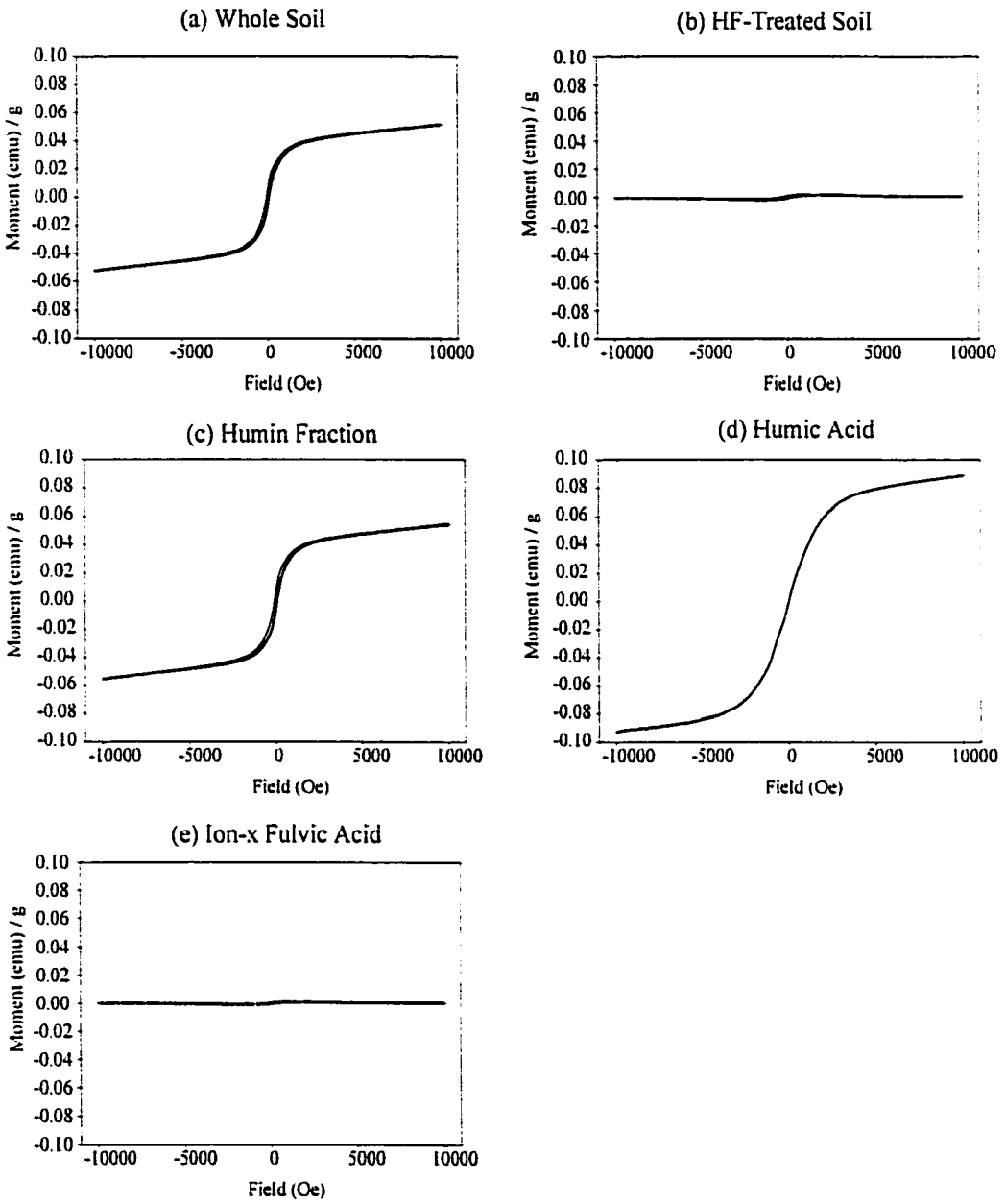

Figure 2.17 Experimental vibrating sample magnetometer data for the Uncompahgre whole soil and its extracts. Plots of the magnetic moment versus the applied external field for (a) the Uncompahgre whole soil, (b) the HF-treated whole soil, (c) the humin fraction, (d) the humic acid fraction, and (e) the fulvic acid fraction. The humic acid did not give reproducible VSM results; the data shown in the humic acid plot is believed to be the most representative.

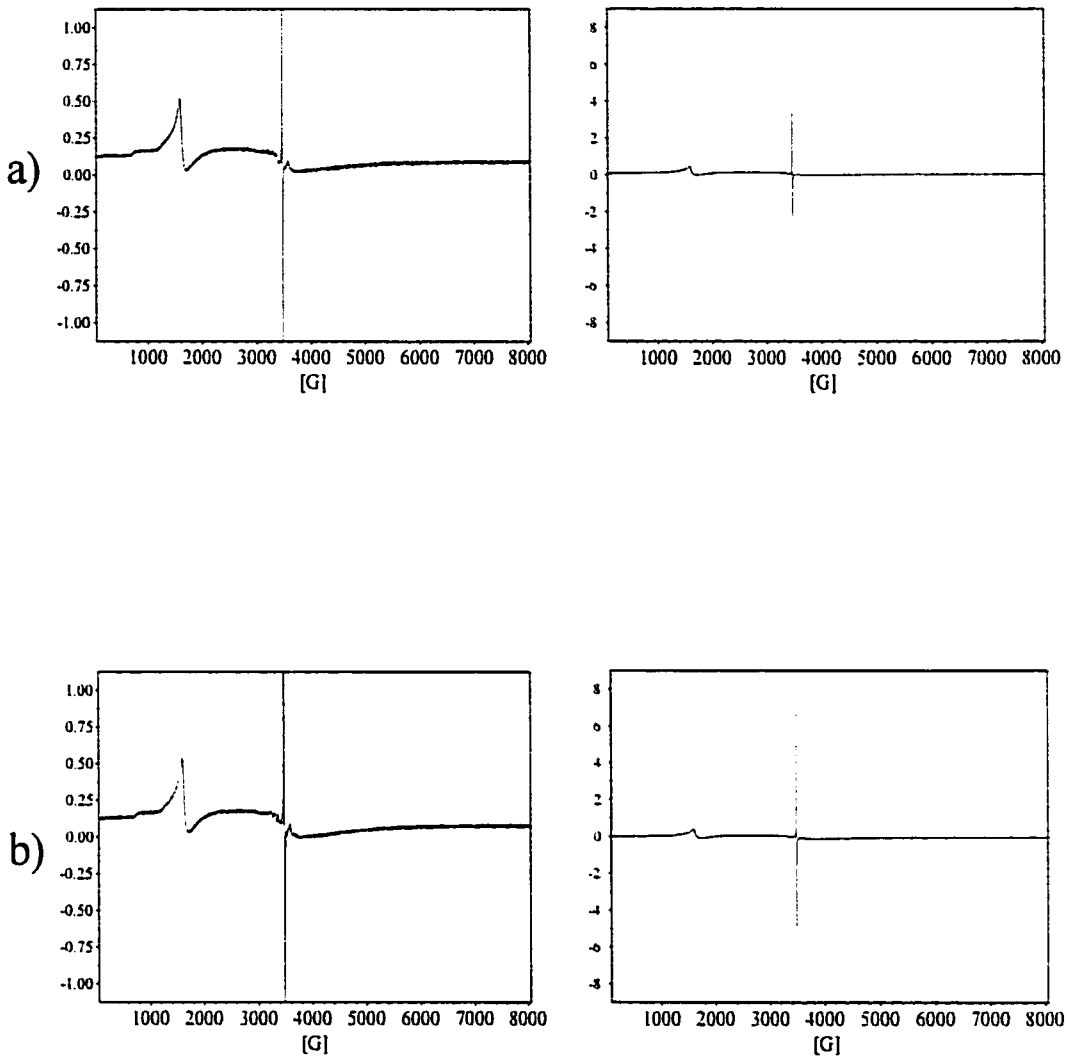

Figure 2.18 Electron spin resonance spectra of humic acid, a) before and b) after treatment with sodium dithionite as a reducing agent. The leftmost spectra are scaled in the amplitude dimension to show detail. The spectra were acquired with equal quantities of humic material and with identical instrumental parameters. Both samples were sealed under nitrogen to prevent air oxidation.

References

1. Gerothanassis, I. P. Methods of Avoiding the Effects of Acoustic Ringing in Pulsed Fourier Transform Nuclear Magnetic Resonance Spectroscopy, *Prog. NMR Spec.* **1987**, *19*, 267-329.

2. Stejskal, E. O.; Schaefer, J Removal of Artifacts from Cross-polarization NMR Experiments. *J. Magn. Reson.* **1975**, *18*, 560-3.

3. Hatcher, P. G.; Breger, I. A.; Dennis, L. W.; Maciel, G. E. "Solid-state ^{13}C NMR of Sedimentary Humic Substances: New Revelations on Their Chemical Composition" in Terrestrial and Aquatic Humic Materials, R.F. Christman and O. Gjessing, eds., Ann Arbor Science Press, **1983**, p. 47.

4. Torchia, D. A. The Measurement of Proton-Enhanced Carbon-13 T_1 Values by a Method Which Suppresses Artifacts. *J. Magn. Reson.* **1978**, *30*, 613-616.

5. Fukushima, E.; Roeder, S. B. W. Relaxation. *Experimental Pulse NMR*. Addison-Wesley: Reading, MA, 1981; pp 125-216.

6. Tan, K. H. Principals of Soil Chemistry, 3nd Ed., M. Dekker, New York. 1998.

7. Horii, F.; Hirai, A.; Kitamaru, R. CP/MAS carbon-13 NMR study of spin relaxation phenomena of cellulose containing crystalline and noncrystalline components. *J. Carbohydr. Chem.* **1984**, *3*, 641-662.

8. Teeaar, R.; Lippmaa, E. Solid State carbon-13 NMR of cellulose. A relaxation study. *Polym. Bull.* **1984**, *12*, 315-318.

9. Newman, R. H.; Hemmingson, J. A. Carbon-13 NMR distinction between categories of molecular order and disorder in cellulose. *Cellulose* **1994**, *2*, 95-110.

10. Maciel, G. E.; Kolodziejski, W, L.; Bertran, M. S.; Dale, B. E. ^{13}C NMR and Order in Cellulose *Macromolecules* **1982**, *15*, 686-687.

11. Metson, A. J.; Blakemore, L. C.; Rhoades, D. A. Methods for the determination of soil organic carbon: a review, and application to New Zealand soils. *New Zealand J. Sci.* **1979**, *22*, 205-28.

12. Tabatabai, M. A. Soil Organic Matter Testing: An Overview. In *Soil Organic Matter: Analysis and Interpretation.* SSSA Special Publication no. 46; Soil Science Society of America: Madison, WI, **1996**, 1-9.

13. Matejovic, I. Determination of carbon, hydrogen, and nitrogen in soils by automated elemental analysis (dry combustion method). *Commun. Soil Sci. Plant Anal.* **1993**, *24*, 2213-2222.

14. Jimenez, R. R.; Ladha, J. K.; Automated Elemental Analysis: A rapid and reliable but expensive measurement of total carbon and nitrogen in plant and soil samples. *Commun. Soil Sci. Plant Anal.* **1993,** *24*, 1897-1924.

15. Malcolm, R. L. The Uniqueness of humic substances in each of soil, stream and marine environments. *Anal. Chim. Acta.* **1990**, *232*, 19-23.

16. Mao, J-D.; Hu, W.; Schmidt-Rohr, K.; Davies, G.; Ghabbour, E. A.; Xing, B. Quantitative Characterization of Humic Substances by Solid-State Carbon-13 Nuclear Magnetic Resonance. *Soil Sci. Soc. Am. J.* **2000**, *64*, 873-884.

17. Mao, J.; Hu, W.; Schmidt-Rohr, K.; Davies, G.; Ghabbour, E. A.; Xing, B. Structure and Elemental Composition of Humic Acids: Comparison of Solid-State 13C NMR Calculations and Chemical Analyes. *Royal Soc. Chem., G. Britain* **1999**, *228*, 79-90.

18. Hatfield, G. R.; Maciel, G. E.; Erbatur, O.; Erbatur, G. Qualitative and Quantitative Analysis of Solid Lignin Samples by Carbon-13 Nuclear Magnetic Resonance Spectrometry. *Anal. Chem.* **1987**, *59*, 172-179.

19. Guggenberger, G. ; Zech, W. ; Haumaier, L. ; Christensen, B. T. Land-use Effects on the Composition of Organic Matter in Particle-size Separates of Soils: II. CPMAS and Solution 13C NMR Analysis. *Euro. J. Soil Sci.* **1995**, *46*, 147-158.

20. Maciel, G. E., Haw, J. F., Smith, D. H., Gabrielsen, B. C., Hatfield, G. R., Carbon-13 nuclear magnetic resonance of herbaceous plants and their components using cross polarization and magic angle spinning, *J. Ag. and Food Chem.* **1985**, *33*, 185-191.

21. Watanabe, A., TsuTsuki, K., Kuwatsuka, S., 13C NMR Investigation of Humic and Fulvic Acids Obtained from some Typical Japanese Soils, *Sci. Tot. Environ.* **1989**, *81-82*. 195-200.

22. Preston, C. M. The Application of NMR to Organic Matter Inputs and Processes in Forest Ecosystems of the Pacific Northwest, *Sci. Tot. Environ.* **1992**, *114*, 107-120.

23. Pfeffer, P. E.; Gerasimowicz, W. V.; Piotrowski, E. G. Effect of paramagnetic iron on quantitation in carbon-13 cross polarization magic angle spinning nuclear magnetic resonance spectrometry of heterogeneous environmental matrices. *Anal. Chem.* **1984**, *56*. 734-741.

24. Vassallo, A. M.; Wilson, M. A.; Collin, P. J.; Oades, J. M.; Waters, A. G.; Malcolm, R. L. Structural analysis of geochemical samples by solid-state nuclear magnetic resonance spectometry. Role of paramagnetic material. *Anal. Chem.* **1987**, *59*, 558-562.

25. Arshad, M. A.; Ripmeester, J. A.; Schnitzer, M. Attempts to improve solid state ^{13}C NMR spectra of whole mineral soils. *Can. J. Soil Sci.* **1988,** *68*, 593-602.

26. Holmgren, G. G. S. A Rapid Citrate-Dithionite Extractable Iron Procedure. *Soil Sci. Soc. Am. Proc.* **1967**, *31*, 210-211.

27. Skjemstad, J. O.; Clarke, P.; Taylor, J. A.; Oades, J. M.; Newman, R. H. The Removal of Magnetic Material from Surface Soils. A Solid State ^{13}C CP/MAS n.m.r. Study. *Aust. J. Soil Res.* **1994**, *32*, 1215-1229.

28. Preston, C. M.; Schnitzer, M.; Ripmeester, J. A. A Spectroscopic and Chemical Investigation on the De-ashing of a Humin. *Soil Sci. Soc. Am. J.* **1989**, *53*, 1442-1447.

29. Chikazumi, S. *Physics of Ferromagnetism*, Oxford Press, New York, NY, **1997**, pp. 110-117.

30. Chikazumi, S. *Physics of Magnetism*, John Wiley & Sons, New York, NY, **1963**, p. 100.

31. Foner, S. Versatile and Sensitive Vibrating-Sample Magnetometer. *Rev. Sci. Instru.* **1959**, *30*, 548-557.

32. Chikazumi, S. *Physics of Magnetism*, John Wiley & Sons, New York, NY, **1963**, pp. 15-35.

33. Senesi, N. Application of Spin Resonance (ESR) Spectroscopy in Soil Chemistry. In *Advances in Soil Science*; Volume 14; Springer-Verlag, New York,1990, pp. 77-130.

34. Adhikari, M.; Chakrabarti, K. K.; Chakrabarti, G. Infra-red studies on humic and fulvic acid complexes with metal salts and their sols. *Sci. Cult.* **1978**, *44*, 287-8

35. Byler, D. M.; Gerasimowicz, W. V.; Susi, H.; Schnitzer, M. FT-IR spectra of soil constituents: Fulvic acid and fulvic acid complex with ferric ions. *Appl. Spectosc.* **1987**, *41*, 1428-30.

36. Senesi, N.; Sposito, G.; Martin, J. P. Copper(II) and Iron(III) Complexation by Soil Humic Acids: An IR and ESR Study. *Sci. Tot. Environ.* **1986**, *55*, 351-362.

37. Senesi, N.; Griffith, S. M.; Schnitzer, M. Binding of Fe^{3+} by humic materials. *Geochim. Cosmochim. Acta* **1977**, *41*, 969-976.

38. Senesi, N. Application of electron spin resonance and fluorescence spectroscopy to the study of soil humic substances. *Dev. agric. managed-for. ecol.* **1992**, *25*, 11-26.

39. Cheshire, M. V.; McPhail, D. B. Hyperfine splitting in the electron spin resonance solution spectra of humic substances. *Euro. J. Soil Sci.* **1996**, *47*, 205-213.

40. Cheshire, M. V.; Goodman, B. A.; McPhail, D. B.; Sparling, G. P. Electron paramagnetic resonance characteristics of the humic acids from a podzol. *Org. Geochem.* **1985**, *8*, 427-440.

Chapter 3

SOLID STATE NMR STUDIES OF UNCOMPAHGRE FOREST SOIL AND ITS SEPARATED SOIL COMPONENTS BY ^{1}H-TO-^{13}C CP-MAS SPIN-COUNTING METHODS

3.1 Introduction

Of the available solid state NMR methods, the cross-polarization magic angle spinning (CP-MAS) technique is the most popular for the analysis of soils and their extracts and samples of organic-geochemical origin. The CP-MAS experiment provides a significant signal-to-noise enhancement over the DP-MAS experiment described in Chapter 2 of this thesis. While technically more straightforward, ^{13}C DP-MAS experiments suffer from the typically long ^{13}C T_1 relaxation times of soil and soil components. The short ^{1}H T_1 relaxation times of soil and soil components allow for a greater number of CP-MAS signal acquisitions in a given period of time over DP-MAS. This advantage, coupled with a maximum cross-polarization enhancement factor of four, makes CP-MAS the typical first choice of solid state ^{13}C NMR experiments for soil and soil extracts. Moreover, CP-MAS experiments on soil and soil components rarely suffer from the baseline distortions commonly encountered in DP-MAS experiments.

Spin counting by CP-MAS has been completed on a number of complex organic samples, including coals and cellulose chars[1-10]. CP-MAS spin counting on coals of various ranks was able to account for a low of 50 percent of the carbon[2], to as much as 97 percent[5], compared to that from elemental analysis. The missing carbon has been correlated to the concentration of unpaired electrons[11] (in the form of organic radicals), and in some cases attributed to the nature of the protons in the organic structures in coal and their location relative to carbons[2]. While some of the issues that plague quantitative analysis of coals by NMR parallel those in soil, the clear difference in chemical make-up forces an independent analysis for solving this problem in soil analysis.

An extensive literature search shows that there have been no spin-counting results to date on soil and soil extracts by ^{13}C CP-MAS NMR, with the exception of a study by Vassallo et al.,[12] in which spin-counting was attempted on Swannee River fulvic acid. While there have been few quantitative spin-counting NMR results on soil components reported in the literature, there have been a number of studies with corrections made to the CP intensities of CP-MAS experiments on soils and soil extracts, ostensibly yielding relative quantitative spectral intensities[13-15]. This is the precursor to *absolute* quantitative results on soil and soil extracts. The CP-MAS studies presented in this chapter will extend beyond the relative quantitative corrections made to spectra and into the absolute quantification of carbon in soil and soil extracts. The results reported in this chapter are compared to the spin-counting DP-MAS results of Chapter 2. Tables and figures are collected at the end of the text in this chapter for convenience.

3.2 Results

3.2.1 ^{1}H Spin-Lattice Relaxation Times (T_1) for the Uncompahgre Forest Soil and its Extracts

^{1}H T_1 values were determined via ^{13}C signals by a ^{1}H version of the Torchia-style pulse-program,[16] for which the ^{13}C intensities are plotted versus the τ delay period. The ^{13}C spectra obtained in the ^{1}H T_1 determinations for each soil component are shown in Figures 3.1-3.5 for the whole soil, HF-treated soil, humin, humic acid and fulvic acid, respectively. These relaxation data indicate that all the ^{13}C signals generated by ^{1}H-^{13}C cross-polarization for each soil component have decayed almost into the noise within about 300 ms, which is much shorter than the 1 s pulse delay employed in the CP-MAS spin counting experiments used here; hence, no ^{1}H T_1 based correction (C_{T_1}) to the peak intensities in the soil or soil components is necessary. For this reason, the spectra in Figures 3.1-3.5 were not deconvoluted or further examined.

3.2.2 Time Constants and Correction Terms for Spin-Counting by ^{13}C CP-MAS

Algebraic corrections are needed when seeking to make quantitative comparisons among peak areas by cross-polarization (CP) spin-counting experiments. The corrections (A_{corr}^{DP}) to the deconvoluted peak areas of the ^{13}C DP-MAS spin-counting spectra in Chapter 2 are based on the relaxation times of the ^{13}C nuclei for each corresponding peak (Eqs. 2.1, 2.2, 2.3). This kind of correction based on longitudinal relaxation also applies to ^{1}H-to-^{13}C CP spin-counting experiments, but in this case using the T_1 for the nucleus from which polarization is generated (in our case, ^{1}H). The ^{1}H T_1's for the whole soil

and its extracts are significantly shorter than the ^{13}C T_1's of the same samples. Approximately 99 percent of the ^1H magnetization appears to be lost after delay periods of 360 ms for the whole soil (Fig. 3.1), 200 ms for HF-treated whole soil (Fig. 3.2), 200 ms for humin (Fig. 3.3), 200 ms for humic acid (Fig. 3.4) and 50 ms for fulvic acid (Fig. 3.5). In all of the CP spin-counting experiments on the soil and its extracts, repetition delays of 1 s were used, removing the need to make ^1H T_1 corrections to deconvoluted peak areas of CP-MAS spin-counting experiments on soil and soil components. The ^1H T_1 of the external reference is significantly longer (0.78 s) than that of the soil and its extracts and hence requires a correction to its deconvoluted peak area in CP-MAS spin-counting experiments. In addition to the T_1 correction (C_{T_1}) for the ^{13}C CP-MAS spin-counting peak of the reference material, a correction is needed to compensate for the unique cross-polarization (C_{CP}) dynamics of each deconvoluted peak. The ^{13}C CP-MAS spin-counting peak areas (A_{exp}^{CP}) of the various soil-component peaks and of the ^{13}C labeled [3.2.1] bicyclo compound were corrected on the basis of equations 3.1-3.6.

$$A_{corr}^{CP} = (A_{exp}^{CP})(C_{T_1})(C_{CP}) \qquad (3.1)$$

where

$$C_{T_1} = \frac{1}{\left(1 - e^{-t_d / T_{1H}}\right)} \qquad (3.2)$$

Relative to a direct-polarization experiment, cross-polarization can generate a maximum signal enhancement equal to the ratio of the gamma values for the nuclei involved in the polarization transfer (in the case of ^1H-to-^{13}C cross polarization, this ratio is 3.98). The rate of growth and decay of that enhancement during the cross-polarization period is governed by two characteristic times (inverse of corresponding first order rate

constants), T_{CH} and $T_{1\rho}$. The time constant T_{CH} describes ^{1}H-to-^{13}C polarization transfer process leading to the growth of the ^{13}C magnetization along the ^{13}C RF field axis and $T_{1\rho}^{H}$ describes the decay of the spin-locked proton magnetization during cross-polarization. The maximum cross-polarization enhancement factor would be obtained with an infinitely short T_{CH} and infinitely long $T_{1\rho}^{H}$. The theoretical maximum for a particular cross-polarization enhanced peak is referred to here as its "M infinity" (typically shown as M^{∞} or $M^{\bullet}$) value. Every cross-polarization enhanced peak in an experimental spectrum will have one $M^{\bullet}$ value, which is the number that is directly proportional to the corresponding number of nuclei – i.e., the quantity we seek for *quantitative* analysis. The relationship between $M^{\bullet}$ and the CP-generated magnetization *M(t)* for a specific CP period *t* is given in terms of the cross-polarization time constants in equation 3.3[17]

$$M^{\bullet} = \frac{M(t)}{\left(\frac{1}{(1 - T_{CH}/T_{1\rho}^{H})}\right)\left(e^{-t/T_{1\rho}}\right)\left(1 - e^{-t/T_{CH}}\right)} \qquad (3.3)$$

where T_{CH} and $T_{1\rho}$ are the aforementioned time constants. In the case where two exponential factors are needed to describe the cross-polarization process corresponding to a specific peak, equation 3.4 applies:

$$M^{\bullet} = \frac{M(t)}{\left(\left(\frac{\beta}{(1 - T_{CH(1)}/T_{1\rho(1)}^{H})}\right)\left(e^{-t/T_{1\rho(1)}^{H}}\right)\left(1 - e^{-t/T_{CH(1)}}\right)\right) + \left(\left(\frac{(1-\beta)}{(1 - T_{CH(2)}/T_{1\rho(2)}^{H})}\right)\left(e^{-t/T_{1\rho(2)}^{H}}\right)\left(1 - e^{-t/T_{CH(2)}}\right)\right)} \qquad (3.4)$$

where β is the fraction of component 1, and $T_{CH(1)}$, $T_{CH(2)}$, $T_{1\rho(1)}$, and $T_{1\rho(2)}$ are the relevant time constants for both components. The corresponding correction factors (C_{CP}) for equations 3.3 and 3.4 are shown below in equations 3.5 and 3.6, respectively. For the

case where a single exponential can be used to describe cross polarization for a specific peak,

$$C_{CP} = \frac{1}{\left(\frac{1}{(1 - T_{CH} / T_{1\rho}^{H})}\right)\left(e^{-t/T_{1\rho}}\right)\left(1 - e^{-t/T_{CH}}\right)} \tag{3.5}$$

and for cases where more than one exponential time constant is needed to describe the cross-polarization behavior,

$$C_{CP} = \frac{1}{\left(\left(\frac{\beta}{(1 - T_{CH(1)} / T_{1\rho(1)}^{H})}\right)\left(e^{-t/T_{1\rho(1)}^{H}}\right)\left(1 - e^{-t/T_{CH(1)}}\right)\right) + \left(\left(\frac{(1-\beta)}{(1 - T_{CH(2)} / T_{1\rho(2)}^{H})}\right)\left(e^{-t/T_{1\rho(2)}^{H}}\right)\left(1 - e^{-t/T_{CH(2)}}\right)\right)} \tag{3.6}$$

Both equations hold true only for a particular experimental value of t. This is the contact period used in the experiment from which the quantitative comparison between peak areas is to be made – i.e., the spin counting experiment.

All of the above-mentioned time constants have to be determined experimentally for each peak of interest in the sample, as well as for the spin-counting reference (the reference material from which a relationship between peak area and a number of spins will be drawn). For the experiments reported in this chapter, ^{1}H relaxation time constants of the soil or soil components were determined (or estimated) to be much shorter than the experimental repetition delay and therefore a ^{1}H T_1 correction factor was not needed for these peaks in a cross-polarization experiment. The time constants (T_{CH} and $T_{1\rho}$) and β were determined by measuring $M(t)$ as a function of t (Figures 3.6(a)-3.10(a)) and fitting the data to a single or multiple exponential growth and decay curve (Figures 3.6(b)-3.10(b)), using SigmaPlot 5.0.

The raw data (CP-MAS spectra) from this portion of the spin-counting scheme are shown in Figures 3.6(a)-3.10(a) and the deconvoluted peak intensities are shown plotted versus CP contact time in Figures 3.6(b)-3.10(b) for the whole soil, HF-treated soil, humin, humic acid, and fulvic acid, respectively. Each of the CP-MAS spectra of soil or soil extract in Figures 3.6(a)-3.10(a) is shown with its corresponding deconvolution data in Figures A3-6 to A3-10 of the appendix. In each set of spectra in Figures A3-6 to A3-10, the uppermost trace is the unadulterated spectrum, followed by the "synthetic" spectrum (equal to the sum of the deconvoluted peaks), followed by the individual deconvoluted peaks, and the lowermost trace is the "difference" spectrum (the difference between the "synthetic" and raw spectrum.) The intensities of deconvoluted peaks were analyzed in terms of Eqs. 3.3-3.6. The results are summarized in Tables 3.1-3.5.

^{13}C CP-MAS the spin-counting spectra are presented, with arbitrary scaling for visual comparison, in stacked format in Figure 3.11 for each of the soil or soil component samples. The ^{13}C CP-MAS spin-counting spectra for each soil component and whole soil are shown individually in Figures 3.12-3.16. In each of these figures, the experimental spectrum a) is shown plotted at the top; b) is the "synthetic" spectrum, equal to the sum of the deconvoluted peaks shown in c) and d) is the "difference" spectrum, equal to the difference between the "synthetic" and experimental spectrum. In each experimental spectrum the peak due to the ^{13}C labeled external reference appears at 217 ppm. The deconvoluted peak areas illustrated in these figures form the basis for all of the spin-counting and related results of this chapter.

The correction factors used to normalize the cross-polarization enhancement were calculated according to equations 3.5 and 3.6, with equation 3.5 used for single-

component rate constants and 3.6 used for two-component rate constants. The calculated cross-polarization correction factor (calculated according to equations 3.5 or 3.6) for each peak is given in the column titled (C_{CP}) in Tables 3.1-3.5. The CP-corrected spin-counting peak integrals are given in the column titled (A_{corr}^{CP}), and were calculated on the basis of equation 3.1. While there was no ^{1}H T_1 correction necessary for the soil components (as mentioned in section 3.2.1), the ^{1}H T_1 of the external reference is 780 ms, much longer than that of the soil and/or soil extracts, and hence requires a correction. The T_1 correction factor for the 3.2.1 external reference and a 1 s relaxation delay is 1.38, calculated according to equation 3.2, and is included in the correction term (A_{corr}^{CP}) for that particular peak.

3.2.3 Empirical Calibration of the [3.2.1] bicyclo-4-pyrrolidino-N-methyl-octan-8-one triflate External Reference

The calibration experiments on the [3.2.1] bicyclo-4-pyrrolidino-N-methyl-octan-8-one triflate[18] (abbreviated here as [3.2.1] bicyclo compound) are summarized in Table 3.7. The calculated number of milligrams of carbon is reported for the 6.49 mg [3.2.1] bicyclo compound external reference (contained in a capillary) for each calibration compound (as a function of the peak position for the compound). The average of these calibration values was used in Tables 3.1-3.5 to determine the percent carbon and milligrams of carbon in each deconvoluted peak by CP-MAS spin-counting for the soil and soil extracts.

Once the external reference was calibrated, and all peak areas of the spin-counting spectrum were "corrected", for each peak a calculated a number of milligrams of carbon

was computed. The milligrams of carbon reported for each peak in Table 3.1-3.5 is for the particular sample weight that was put in the spinner for spin counting. The sample size for the spin-counting experiment for each soil sample is written in the title of each table.

3.2.4 Percent Carbon by ^{13}C CP-MAS Spin Counting

The combination of the calibration data of Table 3.7 and the corrected peak areas of Tables 3.1-3.5 was used to generate the percent carbon by CP-MAS spin counting. The percent carbon detected by CP-MAS for each soil component is written to the right of the cell labeled "total percent carbon by CP-MAS spin counting" in Tables 3.1-3.5. This value was calculated from the total of the corrected CP integrals for the soil component (also reported in Tables 3.1-3.5), multiplied by the ratio of the mass of carbon (established from the calibrations) to the corrected peak area of the external reference.

3.2.5 RF-field Mapping and Field Simulations for the Large Volume Spinning System

While often overlooked in routine ^{13}C MAS NMR experiments where relatively quantitative peak integrals are not critical, the radio-frequency (RF) excitation profile within the NMR coil plays a significant role in quantification by MAS NMR[24]. The unusually large NMR coil of the large-volume spinning system employed in this study requires significantly more RF power than the coils employed in other commercial MAS systems to achieve what is considered the lowest acceptable decoupling and spin-lock B_1 fields for organic solids (roughly 40 kHz[22]). This fact, in conjunction with the large systematic error associated with the empirical calibration of the external reference and the

rather low percent carbon of the soil components accounted for by ^{13}C MAS NMR, prompted an investigation of the RF field profile generated in our particular MAS/coil assembly. A procedure known as field mapping was used to determine the relationship between the *x*-*y* directional component of the $\mathbf{B_1}$ intensity and position within the NMR coil (i.e., the sample area) in the MAS spinner. In a second experiment, DP- and CP-MAS signal intensity was measured (for the three different organic functional groups in L-alanine) as a function of position within the sample area of the MAS spinner.

The apparatus used to map the RF-field in the large-volume spinning system employed in this thesis is illustrated in Figure 3.17. The observation sample (83 mg of ^{13}C-3-L-alanine) insert was contained in a disk that is moveable (in the spinner's axial direction) and machined from Vespel plastic. This arrangement is represented Figure 3.17(a). A 1:1 scale representation of the coil, coil area, spinner, spinner sample area, and the home-built Kel-F stator is shown in Figure 3.17(b). The spinner sample area is slightly offset, in the axial direction, from the center of the coil area (due to a machining error in the home-built MAS module). Figure 3.17(b) was generated from careful measurements on the assembled spinning system.

An RF-field strength is typically measured in solid-state ^{13}C NMR by observing the null-intensities (π, 2π) of a standard (e.g., hexamethylbenzene), using either DP-MAS or CP-MAS experiments. Once the pulse widths are established (typically measured in milliseconds), the field is estimated using the below equation[19].

$$\text{RF-field (kHz)} = [2 \times 10^{-3} \times (2\pi \text{ pulse width (ms)}) - (\pi \text{ pulse width (ms)})]^{-1} \qquad (3.8)$$

The results from mapping the RF-field intensity in this manner are shown in Figure 3.18(a). This figure was generated by measuring the ^{1}H 180° (π) and 360° (2π) pulse widths (using the methyl-group CP-MAS signal from $^{13}CH_3CHNH_2CO_2H$), and calculating the field strength in kHz according to equation 3.8. Field mapping was carried out by first positioning the moveable disk in the large-volume spinner and then noting the disk's position relative to the center of the coil, using a digital caliper. The disk and spinner were spun at a magic-angle spinning speed of 2.0 kHz and, as described above, ^{13}C CP-MAS experiments were used to determine the B_1 field strength of the disk at that particular position. The disk would then be axially re-positioned in a 1 mm increment and the B_1 field determined at the new location. This was repeated until the entire volume of the sample spinner was mapped. The results are represented by solid points in the plots shown in Figure 3.18(a) and are normalized, with the highest point representing a field strength of 53 kHz.

A second set of experiments was performed for the purpose of mapping ^{13}C DP- and CP-MAS signal responses as a function of position within the sample area. These experiments were carried out with a disk containing a mixture of three ^{13}C labeled compounds (^{13}C-1-L-alanine, ^{13}C-2-L-alanine, ^{13}C-3-L-alanine) in a 1:1:1 molar ratio. The disk that was used to hold this mixture was identical to the Vespel disk used to map the RF-field shown in Figure 3.18(a). The ^{13}C DP- and CP-MAS signal integral of the labeled carbon in each compound was measured as function of sample position as was done in the aforementioned RF field mapping experiment. The signal integral for each carbon type is plotted as a function of sample position and separated into DP-MAS (Fig. 3.18(b)) and CP-MAS (Fig. 3.18(c)) plots.

3.2.6 Calculations for RF-field Mapping and Field Simulations

A magnetic field can be calculated for a given distribution of currents in the surrounding space. The NMR coil is a medium that directs current flow, typically through a wire surrounding the sample, to create a magnetic field and/or receive a low voltage signal emanating from the sample. The law of Biot and Savart can be used to calculate the magnitude and direction of the magnetic field (***B***) at a point by a given current element,[20,21] using the following expression:

$$d\boldsymbol{B} = \left(\frac{\mu_0}{4\pi}\right)\frac{i d\boldsymbol{l} \times \boldsymbol{a}}{a^3} \tag{3.9}$$

where μ_0 is the permeability constant of vacuum, i is the current with $d\boldsymbol{l}$ being the differential element of length pointing tangent to the current flow in the wire, and a is the magnitude of $\boldsymbol{a}$, which describes the vector that points from the current element to the point P at which we wish to know the field. The relationship between the differential field element at point P and the aforementioned current element is shown diagrammatically in Figure 3.19(a). Expansion of Equation 3.9 by integration to find the total magnetic field in the z direction (B_{Iz}) at an external point (in a Cartesian axis system) and with the proper geometric substitutions to describe a standard solenoid coil yields:

$$B_{Iz}(x,y,z) = \int_{-n\pi}^{n\pi} \frac{r^2 - r(y\sin\varphi + x\cos\varphi)}{\left[(x - r\cos\varphi)^2 + (y - r\sin\varphi)^2 + (z - zSPC(\varphi))^2\right]^{3/2}} d\varphi \tag{3.10}$$

where r is the radius of the coil, φ is the phase of the coil turn in radians (i.e., looking down along the coil axis, a 360° turn along the coil would be $\varphi = 2\pi$ radians, two turns

would be $\varphi = 4\pi$ radians, etc..), x, y, z determines the position of the point where we wish to know the z-component of the magnetic field. The quantity $zSPC(\varphi)$ is a function to describe the current path along the z direction:

$$zSPC(\varphi) = \frac{\varphi s}{2\pi} \tag{3.11}$$

where s is a pitch constant to describe the spread between the turns along the length of the coil, as shown in Figure 3.19(b). Figure 3.19(b-g) shows, in detail, the coil shapes and their corresponding functions to describe the pitch and radius along the coil.

The solid line in Figure 3.18(a) represents the field calculated using Equations 3.10 and 3.11, based on a current path in the center of the simple wire solenoid illustrated in position in Figure 3.17(b) and shown in a cut-away view in Figure 3.19(b). This field was calculated for x = 3.53 mm, y = 0 mm, and z varied along the length of the sample volume. The value of 3.53 mm for the x position was used because it represents the radial boundary at which the inner volume equals the outer volume of the sample area (the average of the sample region, which has a maximum radius of 5.47 mm). The sample region and average radius relative to the coil are illustrated in Figure 3.19(b). The solid line in the plot of Figure 3.18(a) is essentially a slice taken at x = 3.53 of the field simulation of Figure 3.19(c). The simulated RF-field calculations were not performed in an absolutely rigorous fashion. An absolutely quantitative and rigorous simulation would require a more extensive investigation into the electrical characteristics, e.g., the resistance and capacitance characteristics, of the coil. The solid line representing the simulated field was normalized to make the maximum value equal to unity for visual comparison to the experimental data.

The RF-field simulations for two more theoretical coil configurations are shown in Figure 3.19(d-g). The details of each calculation are shown with the corresponding coil configuration. Figure 3.19(d, e) represents a relatively simple coil modification and illustrates the effect that this modification has on the field profile. Figure 3.19(f, g) represents a more complex coil shape and the nearly flat RF-field profile it can produce (the goal of this coil simulation).

Figures 3.18(b) and 3.18(c) show plots of signal integrals versus sample position for the standard solenoid coil used in this thesis for ^{13}C DP-MAS and CP-MAS experiments, respectively. In Figure 3.18(b), the ^{13}C DP-MAS signal integrals for the three different carbon sites of L-alanine are plotted as a function of sample position. As shown and discussed earlier, the insert shown in Figure 3.17(a) was used to probe the behavior of signal intensity (for the three functional groups of L-alanine) at different positions within the sample area. The insert contained a 1:1:1 mixture of $^{13}CH_3CHNH_2CO_2H$ (peak at 21.2 ppm), $CH_3{}^{13}CHNH_2CO_2H$ (peak at 54.0, 50.4 ppm), and $CH_3CHNH_2{}^{13}CO_2H$ (peak at 178.5 ppm). Each peak is represented by a different line type, as shown in the legend. Analogous ^{13}C CP-MAS results are shown in Figure 3.18(c). The plots show slightly greater signal variations for the CP-MAS version of the experiment.

3.3 Discussion

3.3.1 Error Analysis of ^{13}C CP-MAS Spin-Counting Results

The errors associated with many of the measurements included in this thesis are estimated in the face of a lack of a large number of experimental trials (repetitions) from which to derive a standard deviation. This is primarily due to the overall length of each experiment; a complete investigation of the random and systematic errors associated with spin-counting of soils by solid-state NMR is beyond the realm of what is realistic or practical at the current level of measurement technology. Rather, errors are estimated on the basis of more practical/realistic experiments on pure solid compounds and by analyzing and isolating the factors likely to dominate the error.

3.3.1.1 Random Error

The random error associated with the measurements made in this chapter represent the limitations of physical measurements by solid-state NMR and in our ability to reproducibly read the experimental output. The signal-to-noise ratio, or ratio of peak intensity to that of the noise level, of the spin-counting spectra in this thesis is typically in excess of 250 to one for the most intense peak in the soil spectra, and 70 to one for the least intense peaks that are readily distinguished in the spectra. In order to assess the random error inherent in our ^{13}C CP-MAS experiments, we carried out series of 10 CP-MAS experiments on glycine, refilling the sample container with a new weighed amount of sample between each experiment. The carbonyl peak of glycine was deconvoluted each time and the resulting peak area was used to estimate the random error associated with our measurements. The signal-to-noise ratio was roughly 1000 to 1 for glycine's carbonyl peak, yet the relative standard deviation associated with this multiple

measurement was found to be ± 1.4 percent. This indicates that the spectral noise is not the only source of random error.

Error associated with the dependent variable in the ^{13}C variable contact time (VCT) plots of Figures 3.6-3.10(b) was propagated to the correction factor (C_{CP}) and presented as a relative deviation in Tables 3.1-3.5. This error was calculated from the standard error of the estimate (SEE) on each VCT regression analysis, and was determined using the SigmaPlot 5.0 program. The standard error of the estimate is an example of a root mean square error estimate, and is a measure of the precision of a regression analysis.

The estimated relative error associated with the deconvoluted experimental peak areas (A_{exp}^{CP}) presented in Tables 3.1-3.5 is the error generated from 20 individual deconvolutions for the corresponding *individual* spin-counting spectrum of the whole soil or soil component. The rather large estimated errors for some peaks, namely the peaks at 198, 40, 30, and 20 ppm, indicate that these peaks are difficult to distinguish (deconvolute) clearly and reproducibly. The total error reported for the corrected peak areas (A_{corr}^{CP}) is the propagated error of the cross-polarization correction term (C_{CP}) and that of the experimental peak areas (A_{exp}^{CP}).

The total experimental peak area and the total corrected peak area are reported below the corresponding columns of peak data. The errors associated with these values are equal to the propagated error of the sum of the individual peak areas, not including that of the external reference peak. The error associated with the total percent carbon is the propagated error of the total corrected peak area, the corrected peak area of the external reference, and the error associated with the external calibration procedure (± 7.0

percent). By analogy to the discussion in Chapter 2 for spin counting by DP-MAS, the *total* experimental integral (A_{exp}^{CP}) for the *entire* ^{13}C CP-MAS spectrum of soil components remained relatively consistent (± 0.9, 0.6, 1.0, 2.1, 1.6 percent for the whole soil, HF-treated soil, humin, humic acid, and fulvic acid, respectively). However, spin-counting by CP-MAS *requires* that individual peak intensities be corrected to account for cross-polarization characteristics; hence, the error associated with each *individual* peak area, rather than the error associated with the *entire* ^{13}C CP-MAS spectrum, is propagated to the final error associated with spin-counting.

3.3.1.2 Systematic Error and B_1 Field Homogeneity

The dominant source of *identified* systematic error in this study originates from the empirical calibration of the external reference material. Table 3.7 shows the different calibration trial results for a number of pure organic compounds. The average of the results for the comparisons against various organic compounds was used to calibrate the external reference. A percent standard deviation was reported on this average value to illustrate the rather large spread of values associated with the calibration.

The large (± 7.00 percent) relative percent deviation of the calibration trial is rather surprising, considering the extreme care that was taken in the calibration experiments. There are, however, a number of assumptions made during these CP-MAS calibration measurements that may ultimately be proven to be poor. Intense proton decoupling and efficient spin-locking power are essential for quantitative cross-polarization to be realized in the analysis of most organic materials. The data in Figure 3.18(a) suggests that the radio-frequency power drops dramatically near the ends of the

rotor, to nearly half of that near the center of the sample. Due to the limitations of the hardware, the maximum applied RF field intensity rarely exceeded 50 kHz, implying that RF fields of 30 kHz or less were experienced through roughly 40 percent of the sample. As was shown in a past study by VanderHart, Earl, and Garroway, protons in methylene and methine functionality typically need greater than 40 kHz proton decoupling and proton spin-locking power in order for quantitative ^{13}C NMR MAS peak integrals of organic polymers to be realized[22]. Reduced ^{13}C CP-MAS NMR integrals for methylene carbons are noticed in the calibration trials presented in Table 3.7, where the methylene carbons of glycine and monoethylfumarate are seen to give high results (as a result of smaller-than-average peak integrals). It should be noted that similar trends were noticed (smaller-than-average peak integrals) for methylene carbons in the DP-MAS calibration trials of Chapter 2.

Cross-polarization efficiency is very dependent on establishing the Hartmann-Hahn match, a condition in which the rotating-frame precession frequencies for the two nuclides involved in the polarization transfer are set equal. Magic angle spinning and molecular motion can make some organic compounds more sensitive to this match condition by essentially modulating the match characteristics[23]. An inhomogeneous B_1 field can create a situation in which the match condition is not met throughout the sample, which will introduce inaccuracies in cross-polarization generated peak intensities for match-sensitive compounds[24]. For this reason, ^{13}C CP-MAS NMR signals would be expected to show greater variation in intensity as a function of position within the sample area compared to signals generated from ^{13}C DP-MAS. This general effect is noticed in the plots of Figure 3.18, where one sees that ^{13}C DP-MAS signal intensities for the

different ^{13}C labeled carbons of a mixture of ^{13}C labeled L-alanine compounds follow essentially the same smooth curve as a function of sample position along the rotor axis. The plotted intensities of ^{13}C CP-MAS NMR generated signals in Figure 3.18(c) show much greater intensity variation for the different L-alanine sites as a function of sample position compared to the plotted ^{13}C DP-MAS signal intensities in Figure 3.18(b).

A potential solution to this systematic error in ^{13}C CP- and DP-MAS intensities as a function of position in the MAS rotor and organic functional group would be to produce a coil configuration that would yield a more homogeneous radio-frequency excitation profile and to employ greater proton decoupling and spin-locking power. The author has proposed two changes to the standard solenoid type coil configuration that may yield improved RF performance and more accurate spin-counting results. Those coil configurations are presented in Figure 3.19(b-g) and were generated using the calculations described in section 3.2.6. The variable pitch and variable radius coil described in Figure 3.19 (f, g) may require changes in the accompanying probe electronics to allow for the use of greater RF power to compensate for the loss in overall field intensity that an increased coil diameter brings. The variable radius and pitch coil of Figure 3.19 (d, e) is estimated to have 70 percent of the field intensity at the center of the coil compared to that of the standard solenoid coil for a given current through the windings. It may be necessary to move to an overall smaller coil radius and smaller spinning system to get both a flat RF-field profile and greater decoupling/spin-locking power or to employ probe circuitry that is capable of withstanding much greater power levels.

3.3.2 A Comparison of Spin-Counting Results from ^{13}C CP-MAS and DP-MAS

Appropriately corrected DP-MAS and CP-MAS peak areas (A_{corr}^{CP} , A_{corr}^{DP}) for a particular peak of a soil component spectrum should be equal, assuming the correction factors are accurate and our models describing CP and DP in these samples are correct. However, in comparing the normalized and corrected intensities for each of the soil component samples analyzed in Chapters 2 and 3, the DP-MAS spin-counting results for each soil component did not compare well to their CP-MAS counterparts. These results are summarized in a normalized fashion for ease in comparison in Table 3.8. There are a few trends that emerge from Table 3.8. The largest intensities are often shared between the aromatic region (peaks at 130, 150 ppm) and the carbohydrate region (peaks at 72, 104 ppm) in the DP-MAS spectra, while in the CP-MAS spectra, the peaks in the carbohydrate region are often largest, with the aromatic region being proportionally smaller. While such a difference can be attributed to a number of factors (such as improper CP correction terms), it does appear to reinforce previous observations reported in the literature that the aromatic intensities in CP-MAS spectra of soils and soil components tend to be smaller than expected[9,10]. Moreover, these apparent intensity losses in the CP-MAS spin-counting spectra may contribute to the smaller percentages of observed carbon reported in Table 3.8 (the carbon spin-counted by CP-MAS NMR relative to that determined by elemental analysis).

Upon examination of the error analysis associated with the ^{13}C CP-MAS spin counting results, one notices some similar trends with the results of Chapter 2 of this thesis. The error associated with the total percent carbon for ^{13}C CP-MAS spin counting is similar to that of DP-MAS spin counting, where values around +/- 10 percent were

common. The largest source of *random* error in both the ^{13}C CP and DP-MAS spin counting experiments on soil components was due to the necessary deconvolution of the spectra into individual peaks. The largest identified source of *systematic* error for both methods was associated with the calibration of the external reference with pure organic compounds.

3.4 Conclusions

Cross-polarization was used to spin count the carbon in the Uncompahgre soil and its extracts, accounting for 48.4, 82.0, 54.6 68.5, and 65.8 percent of the carbon detected by elemental analysis in the whole soil, HF-treated soil, humin, humic acid and fulvic acid, respectively. The large volume spinning system proved to be valuable for producing ^{13}C CP-MAS NMR spectra of soil and soil components with very high signal-to-noise ratios. In comparing the DP-MAS spin counting results with the corresponding CP-MAS results, CP-MAS intensities, corrected to account for cross-polarization and ^{1}H T_1 relaxation behavior, in the aromatic region tended to be lower than that predicted by DP-MAS for all fractions. The total percent carbon detected by ^{13}C CP-MAS spin counting was within the experimental error of that predicted by DP-MAS; however, both methods suffer from low estimates for total carbon, relative to that detected by elemental analysis.

The accuracy of both the CP-MAS and DP-MAS spin-counting results was found to depend strongly on the quality of the empirical calibration of the external reference material. For both methods, the calibration was highly dependent on the functionality and compound by which the calibration was made. Ways for improving the accuracy of

these experiments were suggested. Of these suggestions, improving the field profile and NMR characteristics of the standard solenoid coil employed in this thesis was examined in detail. The variable-pitch and variable-radius solenoid is predicted to generate a nearly flat RF field profile for the large volume spinning system. Employing this coil design in future spin-counting studies should reduce the systematic error associated with the calibration of the external reference when used in conjunction with high power ^{1}H decoupling (>40 kHz).

Table 3.1 ^{13}C CP-MAS spin-counting results for the Uncompahgre whole soil (2.237 g).

ppm	Polarization transfer rate constants (ms)[a]				β	C_{CP}[b] (± SEE %)	A_{exp}^{CP}[c] (± ERE %)	A_{corr}^{CP}[d] (± Total % error)	mg of carbon[e]	% of total[f] (p_i)
	T_{CH}		$T_{1\rho}$							
	(1)	(2)	(1)	(2)						
197	0.422	0.528	2.110	6.356	0.75	1.45 (± 8.43 %)	131.1 (± 16.7 %)	190.7 (± 18.7 %)	5.70	2.84
172	0.331	0.210	3.311	7.451	0.64	1.23 (± 2.12 %)	415.2 (± 10.9 %)	511.7 (± 11.1 %)	15.30	7.62
160										
150	0.289		7.230		1.00	1.14 (± 3.07 %)	404.5 (± 9.1 %)	462.7 (± 9.6 %)	13.84	6.89
130	0.060	0.570	2.147	7.301	0.46	1.42 (± 1.83 %)	550.2 (± 9.0 %)	779.8 (± 9.2 %)	23.32	11.61
115	0.027	0.285	4.151	8.672	0.80	1.23 (± 4.20 %)	339.7 (± 8.2 %)	418.9 (± 9.2 %)	12.53	6.24
104	0.033	0.434	2.479	9.737	0.65	1.36 (± 3.02 %)	481.7 (± 3.8 %)	656.7 (± 4.8 %)	19.64	9.78
86	0.033	0.482	1.230	6.560	0.61	1.71 (± 3.89 %)	354.2 (± 8.6 %)	606.5 (± 9.4 %)	18.14	9.03
72	0.203	0.030	16.09	3.440	0.18	1.27 (± 3.52 %)	1010.6 (± 6.3 %)	1281.2 (± 7.2 %)	38.32	19.07
56	0.034		5.826		1.00	1.18 (± 3.54 %)	539.5 (± 9.4 %)	636.7 (± 10.0 %)	19.04	9.48
39	0.025	0.025	4.752	0.968	0.60	1.57 (± 5.94 %)	204.9 (± 32.1 %)	320.8 (± 32.7 %)	9.60	4.78
30	0.036	0.035	3.113	16.49	0.83	1.30 (± 3.15 %)	336.9 (± 13.7 %)	438.3 (± 14.0 %)	13.11	6.53
20	0.047	0.047	4.495	4.862	0.27	1.22 (± 4.05 %)	338.5 (± 15.6 %)	413.5 (± 16.1 %)	12.37	6.16
217[g]	0.420		198.00		1.00	1.53 (± 1.13 %)	487.2 (± 2.1 %)	743.4 (± 2.3 %)	22.23 (± 7.0 %)[h]	
	Total (not including reference at 0 ppm)						5107.1 (± 3.0 %)[i]	6717.5 (± 3.3 %)[i]	200.91	100 %
	total percent carbon by CP-MAS spin counting						9.0 (± 8.1 %)[j]			

[a] Cross-polarization rate constant reported as single or multiple component values. For single exponential component growth/decay, one constant is reported for T_{CH} and $T_{1\rho}$. For multiple component exponential behavior, the value for each component is listed under (1) and (2), with the contribution from component (1) reported in the column titled with the β symbol. The contribution from component 2 will then be (1-β.)

[b] Calculated cross-polarization correction factors for each peak from equations 3.5 and 3.6, with error estimated from the standard error of the estimate (SEE).

[c] Experimental peak areas for each deconvoluted peak. The estimated relative error (ERE) is given as a percent error in parenthesis. The estimated relative error is based on 20 independent deconvolutions (see section 3.3.2.1).

[d] Experimental peak areas multiplied by the ^1H T_1 relaxation correction factor (C_{T_1}) and cross polarization correction factor (C_{CP}). The ^1H T_1 correction factor will be 1 for all the peaks of the soil or soil extract, and 1.38 for the external reference (peak at 217 ppm). The total error is given as a percent error in parenthesis. The total error is the propagated error of the correction term and experimental peak area.

[e] Amount of carbon in milligrams per deconvoluted peak out of the whole spinner sample (2.237 g).

[f] Percent carbon contribution from this peak out of the total CP-MAS detected carbon, p_i = 100*(mg C for peak i)/(sum of mg C for all peaks).

[g] Peak due to [3.2.1] bicyclo compound external reference.

[h] Result from the calibration of the 3.2.1 spin-reference compound.

[i] Sum of the individual peak integrals in the same column, excluding the integral due to the reference material at 217 ppm. The error for this total is the propagated error of the sum of the aforementioned integrals.

[j] The total percent carbon with relative error given in parenthesis. Error for this total is the propagated error of the total corrected peak integral, and the errors associated with the external reference.

Table 3.2 CP-MAS spin-counting results for the HF-treated Uncompahgre whole soil (1.178 g).

ppm	Polarization transfer rate constants (ms)[a]					C_{CP}[b] (± SEE %)	A_{exp}^{CP}[c] (± ERE %)	A_{corr}^{CP}[d] (± Total % error)	mg of carbon[e]	% of total[f] (p_i)
	T_{CH}		$T_{1\rho}$		β					
	(1)									
197	0.678		5.117			1.46 (± 4.08 %)	143.0 (± 11.6 %)	208.9 (± 12.3 %)	5.54	1.92
172	0.390		4.183			1.28 (± 1.57 %)	660.9 (± 5.2 %)	843.7 (± 5.5 %)	22.36	7.76
160										
150	0.658		5.841			1.42 (± 1.91 %)	656.2 (± 8.8 %)	933.2 (± 9.0 %)	24.73	8.58
130	0.038	0.547	0.408	5.031	0.26	1.75 (± 1.49 %)	978.7 (± 6.9 %)	1711.1 (± 7.1 %)	45.35	15.74
115	0.024	0.947	7.326	2.437	0.53	1.42 (± 2.76 %)	457.8 (± 11.1 %)	648.8 (± 11.5 %)	17.19	5.97
104	0.031	0.372	5.377	2.020	0.53	1.32 (± 2.11 %)	568.3 (± 8.3 %)	752.5 (± 8.5 %)	19.94	6.92
86	0.046		4.305		1.00	1.25 (± 5.18 %)	292.5 (± 24.2 %)	365.0 (± 24.7 %)	9.67	3.36
72	0.027	0.321	1.726	4.867	0.61	1.50 (± 2.76 %)	1614.6 (± 8.2 %)	2417.2 (± 8.6 %)	64.06	22.23
56	0.423	0.029	1.974	5.069	0.30	1.29 (± 2.14 %)	801.1 (± 5.0 %)	1037.3 (± 5.5 %)	27.49	9.54
39	0.026		3.569			1.31 (± 4.66 %)	471.4 (± 6.5 %)	619.3 (± 8.0 %)	16.41	5.69
30	0.029	0.381	2.629	8.101	0.74	1.36 (± 2.07 %)	488.6 (± 22.5 %)	666.7 (± 22.6 %)	17.67	6.13
20	0.084		4.839			1.21 (± 4.46 %)	555.0 (± 16.9 %)	670.6 (± 17.5 %)	17.77	6.17
217[g]	0.420		198.00			1.53 (± 1.13 %)	549.8 (± 2.2 %)	838.9 (± 2.4 %)	22.23 (± 7.0 %)[h]	
	Total (not including reference at 0 ppm)						7688.3 (± 3.2 %)[i]	10874.2 (± 3.3 %)[i]	288.19	100.00
	total percent carbon by CP-MAS spin counting						24.5 (± 8.1 %)[j]			

[a] Cross-polarization rate constant reported as single or multiple component values. For single exponential component growth/decay, one constant is reported for T_{CH} and $T_{1\rho}$. For multiple component exponential behavior, the value for each component is listed under (1) and (2), with the contribution from component (1) reported in the column titled with the β symbol. The contribution from component 2 will then be (1-β.)

[b] Calculated cross-polarization correction factors for each peak from equations 3.5 and 3.6, with error estimated from the standard error of the estimate (SEE).

[c] Experimental peak areas for each deconvoluted peak. The estimated relative error (ERE) is given as a percent error in parenthesis. The estimated relative error is based on 20 independent deconvolutions (see section 3.3.2.1).

[d] Experimental peak areas multiplied by the ^{1}H T_1 relaxation correction factor (C_{T_1}) and cross polarization correction factor (C_{CP}). The ^{1}H T_1 correction factor will be 1 for all the peaks of the soil or soil extract, and 1.38 for the external reference (peak at 217 ppm). The total error is given as a percent error in parenthesis. The total error is the propagated error of the correction term and experimental peak area.

[e] Amount of carbon in milligrams per deconvoluted peak out of the whole spinner sample (1.178 g).

[f] Percent carbon contribution from this peak out of the total CP-MAS detected carbon, p_i = 100*(mg C for peak i)/(sum of mg C for all peaks).

[g] Peak due to [3.2.1] bicyclo compound external reference.

[h] Result from the calibration of the 3.2.1 spin-reference compound.

[i] Sum of the individual peak integrals in the same column, excluding the integral due to the reference material at 217 ppm. The error for this total is the propagated error of the sum of the aforementioned integrals.

[j] The total percent carbon with relative error given in parenthesis. Error for this total is the propagated error of the total corrected peak integral, and the errors associated with the external reference.

Table 3.3 CP-MAS spin-counting results for the humin fraction (2.198 g).

ppm	Polarization transfer rate constants (ms)[a] T_{CH} (1)		$T_{1\rho}$		β	C_{CP}[b] (± SEE %)	A_{exp}^{CP}[c] (± ERE %)	A_{curr}^{CP}[d] (± Total % error)	mg of carbon[e]	% of total[f] (p_i)
197	0.274	0.567	2.397	2.833	0.30	1.47 (± 7.67 %)	97.7 (± 32.2 %)	143.9 (± 33.1 %)	4.67	3.17
172	0.269		3.899			1.24 (± 1.93 %)	267.1 (± 6.1 %)	331.8 (± 6.4 %)	10.77	7.30
160										
150	0.820	0.139	3.504	7.394	0.60	1.40 (± 1.75 %)	216.8 (± 10.6 %)	304.0 (± 10.8 %)	9.86	6.69
130	0.378	0.045	2.901	7.105	0.51	1.25 (± 1.67 %)	392.4 (± 7.7 %)	489.3 (± 7.8 %)	15.88	10.76
115	0.030		4.430			1.24 (± 5.01 %)	207.6 (± 18.0 %)	258.4 (± 18.7 %)	8.39	5.68
104	0.301	0.031	8.328	2.461	0.28	1.36 (± 2.98 %)	263.0 (± 16.6 %)	358.4 (± 16.8 %)	11.63	7.88
86	0.034		3.576			1.31 (± 3.92 %)	193.8 (± 16.2 %)	253.9 (± 16.7 %)	8.24	5.58
72	0.031	0.260	2.358	8.490	0.77	1.40 (± 3.09 %)	736.3 (± 9.3 %)	1027.9 (± 9.8 %)	33.36	22.61
56	0.035		4.353			1.25 (± 3.78 %)	390.6 (± 17.0 %)	487.6 (± 17.5 %)	15.82	10.73
39	0.021	0.258	1.133	9.754	0.81	1.94 (± 4.86 %)	117.1 (± 28.0 %)	227.5 (± 28.4 %)	7.38	5.00
30	0.041		4.148			1.26 (± 2.98 %)	230.6 (± 20.9 %)	290.5 (± 21.1 %)	9.43	6.39
20	0.034	0.215	1.710	4.877	0.51	1.42 (± 3.40 %)	262.0 (± 21.3 %)	372.9 (± 21.6 %)	12.10	8.20
217[g]	0.420		198.00			1.53 (± 1.13 %)	449.0 (± 3.7 %)	685.1 (± 3.8 %)	22.23 (± 7.0 %)[h]	
	Total (not including reference at 0 ppm)						3374.9 (± 4.5 %)[i]	4546.1 (± 4.7 %)[i]	147.54	100.00
	total percent carbon by CP-MAS spin counting						6.7 (± 9.2 %)[j]			

[a] Cross-polarization rate constant reported as single or multiple component values. For single exponential component growth/decay, one constant is reported for T_{CH} and $T_{1\rho}$. For multiple component exponential behavior, the value for each component is listed under (1) and (2), with the contribution from component (1) reported in the column titled with the β symbol. The contribution from component 2 will then be (1-β.)

[b] Calculated cross-polarization correction factors for each peak from equations 3.5 and 3.6, with error estimated from the standard error of the estimate (SEE).

[c] Experimental peak areas for each deconvoluted peak. The estimated relative error (ERE) is given as a percent error in parenthesis. The estimated relative error is based on 20 independent deconvolutions (see section 3.3.2.1).

[d] Experimental peak areas multiplied by the ^1H T_1 relaxation correction factor (C_{T_1}) and cross polarization correction factor (C_{CP}). The ^1H T_1 correction factor will be 1 for all the peaks of the soil or soil extract, and 1.38 for the external reference (peak at 217 ppm). The total error is given as a percent error in parenthesis. The total error is the propagated error of the correction term and experimental peak area.

[e] Amount of carbon in milligrams per deconvoluted peak out of the whole spinner sample (2.198 g).

[f] Percent carbon contribution from this peak out of the total CP-MAS detected carbon, p_i = 100*(mg C for peak i)/(sum of mg C for all peaks).

[g] Peak due to [3.2.1] bicyclo compound external reference.

[h] Result from the calibration of the 3.2.1 spin-reference compound.

[i] Sum of the individual peak integrals in the same column, excluding the integral due to the reference material at 217 ppm. The error for this total is the propagated error of the sum of the aforementioned integrals.

[j] The total percent carbon with relative error given in parenthesis. Error for this total is the propagated error of the total corrected peak integral, and the errors associated with the external reference.

Table 3.4 CP-MAS spin-counting results for humic acid (1.842 g).

ppm	Polarization transfer rate constants (ms)[a]					C_{CP} [b] (± SEE %)	A_{exp}^{CP} [c] (± ERE %)	A_{corr}^{CP} [d] (± Total % error)	mg of carbon[e]	% of total[f] (p_i)
	T_{CH}		$T_{1\rho}$		β					
	(1)									
197	0.498		3.944			1.36 (± 4.71 %)	1347 (± 12.4 %)	1834.1 (± 13.3 %)	11.75	2.06
172	0.299		3.586			1.27 (± 1.71 %)	8086.9 (± 4.8 %)	10275.9 (± 5.1 %)	65.83	11.53
160										
150	1.284	0.193	2.474	5.559	0.70	1.78 (± 2.05 %)	5574.4 (± 9.0 %)	9909.3 (± 9.3 %)	63.48	11.12
130	0.025	0.411	0.410	4.010	0.26	1.68 (± 2.17 %)	9463.4 (± 7.5 %)	15921.4 (± 7.8 %)	102.00	17.86
115	0.018	1.154	5.403	1.934	0.52	1.56 (± 3.80 %)	3965.6 (± 27.7 %)	6168.1 (± 27.9 %)	39.51	6.92
104	0.047		3.907			1.28 (± 6.75 %)	2146.7 (± 23.4 %)	2739.7 (± 24.3 %)	17.55	3.07
86										
72	0.020	0.350	3.340	0.795	0.63	1.61 (± 3.49 %)	10807.0 (± 5.5 %)	17407.0 (± 6.5 %)	111.51	19.53
56	0.022	0.271	3.941	1.161	0.67	1.44 (± 3.48 %)	5311.8 (± 8.9 %)	7664.4 (± 9.5 %)	49.10	8.60
39	0.020		3.110			1.37 (± 5.72 %)	4097.8 (± 15.9 %)	5615.6 (± 16.9 %)	35.97	6.30
30	0.022	0.239	2.795	6.912	0.74	1.33 (± 3.28 %)	3489.8 (± 26.2 %)	4654.4 (± 26.4 %)	29.82	5.22
20	0.029	0.184	2.336	5.332	0.58	1.35 (± 2.52 %)	5155.3 (± 13.8 %)	6960.9 (± 14.0 %)	44.59	7.81
217[g]	0.420		198.00			1.53 (± 1.13 %)	2274.6 (± 1.9 %)	3470.6 (± 2.2 %)	22.23 (± 7.0 %)[h]	
	Total (not including reference at 0 ppm)						59445.7 (± 3.7 %)[i]	89150.6 (± 3.8 %)[i]	571.12	100.00
	total percent carbon by CP-MAS spin counting						31.0 (± 8.3 %)[j]			

[a] Cross-polarization rate constant reported as single or multiple component values. For single exponential component growth/decay, one constant is reported for T_{CH} and $T_{1\rho}$. For multiple component exponential behavior, the value for each component is listed under (1) and (2), with the contribution from component (1) reported in the column titled with the β symbol. The contribution from component 2 will then be (1-β.)

[b] Calculated cross-polarization correction factors for each peak from equations 3.5 and 3.6, with error estimated from the standard error of the estimate (SEE).

[c] Experimental peak areas for each deconvoluted peak. The estimated relative error (ERE) is given as a percent error in parenthesis. The estimated relative error is based on 20 independent deconvolutions (see section 3.3.2.1).

[d] Experimental peak areas multiplied by the ^{1}H T_1 relaxation correction factor (C_{T_1}) and cross polarization correction factor (C_{CP}). The ^{1}H T_1 correction factor will be 1 for all the peaks of the soil or soil extract, and 1.38 for the external reference (peak at 217 ppm). The total error is given as a percent error in parenthesis. The total error is the propagated error of the correction term and experimental peak area.

[e] Amount of carbon in milligrams per deconvoluted peak out of the whole spinner sample (1.842 g).

[f] Percent carbon contribution from this peak out of the total CP-MAS detected carbon, p_i = 100*(mg C for peak i)/(sum of mg C for all peaks).

[g] Peak due to [3.2.1] bicyclo compound external reference.

[h] Result from the calibration of the 3.2.1 spin-reference compound.

[i] Sum of the individual peak integrals in the same column, excluding the integral due to the reference material at 217 ppm. The error for this total is the propagated error of the sum of the aforementioned integrals.

[j] The total percent carbon with relative error given in parenthesis. Error for this total is the propagated error of the total corrected peak integral, and the errors associated with the external reference.

Table 3.5 CP-MAS spin-counting results for the Fulvic Acid (1.483 g).

ppm	Polarization transfer rate constants (ms)[a] T_{CH} (1)		$T_{1\rho}$		β	C_{CP}[b] (± SEE %)	A_{exp}^{CP}[c] (± ERE %)	A_{corr}^{CP}[d] (± Total % error)	mg of carbon[e]	% of total[f] (p_i)
197	1.453		3.024			2.41 (± 7.77 %)	144.9 (± 24.7 %)	348.4 (± 25.9 %)	9.60	4.52
172	0.261		2.368			1.40 (± 1.21 %)	671.1 (± 6.7 %)	942.1 (± 6.8 %)	25.96	12.22
160	0.375		3.005			1.35 (± 2.36 %)	162.9 (± 12.5 %)	220.2 (± 12.7 %)	6.07	2.85
150	0.400		3.467			1.33 (± 3.49 %)	267.3 (± 10.4 %)	354.2 (± 11.0 %)	9.76	4.59
130	0.036	0.529	3.286	2.080	0.43	1.47 (± 2.27 %)	427.4 (± 8.2 %)	630.1 (± 8.5 %)	17.36	8.17
115	0.034	0.834	3.837	2.286	0.30	1.63 (± 2.51 %)	101.8 (± 19.3 %)	166.2 (± 19.5 %)	4.58	2.16
104	0.033	0.308	2.375	1.600	0.70	1.54 (± 2.70 %)	542.3 (± 7.5 %)	834.1 (± 8.0 %)	22.98	10.82
86										
72	0.034		1.826			1.70 (± 4.23 %)	1575.7 (± 9.6 %)	2673.7 (± 10.5 %)	73.67	34.67
56	0.023		2.378			1.51 (± 5.08 %)	386.8 (± 37.1 %)	583.3 (± 37.4 %)	16.07	7.56
39	0.026	0.516	1.483	3.974	0.76	1.76 (± 3.92 %)	223.7 (± 13.0 %)	393.8 (± 13.6 %)	10.85	5.11
30	0.021		1.880			1.68 (± 3.89 %)	177.4 (± 10.4 %)	298.6 (± 11.1 %)	8.23	3.87
20	0.070		2.466			1.46 (± 4.12 %)	183.5 (± 6.2 %)	267.4 (± 7.5 %)	7.37	3.47
217[g]	0.420		198.00			1.53 (± 1.13 %)	528.8 (± 4.2 %)	806.9 (± 4.3 %)	22.23 (± 7.0 %)[h]	
	Total (not including reference at 0 ppm)						4864.9 (± 4.7 %)[i]	7712.2 (± 5.1 %)[i]	212.50	100.00
	total percent carbon by CP-MAS spin counting						14.3 (± 9.7 %)[j]			

[a] Cross-polarization rate constant reported as single or multiple component values. For single exponential component growth/decay, one constant is reported for T_{CH} and $T_{1\rho}$. For multiple component exponential behavior, the value for each component is listed under (1) and (2), with the contribution from component (1) reported in the column titled with the β symbol. The contribution from component 2 will then be (1-β.)

[b] Calculated cross-polarization correction factors for each peak from equations 3.5 and 3.6, with error estimated from the standard error of the estimate (SEE).

[c] Experimental peak areas for each deconvoluted peak. The estimated relative error (ERE) is given as a percent error in parenthesis. The estimated relative error is based on 20 independent deconvolutions (see section 3.3.2.1).

[d] Experimental peak areas multiplied by the ^{1}H T_1 relaxation correction factor (C_{T_1}) and cross polarization correction factor (C_{CP}). The ^{1}H T_1 correction factor will be 1 for all the peaks of the soil or soil extract, and 1.38 for the external reference (peak at 217 ppm). The total error is given as a percent error in parenthesis. The total error is the propagated error of the correction term and experimental peak area.

[e] Amount of carbon in milligrams per deconvoluted peak out of the whole spinner sample (1.483 g).

[f] Percent carbon contribution from this peak out of the total CP-MAS detected carbon, p_i = 100*(mg C for peak i)/(sum of mg C for all peaks).

[g] Peak due to [3.2.1] bicyclo compound external reference.

[h] Result from the calibration of the 3.2.1 spin-reference compound.

[i] Sum of the individual peak integrals in the same column, excluding the integral due to the reference material at 217 ppm. The error for this total is the propagated error of the sum of the aforementioned integrals.

[j] The total percent carbon with relative error given in parenthesis. Error for this total is the propagated error of the total corrected peak integral, and the errors associated with the external reference.

Table 3.6 Summary of elemental and CP-MAS derived spin-counting data for the Uncompahgre Forest soil and its extracts.

Soil component	weight percent of soil	%C by elemental	% C by CP-MAS spin counting	% of C detected by CP-MAS spin counting[a]	% C by elemental on an ash-free basis[b]
whole soil	100	16.07	9.0	48.4	54.12
HF-treated soil	N/A	29.88	24.5	82.0	52.88
humin	87.42	11.86	6.7	54.6	51.12
humic acid	8.92	43.91	31.0	68.5	52.15
fulvic acid	3.66	21.84	14.3	65.8	41.52

[a] Calculated by (%C by CP-MAS)/(%C by elemental)*100.

[b] Ash and carbon elemental analysis provided by Water, Soil, and Plant Testing Laboratory of CSU and Huffman Laboratories, respectively.

Table 3.7 Summary of CP-MAS calibration[b] data for ^{13}C labeled [3.2.1] bicyclo external reference.

compound	peak position (ppm)	t_d[e] (s)	CT[f] (ms)	C_{CP}[g]	C_{T_1}[g]	calibration of 6.49 mg of [3.2.1] bicyclo cpmd (mg C)[d]
Hexamethylbenzene	131	3	5	1.147	1.000	18.54
Hexamethylbenzene	16.9	3	5	1.116	1.000	18.84
50/50 mixture of hexamethylbenzene in glycine, hexamethylbenzene peaks[a]	131	5	5	1.107	1.000	22.28
50/50 mixture of hexamethylbenzene in glycine, hexamethylbenzene peaks[a]	16.9	5	5	1.125	1.000	21.72
1,4 dimethoxybenzene	56	5	5	1.003	1.006	20.89
1,4 dimethoxybenzene	156	5	5	1.004	1.007	20.69
1,4 dimethoxybenzene	111, 117	5	5	1.002	1.005	21.10
Monoethylfumarate[c]	15.3	9	5	1.014	1.007	22.48
Monoethylfumarate[c]	62.1	9	5	1.014	1.007	24.58
Monoethylfumarate[c]	136.3, 133.8	9	5	1.022	1.008	21.95
Monoethylfumarate[c]	171.8, 165.7	9	5	1.024	1.008	21.67
glycine	175	5	5	1.162	1.000	22.73
glycine	46	5	5	1.172	1.000	24.87
50/50 mixture of glycine in hexamethylbenzene, glycine peaks[a]	175	5	5	1.162	1.000	21.83
50/50 mixture of glycine in hexamethylbenzene, glycine peaks[a]	46	5	5	1.177	1.000	24.33
2,6-dimethoxyphenol	147	15	5	1.006	1.005	20.45
2,6-dimethoxyphenol	134	15	5	1.006	1.005	20.55
2,6-dimethoxyphenol	120	15	5	1.012	1.005	21.08
2,6-dimethoxyphenol	104	15	5	1.006	1.005	21.12
2,6-dimethoxyphenol	55	15	5	1.001	1.005	21.64
average						22.23
standard deviation						1.56
relative deviation						7.00

[a] A 50/50 mixture (by weight) of hexamethylbenzene and glycine.

[b] All calibrations were run with the same radio-frequency field intensities used for the spin-counting experiments on the individual soil samples, matched on the first spinning side-band. Magic angle spinning speeds of 2.0 kHz were used.

[c] MAS speed of 3.5 kHz was used for the monoethylfumarate calibration.

[d] The calibration value empirically assigned to the reference material. The values reported here are based on peak integrals that have been corrected to account for ^1H T_1 relaxation times and cross-polarization dynamics (A_{corr}^{CP}). The external reference has a ^1H T_1 of 0.51 s and a C_{CP} of 1.069 for a contact time of 5.0 ms at 2.0 kHz MAS. At 3.5 kHz MAS, the external reference has ^1H T_1 of 0.59 s and a C_{CP} of 1.036 for a contact time of 5.0 ms.

[e] Repetition delay in seconds between acquisitions during calibration experiments.

[f] Cross-polarization contact period in milliseconds.

[g] Correction factors for the peaks of the calibration compound, calculated according to equations 3.5 and 3.6.

Table 3.8 Summary of normalized and corrected peak areas for DP- and CP-MAS spin counting experiments.

Normalized[a] and Corrected (A_{corr}^{CP}, A_{corr}^{DP}) Peak Areas										
	CP-MAS					DP-MAS				
peak position	whole soil	HF-treated soil	humin	humic acid	fulvic acid	whole soil	HF-treated soil	humin	humic acid	fulvic acid
197	0.09	0.08	0.02	0.12	0.07	0.12	0.49	0.19	0.14	0.07
172	0.26	0.31	0.19	0.64	0.30	0.71	0.61	0.79	0.83	0.51
160					0.06					0.10
150	0.24	0.39	0.13	0.61	0.17	0.45	0.53	0.37	0.55	0.26
130	0.39	0.57	0.27	0.94	0.17	1.00	1.00	1.00	1.00	0.35
115	0.23	0.26	0.13	0.32	0.06	0.22	0.16	0.29	0.36	0.12
104	0.30	0.27	0.29	0.21	0.26	0.23	0.37	0.18	0.24	0.20
72[b]	1.00	1.00	1.00	1.00	1.00	0.92	0.87	0.92	0.65	1.00
56	0.38	0.38	0.33	0.54	0.21	0.29	0.41	0.25	0.35	0.16
39	0.24	0.24	0.21	0.30	0.14	0.06	0.46	0.05	0.13	0.14
30	0.26	0.29	0.12	0.26	0.17	0.25	0.20	0.27	0.37	0.14
20	0.16	0.21	0.29	0.48	0.08	0.17	0.19	0.14	0.27	0.10
percent carbon observed by CP- or DP-MAS spin-counting[c]	48.4	82.0	54.6	68.5	65.8	59.1	85.7	71.7	71.3	68.7

[a] The maximum value for the corrected peak area of a each set of data was normalized to a value of 1.00. All other values for each soil component were made relative to the maximum value.

[b] In many cases, the CP-MAS spin counting experiments were able to resolve a second peak at 86 ppm. This intensity was added to the peak at 72 ppm for comparison to the DP-MAS data where the peak was not resolved.

[c] Percent carbon observed relative to that determined by elemental analysis. Results for DP-MAS are from Chapter 2, Table 2.7 of this thesis.

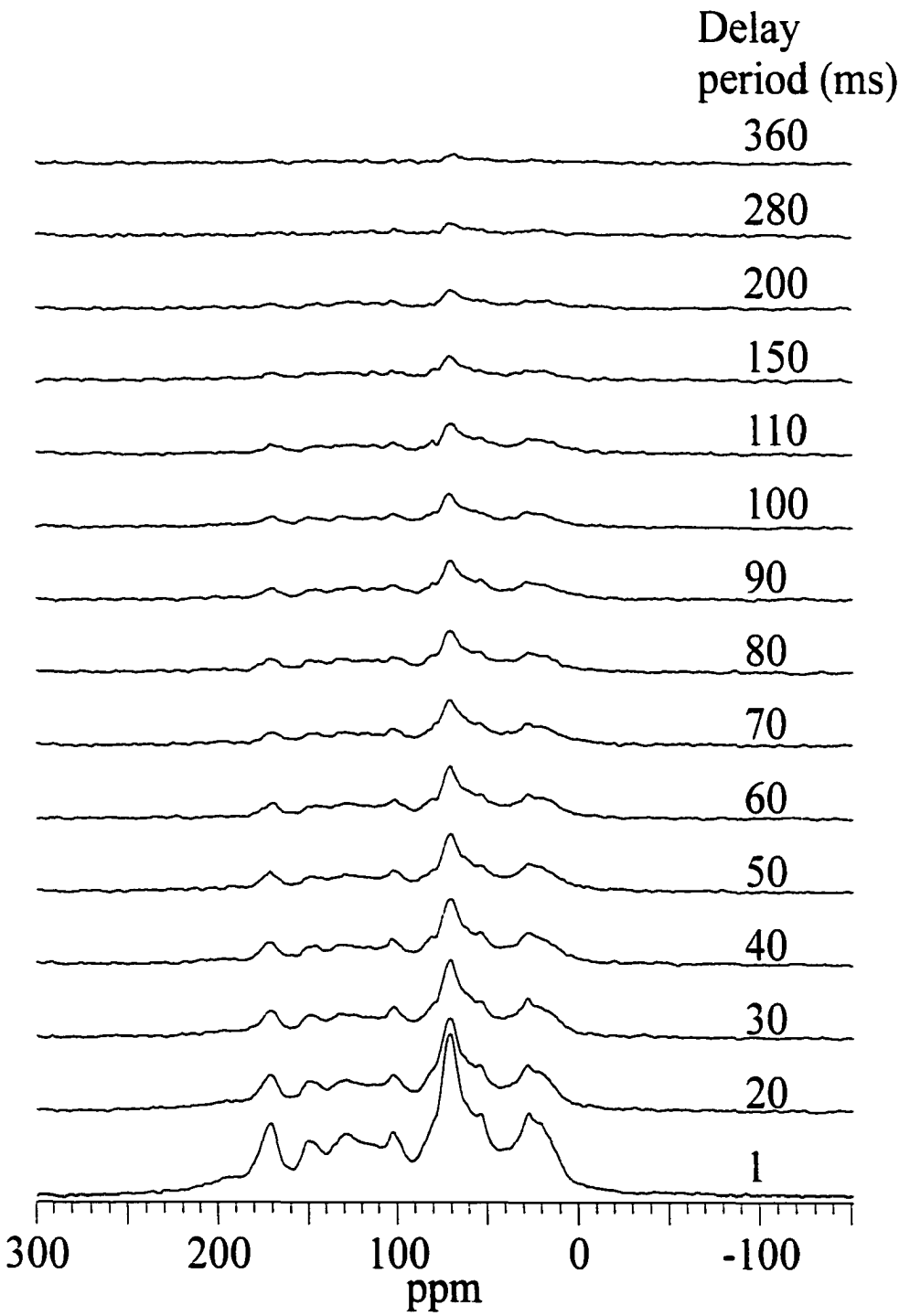

Figure 3.1 CP-MAS based proton T_1 measurement of Uncompahgre whole soil.

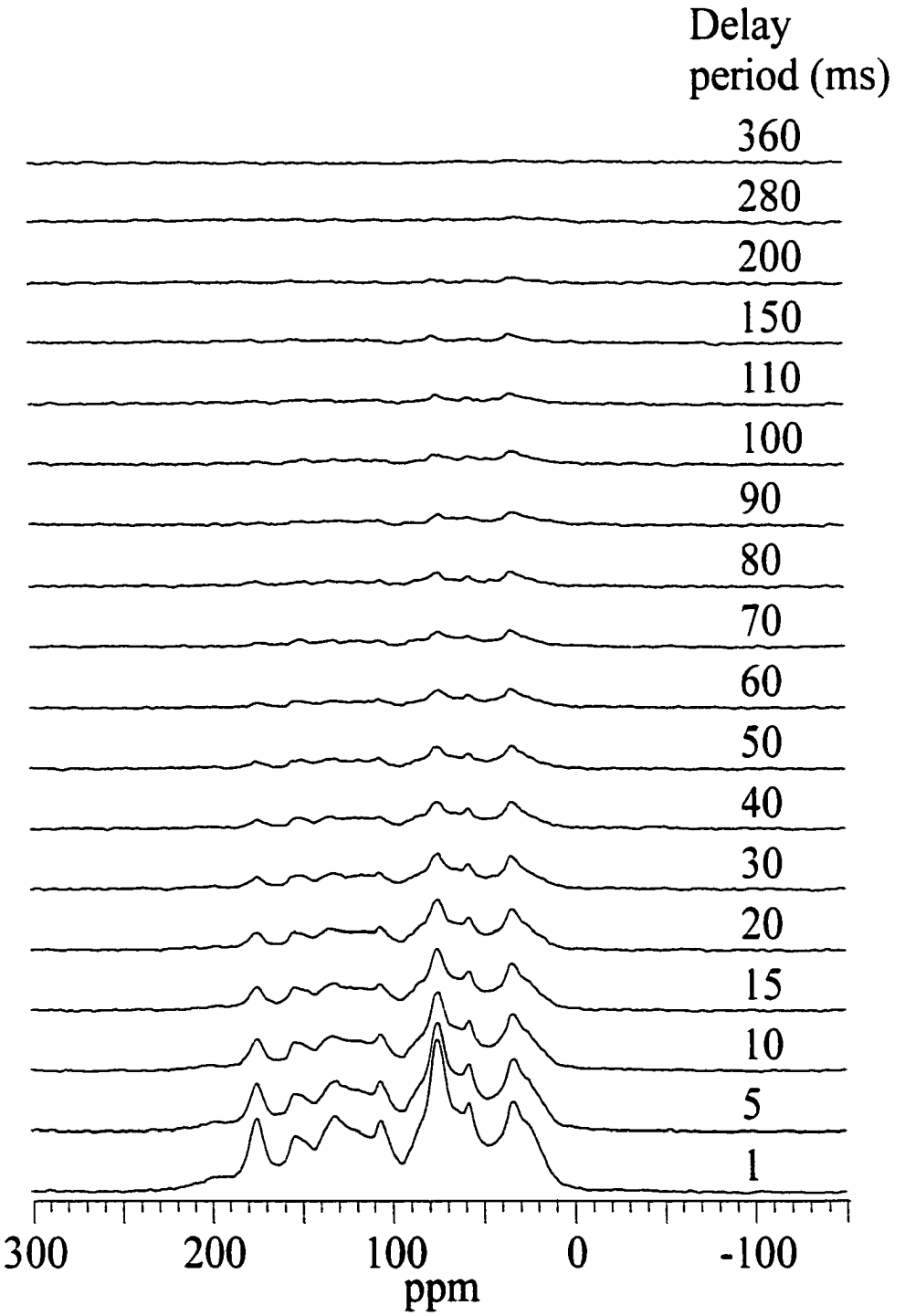

Figure 3.2 CP-MAS based proton T_1 measurement of HF-Treated Uncompahgre whole soil.

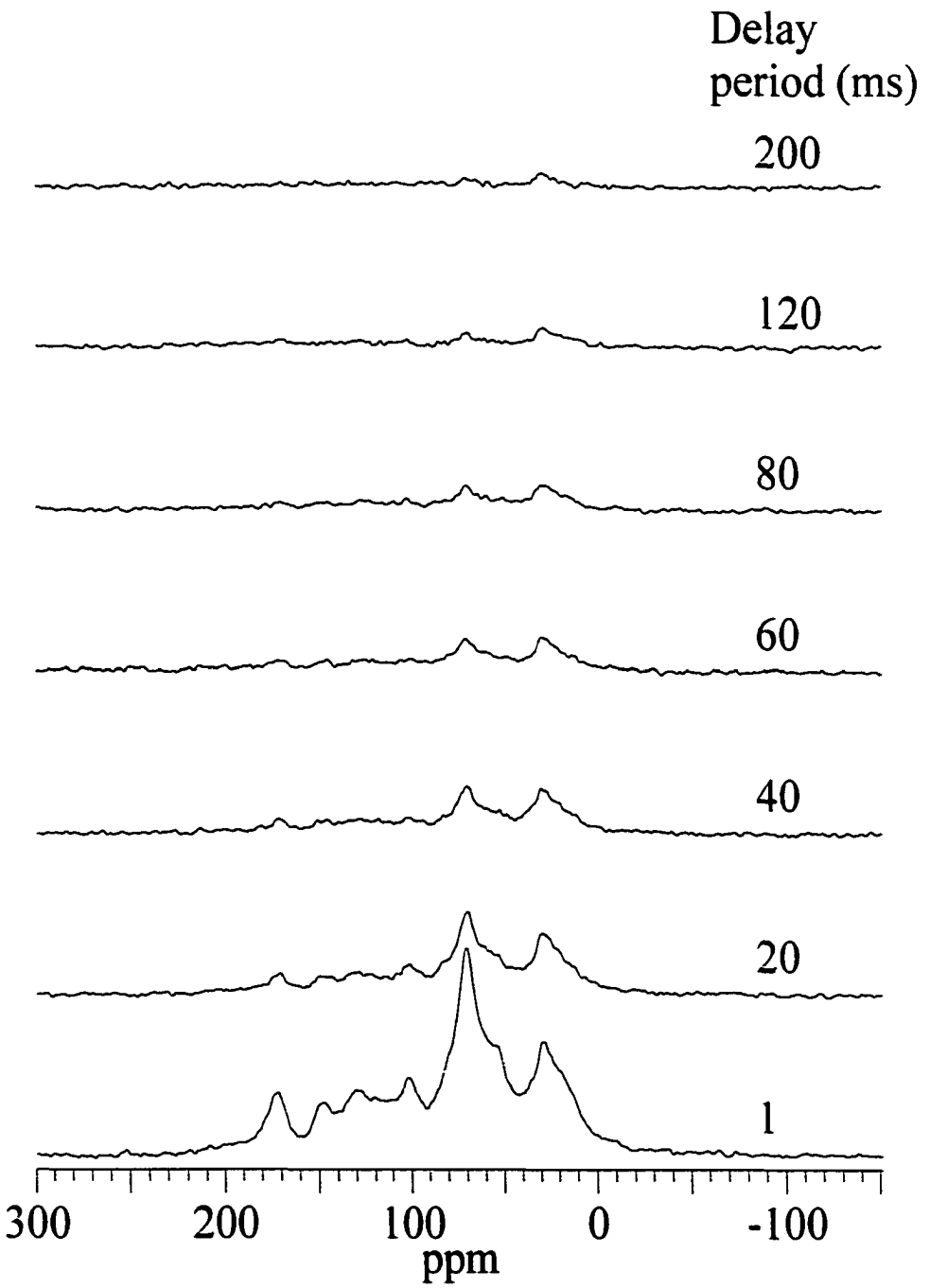

Figure 3.3 CP-MAS based proton T_1 measurement of Uncompahgre soil humin fraction.

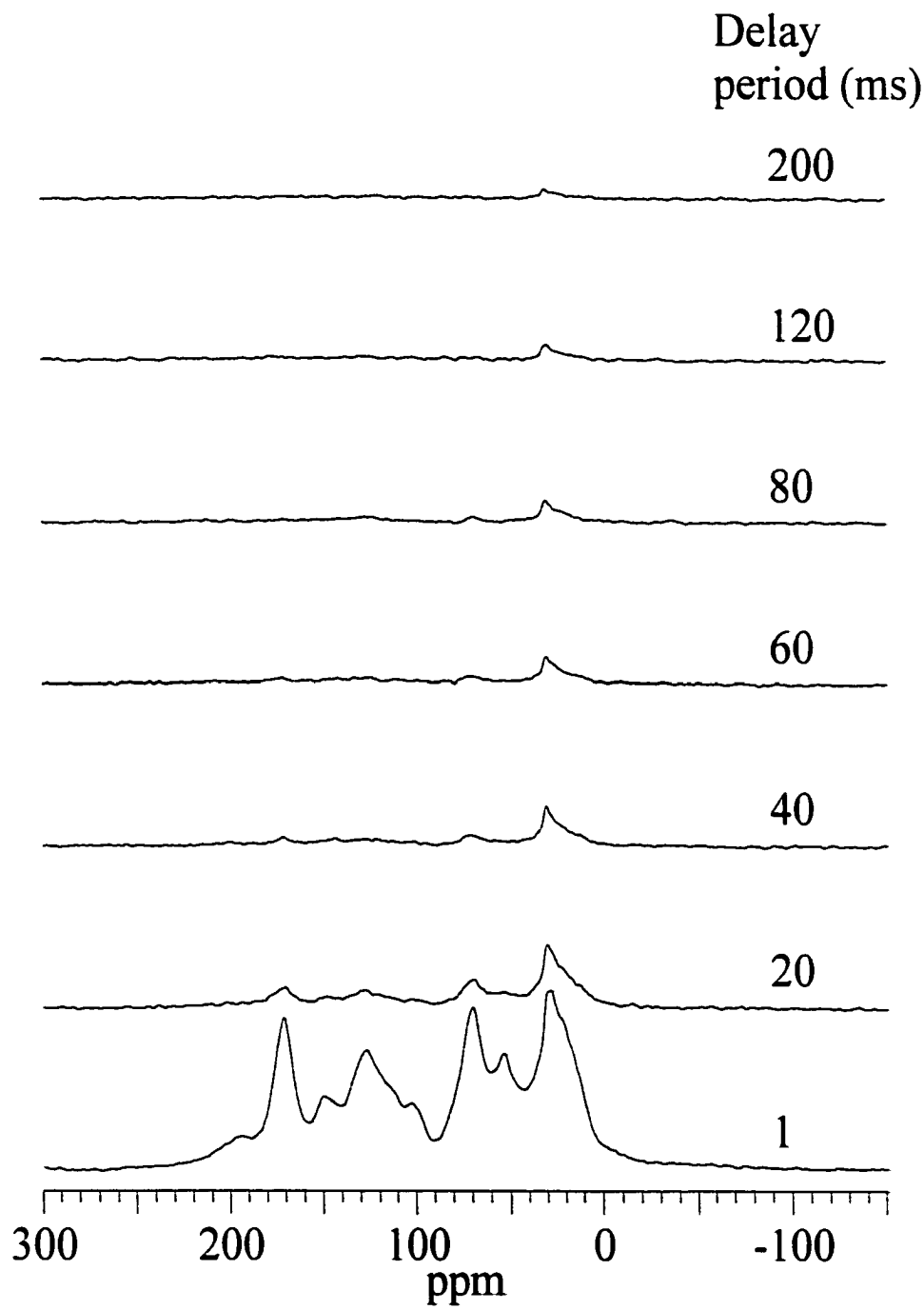

Figure 3.4 CP-MAS based proton T_1 measurement of Uncompahgre humic acid.

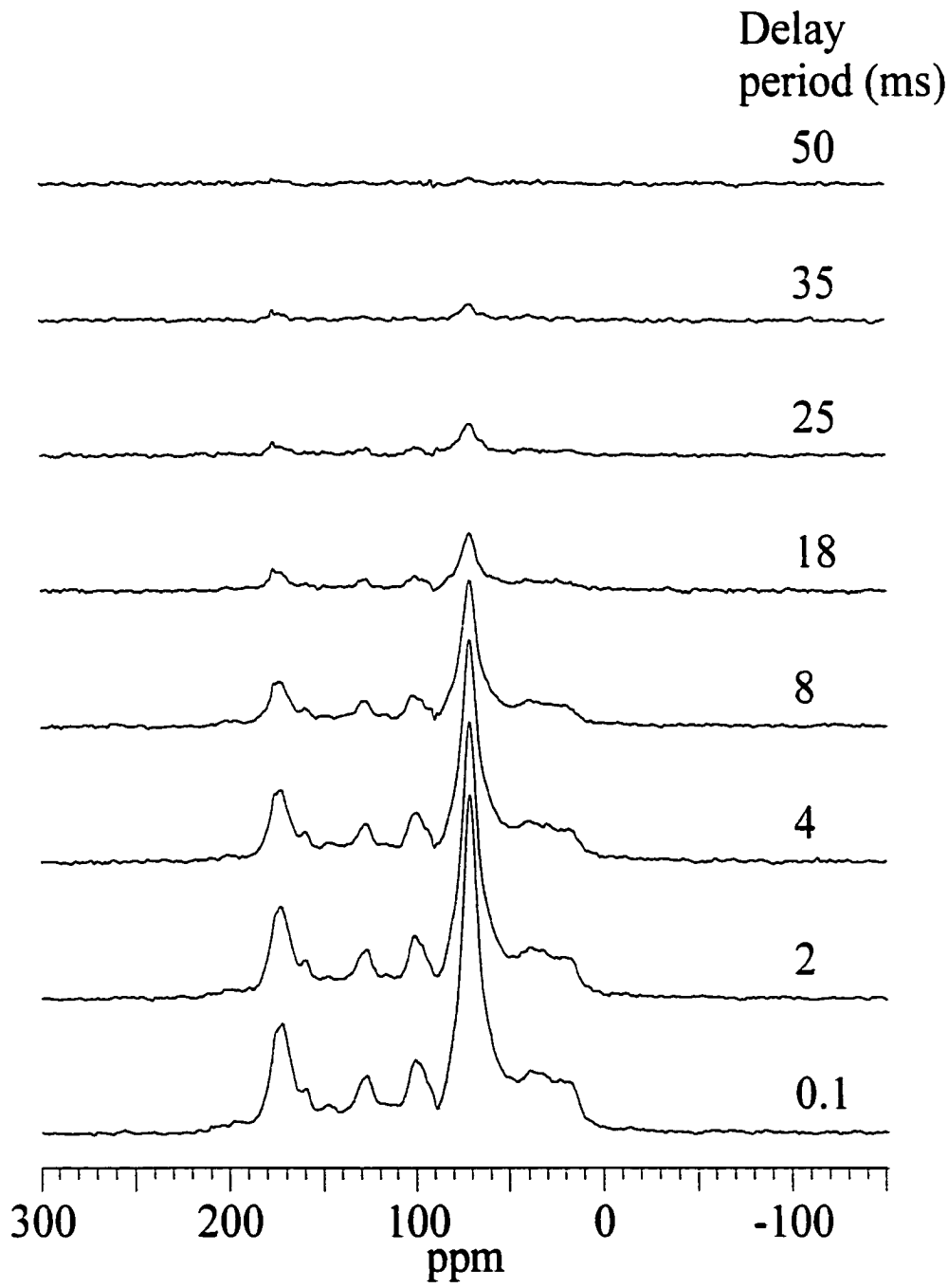

Figure 3.5 CP-MAS based proton T_1 measurement on Uncompahgre fulvic acid.

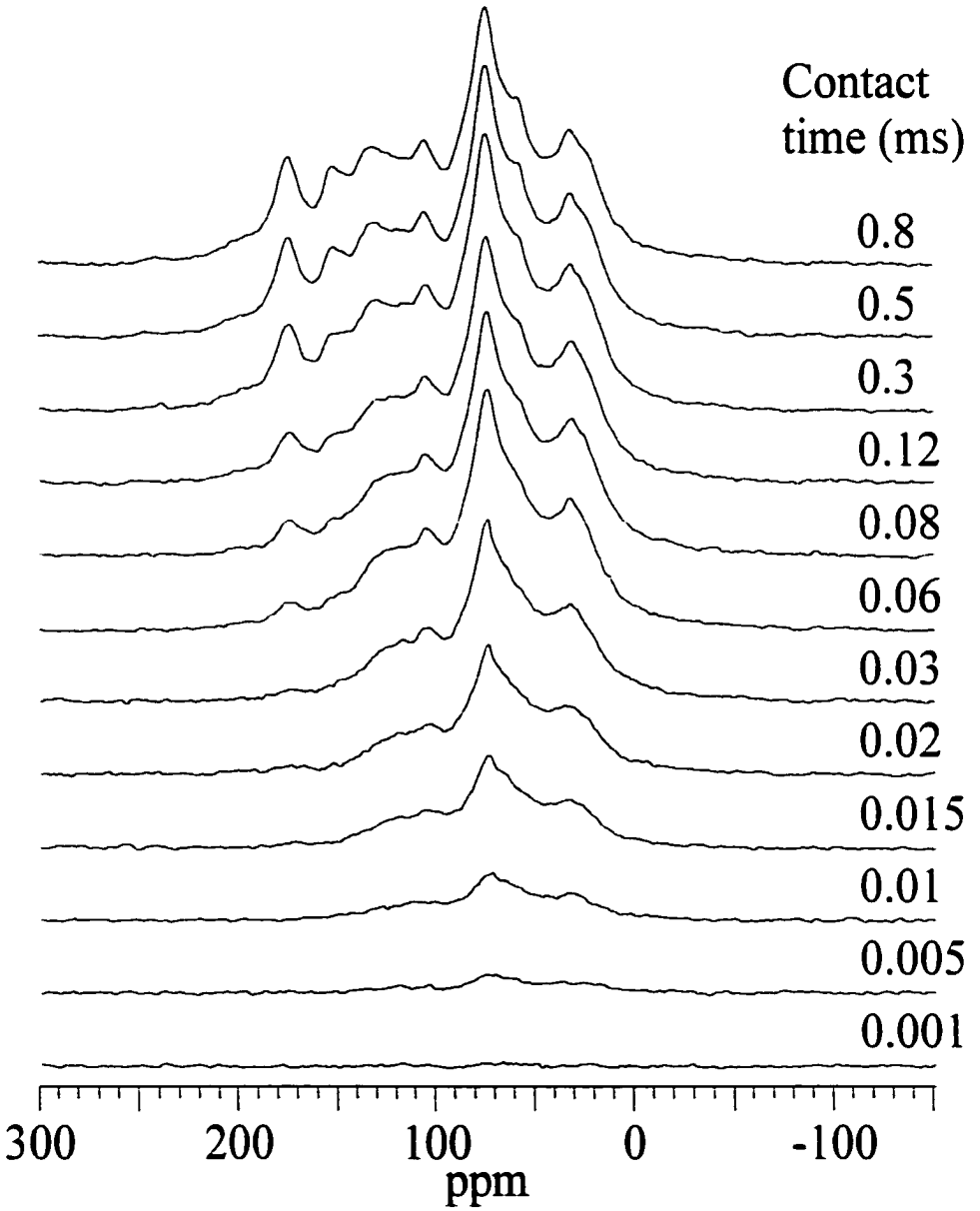

Figure 3.6(a) Variable contact time spectra of Uncompahgre whole soil.

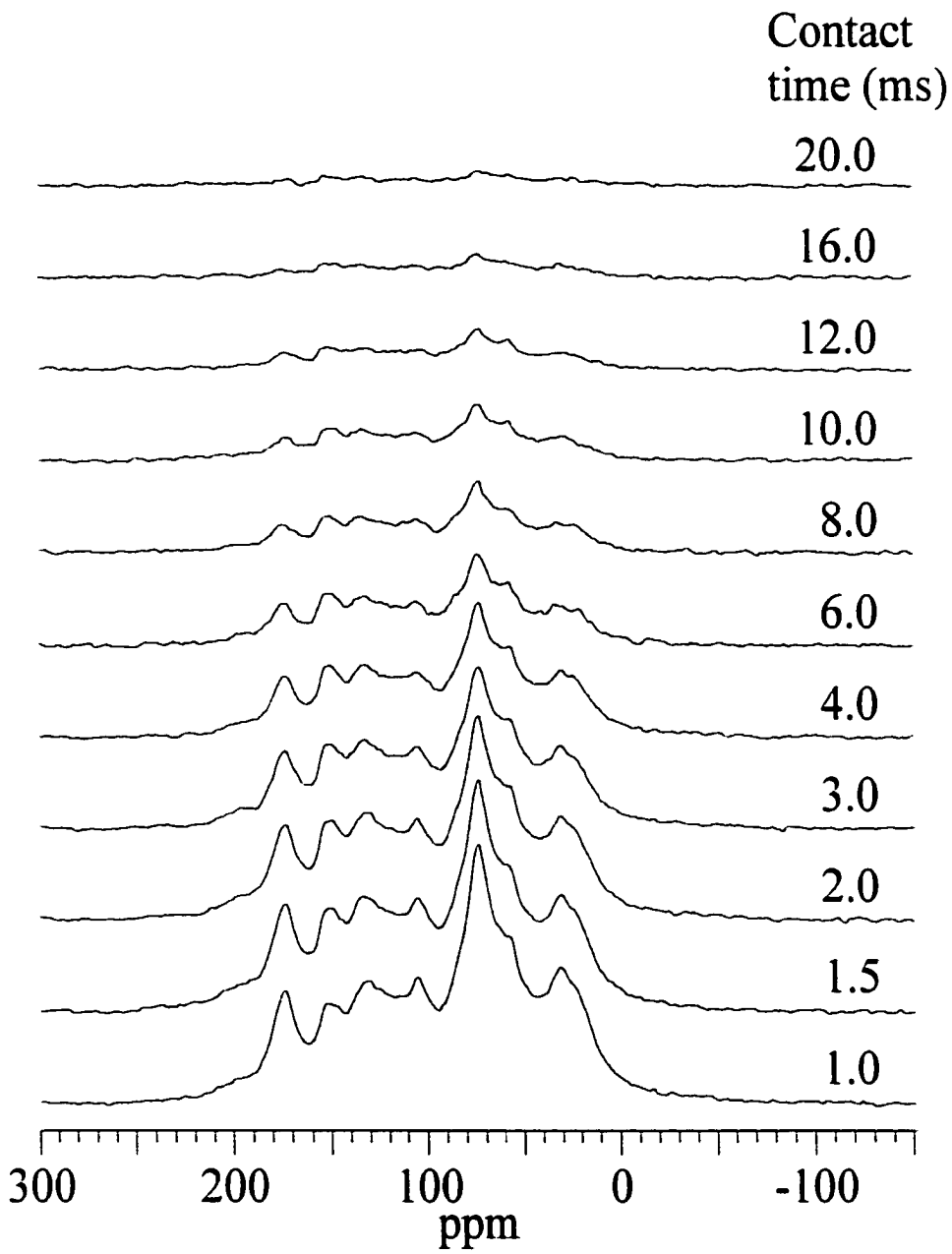

Figure 3.6(a) Variable contact time spectra of Uncompahgre whole soil (continued).

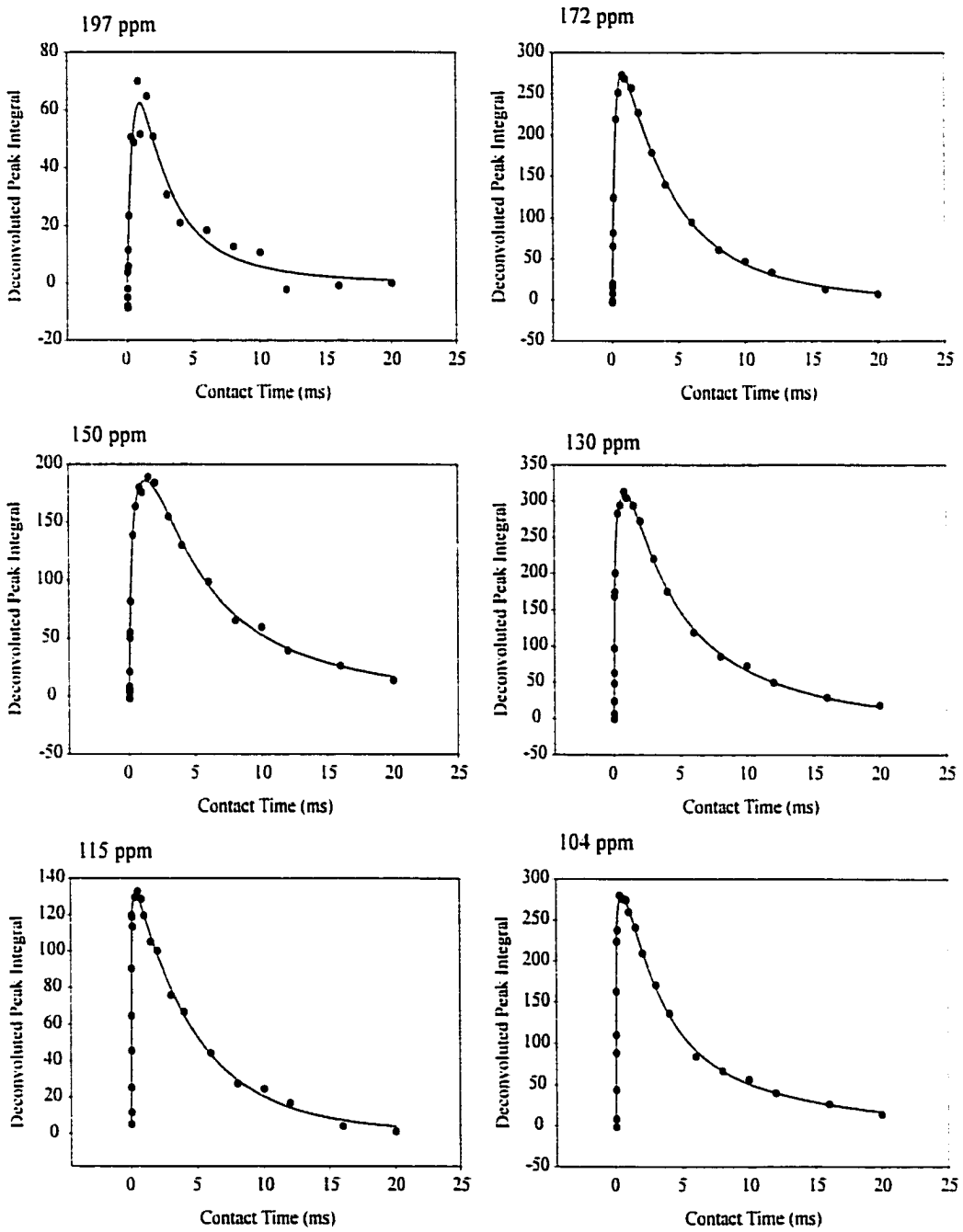

Figure 3.6(b) Plots of variable contact time data from the Uncompahgre whole soil.

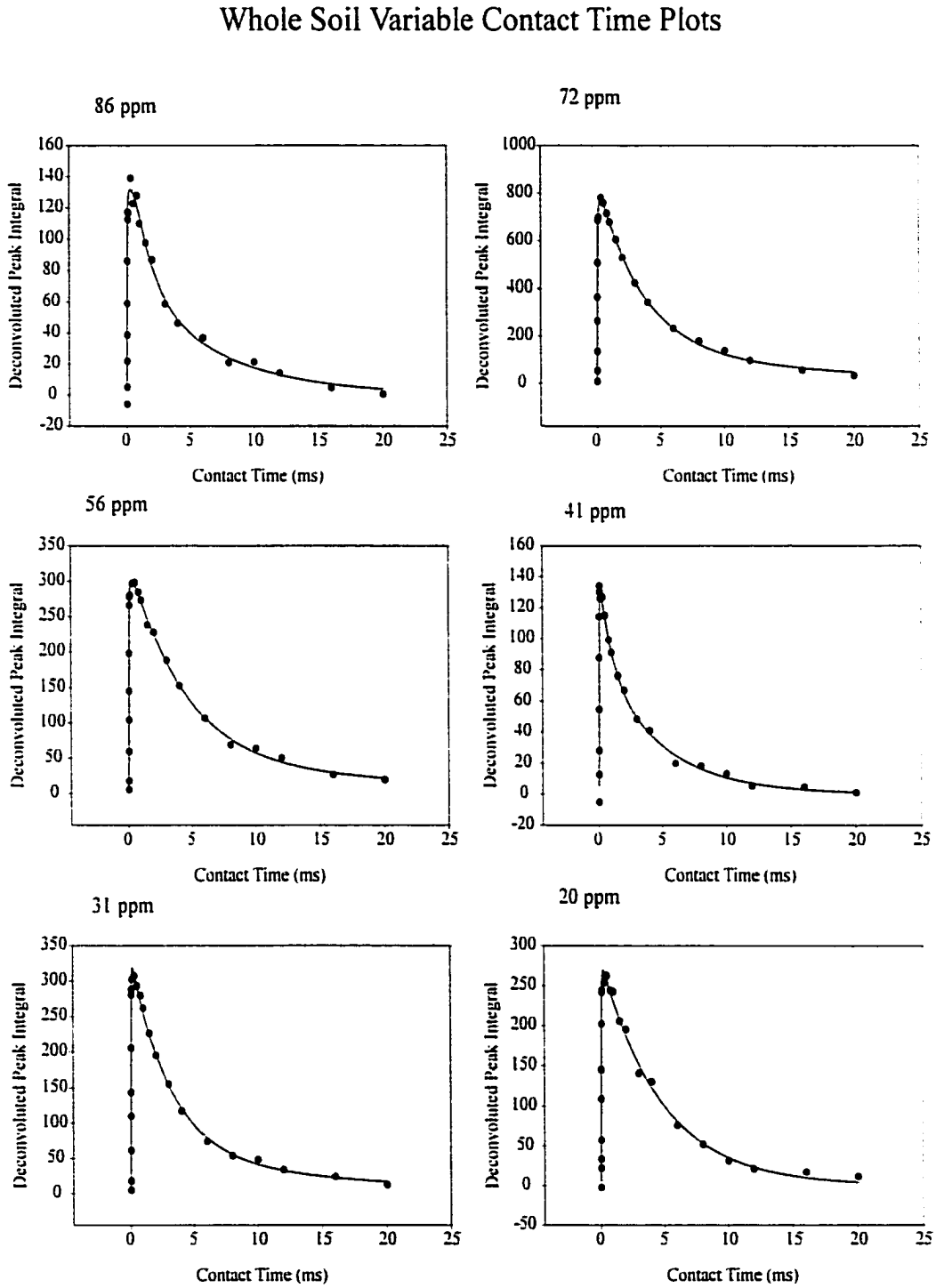

Figure 3.6(b) Plots of variable contact time data from the Uncompahgre whole soil (continued).

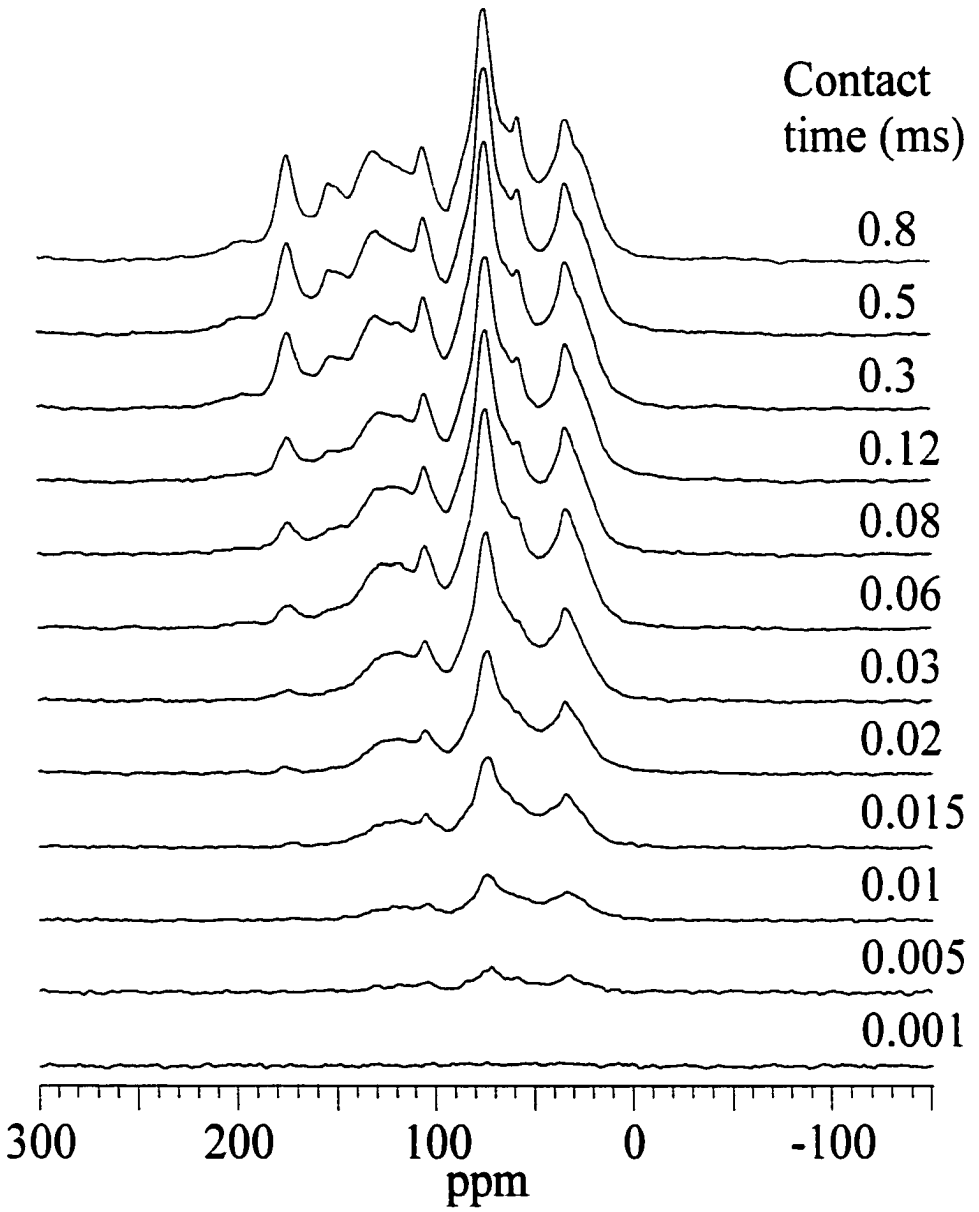

Figure 3.7(a) Variable contact time spectra of HF-Treated Uncompahgre whole soil.

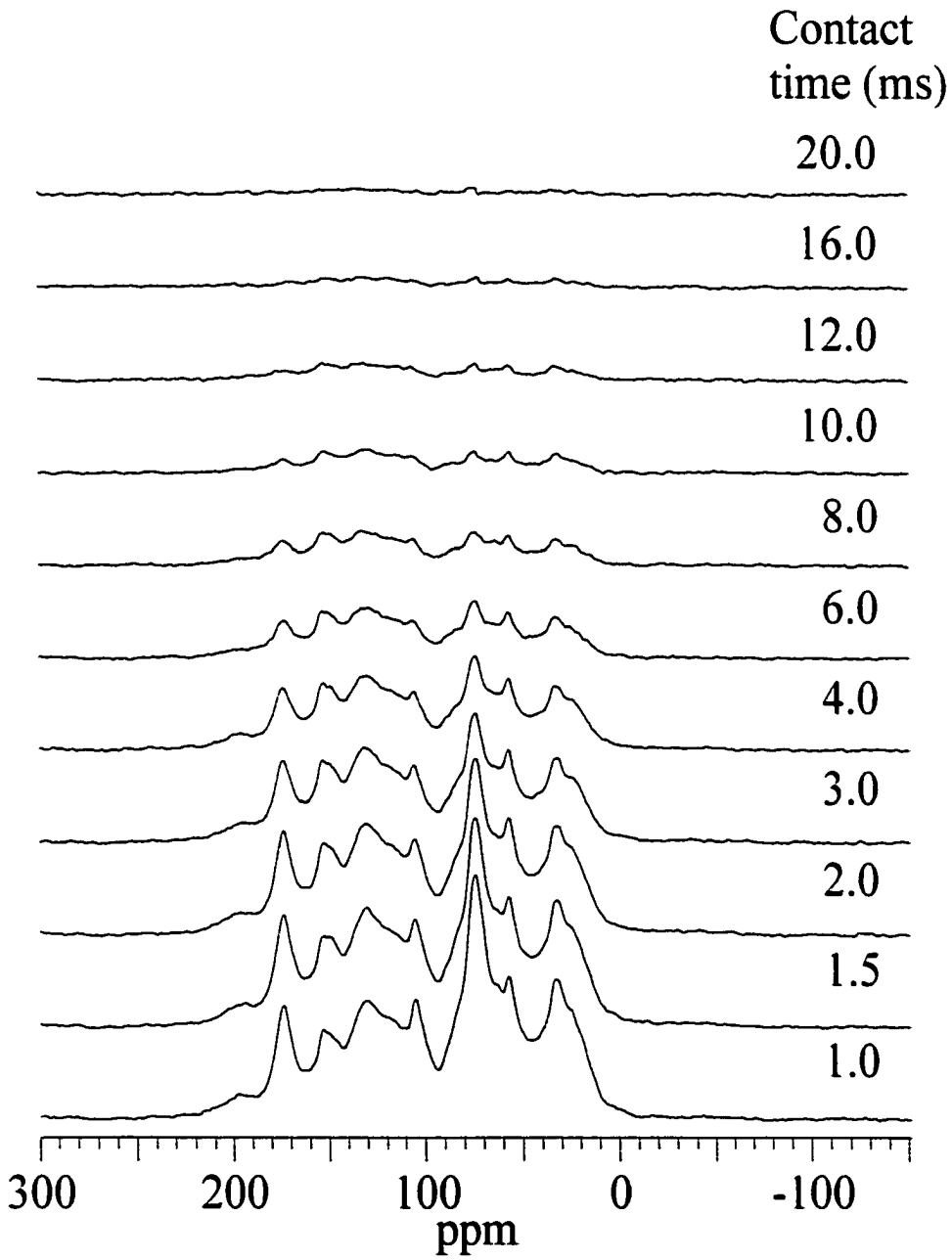

Figure 3.7(a) Variable contact time spectra of HF-Treated Uncompahgre whole soil (continued).

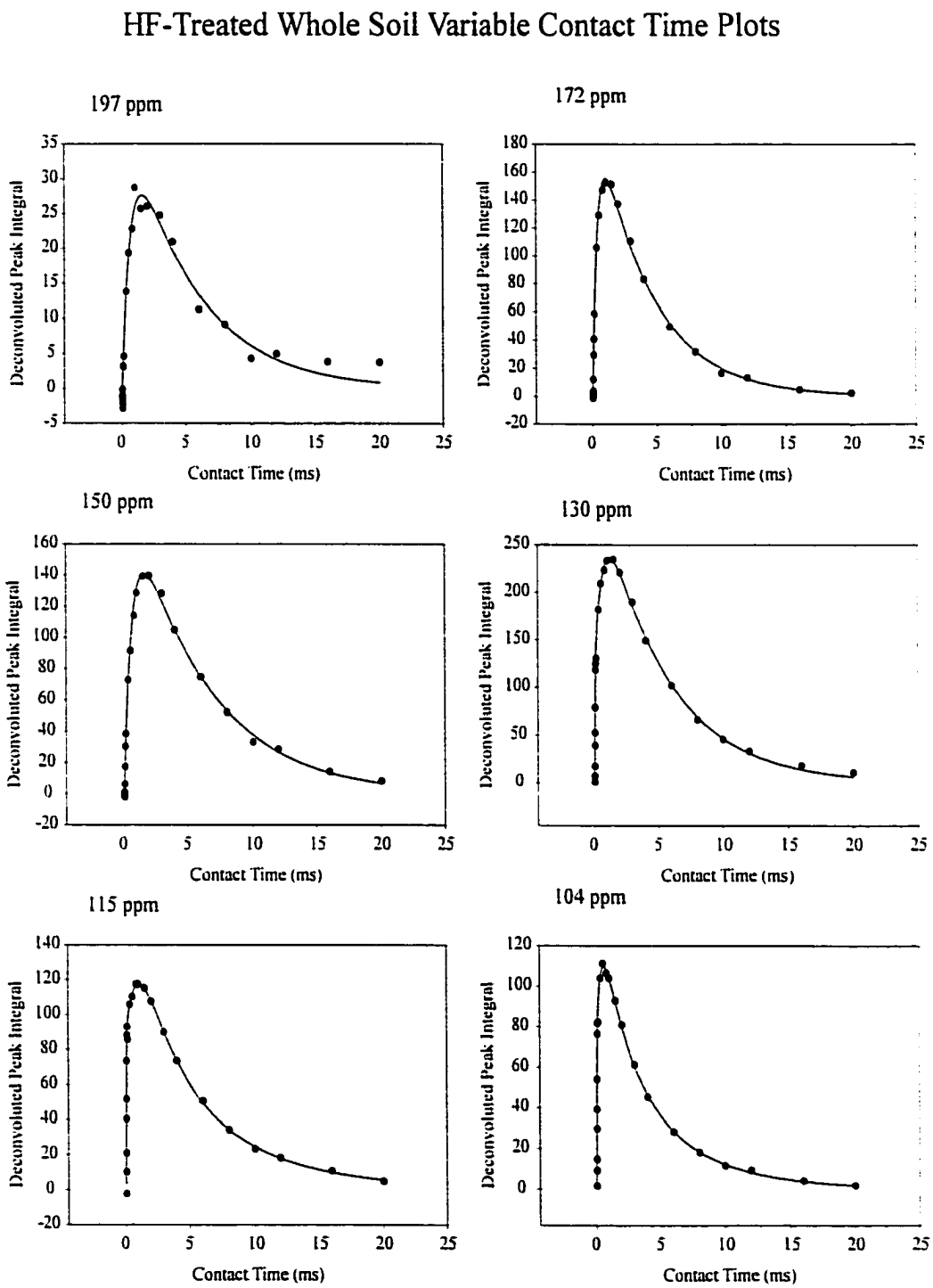

Figure 3.7(b) Plots of variable contact time data from the HF-treated Uncompahgre whole soil.

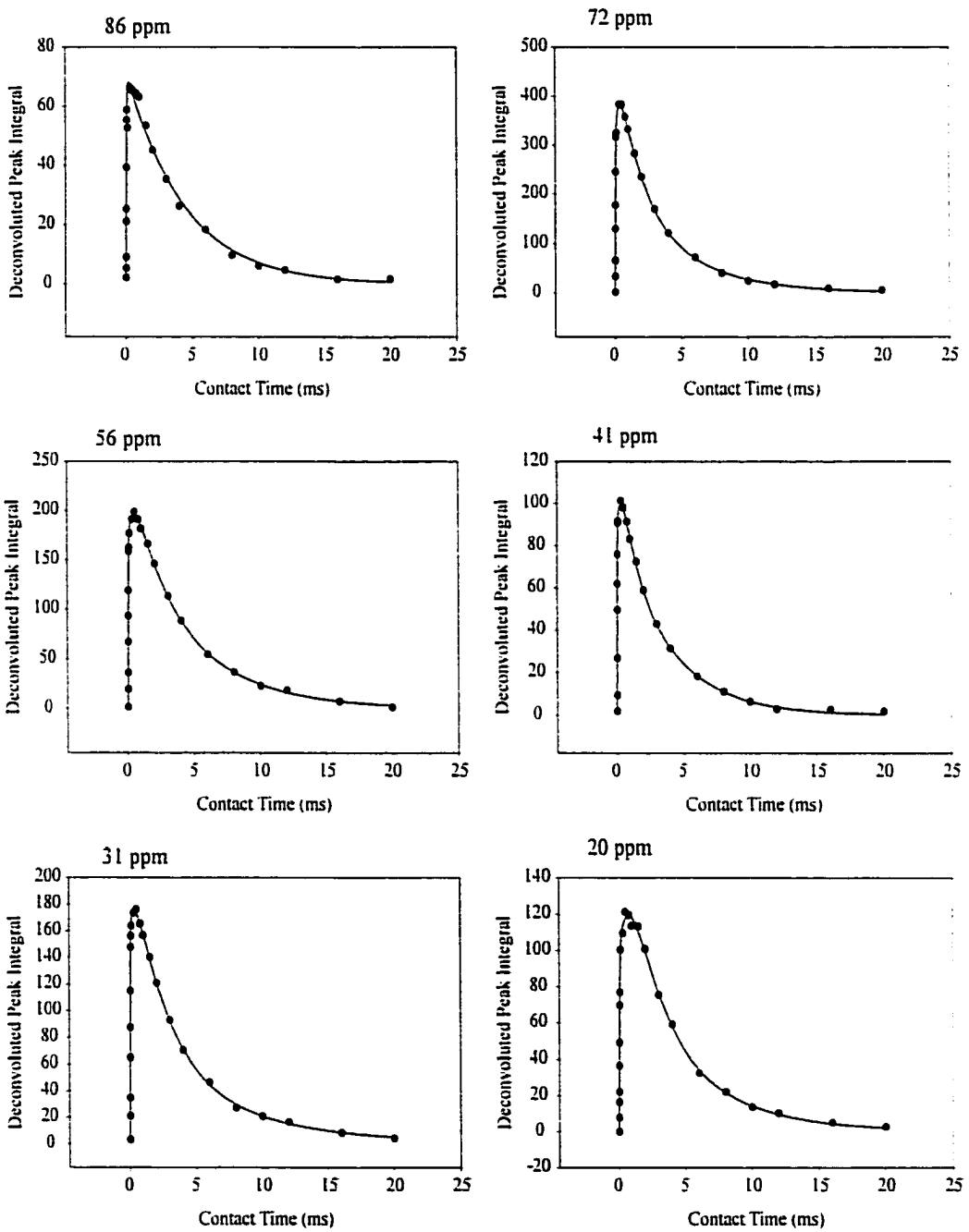

Figure 3.7(b) Plots of variable contact time data from the HF-treated Uncompahgre whole soil (continued).

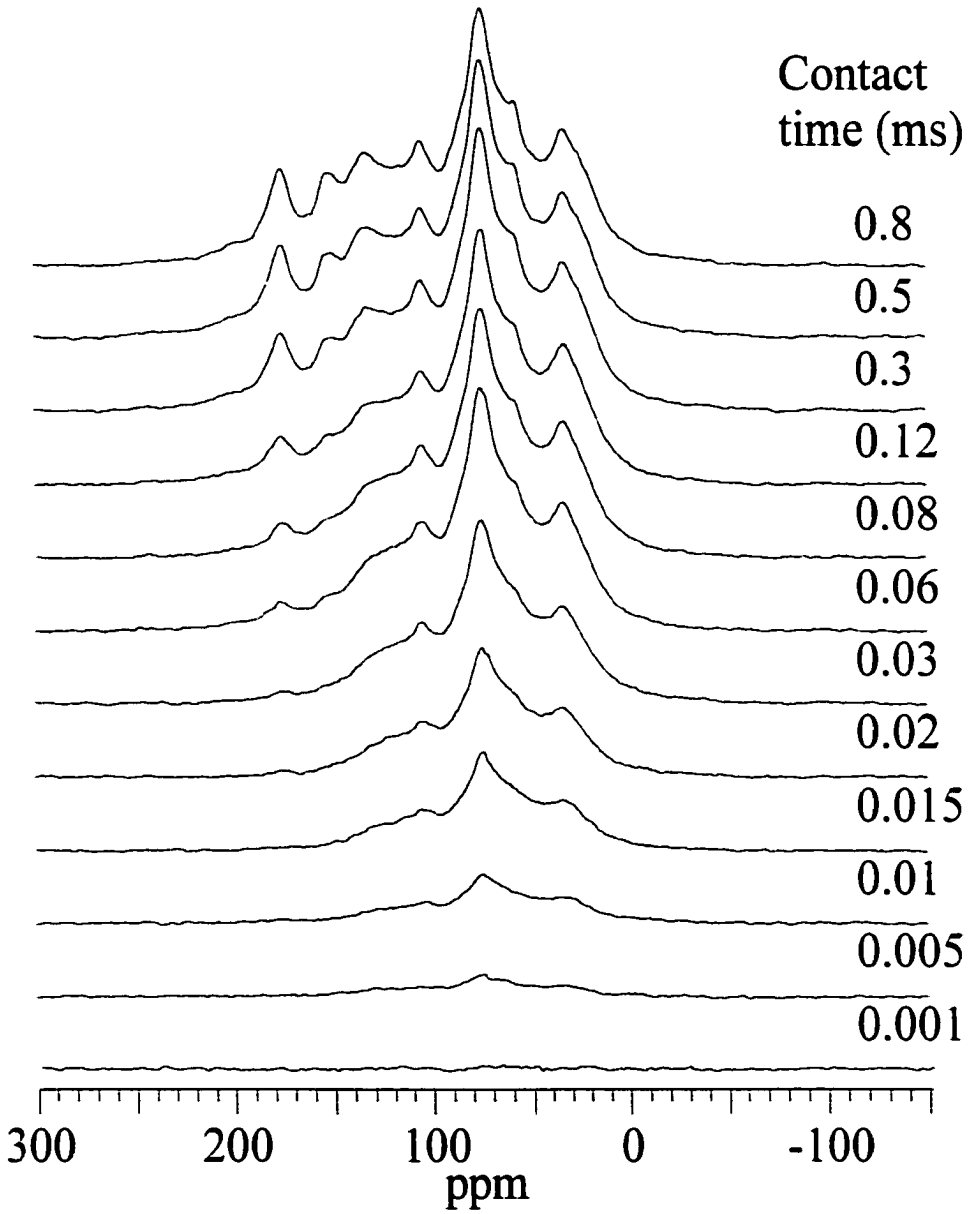

Figure 3.8(a) Variable contact time spectra of Uncompahgre humin fraction.

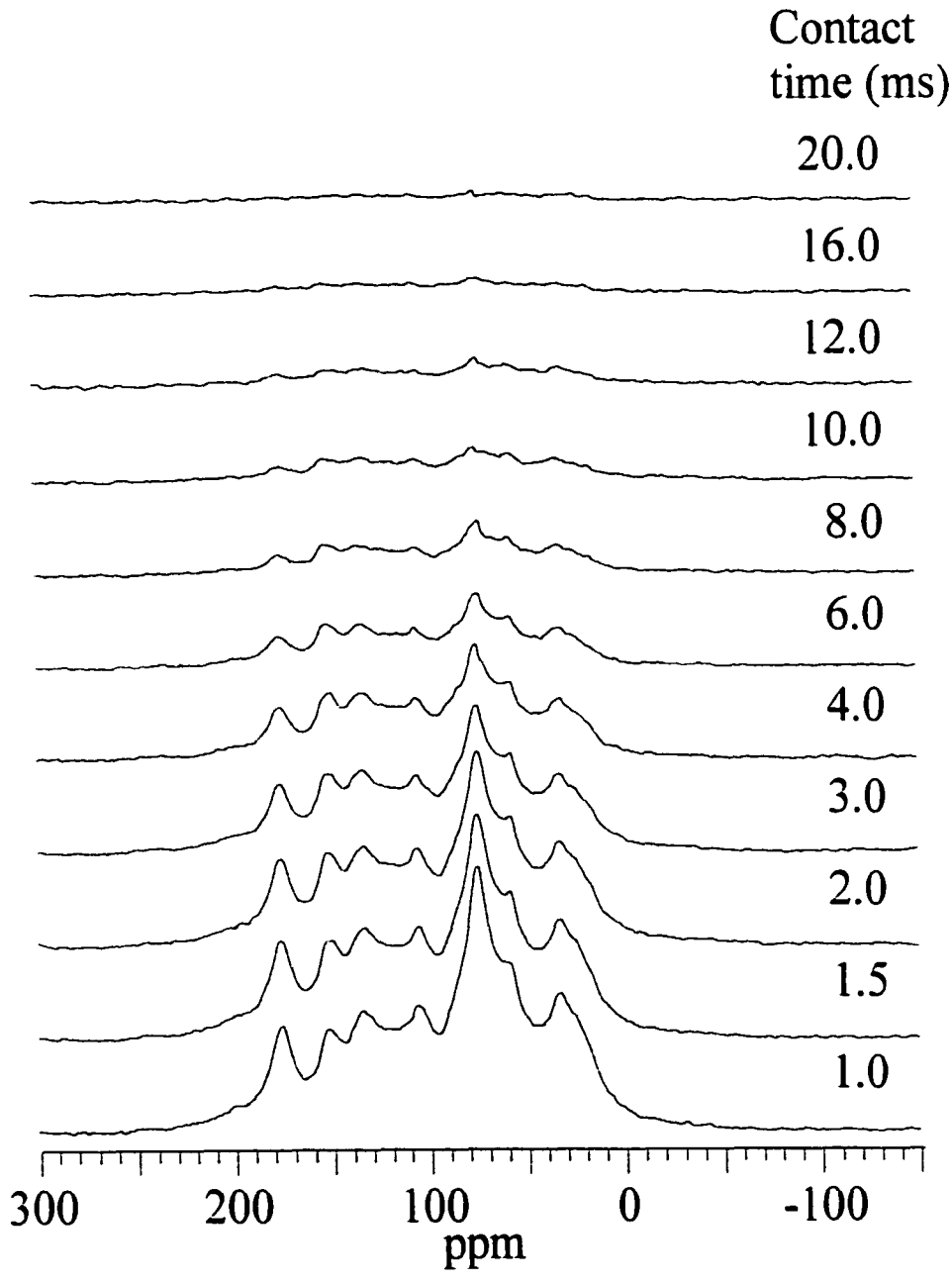

Figure 3.8(a) Variable contact time spectra of Uncompahgre humin fraction (continued).

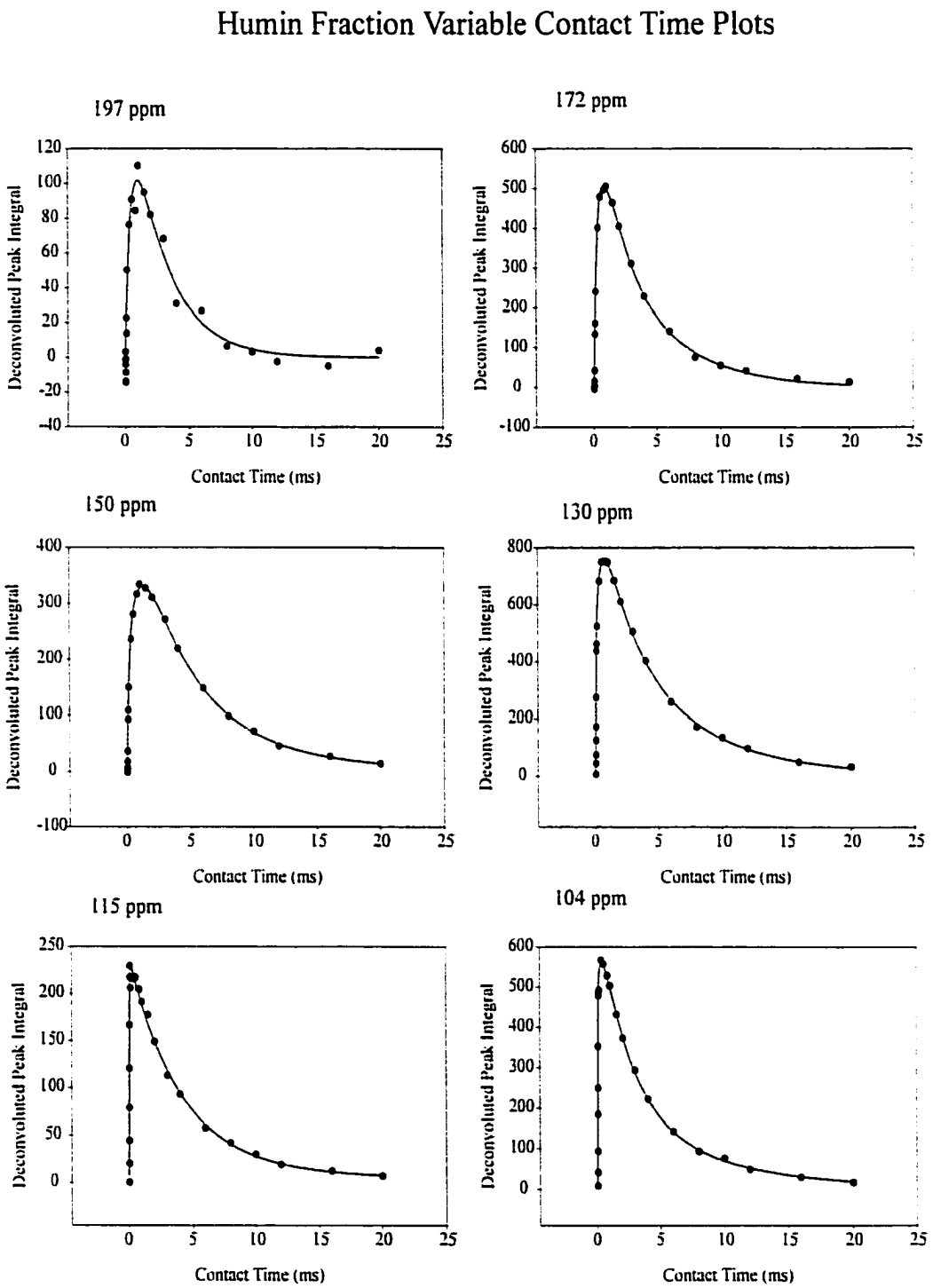

Figure 3.8(b) Plots of variable contact time data from the humin fraction.

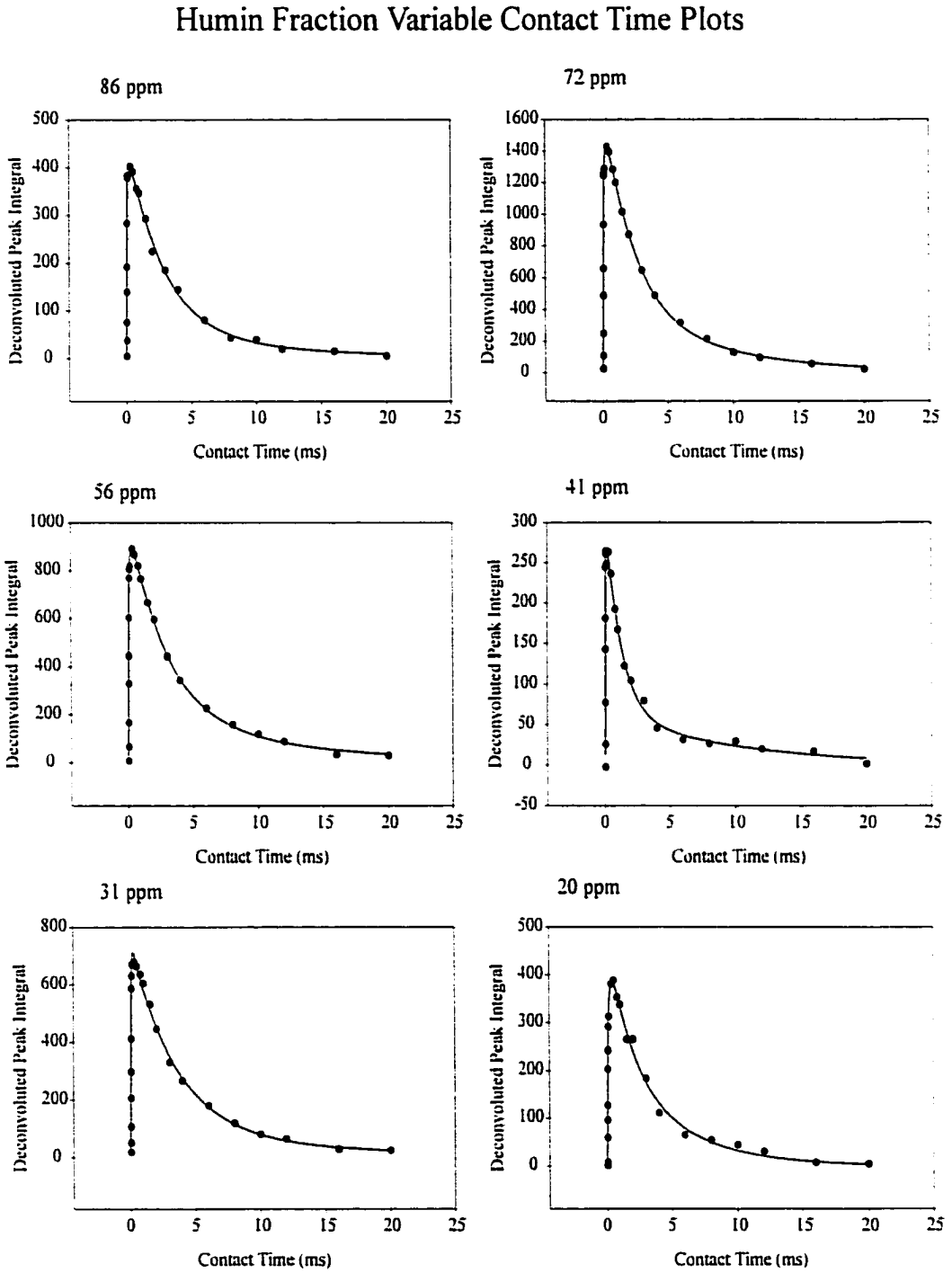

Figure 3.8(b) Plots of variable contact time data from the humin fraction (continued).

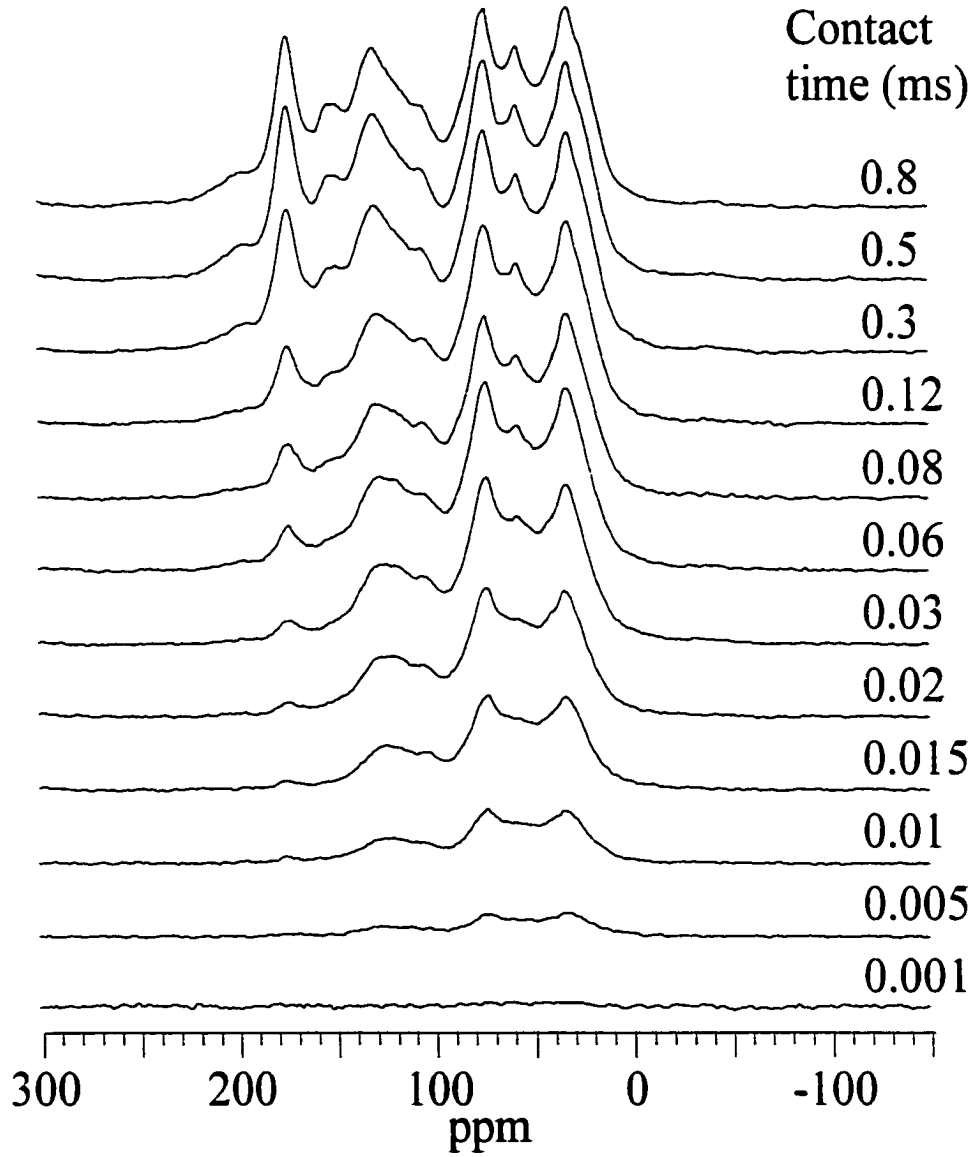

Figure 3.9(a) Variable contact time spectra of Uncompahgre humic soil fraction.

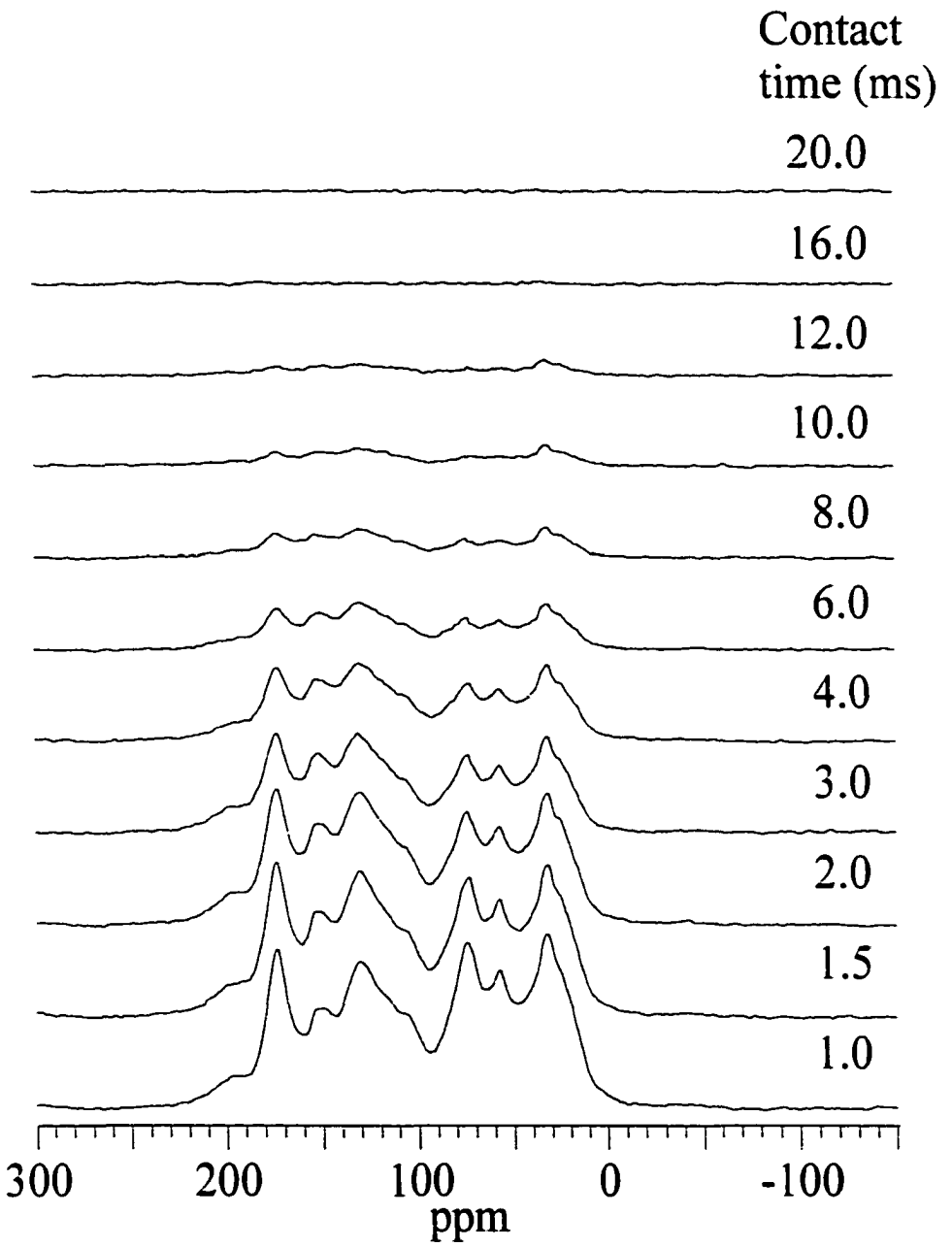

Figure 3.9(a) Variable contact time spectra of Uncompahgre humic soil fraction (continued).

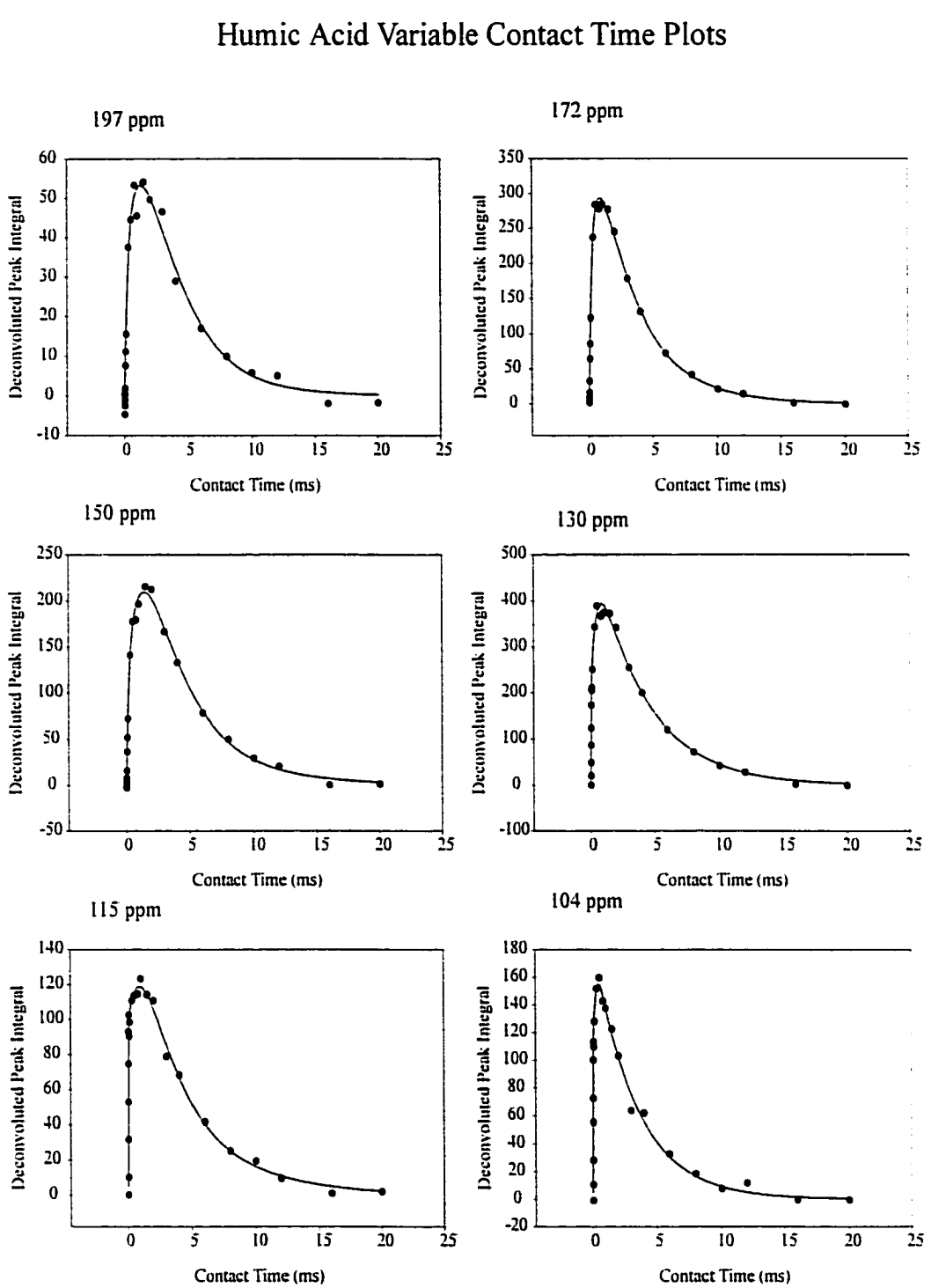

Figure 3.9(b) Plots of variable contact time data from the humic acid fraction.

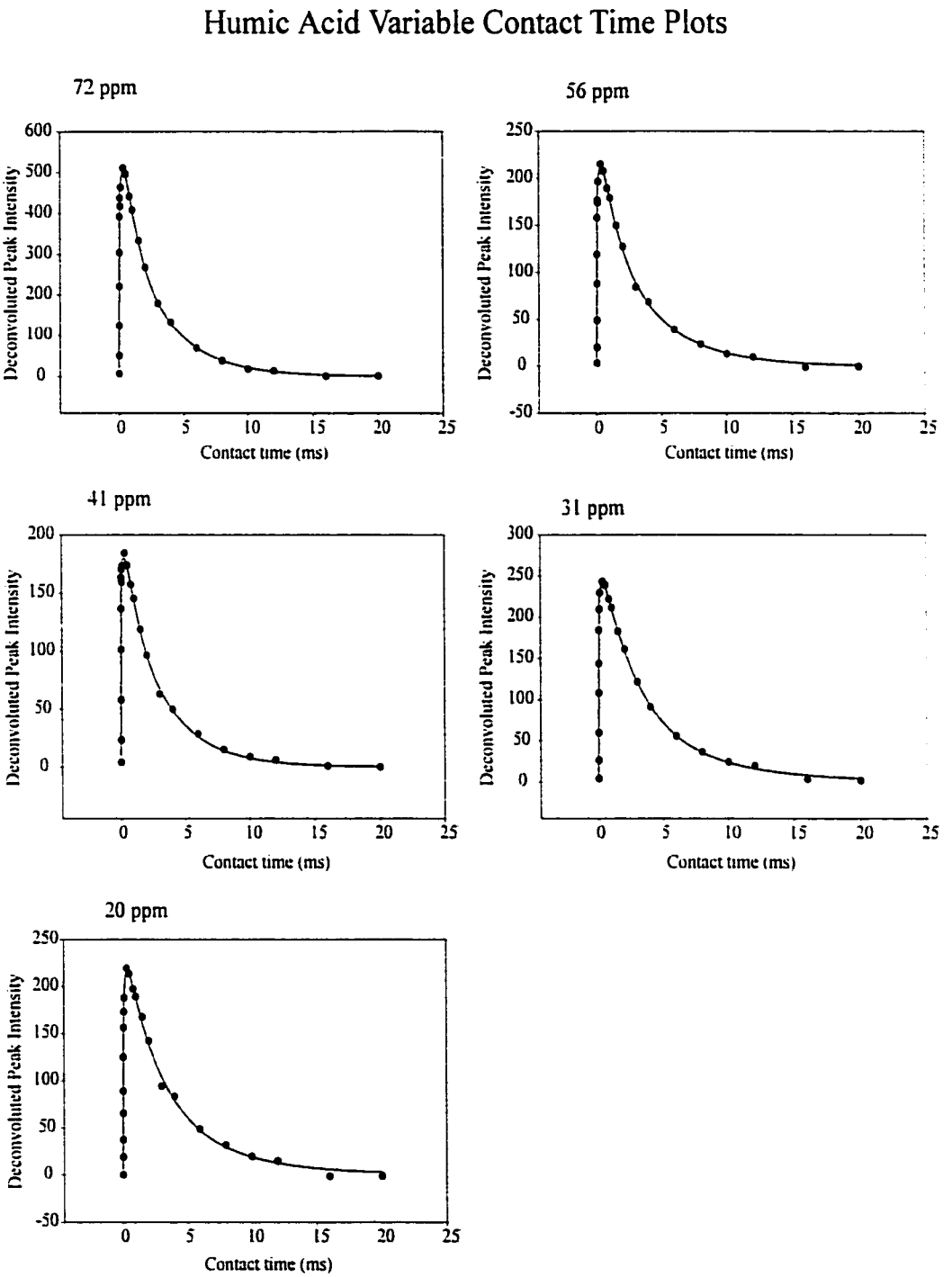

Figure 3.9(b) Plots of variable contact time data from the humic acid fraction (Continued).

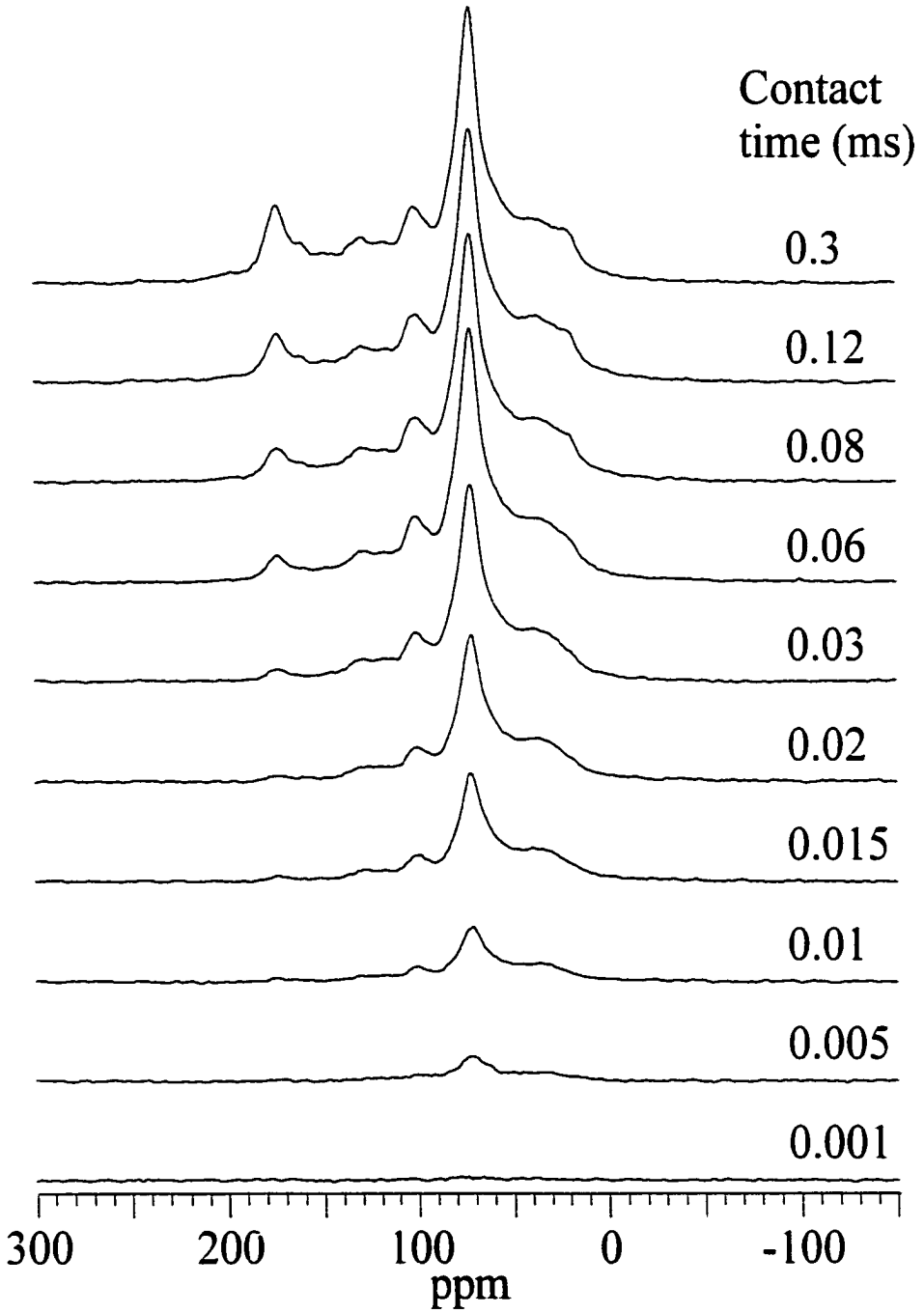

Figure 3.10(a) Variable contact time spectra of Uncompahgre fulvic acid soil fraction.

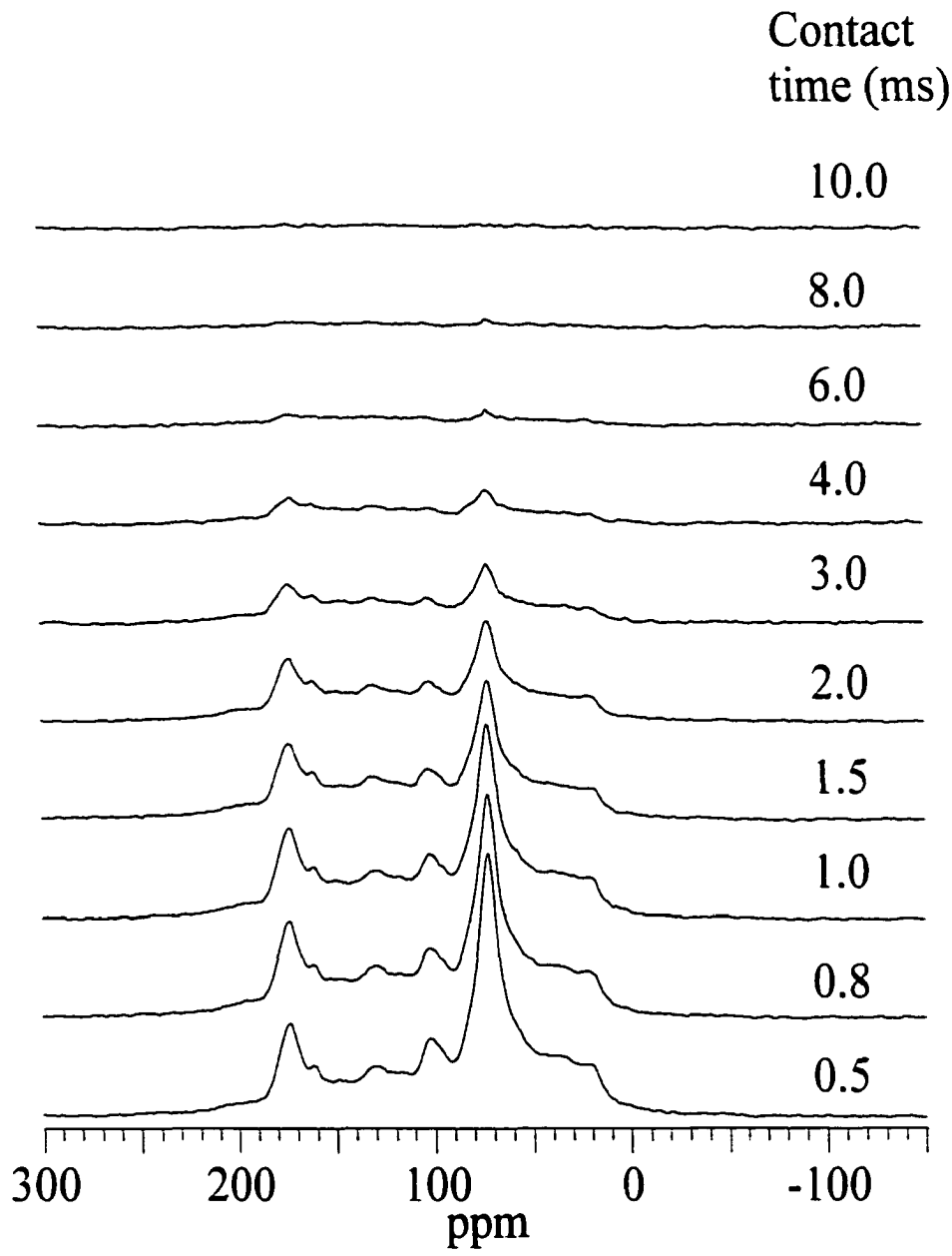

Figure 3.10(a) Variable contact time spectra of Uncompahgre fulvic acid soil fraction (Continued).

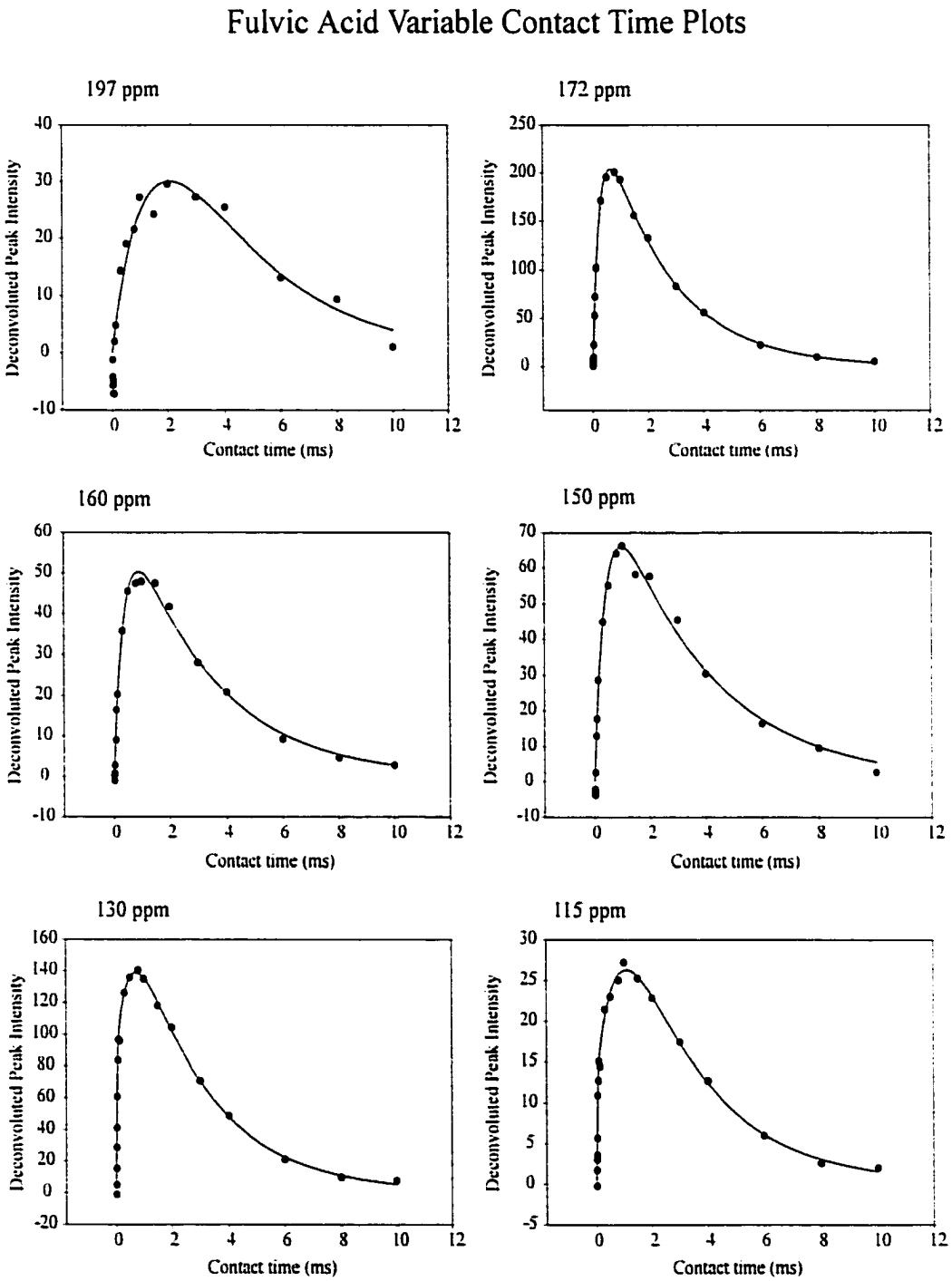

Figure 3.10(b) Plots of variable contact time data from the fulvic acid fraction.

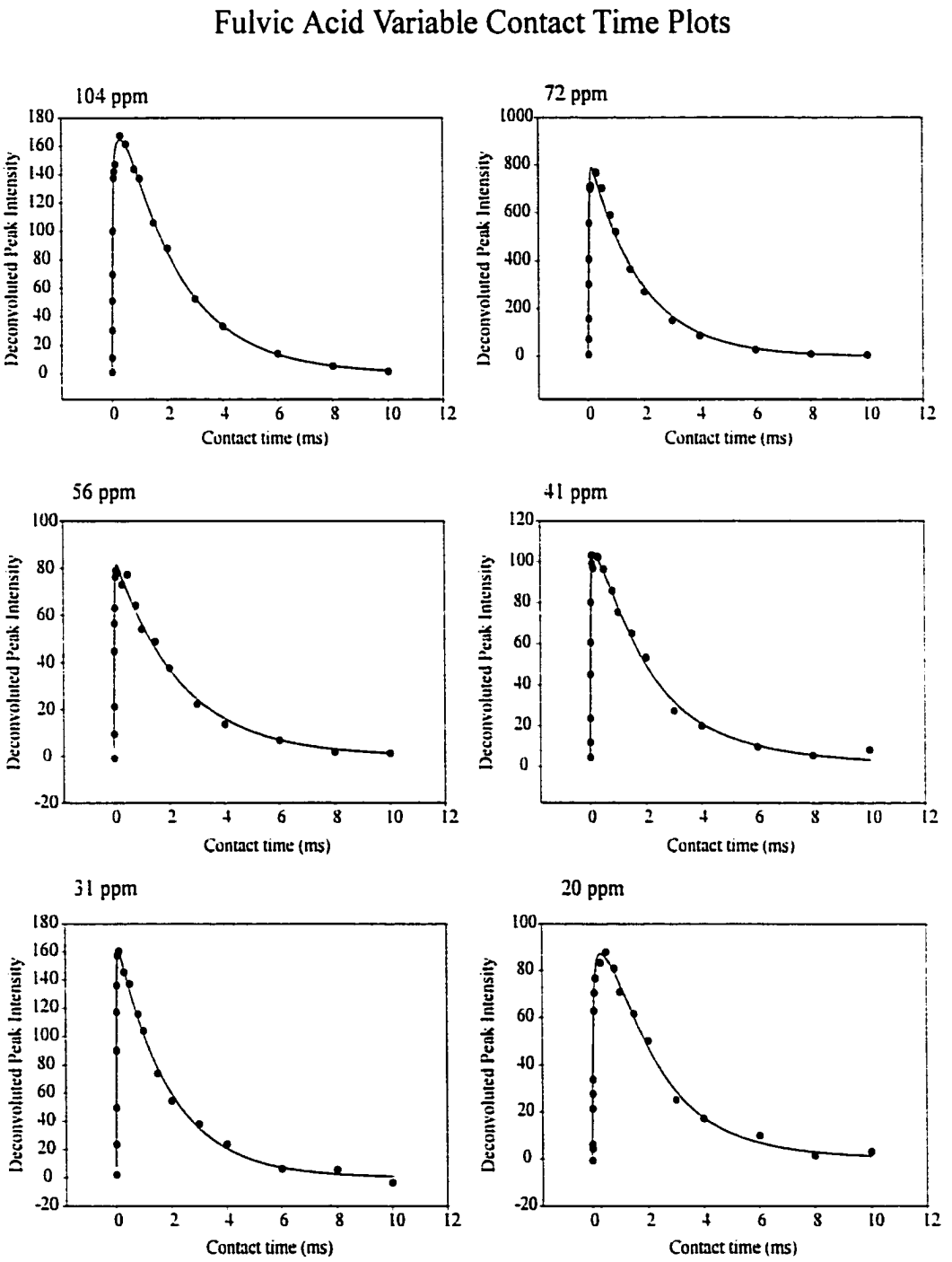

Figure 3.10(b) Plots of variable contact time data from the fulvic acid fraction (Continued).

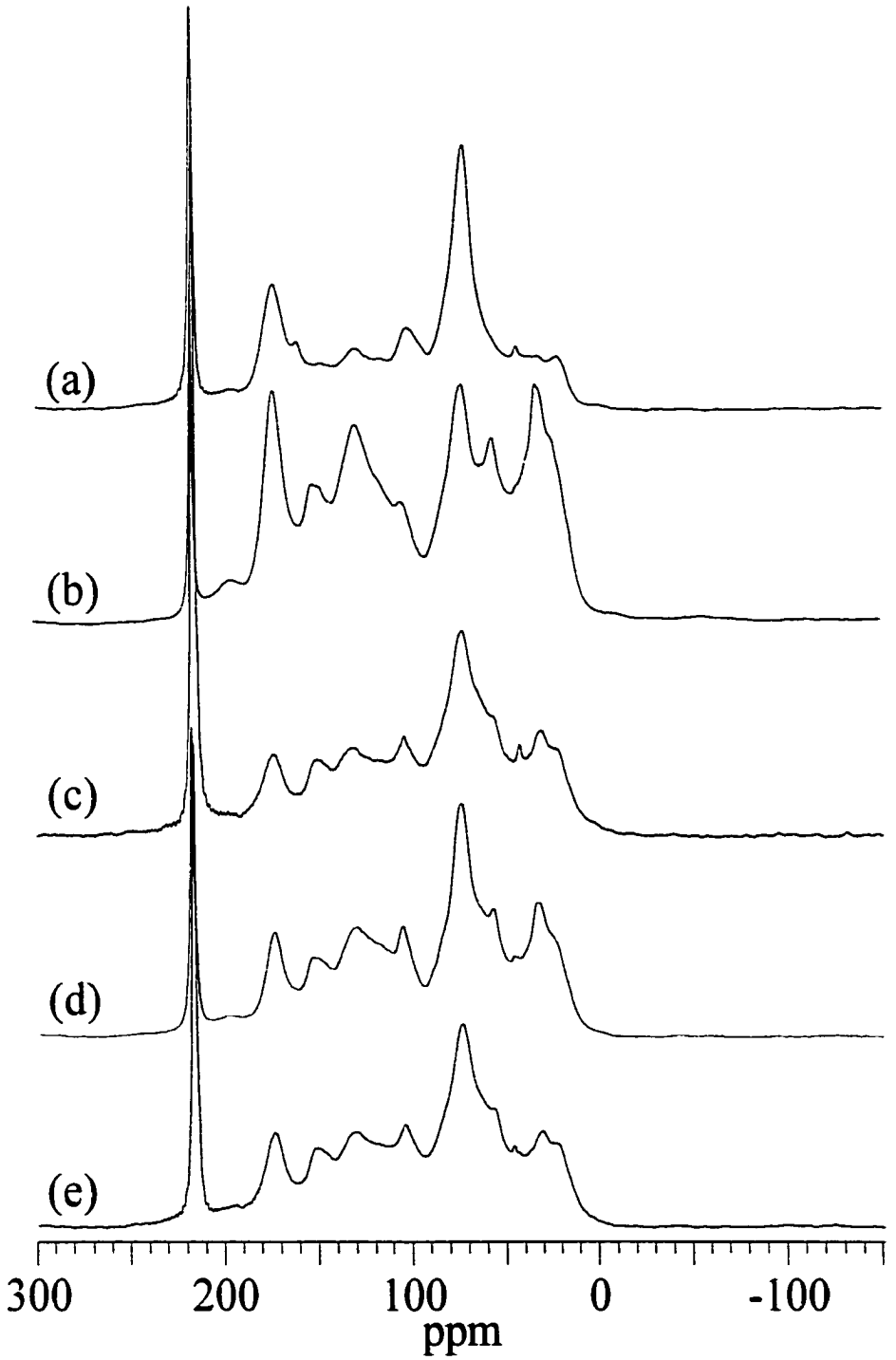

Figure 3.11 ^{1}H to ^{13}C CP-MAS spin-counting spectra of the Uncompahgre whole soil and its extracts, arbitrarily scaled for spectral comparison. In each CP-MAS experiment 6.49 mg of the ^{13}C-labeled CP-MAS spin reference compound [3.2.1] bicyclo-4-pyrrolidino-N-methyl-octan-8-one triflate was added as illustrated in Figure 1.4. Experimental spectrum (a) is of 1.483 g of fulvic acid, (b) 1.841 g humic acid, (c) 2.198 g of humin, (d) 1.178 g of HF-treated soil, and (e) 2.237 g of Uncompahgre whole soil. Each spectrum was acquired with a 1 ms contact period, and 1 s pulse delay.

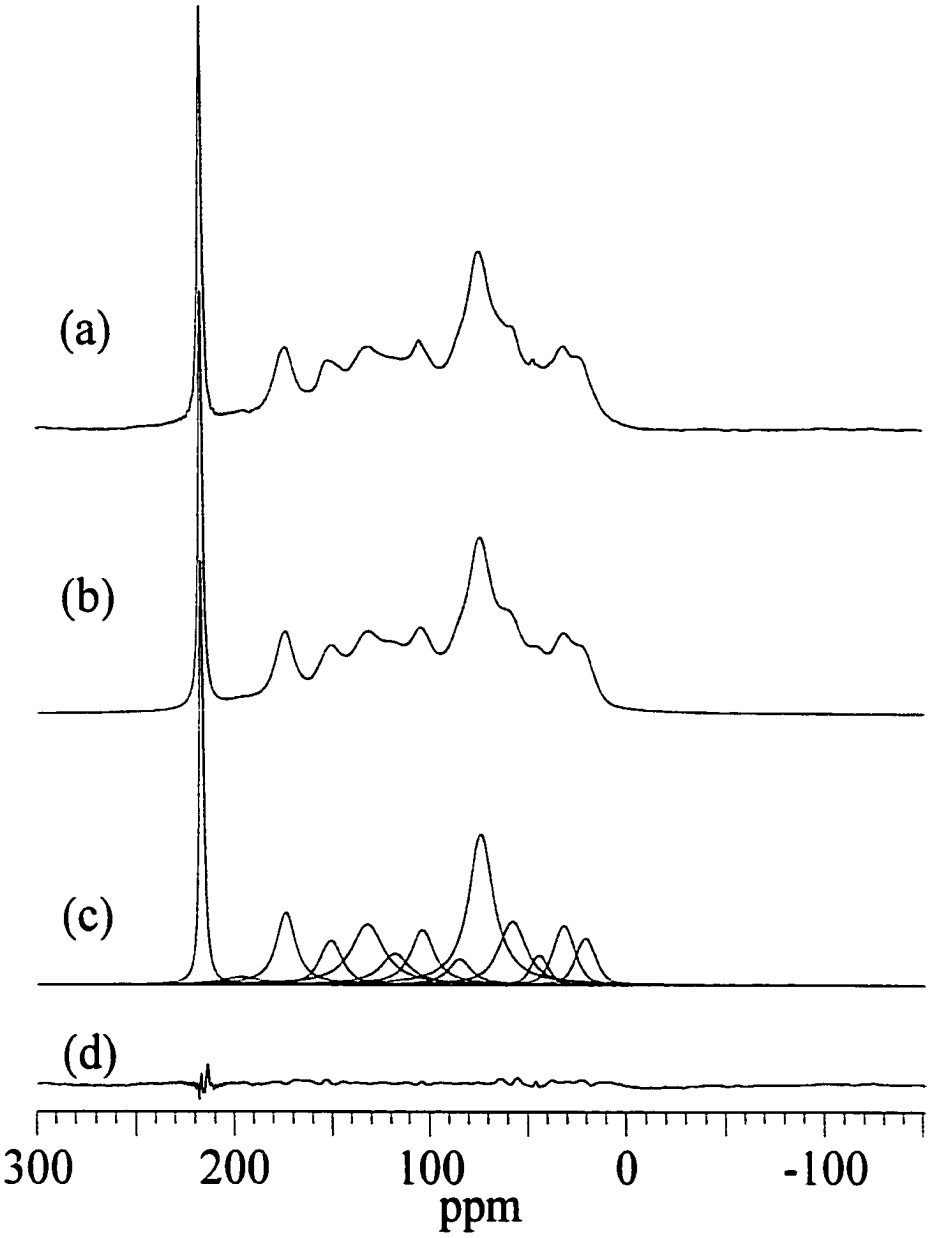

Figure 3.12 ^{13}C CP-MAS spin-counting spectrum of 2.237 g of the Uncompahgre whole soil with 6.49 mg of the ^{13}C-labeled CP-MAS spin reference compound [3.2.1] bicyclo-4-pyrrolidino-N-methyl-octan-8-one triflate. Experimental spectrum (a) is of the Uncompahgre whole soil, (b) is the synthetic spectrum created from the summation of the individual deconvoluted peaks in (c). Spectrum (d) is the difference between the experimental spectrum (a) and the synthetic spectrum (b). The experimental spectrum was acquired with 40000 acquisitions, a 1 ms contact period, and 1 s pulse delay.

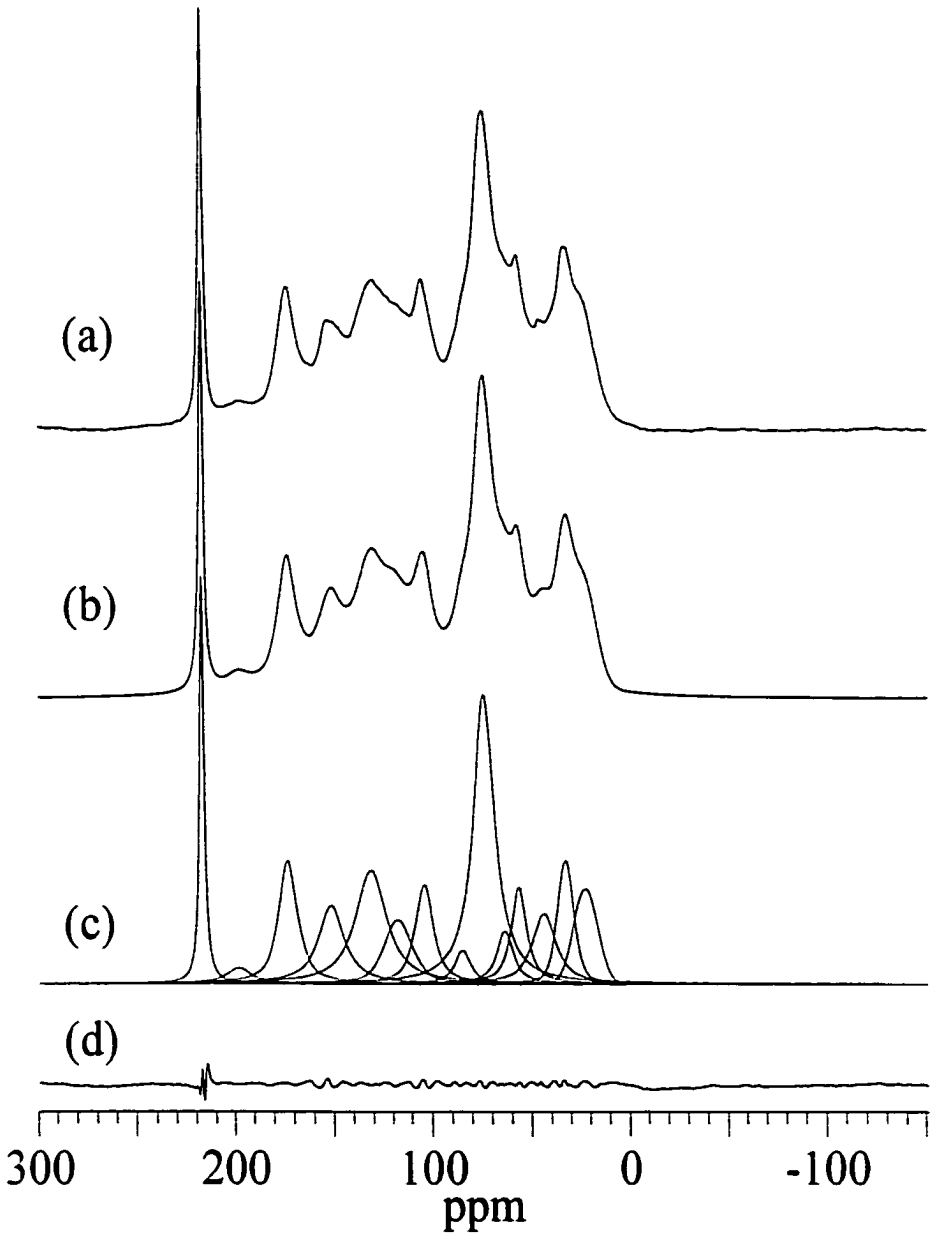

Figure 3.13 ^{13}C CP-MAS spin-counting spectra of 1.178 g of the HF-treated Uncompahgre whole soil with 6.49 mg of the ^{13}C-labeled CP-MAS spin reference compound [3.2.1] bicyclo-4-pyrrolidino-N-methyl-octan-8-one triflate. Experimental spectrum (a) is of the HF-treated Uncompahgre whole soil, (b) is the synthetic spectrum created from the summation of the individual deconvoluted peaks in (c). Spectrum (d) is the difference between the experimental spectrum (a) and the synthetic spectrum (b). The experimental spectrum was acquired with 80000 acquisitions, a 1 ms contact period, and 1 s pulse delay.

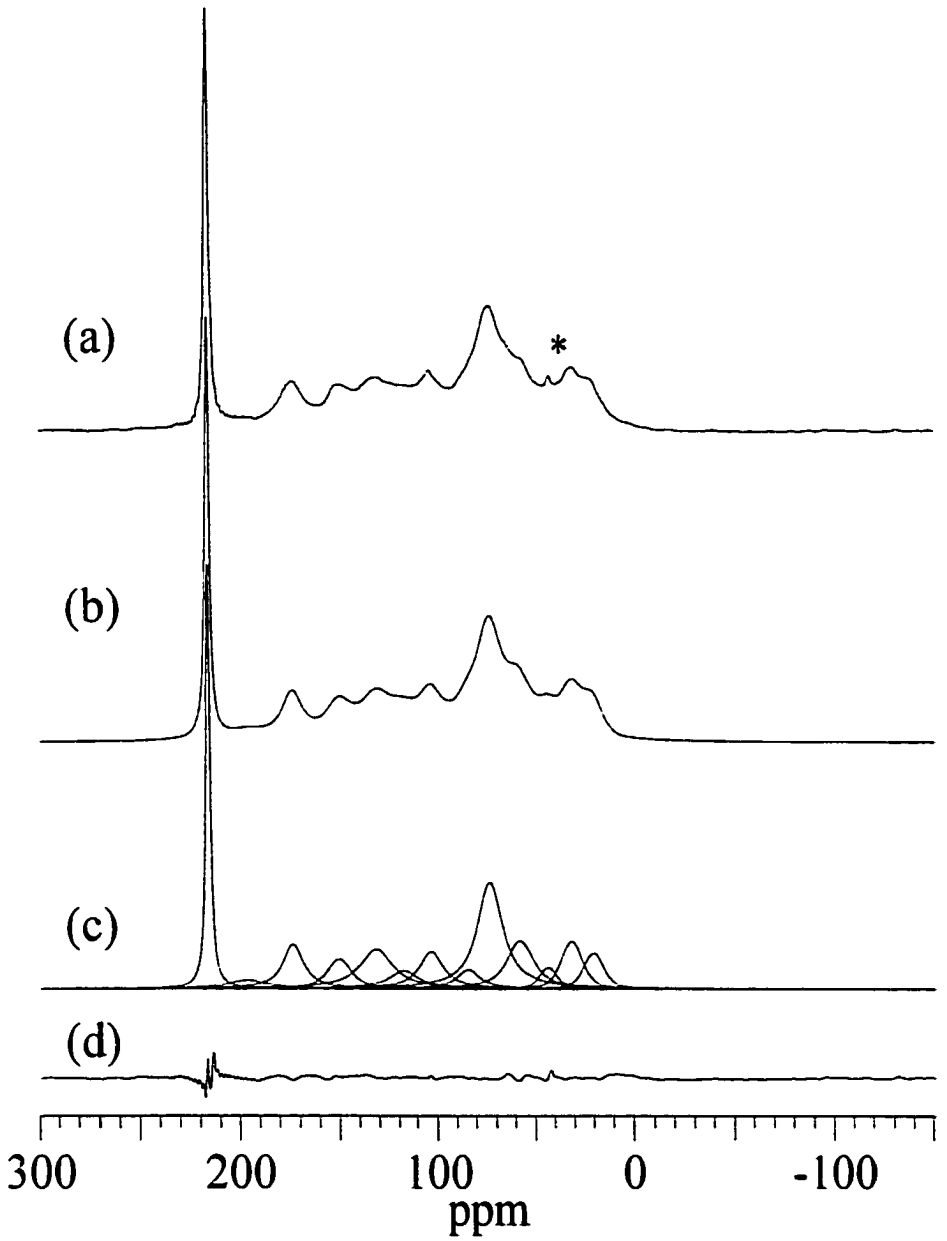

Figure 3.14 ^{13}C CP-MAS spin-counting spectra of 2.198 g of the Uncompahgre soil humin fraction with 6.49 mg of the ^{13}C-labeled CP-MAS spin reference compound [3.2.1] bicyclo-4-pyrrolidino-N-methyl-octan-8-one triflate. The experimental spectrum (a) is of the Uncompahgre soil humin fraction, (b) is the synthetic spectrum created from the summation of the individual deconvoluted peaks in (c). Spectrum (d) is the difference between the experimental spectrum (a) and the synthetic spectrum (b). The experimental spectrum was acquired with 40000 acquisitions, a 1 ms contact period, and 1 s pulse delay. The asterisk above the spectrum marks the position of the spinning sideband of the ^{13}C-labeled CP-MAS spin reference compound and is roughly 0.6 percent of the peak area at 216 ppm.

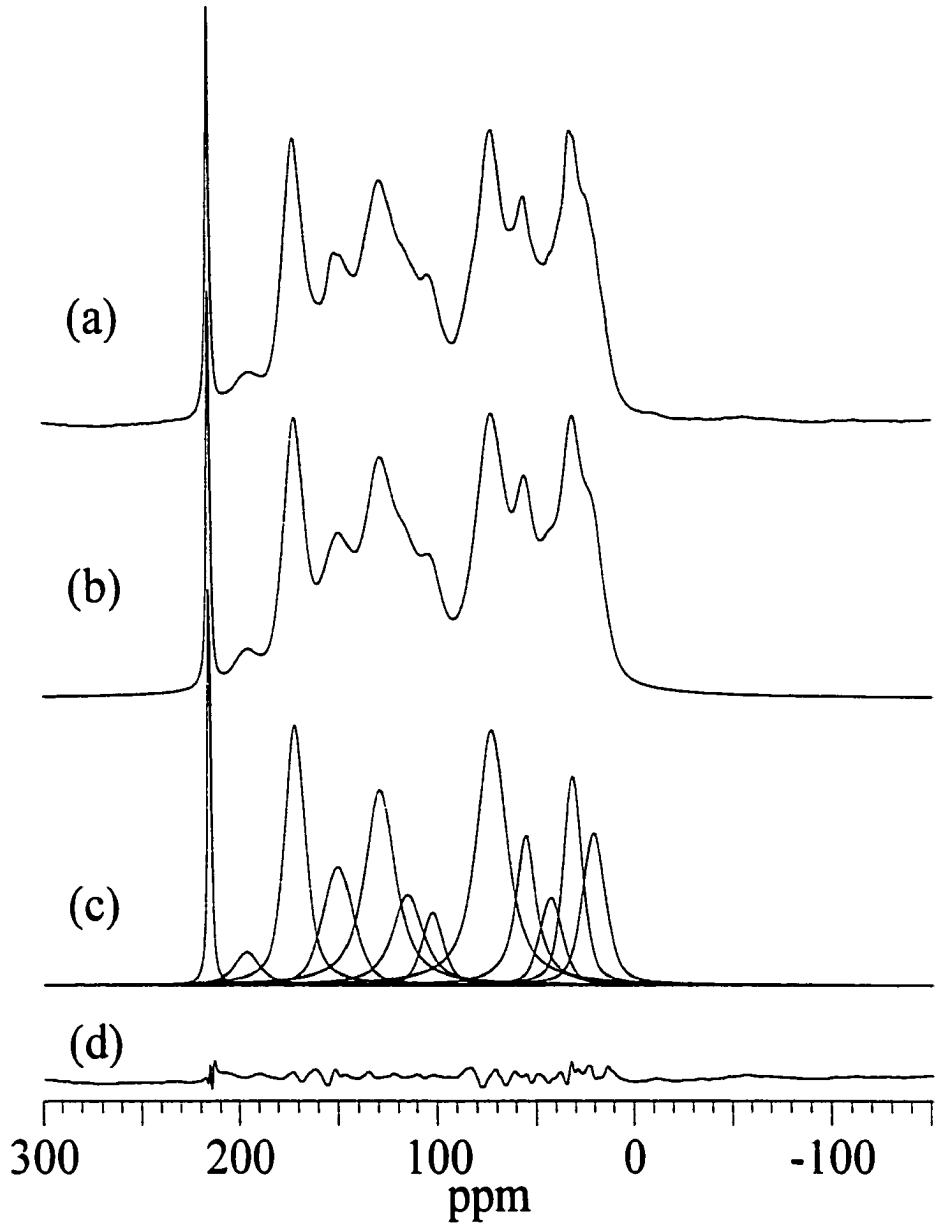

Figure 3.15 ^{13}C CP-MAS spin-counting spectra of 1.841 g of the Uncompahgre soil humic acid with 6.49 mg of the ^{13}C-labeled CP-MAS spin reference compound [3.2.1] bicyclo-4-pyrrolidino-N-methyl-octan-8-one triflate. Experimental spectrum (a) is of the Uncompahgre soil humic acid, (b) is the synthetic spectrum created from the summation of the individual deconvoluted peaks in (c). Spectrum (d) is the difference between the experimental spectrum (a) and the synthetic spectrum (b). The experimental spectrum was acquired with 80000 acquisitions, a 1 ms contact period, and 1 s pulse delay.

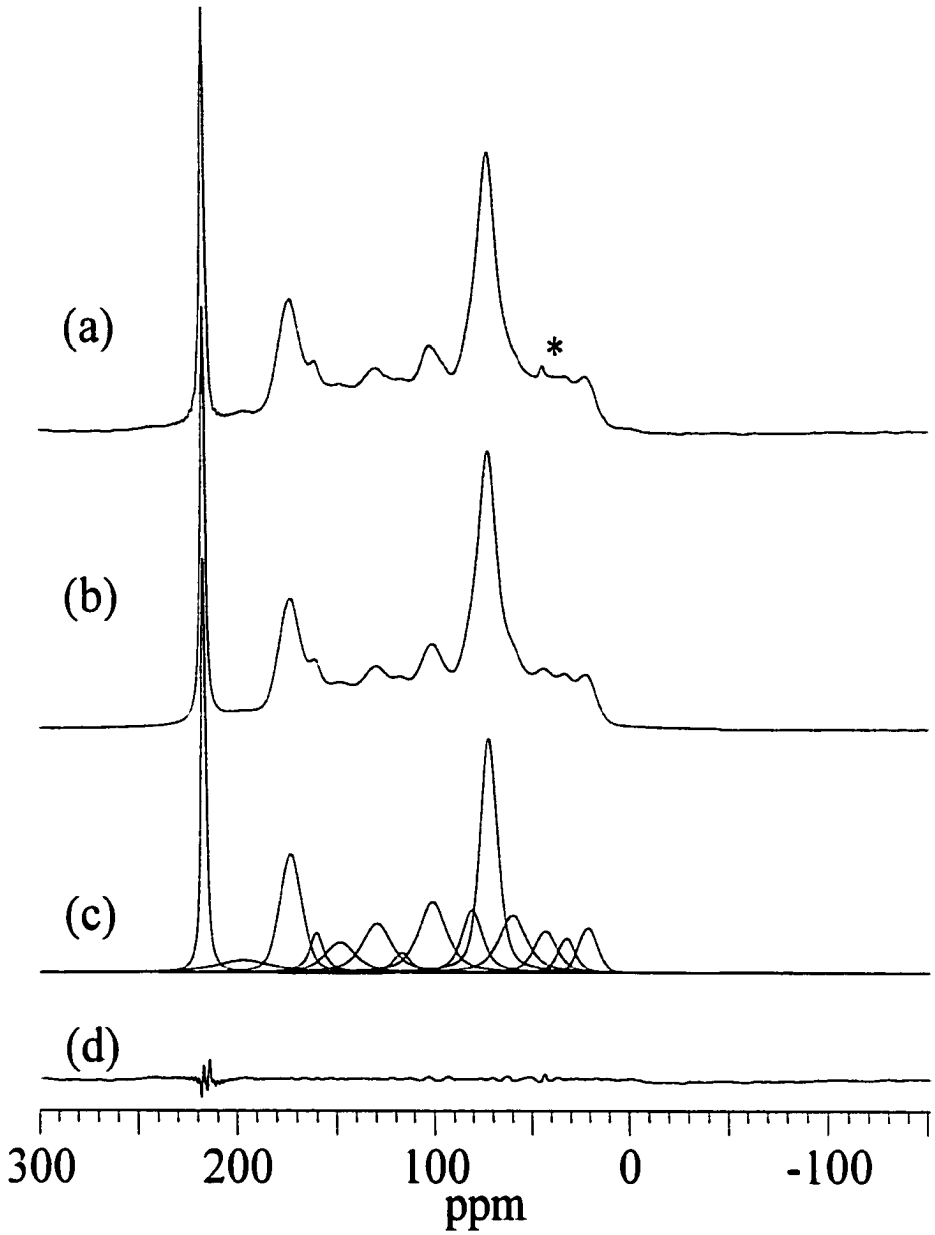

Figure 3.16 ^{13}C CP-MAS spin-counting spectra of 1.483 g of the Uncompahgre soil fulvic acid extract with 6.49 mg of the ^{13}C-labeled CP-MAS spin reference compound [3.2.1] bicyclo-4-pyrrolidino-N-methyl-octan-8-one triflate. The experimental spectrum (a) is of the Uncompahgre soil fulvic acid, (b) is the synthetic spectrum created from the summation of the individual deconvoluted peaks in (c). Spectrum (d) is the difference between the experimental spectrum (a) and the synthetic spectrum (b). The experimental spectrum was acquired with 40000 acquisitions, a 1 ms contact period, and 1 s pulse delay. The asterisk above the spectrum marks the position of the spinning sideband of the ^{13}C-labeled CP-MAS spin reference compound and is roughly 1.2 percent of the peak area at 216 ppm.

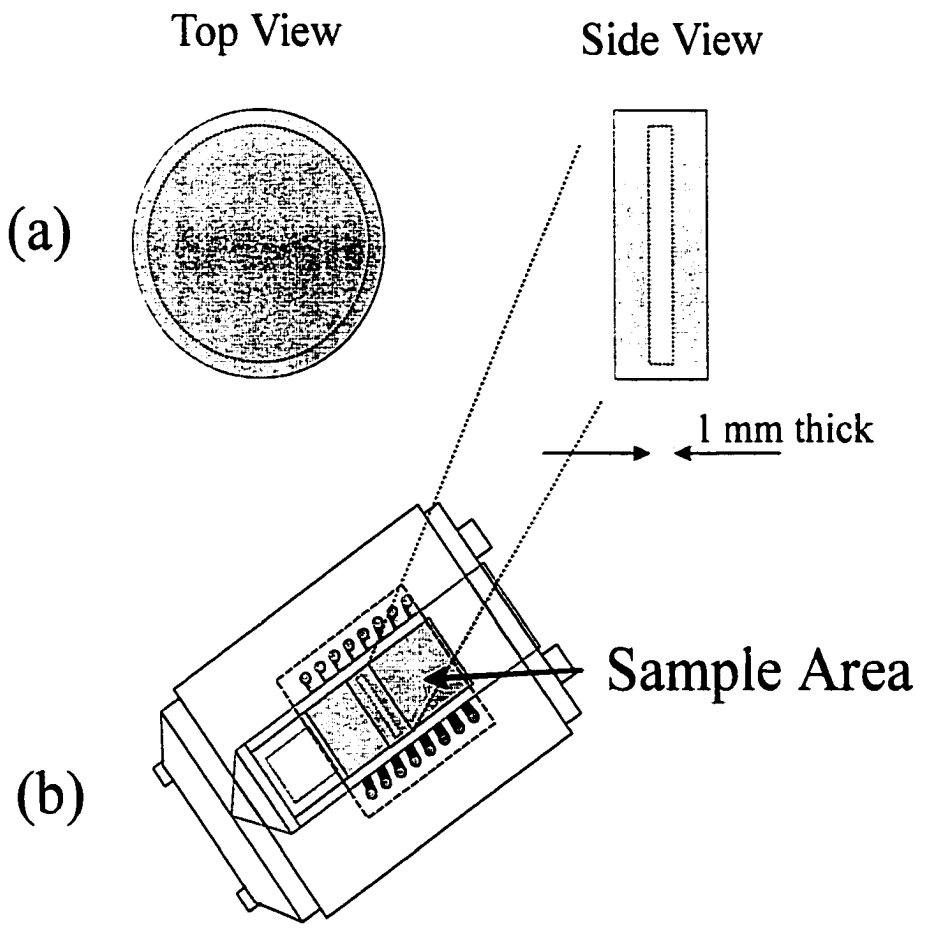

Figure 3.17 (a) Diagram of a Vespel insert (not to scale) containing 1:1:1 (by weight) mixture of ^{13}C-labelled L-Alanine ($^{13}CH_3CHNH_2CO_2H$ (21.2 ppm), $CH_3{}^{13}CHNH_2CO_2H$ (54.0, 50.4 ppm), $CH_3CHNH_2{}^{13}CO_2H$ (178.5 ppm)) occuping a disk-shaped volume. (b) Diagram of the large volume spinning system (drawn to scale) used in the field-mapping experiments. The diagram shows the relative position of the standard solenoid coil (box with dashed line) to that of the sample area with the Vespel insert in place.

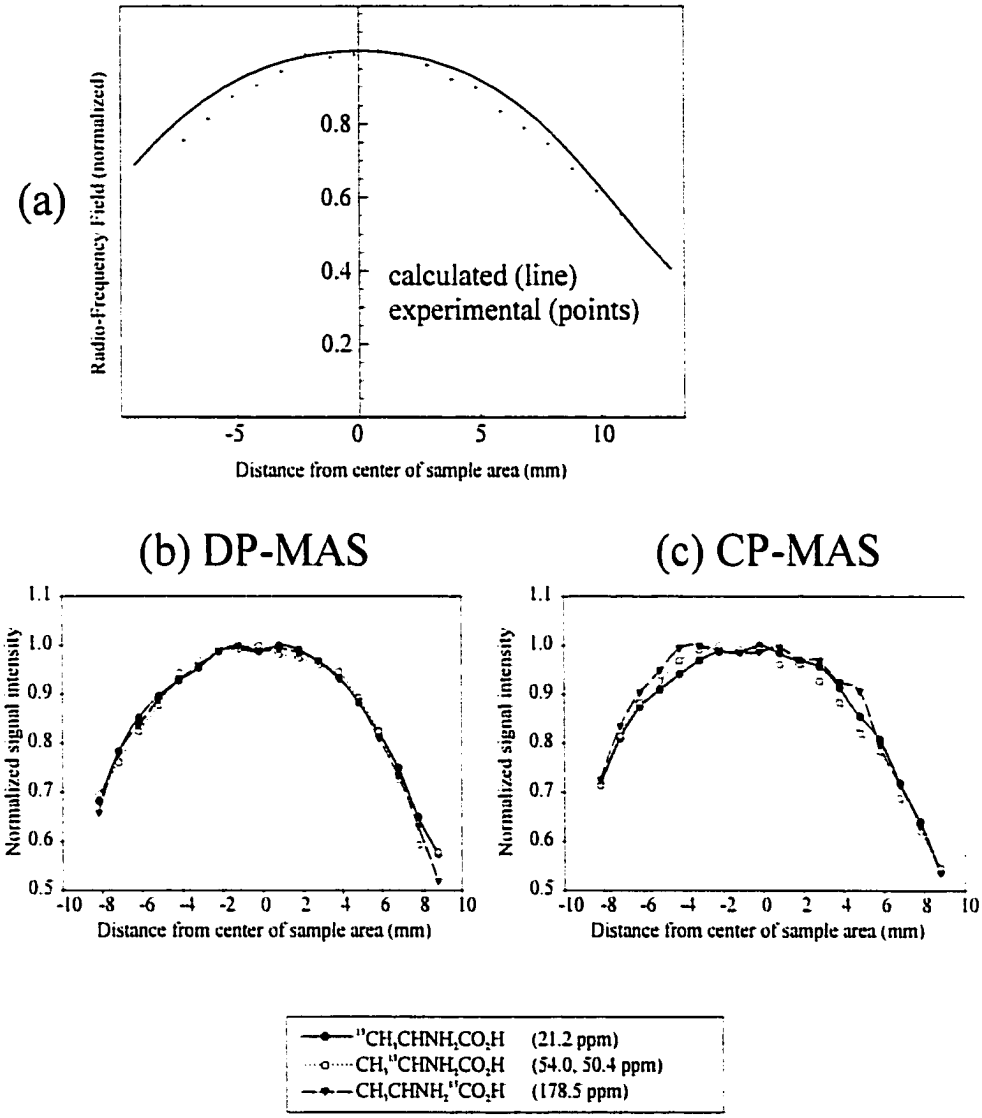

Figure 3.18 (a) Plot of the experimental and calculated RF field for the standard solenoid coil used in the 14 mm spinning system employed in this thesis. These measurements were made from the methyl ^{13}C CP-MAS signal intensity using the disk-shaped container of Figure 3.17(a), and containing 83 mg of $^{13}CH_3CHNH_2CO_2H$. The maximum RF field meausred (53 kHz ^1H RF field at 1 mm) was normalied to a value of 1.0 for comparison to the calculated field profile. The details of this coil configuration are shown in Figure A3-18(a) of the appendix. The simulated field, represented by a solid line, is the field measured at x = 3.53 mm, y = 0 mm and along the length of the sample volume. (b) The DP-MAS and (c) CP-MAS signal intensities of each peak of a 1:1:1 mixture of ^{13}C labeled l-alanines (occupying a disk-shaped volume as shown in Figure 3.17) plotted as a function of position along the spinner axis. The legend below plots (b) and (c) correlates the markings on the plots to the specific peak area measured. The signal intensites were normalized to show the overall field profile. Magic-angle spinning speeds of 4.0 kHz were used.

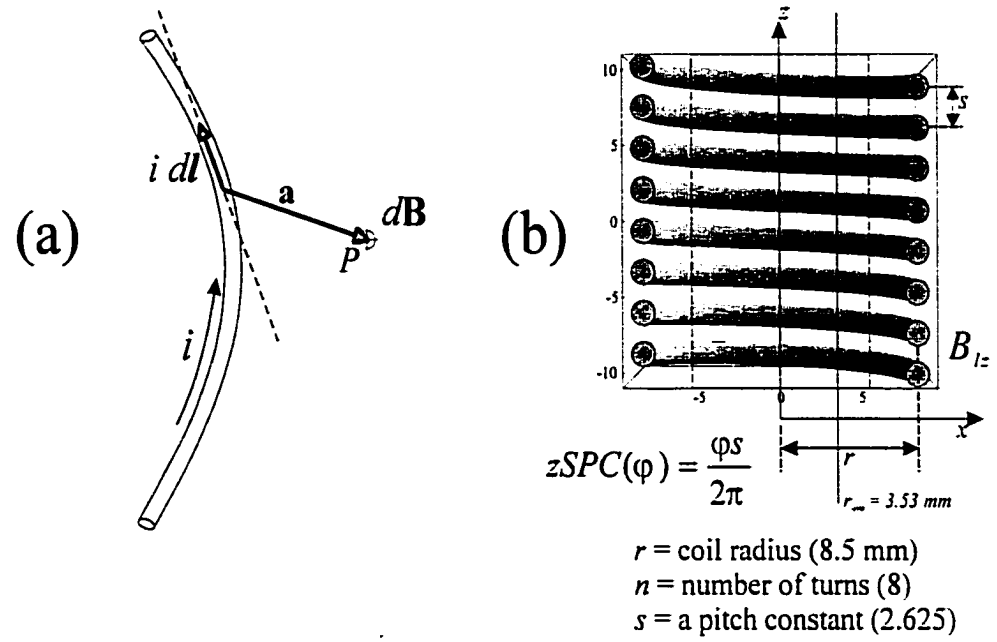

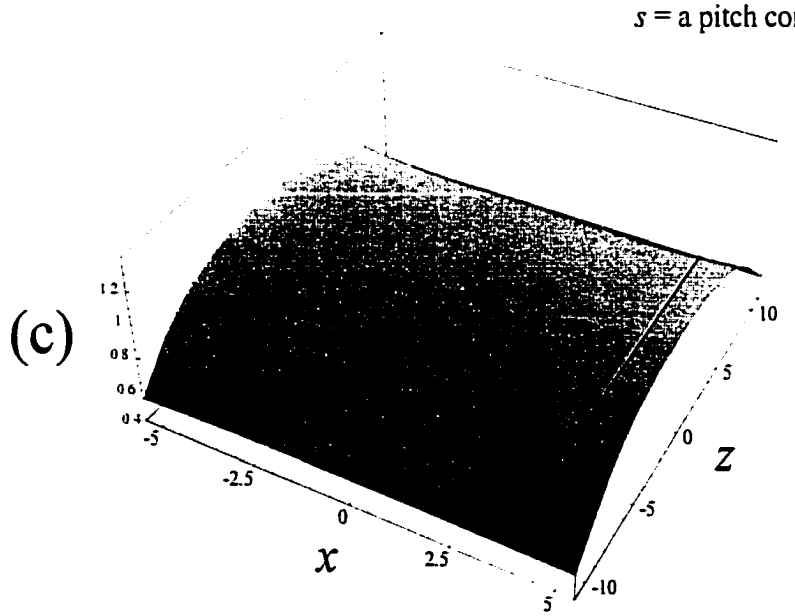

$$B_{1z}(x,y,z) = \int_{-m}^{m} \frac{r^2 - r(y\sin\varphi + x\cos\varphi)}{\left[(x - r\cos\varphi)^2 + (y - r\sin\varphi)^2 + (z - zSPC(\varphi))^2\right]^{3/2}} d\varphi \times \frac{1}{B_{1z0}}$$

Figure 3.19 (a) A pictorial representation of the law of Biot-Savart for current *i* through a wire (see section 3.2.7). A standard solenoid was mathematically generated by creating a function (zSPC(φ)) that would describe a coil with a constant pitch as a function of φ. The parameters describing this coil shape were chosen to reflect the actual coil shape used in the large-volume spinning system of this thesis. (b) The side (cut-away) view of the rendered coil shape with the sample volume outlined in a grey dashed line and the relevant coil parameters marked. The RF field for this coil was calculated using the above B_{1z} equation for a slice on the y axis ($y = 0$) dimension and covering the sample volume (x = -5.47 to 5.47 mm and z = -11.025 to 11.025 mm.) B_{1z0} is the field at the very center of the coil ($B_1(0, 0, 0)$) and assigned a value of 1 to normalize the field plots. (c) The oblique view of the field profile generated from applying the law of Biot-Savart to this current path. The (b) renderings and (c) field profile were calculating using Mathematica 4.0.

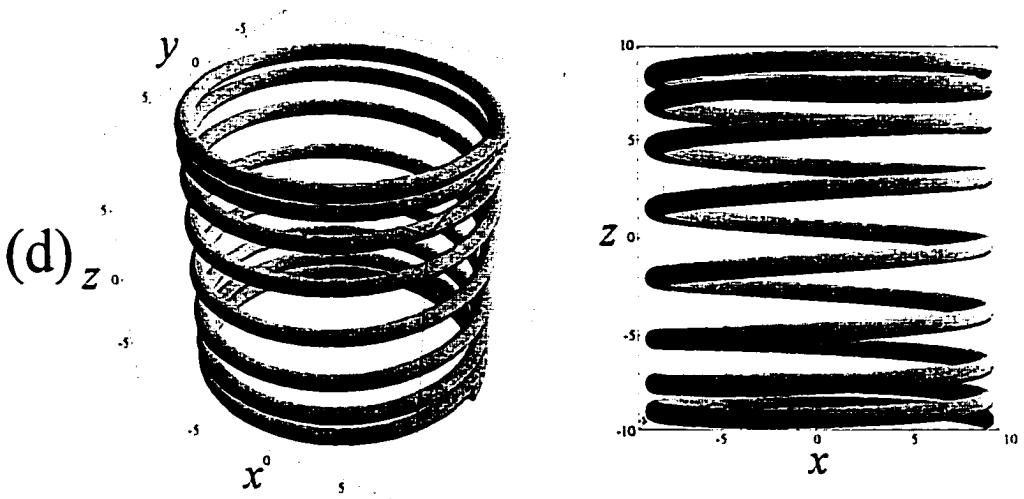

$$zVPC(\varphi) = \frac{ns}{2} \times Tanh[\frac{\varphi k}{n}]$$

r = coil radius (8.5 mm)
k = variable to describe pitch (0.45)
n = number of turns (8)
s = a pitch constant (2.625)

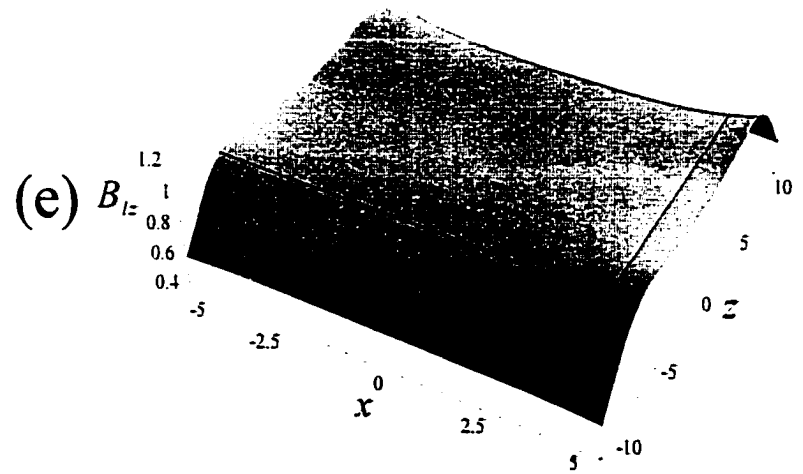

$$B_{1z}(x,y,z) = \int_{-m}^{m} \frac{r^2 - r(y\sin\varphi + x\cos\varphi)}{\left[(x - r\cos\varphi)^2 + (y - r\sin\varphi)^2 + (z - zVPC(\varphi))^2\right]^{3/2}} d\varphi \times \frac{1}{B_{1z0}}$$

Figure 3.19 (continued) A variable pitch solenoid was mathematically generated by creating a function (zVPC(φ)) that would vary the pitch of the coil with changing φ. Coil shapes with various parameters were rendered and visually examined to ensure that the coil maintained realistic properties. (d) The oblique (left) and side (right) views of the rendered coil shapes. The RF field for this coil was calculated using the above B_{1z} equation for a slice on the y axis ($y = 0$) dimension and covering the sample volume (x = -5.47 to 5.47 mm and z = -11.025 to 11.025 mm. (e) The oblique view of the field profile generated from applying the law of Biot-Savart to this current path. The (d) renderings and (e) field profile were calculating using Mathematica 4.0.

(f)

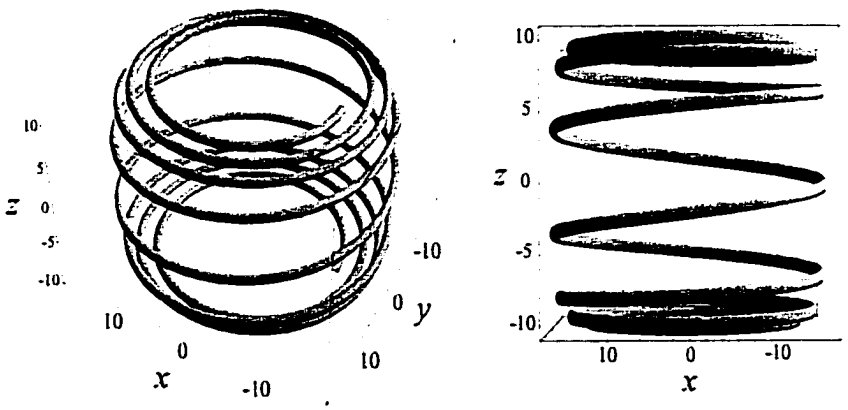

$$r(\varphi) = r_i \times r_f \times \cos[\frac{\varphi}{n\pi}]^v$$

$$\text{zVPC}(\varphi) = \frac{ns}{2} \times Tanh[\frac{\varphi k}{n}]$$

r_i = smallest radius of coil (8.5 mm)
r_f = multiplier to describe maximum radius (2)
k = variable to describe pitch (1.0)
n = number of turns (8)
s = a pitch constant (2.625)
v = variable to describe radial function

(g)

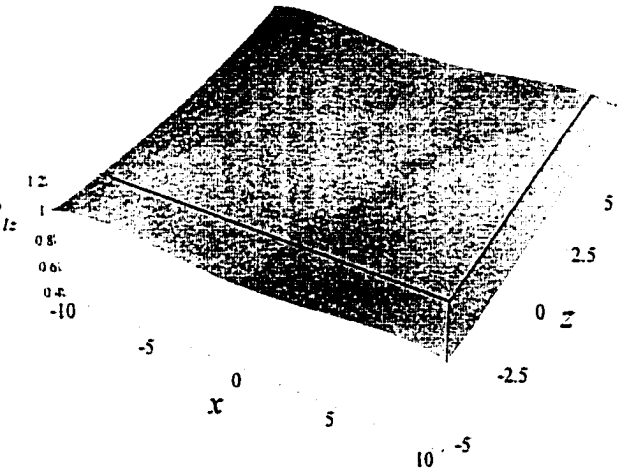

$$B_{l_z}(x,y,z) = \int_{-n\pi}^{n\pi} \frac{r(\varphi)^2 - r(\varphi)(y\sin\varphi + x\cos\varphi)}{\left[(x - r(\varphi)\cos\varphi)^2 + (y - r(\varphi)\sin\varphi)^2 + (z - zVPC(\varphi))^2\right]^{3/2}} d\varphi \times \frac{1}{B_{l=0}}$$

Figure 3.19 (continued) A variable-pitch and -radius coil was mathematically generated using a radial function r(φ) to describe the changes in the coil radius with φ and a pitch function, zVPC(φ). The radial function, pitch function, and constants used to render this coil shape are shown above. (f) The oblique (left) and side (right) views of the rendered coil shapes. The RF field for this coil was calculated using the above B_{l_z} equation for a slice on the y axis ($y = 0$) dimension and covering the sample volume (x = -5.47 to 5.47 mm and z = -11.025 to 11.025 mm. (g) The oblique view of the field profile generated from applying the law of Biot-Savart to this current path. The (f) renderings and (g) field profile were calculating using Mathematica 4.0.

References

1. Jurkiewicz, A.; Maciel, G. E. Spin Dynamics and Spin Counting in the ^{13}C CP-MAS Analysis of Argonne Premium Coals. *Fuel* **1994**, *73*, 828-835.

2. Zhang, M.; Maciel, G. E. Large-sample ^{13}C MAS n.m.r. spectroscopy of coal: relaxation and spin counting. *Fuel* **1990**, *69*, 557-563.

3. Muntean, J. V.; Stock, L. M.; Botto, R. E. Improving the Reliability of Quantitative Solid-State ^{13}C NMR Analysis of Coal. *Energy Fuels* **1988**, *2*, 108-110.

4. Franz, J. A.; Garcia, R.; Linehan, J. C.; Love, G. D.; Snape, C. E. Single-pulse excitation carbon-13 NMR measurements on the Argonne premium coal samples. *Energy Fuels* **1992**, *6*, 598-602.

5. Jurkiewicz, A.; Maciel, G. E. ^{13}C NMR Spin-Lattice Relaxation Properties and Quantitative Analytical Methodology of ^{13}C NMR Spectroscopy for Coals. *Anal. Chem.* **1995**, *34*, 2188-2194.

6. Snape, C. E.; Axelson, D. E.; Botto, R. E.; Delpuech, J. J.; Tekely, P.; Gerstein, B. C.; Pruski, M.; Maciel, G. E.; Wilson, M. A. Quantitative reliability of aromaticity and related measurements on coals by ^{13}C n.m.r. A debate. *Fuel* **1989**, *68*, 547-560.

7. Packer, K. J.; Harris, R. K.; Kenwright, A. M.; Snape, C. E. Quantitative aspects of solid state carbon-13 NMR of coals and related materials. *Fuel* **1983**, *62*, 999-1002.

8. Muntean, J. V.; Stock, L. M.; Botto, R. E. Improving the Reliability of Quantitative Solid-State ^{13}C NMR Analysis of Coal. *Energy Fuels* **1988**, *2*, 108-110.

9. Dudley, R. L.; Fyfe, C. A. Evaluation of the quantitative reliability of the carbon-13 CP/MAS technique for the analysis of coals and related materials. *Fuel*, **1982**, *61*, 651-657.

10. Botto, R. E.; Wilson, R.; Winans, R. E. Evaluation of the Reliability of Solid ^{13}C NMR Spectroscopy for the Quantitative Analysis of Coals: Study of Whole Coals and Maceral Concentrates. *Energy and Fuels* **1987**, *1*, 173-181.

11. Silbernagel, B. G.; Botto, R. E. "Advanced Magnetic Resonance Techniques Applied To Argonne Premium Coals" in *Magnetic Resonance of Carbonaceous Solids*, R. E. Botto, Y. Sanada, eds., Advances in Chemistry Series 229, American Chemical Society, Washington, DC, **1993**, pp. 629-643.

12. Vassallo, A. M.; Wilson, M. A.; Collin, P. J.; Oades, J. M.; Waters, A. G.; Malcolm, R. L. Structural analysis of geochemical samples by solid-state nuclear magnetic resonance spectometry. Role of paramagnetic material. *Anal. Chem.* **1987**, *59*, 558-562.

13. Mao, J-D.; Hu, W.; Schmidt-Rohr, K.; Davies, G.; Ghabbour, E. A.; Xing, B. Quantitative Characterization of Humic Substances by Solid-State Carbon-13 Nuclear Magnetic Resonance. *Soil Sci. Soc. Am. J.* **2000**, *64*, 873-884.

14. Mao, J.; Hu, W.; Schmidt-Rohr, K.; Davies, G.; Ghabbour, E. A.; Xing, B. Structure and Elemental Composition of Humic Acids: Comparison of Solid-State ^{13}C NMR Calculations and Chemical Analyes. *Royal Soc. Chem., G. Britain* **1999**, *228*, 79-90.

15. Frund, R.; Ludemann, H.-D. The quantitative analysis of solution- and CPMAS-C-13 NMR spectra of humic material. *Sci. Tot. Environ.* **1989**, *81/82*, 157-168.

16. Torchia, D The measurement of proton-enhanced carbon-13 T_1 values by a method which suppresses artifacts. *J. Magn. Reson.* **1978**, *30*, 613-616.

17. Mehring, M. *Principles of High Resolution NMR in Solids*, Springer-Verlag, New York, USA, **1982**, pp. 152-154.

18. Hall, R. A.; Jurkiewicz, A.; Maciel, G. E. A Bicyclic Ketone as a Solid-State ^{13}C NMR Intensity Reference. *Anal. Chem.* **1993**, *65*, 534-538.

19. Fukushima, E.; Roeder, S. B. W. Experimental Pulse NMR: A Nuts and Bolts Approach, Addison-Wesley Publishing Co., Inc., London, 1981, Chapter 6.

20. Privalov, A. F.; Dvinskikh, S. V.; Vieth, H.-M. Coil Design for Large-Volume High-B_1 Homogeneity for Solid-State NMR Applications. *J. Magn. Reson. Ser. A.* **1996**, *123*, 157-160.

21. Idziak, S; Haeberlen, U. Design and construction of a high homogeneity rf coil for solid-state multiple-pulse NMR. *J. Magn. Reson.* 1983, *50*, 281-288.

22. VanderHart, D. L.; Earl, W. L.; Garroway, A. N. Resolution in ^{13}C NMR of Organic Solids Using High-Power Proton Decoupling and Magic-Angle Sample Spinning. *J. Magn. Reson.*, **1981**, *44*, 361-401.

23. Sardashti, M; Maciel, G. E. Effects of Sample Spinning on Cross Polarization *J. Magn. Reson.*, **1987**, *72*, 467-474.

24. Campbell, G. C.; Galya, L.G.; Beeler, A. J.; English, A. D. Effect of RF inhomogeneity upon quantitative solid-state NMR measurements. *J. Magn. Reson. Ser. A.* **1995**, *112*, 225-228.

Chapter 4

^{13}C NMR SPECTRAL EDITING OF HUMIC MATERIAL EXTRACTED FROM UNCOMPAHGRE NATIONAL FOREST SOIL

4.1 Introduction

During the past 20 years, ^{13}C NMR has emerged as one of the premier experimental approaches for characterizing solid samples of organic-geochemical origin[1-4], including coal[5-19], oil shale[20-27], humic materials[28-34] and peats[35-38]. All of this work has included magic-angle spinning (MAS) for averaging (narrowing) line broadening due to chemical shift anisotropies (CSA)[39-42], as well as inhomogeneities and discontinuities in local magnetic susceptibilities throughout a sample, and high-power ^{1}H decoupling for averaging (narrowing) line broadening due to ^{1}H-^{13}C magnetic dipole-dipole interactions[39]. While there may be an advantage in *directness* of quantitation in using direct polarization (DP) in generating ^{13}C magnetization *via* ^{13}C spin-lattice relaxation (characterized by the relaxation time, T_1^C)[43,44], the overwhelming portion of previously published work has employed ^{1}H to ^{13}C cross polarization (CP) for generating observable ^{13}C magnetization[45,46]. The main advantage of CP over DP approaches lies in sensitivity,

or signal-to-noise (S/N), because the CP approach, which depends on ^{1}H-^{13}C magnetic dipole-dipole interactions, yields a substantial ^{13}C signal enhancement (roughly γ^{H}/γ^{C}, where γ is the nuclear magnetogyric ratio), and the relaxation parameter that limits the repetition rate in multi-scan CP experiments is T_1^{H}, rather than the usually much larger T_1^{C}.

The main parameter/criterion used in making structural identifications (peak assignments) in ^{13}C MAS studies of solid organic-geochemical samples has been the ^{13}C chemical shift, which has a range of more than 200 ppm for diamagnetic samples and provides a high degree of shift-vs-structure selectivity. Use of this parameter has been aided by various time-domain strategies. Most prominent and popular of these has been "interrupted-decoupling" or "dipolar dephasing"[45-48].

In a dipolar-dephasing CP-MAS ^{13}C NMR experiment, an interrupt period is inserted between the end of the CP period and the beginning of data acquisition; during this interrupt period both the ^{13}C and ^{1}H (decoupler) channels are turned off and transverse ^{13}C magnetization is allowed to evolve under the influence of ^{1}H-^{13}C dipolar interactions prior to turning on the ^{1}H decoupler for data acquisition. The ^{13}C magnetization of CH and CH_2 groups dephases rapidly during the interrupt period (e.g., almost completely in about 70 μs), while >C< groups dephase much more slowly, because they have no directly attached hydrogen atoms. CH_3 groups typically behave substantially like >C< groups, because rapid methyl-group rotation largely averages ^{1}H-^{13}C dipolar interactions.

A more refined and sophisticated method of ^{13}C CP-MAS spectral editing, also based on behavior grounded in ^{1}H-^{13}C dipolar interactions, was introduced by Wu, Burns,

and Zilm[49]. This method is based on a detailed analysis of the behaviors of CH_3, CH_2, CH and $>C<$ moieties under conditions of cross polarization, depolarization (*vide infra*) and polarization inversion. The results of four separate CP-MAS experiments, with carefully chosen periods of cross polarization, depolarization and polarization inversion, are combined to produce three subspectra, representing CH groups, CH_2 groups and CH_3 + $>C<$ groups. Because this approach *combines* individual spectra, each of which has a lower S/N than can potentially be obtained by CP-MAS, it suffers from basic sensitivity constraints and is correspondingly very time consuming. The study reported here was undertaken to see if this approach could profitably be applied to a humic sample. Such a study had not previously been reported, although a somewhat similar study has been reported on dried pine needles[50]. The work presented here is part of an extensive ^{13}C NMR study of a suite of humic samples isolated from soil in the Uncompahgre National Forest of southwestern Colorado. Most details of that study will be reported elsewhere.

One of the main areas of emphasis in our ^{13}C NMR study of Uncompahgre samples is the issue of quantitation. This matter, and its relation to the static magnetic field strength of the NMR spectrometer has been discussed previously for organic-geochemical solids[51]. After considering all relevant issues, e.g., 1) spinning sideband intensity and its relationship to CSAs and MAS speed, 2) the relationship between MAS speed and sample size and 3) the relationship between MAS speed and CP efficiency/dynamics (certainly improved by modulated CP techniques[52-55]), we concluded that for typical soil organics, when large amounts of samples are available, the optimal spectrometer field for maximum S/N in ^{13}C MAS experiments is close to 2.35 T (100 MHz ^{1}H, 25.1 MHz ^{13}C). At this field, a large sample volume (roughly 2 cm^3) can be

spun at about 4.6 kHz, a MAS speed for which MAS sidebands have small intensities with little or no overlap over the spectral regions of interest.

4.2 Experimental Section

4.2.1 Extraction of Humic Substances

Topsoil collected from an Aspen tree stand in the Uncompahgre National Forest in southern Colorado was dried at 55 °C until a constant weight was achieved. The dried soil was passed through a 24 mesh screen to remove large pieces of un-decomposed leaf-litter and stones. The soil (4.0 Kg) was then placed into a polyethylene carboy with a magnetic stirrer (to remove ferromagnetic particles) and 40 L of 0.1 M NaOH. The soil/base mixture was agitated overnight under flowing N_2. The insoluble fraction was filtered off from the mixture and rinsed several times with a total of 4 L of HPLC grade water. Smaller clay particles were separated from the base solution by centrifugation at 9000 rpm. The washings and filtrate were combined and placed into a polyethylene carboy where the pH was adjusted to 2 using concentrated HCl. The solution was allowed to sit undisturbed overnight. A dark brown precipitate (humic acid) formed overnight which was separated from the remaining solution by centrifugation at 9000 rpm. The humic acid was dried by rotary evaporation at 15 mbar and 50 °C for a total humic acid yield of 322 g. Elemental analysis provided by Huffman Laboratories gave 44.87 percent carbon, 39.4 percent oxygen, and 5.2 percent hydrogen. The remaining fulvic acid and humin fractions were collected for further experiments not described in this publication.

4.2.2 NMR Spectroscopy

All of the solid-state NMR experiments were completed on a home-built spectrometer with a Chemagnetics Phoenix data system upgrade and Spinsight acquisition software. This spectrometer operates at a ^{1}H frequency of 100.5 MHz and a ^{13}C frequency of 25.2 MHz. Cross polarization was achieved for all experiments with 50 kHz, or greater, RF fields and repetition delays of 1 s. A home-built magic angle spinning probe with a Chemagnetics-style 9.5 mm (o.d.) MAS rotor was employed for spectral-editing experiments. A MAS spinning speed of 5.2 kHz and 700 mg of humic acid were used for the humic acid spectral-editing experiments. A home-built two-channel probe utilizing Chemagnetics-style 14 mm (o.d.) zirconia rotors was employed for the interrupted-decoupling experiments, with a MAS spinning speed of 4.6 kHz and 1.8 g humic acid sample.

4.3 Results

4.3.1 Dipolar Dephasing

^{13}C CP-MAS experiments with dipolar dephasing were carried out on the Uncompahgre humic acid as a function of the dipolar-dephasing period, τ_{dd}. The results are shown in Figure 4.1. In that figure one sees that ^{13}C NMR intensity in the 150-180 ppm region, in the region around 57 ppm and in the 10-30 ppm region substantially survives even a dephasing period of 150 μs. These regions can be identified primarily with carbonyl groups of ketones and carboxyl moieties (~ 180-160 ppm), OH-substituted

carbons of phenolic moieties (~165-150 ppm) and methyl carbons in OCH_3 (57 ppm) or $C\text{-}CH_3$ moieties (~35-10 ppm).

4.3.2 WBZ Spectral Editing

The spectral-editing approach introduced by Wu, Burns and Zilm (WBZ), based on a series of studies from that group[49,56-58], was also applied to the Uncompahgre humic acid. This method is based on a prescribed combination of four different CP-MAS experiments. These four experiments, denoted by the abbreviations SCP, SCPPI, SCPD and LCPD, are represented in the timing diagrams in Figure 4.2.

The SCP experiment shown in Fig. 4.2B is a cross polarization experiment with a short CP contact period, $2\tau_{CP}$ (40 μs). The phase alternation indicated in the CP contact period is included to minimize sensitivity to CP mismatch[56,57]. The spin-lock periods, τ^{I}_{SL} and τ^{S}_{SL}, were included by Wu, Burns and Zilm to maintain equal spin-lock times, in each channel, among the four experiments. Aside from the use of a very short CP contact

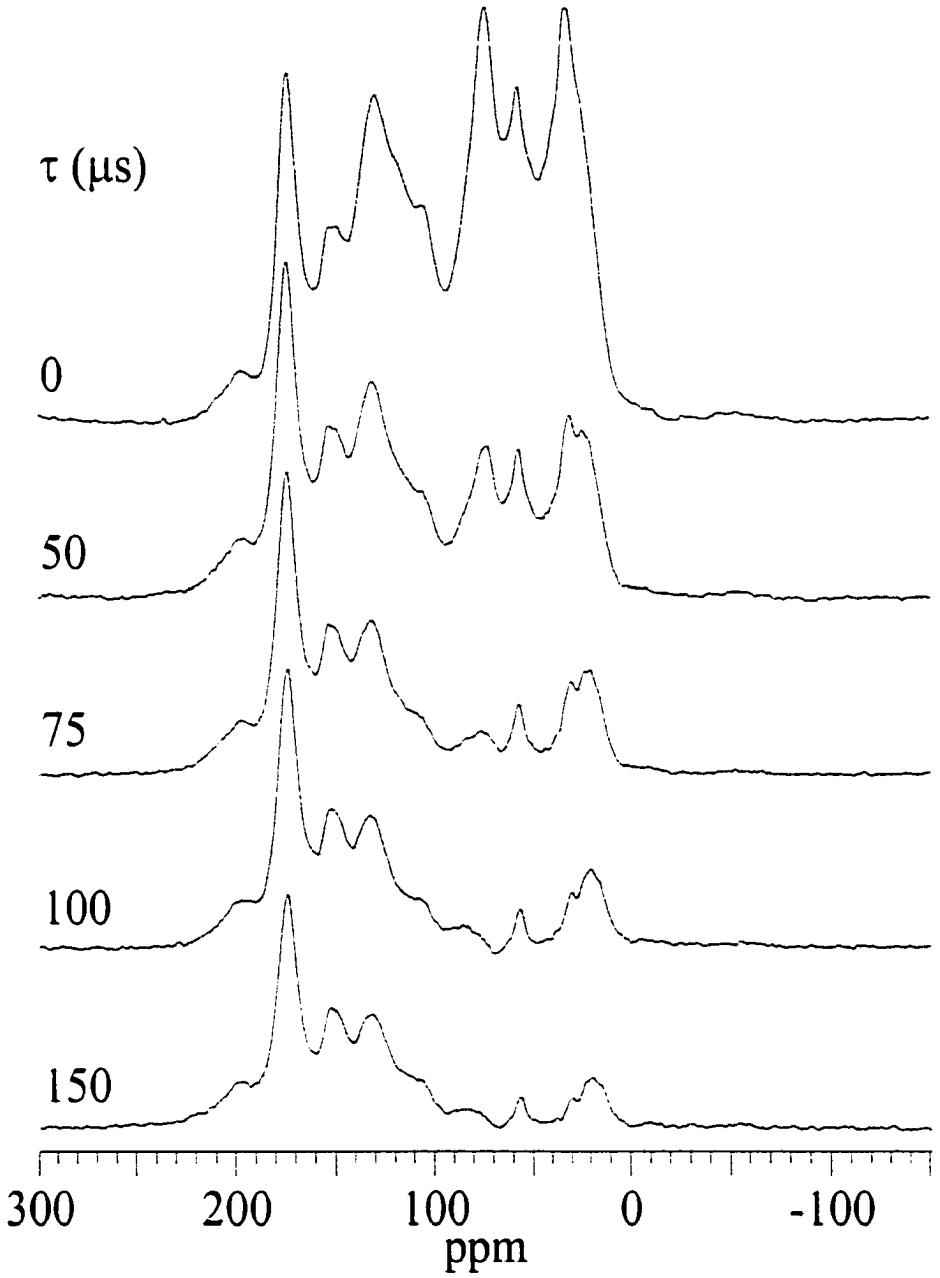

Figure 4.1 Dipolar-dephasing ^{13}C CP-MAS spectra of Uncompahgre humic acid. Dipolar dephasing periods τ are printed to the left of each spectrum. Each spectrum was the result of 16.000 acquisitions, acquired with a 1 s repetition delay and a 1 ms CP contact time period.

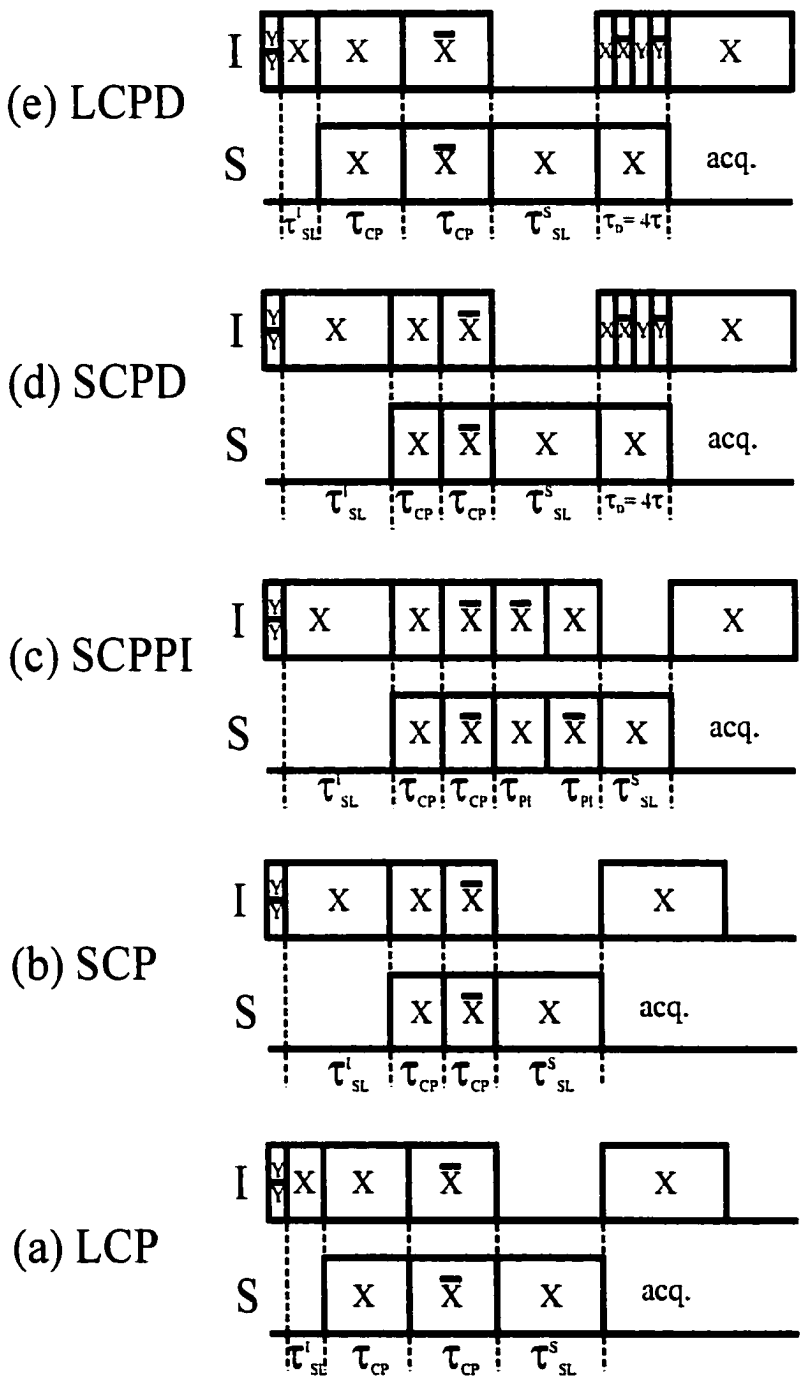

Figure 4.2 ^{13}C CP-MAS pulse sequences utilized for obtaining (a) LCP, (b) SCP, (c) SCPPI, (d) SCPD, and (e) LCPD spectra. I stands for ^{1}H and S stands for ^{13}C. CP contact periods are labeled τ_{CP}; depolarization periods are denoted τ_D; spin-lock periods are labeled τ_{SL}, and polarization inversion periods are given as τ_{PI}.

period with phase alternation, and inclusion of the spin-lock periods τ^{I}_{SL} and τ^{S}_{SL}, the SCP experiment is very similar to a "standard" CP-MAS experiment, but with a much shorter CP contact period. A corresponding experiment with a long CP period (LCP) is shown in Figure 4.2A. Because the 40 μs CP contact period of the SCP experiment is so short, it is primarily the rigid CH and CH_2 carbons that are polarized during the $2\tau_{CP}$ period, and the quasi-equilibrium polarizations that these carbons acquire during this period are only 1/2 and 2/3, respectively, of the corresponding "normal" CP polarization in a LCP experiment. These attenuations are due to the fact that within 40 μs there is not sufficient time for the CH and CH_2 protons to be repolarized from other protons (via ^{1}H-^{1}H flip-flops), following the partial transfer of polarization to ^{13}C. Thus, if one compares the LCP and SCP spectra obtained on the Uncompahgre humic acid, in Figures 4.3A and 4.3B, respectively, one sees a substantial diminution in Fig. 4.3B (relative to 4.3A) in the same spectral regions that survive interrupted decoupling most strongly (Fig. 4.1) – i.e., regions corresponding to CH_3 and $>C<$ groups.

Figure 4.2C shows the timing sequence of the SCPPI experiment, i.e., a cross polarization experiment carried out with a short CP contact period (40 μs), followed by a period of polarization inversion brought about by a suitable alteration of the relative phases of the ^{1}H and ^{13}C spin-lock (RF) fields (with $2\tau_{PI}$ = 32.8 μs in Fig. 4.2). This experiment leads, ideally, to a nulled CH signal and a CH_2 signal that is –2/9 (inverted in phase) of the optimized CP intensity. Since one expects only a minor CH_3 and $>C<$ intensity from a short-CP experiment, the SCPPI experiment ideally yields a CH_2-only spectrum (with inverted and attenuated amplitude). One sees in Figure 4.3C that the SCPPI spectrum of the Uncompahgre humic acid is a low-S/N spectrum.

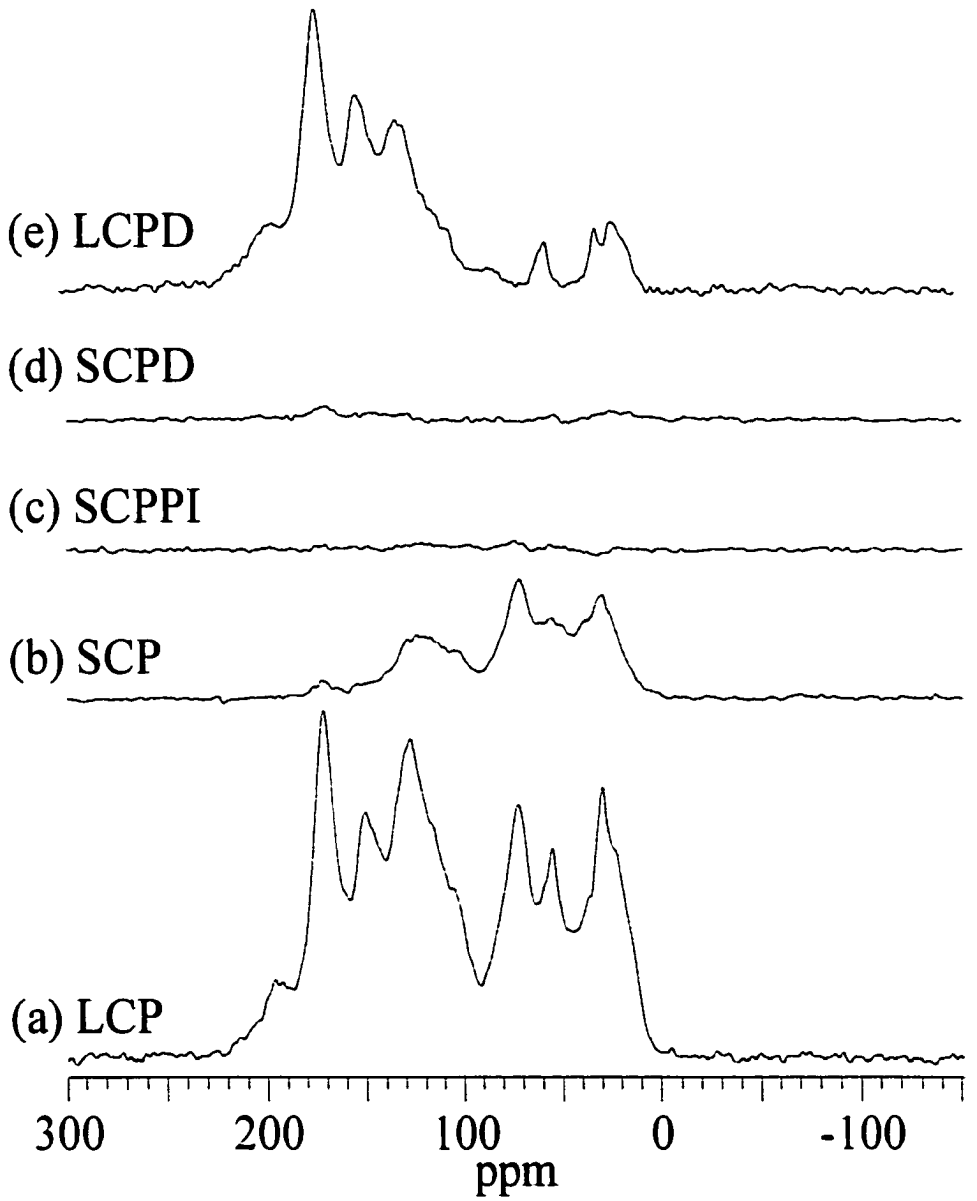

Figure 4.3 ^{13}C CP-MAS spectra of Uncompahgre humic acid (700 mg) obtained at a spinning speed of 5.2 kHz. (a) LCP, with $2\tau_{CP}$ = 1.5 ms, τ^{I}_{SL} = 140 μs, τ^{S}_{SL} = 400 μs, after 48000 acquisitions; (b) SCP, with $2\tau_{CP}$ = 40 μs, τ^{I}_{SL} = 1.6 ms, τ^{S}_{SL} = 400 μs, after 172,000 acquisitions; (c) SCPPI, with $2\tau_{CP}$ = 40 μs, τ^{I}_{SL} = 1.6 ms, τ^{S}_{SL} = 367 μs, $2\tau_{PI}$ = 32.8 μs, after 172,000 acquisitions; (d) SCPD, with $2\tau_{CP}$ = 40 μs, τ^{I}_{SL} = 1.6 ms, τ^{S}_{SL} = 300 μs, $4\tau_{D}$ = 120 μs, after 172,000 acquisitions; (e) LCPD, with $2\tau_{CP}$ = 1.5 ms, τ^{I}_{SL} = 140 μs, τ^{S}_{SL} = 400 μs, $4\tau_{D}$ = 120 μs, after 48,000 acquisitions.

Figure 4.2D shows the timing sequence of the SCPD experiment, executed with a short CP contact period that is followed by a period of proton depolarization and associated ^{13}C depolarization of CH and CH_2 groups (with $4\tau_D$ = 120 μs in Fig. 4.2). The net result expected of this experiment is a spectrum consisting primarily of small $>C<$ and CH_3 intensities that are generated during the short CP contact period. Figure 4.3D shows that the SCPD spectrum of the Uncompahgre humic acid has very poor S/N.

Figure 4.2E represents the LCPD experiment, i.e., a CP experiment carried out with a long CP contact period (in this case 1.5 ms) to permit, ideally, full polarization for all carbons, followed by a depolarization period designed to eliminate signals due to CH and CH_2 moieties. Hence, this experiment is expected to yield ideally a (CH_3 + $>C<$)-only spectrum. One can see that the LCPD spectrum of the Uncompahgre humic acid, shown in Figure 4.3E, resembles the dipolar dephasing spectrum of Figure 4.1, obtained with a 75 μs dephasing period.

The typical goal of a spectral editing procedure for ^{13}C NMR is to generate a CH-only subspectrum, a CH_2-only subspectrum, a CH_3-only subspectrum and a subspectrum representing only quaternary ($>C<$) carbons. The WBZ method generates CH-only and CH_2-only subspectra, and a third subspectrum representing only the combination of CH_3 and $>C<$ groups; the two contributions in the last subspectrum were partitioned by Wu, Burns and Zilm by recognizing that, in the samples of immediate interest to them, CH_3 resonances always occur at chemical shifts < 35 ppm and $>C<$ resonances always occur at > 35 ppm.

The WBZ recipe for generating the three basic subspectra is to take appropriate linear combinations of the SCP, SCPPI, SCPD and LCPD spectra discussed above. The

coefficients in these linear combinations were chosen empirically, based on model compounds, but show a close correspondence with theoretical considerations of the type outlined above (e.g., the –2/9 factor for CH_2 groups in the SCPPI experiment). Figure 4.4 shows diagrammatically the specific linear combinations of SCP, SCPPI, SCPD and LCPD spectra that are used to generate the three basic subspectra in the WBZ method. The combination factors shown above the arrows in that figure are those of Wu, Burns and Zilm; the factors presented in brackets below the arrows were empirically determined in this study based on intensities and combination properties of SCP, SCPPI, SCPD and LCPD spectra of monoethyl fumarate. This latter set are the values used for the work presented here.

In order to implement the WBZ procedure represented in Figure 4.4, one must be able to distinguish between CH_3 and $>C<$ contributions to the LCPD spectrum, because these two components are not distinguished by the time-domain editing in the WBZ process. Also, different combination factors (empirically 1.86 and 1.21) are used to generate CH_3-only and $>C<$-only subspectra and are used in generating the CH-only subspectrum. Although, as indicated above, Wu, Burns and Zilm were able to use a chemical-shift criterion for partitioning the LCPD spectrum into $>C<$ -only and CH_3-only contributions, we cannot use that criterion for the Uncompahgre humic acid case, because we believe that OCH_3 groups are major contributors to intensity in the 50-60 ppm region. This belief is at least partially grounded in the dipolar-dephasing behavior shown pictorially in Figure 4.1; detailed spectral deconvolutions of those spectra (not shown here), reveal that the peak centered at about 57 ppm behaves much more like a methyl peak than a quaternary carbon contribution, as characterized by Hatcher and co-

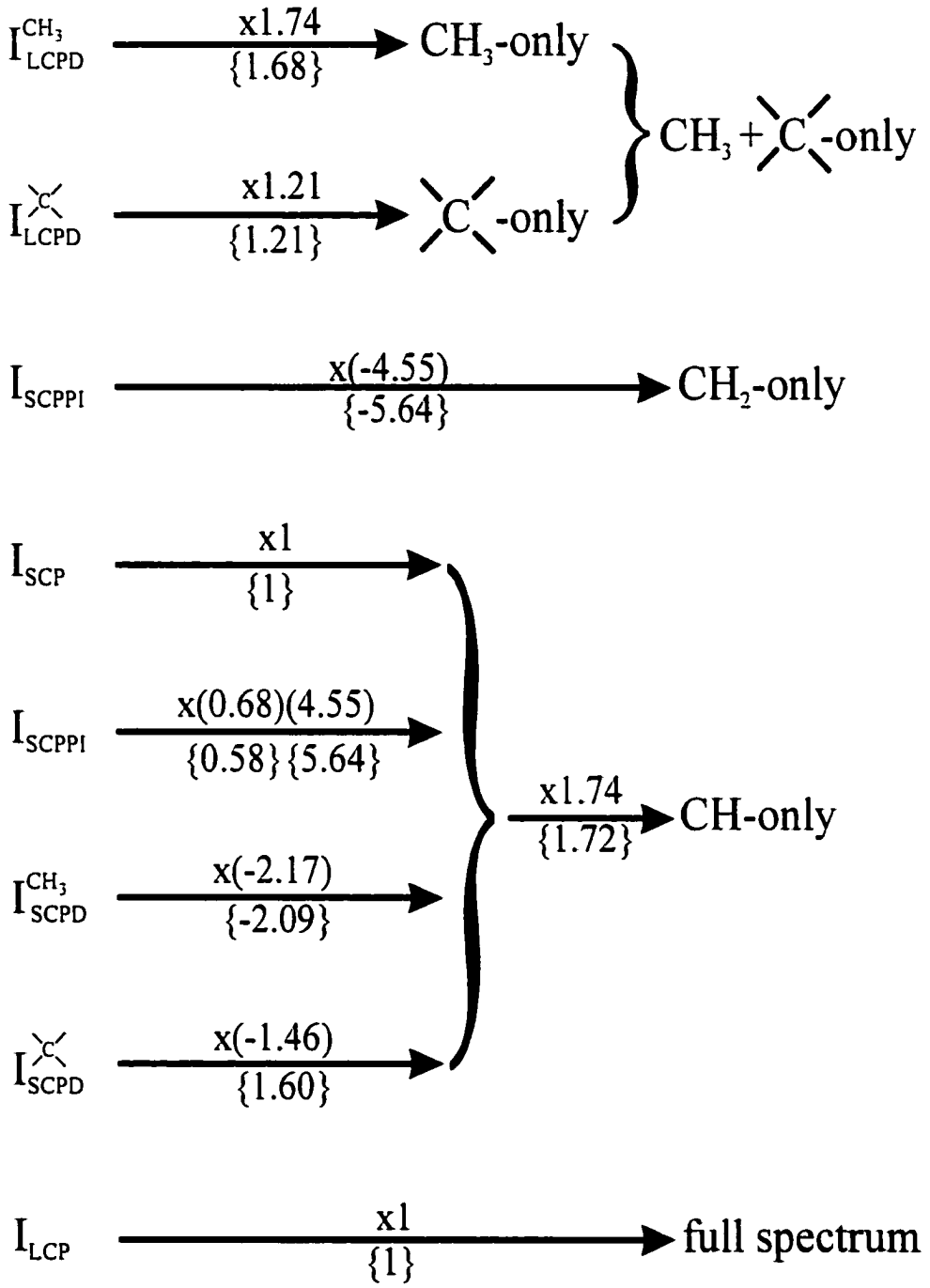

Figure 4.4 The WBZ scheme for generating the ($CH_1 + C_0$)-only, CH_2-only, and CH-only subspectra, and the full spectrum, showing combination factors suggested by Wu, Burns, and Zilm (above arrows) and those determined empirically in this study from experiments on monoethylfumarate (below arrows, in brackets).

workers[47,59-61]; this peak is attenuated much more slowly than are CH or CH_2 peaks (e.g., 32 ppm or 72 ppm peaks), but much faster than is the carbonyl peak (170-180 ppm) under dipolar-dephasing conditions. On this basis, we set 60 ppm, rather than 35 ppm, as the border between >C<-only contributions (>60 ppm) and CH_3-only contributions (< 60 ppm) in the LCPD spectrum. To the extent that this demarcation is invalid, i.e., to the extent that there is some >C< intensity in the 0-60 ppm region, the (CH_3 + >C<)-only subspectrum will have slightly too much intensity in that region, and the CH-only subspectrum will have slightly too little intensity in that region.

Figure 4.5 shows for the Uncompahgre humic acid the full (LCP) spectrum (4.5A), the CH-only subspectrum (4.5B), the CH_2-only subspectrum (4.5C) and the (CH_3 + >C<)-only subspectrum (4.5D) derived from the procedure represented in Figure 4.4. Figure 4.6 shows a comparison of the full (LCP) spectrum of the Uncompahgre humic acid (4.6A) with the synthetic spectrum (4.6B) constructed by adding the three (4.5B, 4.5C and 4.5D) subspectra together, each of which was generated according to the scheme shown in Figure 4.4. This comparison is most easily seen in the difference spectrum (4.6C), corresponding to: spectrum 4.6B – spectrum 4.6A.

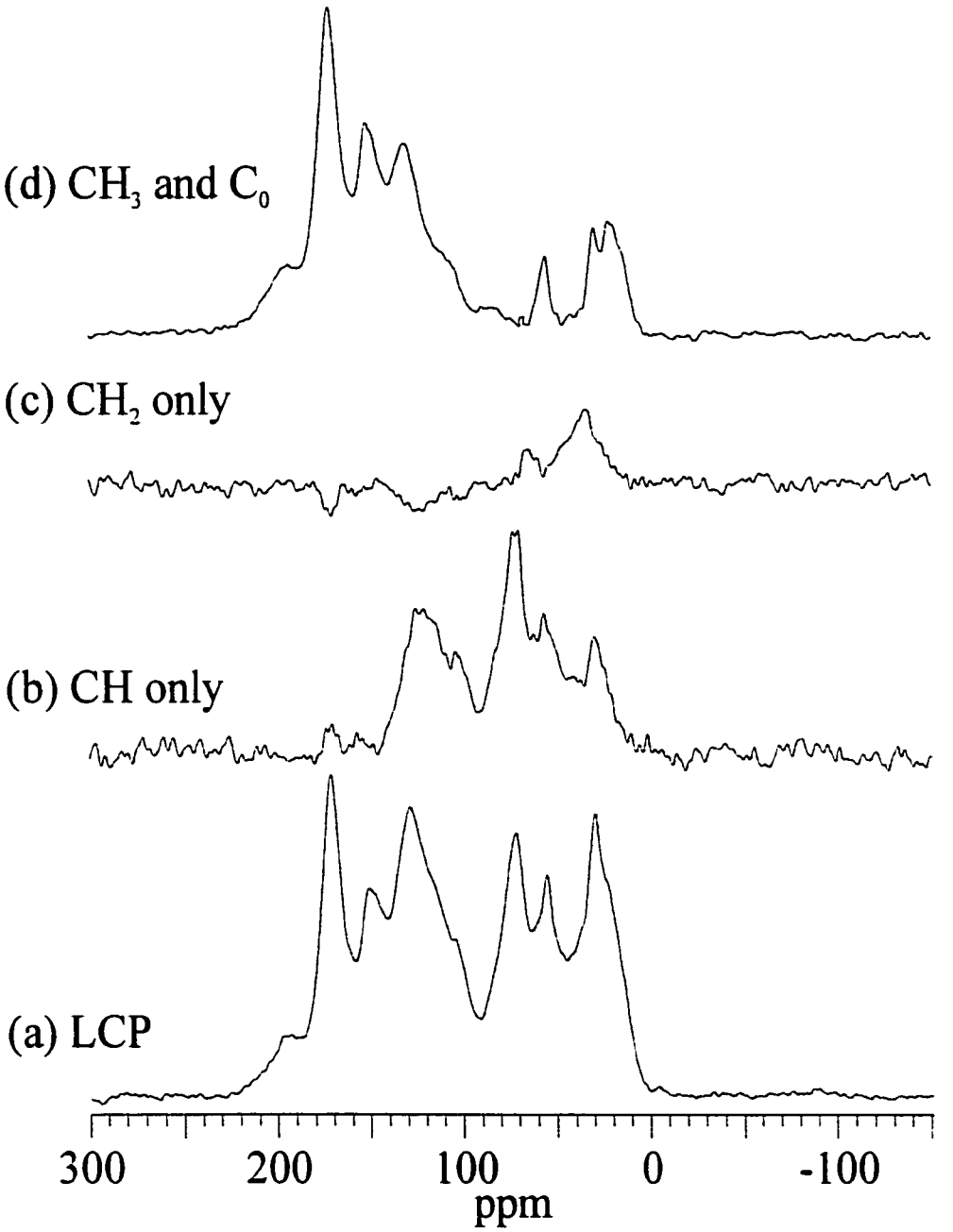

Figure 4.5 ^{13}C CP-MAS subspectra of Uncompahgre humic acid. (a) full (LCP) ^{13}C CP-MAS spectrum; (b) CH-only spectrum; (c) CH_2-only spectrum; and (d) (CH_3 + C_n)-only spectrum.

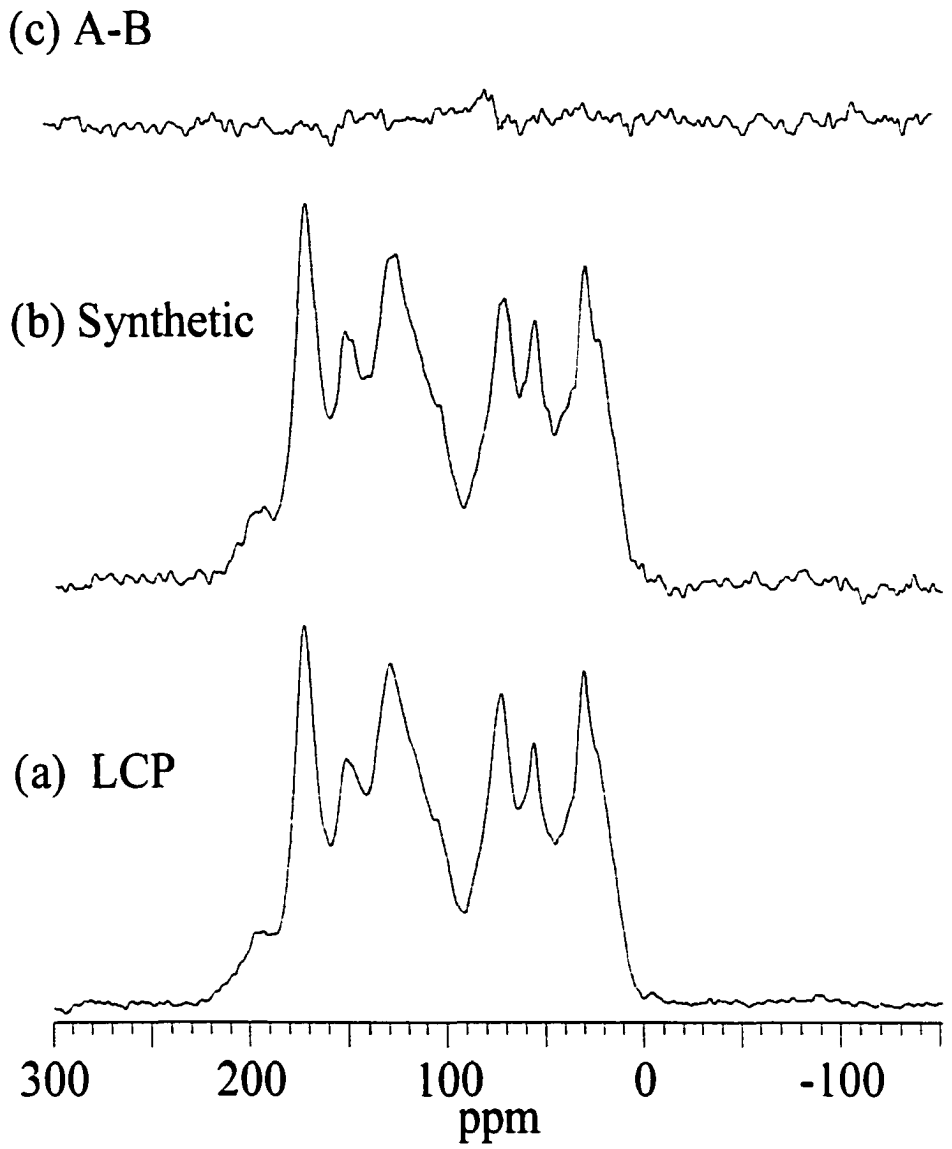

Figure 4.6 (a) full ^{13}C CP-MAS (LCP) spectrum of Uncompahgre humic acid; (b) synthetic ^{13}C CP-MAS spectrum generated by adding 4.5(b), 4.5(c), and 4.5(d) together; and (c) difference spectrum: spectrum 4.6(a) - spectrum 4.6(b).

4.4 Discussion

The "normal" CP-MAS ^{13}C NMR spectrum of the Uncompahgre humic acid (Fig. 4.1, $\tau = 0$ s) has major peaks at 190, 175, 150, 130, 104, 72, 57, 32, and 22 ppm. The broad peak at 22 ppm corresponds to a chemical shift that has typically been assigned to terminal methyl groups of alkyl chains[62-64]. This peak assignment is consistent with its appearance in the (CH_3 + >C<)-only subspectrum (Fig. 4.5D) and with its slow dipolar-dephasing decay, as can be seen in Figure 4.1. The fact that peak intensity at 22 ppm is insignificant in the other subspectra supports this assignment. This chemical shift has also been assigned to the acetyl methyl groups in hemicellulose[65], which is consistent with its occurrence in humic acid spectra.

The peak at 32 ppm corresponds to a chemical shift that has typically been assigned to methylene carbons in alkyl chains[62,63,66], and to CH_3 groups of acetyl groups attached to aliphatic structures[67]. These shift assignments are consistent with the peaks at 32 ppm observed in the CH_2-only subspectrum and (>C< + CH_3)-only subspectrum, respectively. In the CH-only subspectrum, the intensity at this chemical shift is likely due to methine carbons in aliphatic chains. Unlike the resonance at 22 ppm, the peak at 32 ppm has contributions to its intensity from a combination of markedly different chemical structures. This hypothesis that the 32 ppm peak contains contributions from CH_2 moieties, CH_3 groups, and possibly >C< moieties, is supported by the faster dipolar dephasing of this peak, relative to the entirely methyl peak at 22 ppm, suggesting that the intensity at 32 ppm is not entirely due to methyl-group functionality, and by the presence of intensity at 32 ppm in each of the three subspectra.

A major peak at about 57 ppm is often assigned to OCH_3 groups[61-64,68-69] and to amino-acid (HOOC-RC*H-NH-) carbons[64,67]. The CH_2 subspectrum has no significant intensity at this position, which is consistent with the proposed structure assignments. The small peak at 57 ppm in the CH-only subspectrum suggests a minor contribution from the amino-acid moieties. The characteristically slow dipolar-dephasing behavior for the 57 ppm peak, shown in Figure 4.1, is consistent with a methoxy chemical shift assignment, with a minor or no contribution to the 57 ppm peak from amino-acids.

A peak at 72 ppm is generally associated with secondary alcohol carbons, including those of cellulose and hemicellulose[65,70-72], which is consistent with the fact the intensity at 72 ppm was found in the CH subspectrum, but in neither the (CH_3 + >C<)-only nor the CH_2-only subspectra. Intensity in this region in the spectrum of Fig. 4.1 (τ = 0) is spread over roughly 20 ppm, covering the chemical shifts characteristic of C_2, C_3, C_4, C_5 and C_6 (all but the anomeric carbons -- C_1) of cellulose and similar polymeric carbohydrate structures[65,68,70,71]. The 72 ppm peak in Figure 4.1 displays the fastest dipolar-dephasing of all carbons in this humic acid, being completely diminished after only 75 μs of dephasing time. This behavior is consistent with both CH and CH_2 groups.

For interpreting the peak centered at 104 ppm in the ^{13}C CP-MAS spectrum of the Uncompahgre humic acid, we note that the anomeric carbon of a glucose fragment in a carbohydrate, e.g., cellulose, is generally accepted to have a chemical shift of about 104 ppm[65,70], the exact value depending on the identity of the next sugar unit to which it is linked. Intensity at 104 ppm appears in the CH subspectrum (Fig. 4.5B). The C_2 carbons of both guaiacyl and syringyl lignin structures and the C_6 carbon of syringyl units also show ^{13}C NMR intensity in the 105 ppm region[72-74]; such structural moieties would be

expected to show intensity in a CH subspectrum. Upon close observation, there also appears to be small intensity in the (CH_3 + $>C<$)-only subspectrum (Fig. 4.5D) centered at about 105 ppm. The $>C<$ groups of hemi-ketal structures in sugars, if present, would contribute intensity at this chemical shift in the (CH_3 + $>C<$)-only subspectrum, while hemi-acetal structures[67,69] would contribute intensity in this region in the CH-only subspectrum. A relatively fast dipolar dephasing is observed (Fig. 4.1) for the peak centered at roughly 105 ppm, which is consistent with a CH (or CH_2) moiety (hemi-acetal), not a $>C<$ structure (hemi-ketal).

Centered at about 130 ppm is a broad peak (~30 ppm width) that manifests itself in both the CH-only and (CH_3 + $>C<$)-only subspectra. Chemical shifts in this region are generally identified with a wide variety of aromatic structures, including the C_1 quaternary carbons of guaiacyl and syringyl lignin units and the C_6 carbon of guaiacyl[72,74]. Nearly all the signal intensity at 150 ppm in the ^{13}C CP-MAS spectrum of the Uncompahgre humic acid manifests itself in the (CH_3 + $>C<$)-only subspectrum, corresponding to substituted aromatic carbons. The relatively slow dipolar dephasing observed for this peak in Figure 4.1 is consistent with this quaternary carbon assignment. The 150 ppm chemical shift is frequently identified with O-substituted carbons in aromatic structures, including both $-OCH_3$ groups (e.g., C_3 and C_5 of syringyl and C_3 of guaiacyl)[72,75,76] and –OH groups (e.g., C_4 of syringyl and guaiacyl)[73,74,76]; also consistent with this chemical shift are –COOH substituted aromatic carbons[62,64]. No intensity in the 150 ppm region appears in the CH_2-only and CH-only subspectra of the Uncompahgre humic acid, which is consistent with these chemical shift assignments. The C_4 carbons of guaiacyl units involved in ether linkages to C_β of adjacent lignin units have

also been assigned previously to this chemical shift[65], as have C_4-OH carbons of guaiacyl; such structural assignments are consistent with our spectral editing results.

The major peak centered at 175 ppm is consistent with carbonyl carbons of a variety of structures[62-64,67,69], including those of hemicellulose[65,71] and amides[64,67,69]. Such carbonyl assignments are consistent with our spectral editing results, in which intensity centered at 175 ppm is found only in the (CH_3 + >C<)-only subspectrum. Similarly, ketone carbonyl intensity in the 190 ppm is also manifested only in the (CH_3 + >C<)-only subspectrum. Carbonyl carbons in these structures don't experience a strong dipolar coupling with protons, as is experimentally confirmed by the very slow dipolar-dephasing results observed for the peak centered at 175 ppm in the humic acid spectrum (Fig. 4.1).

In summary, the solid-sample ^{13}C NMR spectral editing procedure introduced by Wu, Burns and Zilm[49] is a practicable technique for humic materials, and accordingly can be applied successfully with a reasonable choice of hardware. Decomposition of the CP-MAS spectrum into CH_2-only, CH-only and (CH_3 + >C<)-only subspectra augments one's ability to assign specific chemical-structural features to specific regions of the spectrum. This approach often confirms, or delineates between, structural assignments based on just ^{13}C chemical shifts. Dipolar-dephasing data provide supporting information. As expected from previously published studies on other types of complex organic samples[49,50], the SCPD and SCPPI spectra prescribed by WBZ have very low S/N, even though they are commonly acquired with an enhanced number of repetitions. Since the CH_2-only subspectrum is derived directly from the latter, the resulting CH_2-only subspectrum has a low S/N.

References

1. D. E. Axelson "Solid State Nuclear Magnetic Resonance of Fossil Fuels: An Experimental Approach." Multiscience Publications, Montreal, Can, 1985.

2. Wind, R. A.; Maciel, G. E.; Botto, R. E. "Quantitation in ^{13}C NMR Spectroscopy of Carbonaceous Solids" in Magnetic Resonance of Carbonaceous Solids, R. E. Botto, Y. Sanada, eds., Advances in Chemistry Series 229, American Chemical Society, Washington, DC, 1993, pp. 175-419.

3. NMR of Humic Substances and Coal: Techniques, Problems, and Solutions. Wershaw, R. L.; Mikita, M. A.; eds., Lewis Publishers, Inc., Chelsea, MI, 1987, p 236.

4. Maciel, G. E.; Erbatur, O. NMR Characterization of Solid Fossil Fuels. Coal and Oil Shale," in *Nuclear Magnetic Resonance in Modern Technology*, Maciel, G. E., ed., NATO ASI Series, Kluwer, Dordrecht, Netherlands, 1994, pp. 165-224.

5. Bartuska, V. J.; Maciel, G. E.; Schaefer, J.; Stejskal, E. O. Prospects for carbon-13 nuclear magnetic resonance analysis of solid fossil-fuel materials. *Fuel* **1977**, *56*, 354-358.

6. Maciel, G. E.; Bartuska, V. J.; Miknis, F. P. Characterization of organic material in coal by proton-decoupled ^{13}C nuclear magnetic resonance with magic-angle spinning. *Fuel* **1979**, *58*, 391-394.

7. Miknis, F. P.; Sullivan, M.; Bartuska, Maciel, G. E. Cross-polarization magic-angle spinning ^{13}C NMR spectra of coals of varying rank. *Org. Geochem.* **1981**, *3*, 19-28.

8. Maciel, G. E.; Sullivan, M. J. "^{13}C NMR Characterization of Solid Fossil Fuels Using Cross-Polarization and Magic-Angle Spinning" in New Methods and Applications in NMR Spectroscopy, ACS Symposium Monograph 191, G.C. Levy, ed., American Chemical Society, pp. 319-343 (1982).

9. Maciel, G. E., Sullivan, M. J.; Petrakis, L.; Grandy, D.W. ^{13}C Nuclear magnetic resonance characterization of coal macerals by magic-angle spinning. *Fuel* **1982**, *61*, 411-414.

10. Sullivan, M. J.; Maciel, G. E., Structural resolution in the carbon-13 nuclear magnetic resonance spectrometric analysis of coal by cross polarization and magic-angle spinning. *Anal. Chem.* **1982**, *54*, 1606-1615.

11. Sullivan, M. J.; Maciel, G. E. Spin dynamics in the carbon-13 nuclear magnetic resonance spectrometric analysis of coal by cross polarization and magic-angle spinning. *Anal. Chem.* **1982**, *54*, 1615-1623.

12. Hatcher, P. G., Breger, I. A.; Szeverenyi, N.; Maciel, G. E. Nuclear magnetic resonance studies of ancient buried wood Ñ II. Observations on the origin of coal from lignite to bituminous coal. *Org. Geochem.* **1982**, *4*, 9-18.

13. Erbatur, G.; Erbatur, O.; Davis, M. F.; Maciel, G. E. Chemical structures of pyridine extracts and residues of coals as indicated by solid state ^{13}C NMR. *J. Mol. Structure* **1984**, *114*, 83-88.

14. Verheyen, V.; Johns, R. B.; Bryson, R. L.; Maciel, G. E.; Blackburn, D. T. A spectroscopic investigation of the banding of lithotypes occurring in Victorian brown coal seams. *Fuel* **1984**, *63*, 1629-1635.

15. Sullivan; M. J.; Szeverenyi, N. M.; Maciel, G. E., "Proton Spin-Lattice Relaxation In Coals of Varying Rank" in Magnetic Resonance. Introduction, Advanced Topics and Applications to Fossil Energy, L. Petrakis and J.P. Fraissard eds., D. Reidel Publishing Company, pp. 607-616 (1984).

16. Erbatur, G.; Erbatur, O.; Davis, M. F.; Maciel, G. E. Investigation of pyridine extracts and residues of coals by solid-state ^{13}C n.m.r. spectroscopy. *Fuel* **1986**, *65*, 1265-1272.

17. Erbatur, G.; Erbatur, O.; Coban, A.; Davis, M. F.; Maciel, G. E. Investigation of the chemical structures of coking and non-coking coals in original and reductively alkylated solid states via ^{13}C n.m.r. and i.r. spectroscopies. *Fuel* **1986**, *65*, 1273-1280.

18. Davis, M. F.; Quinting, G. R.; Bronnimann, C. E.; Maciel, G. E. A nuclear magnetic resonance study of the pyridine extraction of coal. *Fuel* **1989**, *68*, 763-770.

19. Maciel, G. E.; Bronnimann, C. E.; Jurkiewicz, A.; Wind, R. A.; Pan, V. H. Recent advances in coal characterization by ^{13}C and ^{1}H n.m.r. *Fuel* **1991**, *70*, 925-930.

20. Maciel, G. E.; Bartuska, V. J.; Miknis, F. P. Correlation between oil yields of oil shales and ^{13}C nuclear magnetic resonance spectra. *Fuel* **1978**, *57*, 505-506.

21. Maciel, G. E.; Bartuska, V. J.; Miknis, F. P. Improvement in correlation between oil yields of oil shales and ^{13}C n.m.r. spectra. *Fuel* **1979**, *58*, 155-156.

22. Miknis, F. P.; Maciel, G. E.; Bartuska, V. J. Cross polarization magic-angle spinning ^{13}C NMR spectra of oil shales. *Org. Geochem.* **1979**, *1*, 169-176

23. Maciel, G. E.; Dennis, L. W. Comparison of oil shales and kerogen concentrates by ^{13}C nuclear magnetic resonance. *Org. Geochem.* **1982**, *3*, 105-109.

24. Miknis, F. P.; Netzel, D. A.; Smith, J. W.; Mast, M. A.; Maciel, G. E. ^{13}C NMR measurements of the genetic potentials of oil shales. *Geochim. Cosmochim. Acta* **1982**, *46*, 977-984.

25. Miknis, F. P.; Szeverenyi, N. M.; Maciel, G. E. Characterization of the residual carbon in retorted oil shale by solid-state ^{13}C n.m.r. *Fuel* **1982**, *61*, 341-345.

26. Palmer, A. R.; Maciel, G. E. Relaxation behavior in the carbon-13 nuclear magnetic resonance spectrometric analysis of kerogen with cross polarization and magic-angle spinning. *Anal. Chem.* **1982**, *54*, 2194-2198.

27. Miknis, F. P.; G. E. Maciel, "Some Examples of ^{13}C NMR Applications To Oil Shales" in Magnetic Resonance. Introduction, Advanced Topics and Applications to Fossil Energy, L. Petrakis and J.P. Fraissard eds., D. Reidel Publishing Company, pp. 545-555 (1984).

28. Hatcher, P. G.; Maciel, G. E.; Dennis, L. W. Aliphatic structure of humic acids; a clue to their origin. *Org. Geochem.* **1981**, *3*, 43-48.

29. Hatcher, P. G.; Schnitzer, M.; Dennis, L. W.; Maciel, G. E. Aromaticity of humic substances in soils. *Soil Sci. Soc. Am. J.* **1981**, *45*, 1089-1094.

30. Hatcher, P. G., Lyons, P. C.; Thompson, C. L.; Brown, F. W.; Maciel, G. E. Organic matter in a coal ball: peat or coal?. *Science* **1982**, *217*, 831-833.

31. Hatcher, P. G.; Breger, I. A.; Dennis, L.W.; Maciel, G. E. "Solid-state ^{13}C NMR of Sedimentary Humic Substances: New Revelations on Their Chemical Composition" in Terrestrial and Aquatic Humic Materials, R.F. Christman and O. Gjessing, eds., Ann Arbor Science Press, p. 37 (1983).

32. Hatcher, P. G.; Breger, I. A.; Maciel, G. E.; Szeverenyi, N. M. "Geochemistry of Humin" in Humic Substances in Soil, Sediment, and Water: Geochemistry, Isolation, and Characterization, D. M. McKnight (ed.), John Wiley & Sons, Inc., New York, pp. 275-302 (1985).

33. Saiz-Jimenez, C.; Hawkins, B. L.; Maciel, G. E. Cross polarization, magic-angle spinning ^{13}C nuclear magnetic resonance spectroscopy of soil humic fractions. *Org. Geochem.* **1986**, *9*, 277-284.

34. Frye, J. S.; Bronnimann, C. E.; Maciel, G. E."Solid-State NMR of Humic Materials" in NMR of Humic Substances and Coal, R. L. Wershaw and M. A. Mikita, eds., Lewis Publishers, Chelsea, MI, pp. 33-46 (1987).

35. Preston, C. M.; Shipitalo, S.-E.; Dudley, R. L.; Fyfe, C. A.; Mathur, S. P.; Levesque, M. Comparison of ^{13}C CPMAS NMR and chemical techniques for measuring the degree of decomposition in virgin and cultivated peat profiles. *Can. J. Soil Sci.* **1987**, *67*, 187-198.

36. Dudley, R. L.; Fyfe, C. A. ; Preston, C. M. A ^{13}C-CPMAS NMR spectroscopic study of the transformation of plant material to peat and coal. *Can. J. Spectrosc.* **1990**, *35*, 31-38.

37. Preston, C. M.; Axelson, D. E.; Levesque, M.; Mathur, S. P.; Dinel, H.; Dudley, R. L. Carbon-13 NMR and chemical characterization of particle-size separates of peats differing in degree of decomposition. *Org. Geochem.* **1989**, *14*, 393-403.

38. Norden, B; Fyfe, C. A.; McKinnon, M. S. ^{13}C CP/MAS study of peat in the solid state. *Int. Peat J.* **1986**, *1*, 153-164.

39. Andrew, E. R.; Bradbury, A.; Eades, R. G. Nuclear magnetic resonance spectra from a crystal rotated at high speed. *Nature* **1958**, *182*, 1659.

40. Fyfe, C. A. "Solid State NMR for Chemists," CFC Press, Guelph, 1983.

41. Maciel, G. E. High-resolution nuclear magnetic resonance of solids. *Science* **1984**, *226*, 282-288.

42. Maciel, G. E., "Line-Broadening Influences and Line-Narrowing Techniques In Solid State NMR" in Magnetic Resonance. Introduction, Advanced Topics and Applications to Fossil Energy, L. Petrakis and J.P. Fraissard, eds., D. Reidel Publishing Company, pp. 71-110 (1984).

43. Pan, V. H.; Maciel, G. E. The analysis of three representative premium coals by ^{13}C nuclear magnetic resonance. *Fuel* **1993**, *72*, 451-468.

44. Jurkiewicz, A.; Maciel, G. E. Spin Dynamics and Spin Counting in the ^{13}C CP-MAS Analysis of Argonne Premium Coals. *Fuel* **1994**, *73*, 828-835.

45. Opella, S. J.; Frey, M. H. Selection of nonprotonated carbon resonances in solid-state nucear magnetic resonance. *J. Am. Chem. Soc.* **1979**, *101*, 5854-5856.

46. Alemany, L. B.; Grant, D. M.; Alger, T. G.; Pugmire, R. J. Cross polarization and magic angle sample spinning NMR spectra of model organic compounds. 3. Effect of the ^{13}C-^{1}H dipolar interaction on cross polarization and carbon-proton dephasing. *J. Am. Chem. Soc.* **1983**, *105*, 6697-6704.

47. Hatcher, P. G. Chemical structural studies of natural lignin by dipolar dephasing solid-state ^{13}C nuclear magnetic resonance. *Org. Geochem.* **1987**, *11*, 31-39.

48. Zhang, M.; Maciel, G. E. Enhanced signal-to-noise ratios in the nuclear magnetic resonance Analysis of Solids, using large-sample magic-angle spinners. *Anal. Chem.* **1990**, *62*, 633-638.

49. Wu, X.; Burns, S.; Zilm, K. W. Spectral editing in CPMAS NMR. Generating subspectra based on proton multiplicities. *J. Magn. Reson. Ser. A* **1994**, *111*, 29-36.

50. Mao, S-H; Mao, X-A.; Xu, Z-H.; Hu, J-Z.; Yang, B-L.; Li, L-Y.; Ye, C-H.; Saffigna, P. CP/MAS ^{13}C spectral editing of dried pine leaves. *Solid State Nucl. Magn. Reson.* **1998**, *12*, 31-36.

51. Derbyshire, F.; Marzec, A.; Schulten, H.-R.; Wilson, M. A.; Davis, A.; Tekely, P.; Delpuech, J. J.; Jurkiewicz, A.; Bronnimann, C. E.; Wind, R. A.; Maciel, G. E., Narayan, R.; Bartle, K.; Snape, C. Molecular structure of coals: A debate. *Fuel* **1989**, *68*, 1091-1106.

52. Metz, G.; Ziliox, M.; Smith, S. O. Towards quantitative CP-MAS NMR. *Solid State Nucl. Magn. Reson.* **1996**, *7*, 155-160.

53. Peersen, O. B.; Wu, X.; Smith, S. O. Enhancement of CP-MAS signals by variable-amplitude cross polarization. Compensation for inhomogeneous B_1 fields. *J. Magn. Reson. Ser. A* **1994**, *106*, 127-131.

54. Peersen, O. B.; Wu, X.; Kustanovich, I.; Smith, S. O. Variable-amplitude cross-polarization MAS NMR. *J. Magn. Reson. Ser. A* **1993**, 104, 334-339.

55. Zhang, M.; Maciel, G. E. Large-sample ^{13}C MAS n.m.r. spectroscopy of coal: relaxation and spin counting. *Fuel* **1990**, *69*, 557-563.

56. Wu, X.; Zilm, K. W. Heterogeneity of cross relaxation in solid-state NMR. *J. Magn. Reson.* **1991**, *93*, 265-278.

57. Wu, X.; Zilm, K. W. Complete spectral editing in CPMAS NMR. *J. Magn. Reson. Ser. A* **1993**, *102*, 205-213.

58. Wu, X.; Zilm, K. W. Methylene-only subspectrum in CPMAS NMR. *J. Magn. Reson. Ser. A* **1993**, *104*, 119-122.

59. Kogel-Knabner, I.; Hatcher, P. G. Characterization of alkyl carbon in forest soils by CPMAS ^{13}C NMR spectroscopy and dipolar dephasing. *Sci. Tot. Environ.* **1989**, *81/82*, 169-177.

60. Hatcher, P. G.; Schnitzer, M.; Vassallo, A. M.; Wilson, M. A. The chemical structure of highly aromatic humic acids in three volcanic ash soils as determined by dipolar dephasing NMR studies. *Geochim. Cosmochim. Acta* **1989**, *53*, 125-130.

61. Hatcher, P. G.; Dipolar-dephasing ^{13}C NMR studies of decomposed wood and coalified xylem tissue: Evidence for chemical structural changes associated with

defunctionalization of lignin structural units during coalification. *Energy Fuels* **1988**, *2*, 48-58.

62. Jokic, A.; Srejic, R.; Pfendt, P. A.; Zakrzewska, J. Characterization of lake sediment humic acids from the Celije lake system near Krusevac (central Serbia) by ^{13}C and ^{1}H solution NMR and ^{13}C CPMAS NMR. *Water, Air Soil Pollut.* **1995**, *84*, 159-173.

63. Silverstein, R. M.; Bassler, G. C.; Morrill, T. C. "^{13}C NMR Spectrometry. In Spectrometric Identification of Organic Compounds", D. Sawicki, ed., John Wiley and Sons, Inc., New York, 227-265 (1991).

64. Gonzalez-vila, F. J.; Ludemann, H.-D.; Martin, F. ^{13}C-NMR Strucural features of soil humic acids and their methylated, hydrolyzed and extracted derivatives. *Geoderma* **1983**, *31*, 3-15.

65. Preston, C. M. The application of NMR to organic matter inputs and processes in forest ecosystems of the Pacific Northwest. *Sci. Tot. Environ.* **1992**, *114*, 107-120.

66. Kolodziejski, W.; Frye, J. S.; Maciel, G. E. Carbon-13 Nuclear Magnetic Resonance Spectrometry with Cross Polarization and Magic-Angle Spinning for Analysis of Lodgepole Pine Wood *Anal. Chem.* 1982, 54, 1419-1424.

67. Ricca, G.; Severini, F. Structural investigations of humic substances by IR-FT. ^{13}C-NMR spectroscopy and comparison with a maleic oligomer of known structure. *Geoderma* **1993**, *58*, 233-244.

68. Haw, J. F.; Maciel, G. E.; Schroeder, H. A. Carbon-13 Nuclear Magnetic Resonance Spectrometric Study of Wood and Wood Pulping with Cross Polarization and Magic-Angle Spinning. *Anal. Chem.* **1984**, 56, 1323-1329.

69. Skjemstad, J. O.; Frost, R. L.; Barron, P. J. Structural units in humic acids from South-eastern Queensland soils as determined by ^{13}C NMR spectroscopy. *Aust. J. Soil Res.* **1983**, *21*, 539-547.

70. Watanabe, A.; Tsutsuki, K.; Kuwatsuka, S.; Kuwatsuka, K. ^{13}C-NMR investigation of humic acid and fulvic acids obtained from some typical japanese soils. *Sci. Tot. Environ.* **1989**, *81-82*, 195-200.

71. Maciel, G. E., Haw, J. F.; Smith, D. H.; Gabrielsen, B. C.; Hatfield, G. R. Carbon-13 Nuclear Magnetic Resonance of Herbaceous Plants and Their Components, Using Cross Polarization and Magic-Angle Spinning *J. Ag. Food Chem.* **1985**, *33*, 185-191.

72. Guggenberger, G.; Zech, W.; Haumaier, L.; Christensen, B. T. Land-use effects on the composition of organic matter in particle-size separates of soils: II. CPMAS and solution ^{13}C NMR analysis. *Eur. J. Soil Sci.* **1995**, *46*, 147-158.

73. Maciel, G. E.; O'Donnell, J. D.; Ackerman, J. J.; Hawkins, B. H.; Bartuska, V. J. A ^{13}C NMR Study of Four Lignins in the Solid and Solution States. *Makromol. Chem.* **1981**, *182*, 2297-2304.

74. Hatfield, G. R.; Maciel, G. E.; O. Erbatur, O.; Erbatur, G. Qualitative and Quantitative Analysis of Solid Lignin Samples by Carbon-13 Nuclear Magnetic Resonance Spectroscopy. *Anal. Chem.* **1987**, *59*, 172-179.

75. Petsom, A.; Steelink, C. Effect of base on the C-13 NMR spectra of model phenolic acids related to humic acids and lignins. *Environ. Technol. Lett.* **1988**, *9*, 609-620.

76. Bartuska, V. J.; Maciel, G. E.; Bolker, H. K.; Fleming, B. I. Structural Studies of Lignin Isolation Procedures by ^{13}C NMR. *Holzforschung* **1980**, *34*, 214-217.

APPENDIX

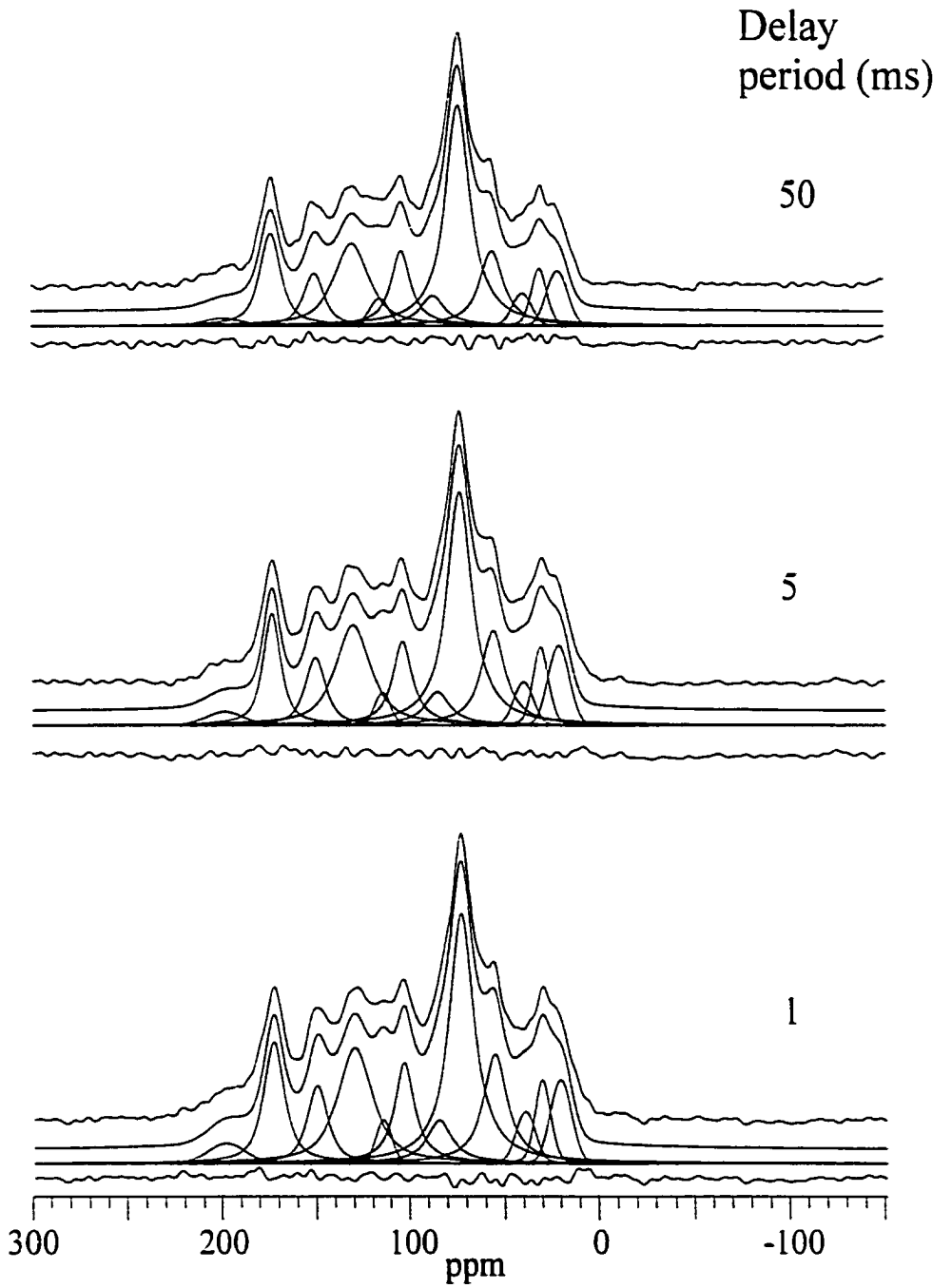

Figure A2-2 Deconvolutions of the ^{13}C T_1 relaxation spectra of the Uncompahgre whole soil data found in Figure 2.2(a). The delay period for each spectrum is written above and to the left of each spectrum. For each delay period, the uppermost spectrum is the experimental spectrum, the next lower trace is the "synthetic" spectrum, the next lower are the individual deconvoluted peaks, and the lowermost spectrum is the "difference spectrum". The synthetic spectrum was generated by adding the peak areas of the deconvoluted peaks (third trace from top). The difference spectrum is generated by subtracting the experimental spectrum from the synthetic spectrum and gives an indication of the success of the deconvolution procedure.

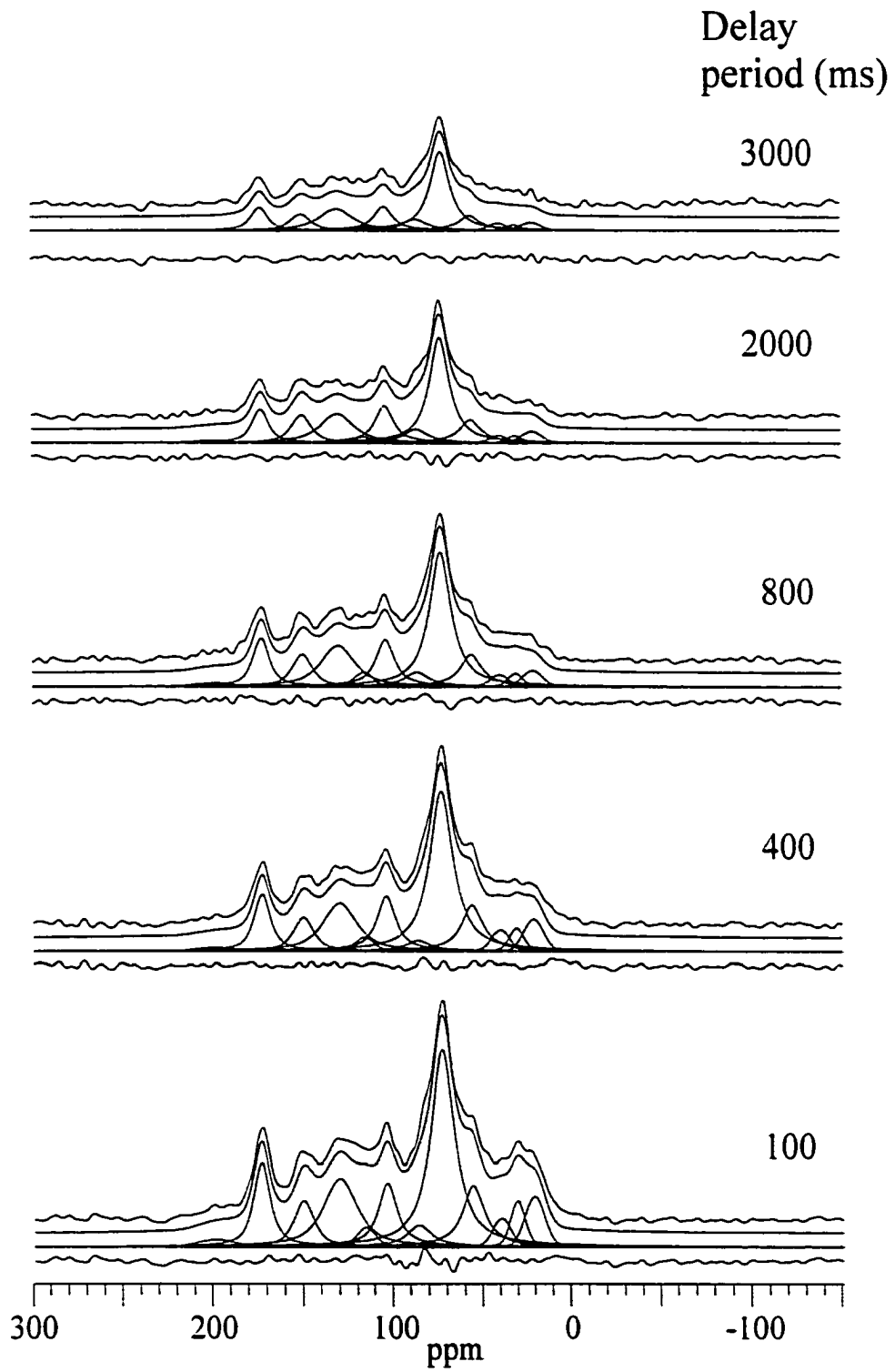

Figure A2-2 (Continued).

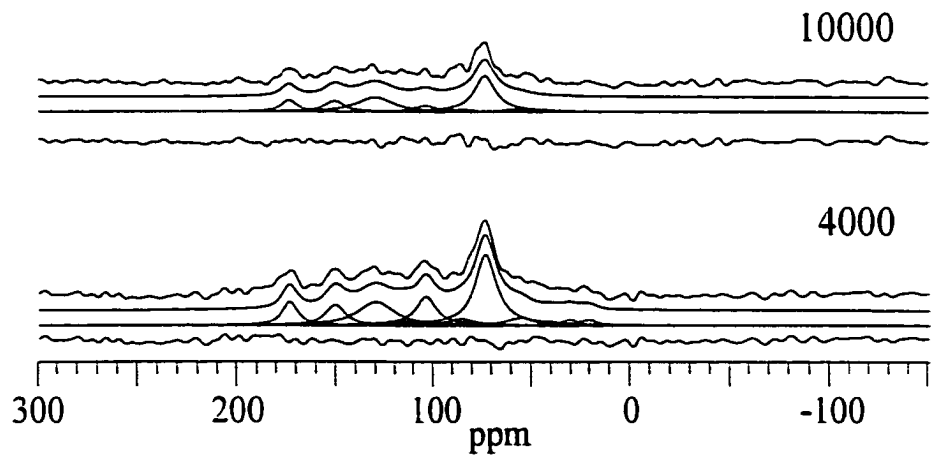

Figure A2-2 (Continued).

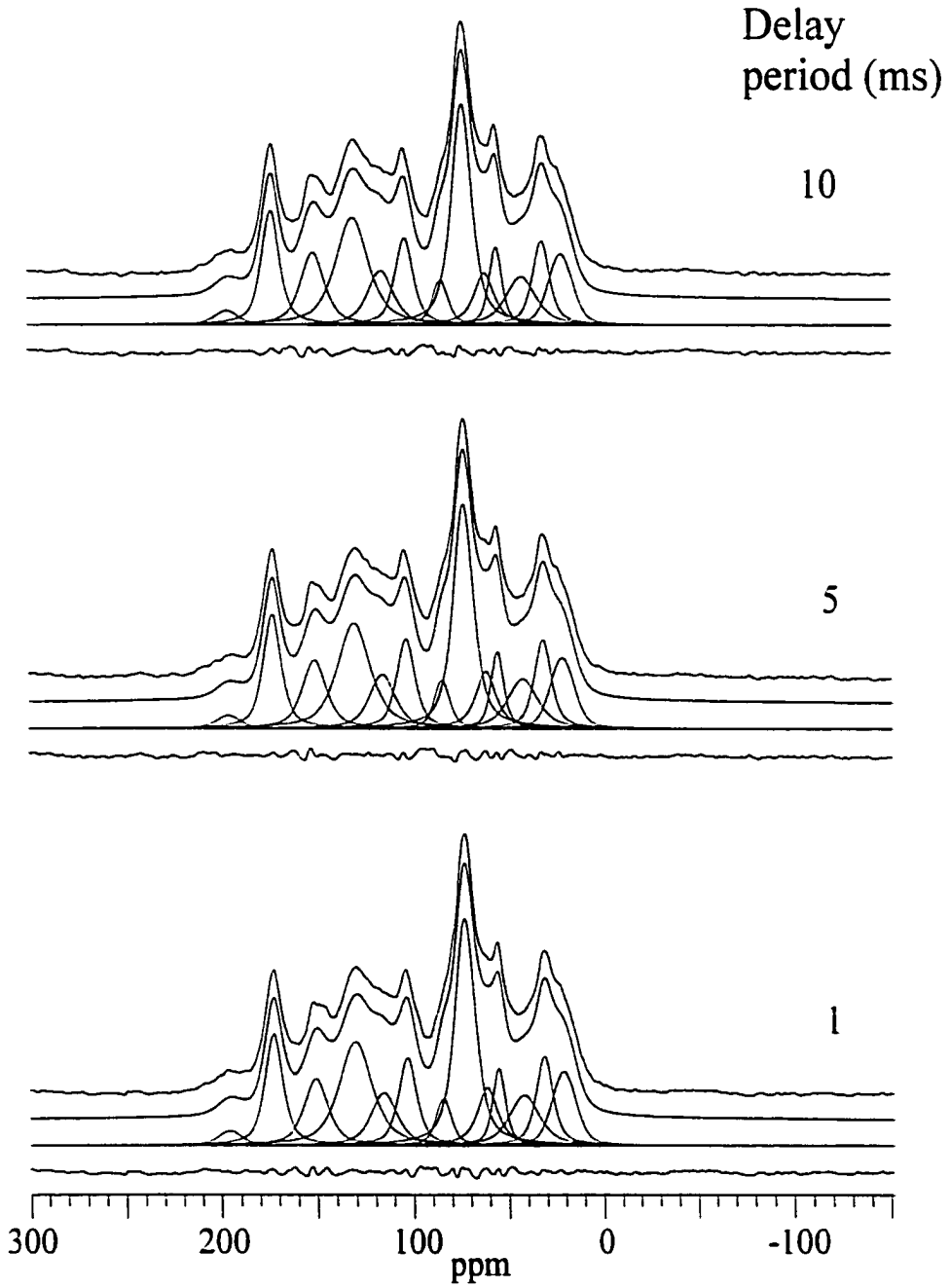

Figure A2-3 Deconvolutions of the ^{13}C T_1 relaxation spectra of the HF-treated Uncompahgre whole soil data found in Figure 2.3(a). The delay period for each spectrum is written above and to the left of each spectrum. For each delay period, the uppermost spectrum is the experimental spectrum, the next lower trace is the "synthetic" spectrum, the next lower are the individual deconvoluted peaks, and the lowermost spectrum is the "difference spectrum". The synthetic spectrum was generated by adding the peak areas of the deconvoluted peaks (third trace from top). The difference spectrum is generated by subtracting the experimental spectrum from the synthetic spectrum and gives an indication of the success of the deconvolution procedure.

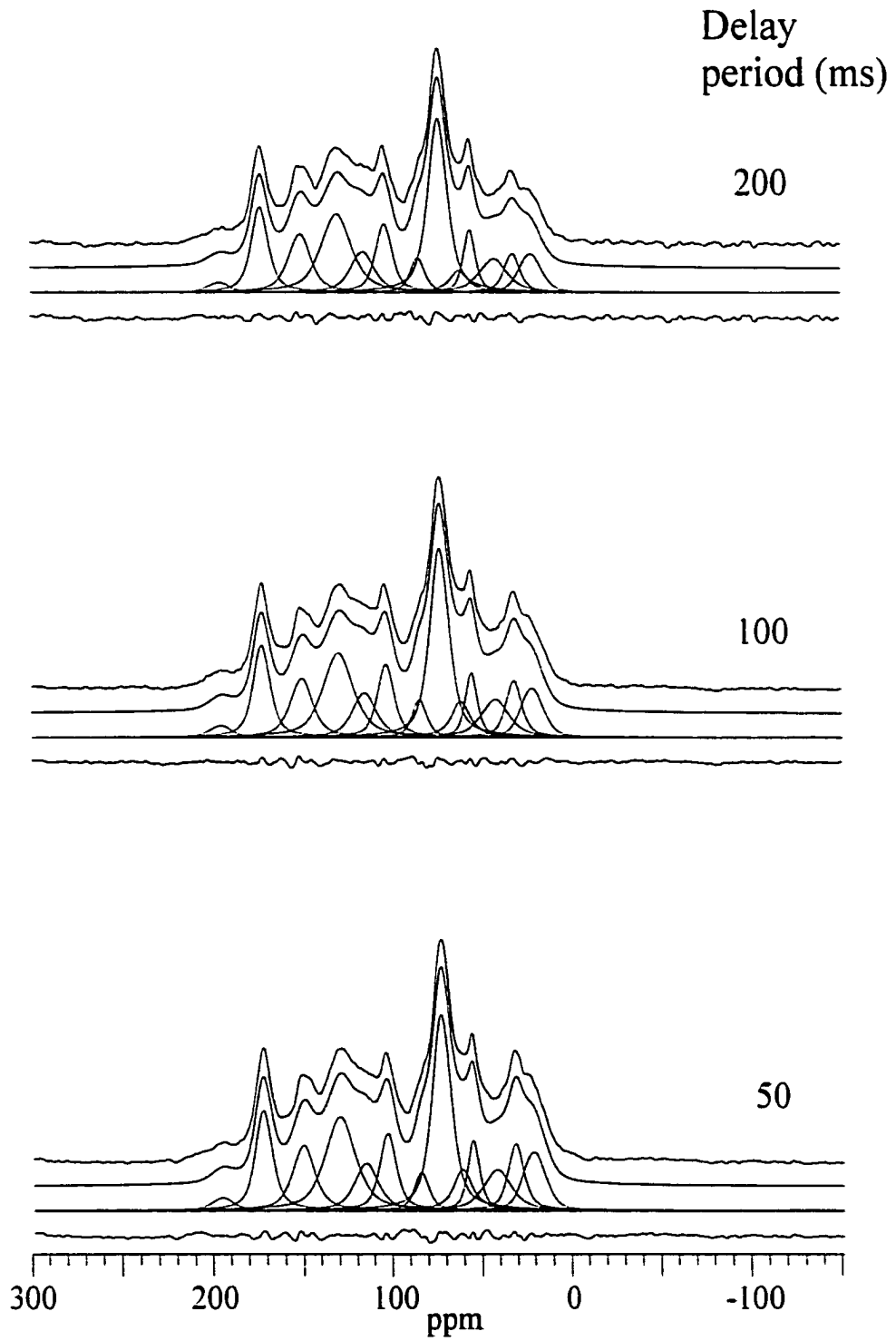

Figure A2-3 (Continued).

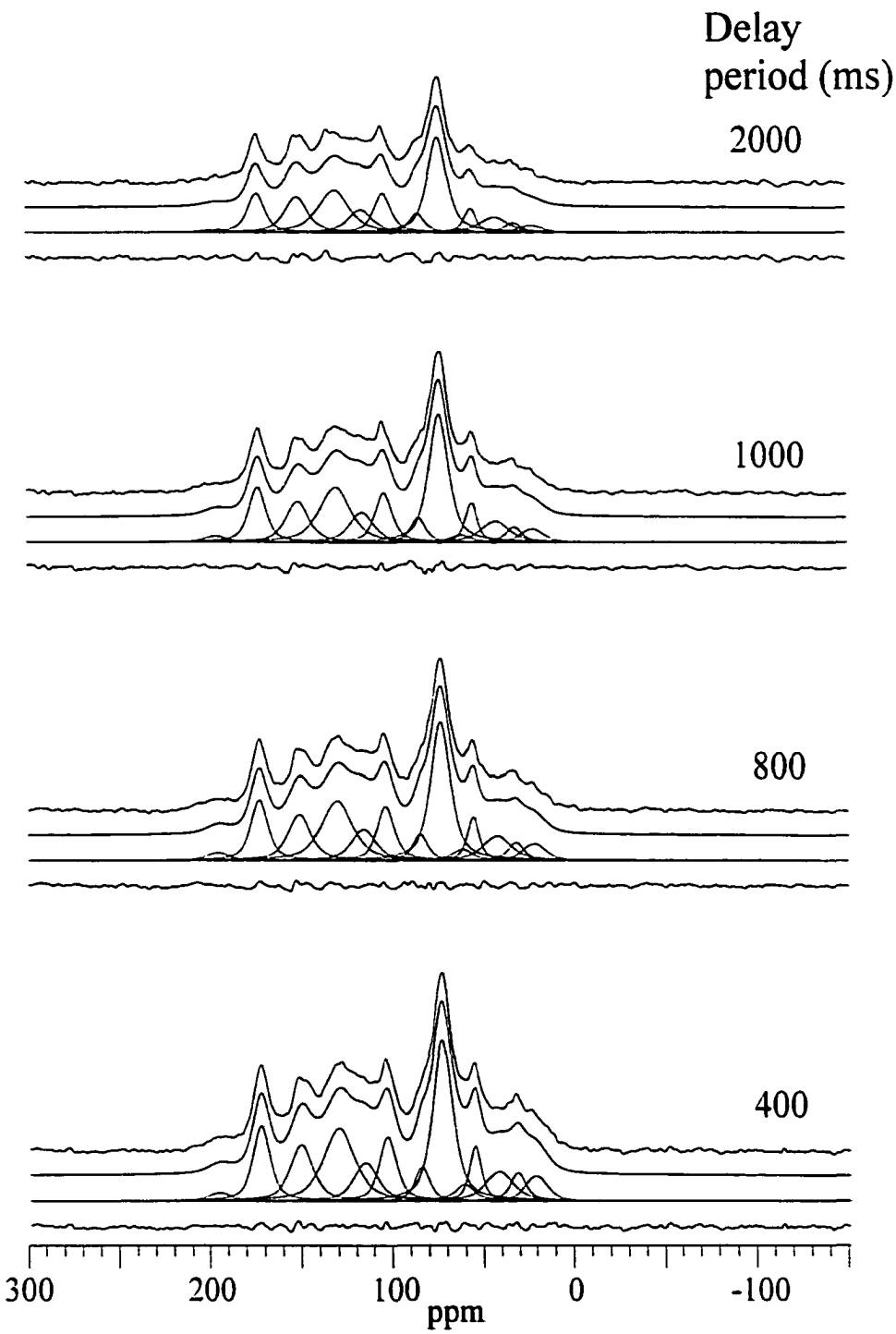

Figure A2-3 (Continued).

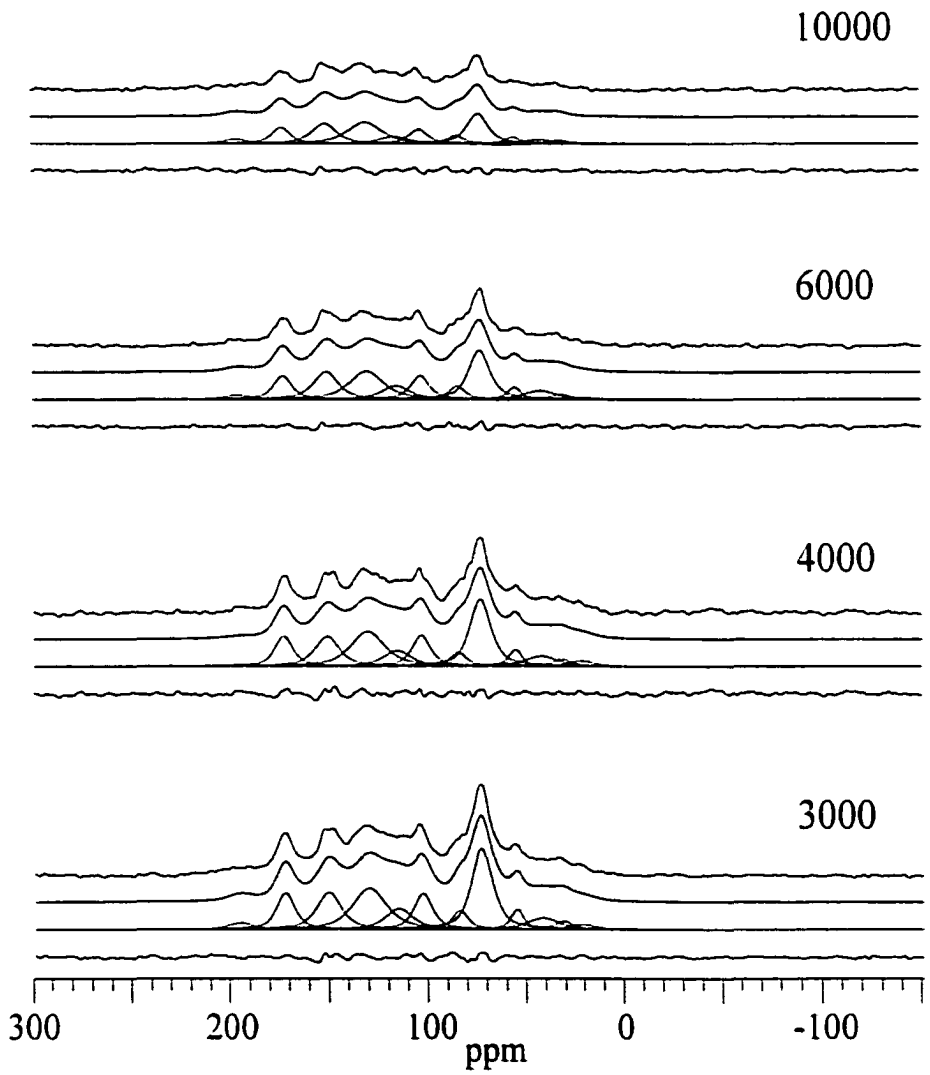

Figure A2-3 (Continued).

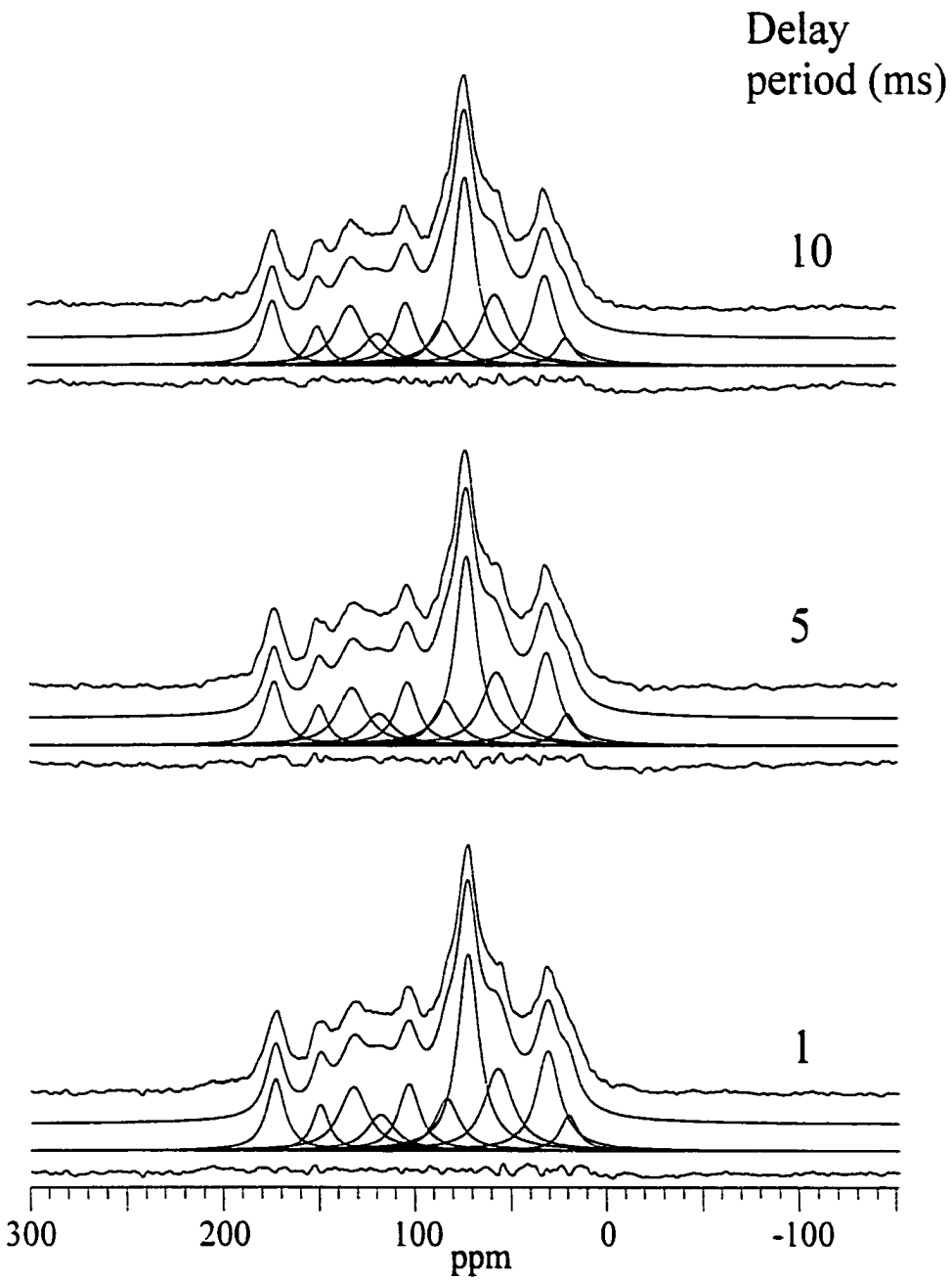

Figure A2-4 Deconvolutions of the ^{13}C T_1 relaxation spectra of the humin fraction data found in Figure 2.4(a). The delay period for each spectrum is written above and to the left of each spectrum. For each delay period, the uppermost spectrum is the experimental spectrum, the next lower trace is the "synthetic" spectrum, the next lower are the individual deconvoluted peaks, and the lowermost spectrum is the "difference spectrum". The synthetic spectrum was generated by adding the peak areas of the deconvoluted peaks (third trace from top). The difference spectrum is generated by subtracting the experimental spectrum from the synthetic spectrum and gives an indication of the success of the deconvolution procedure.

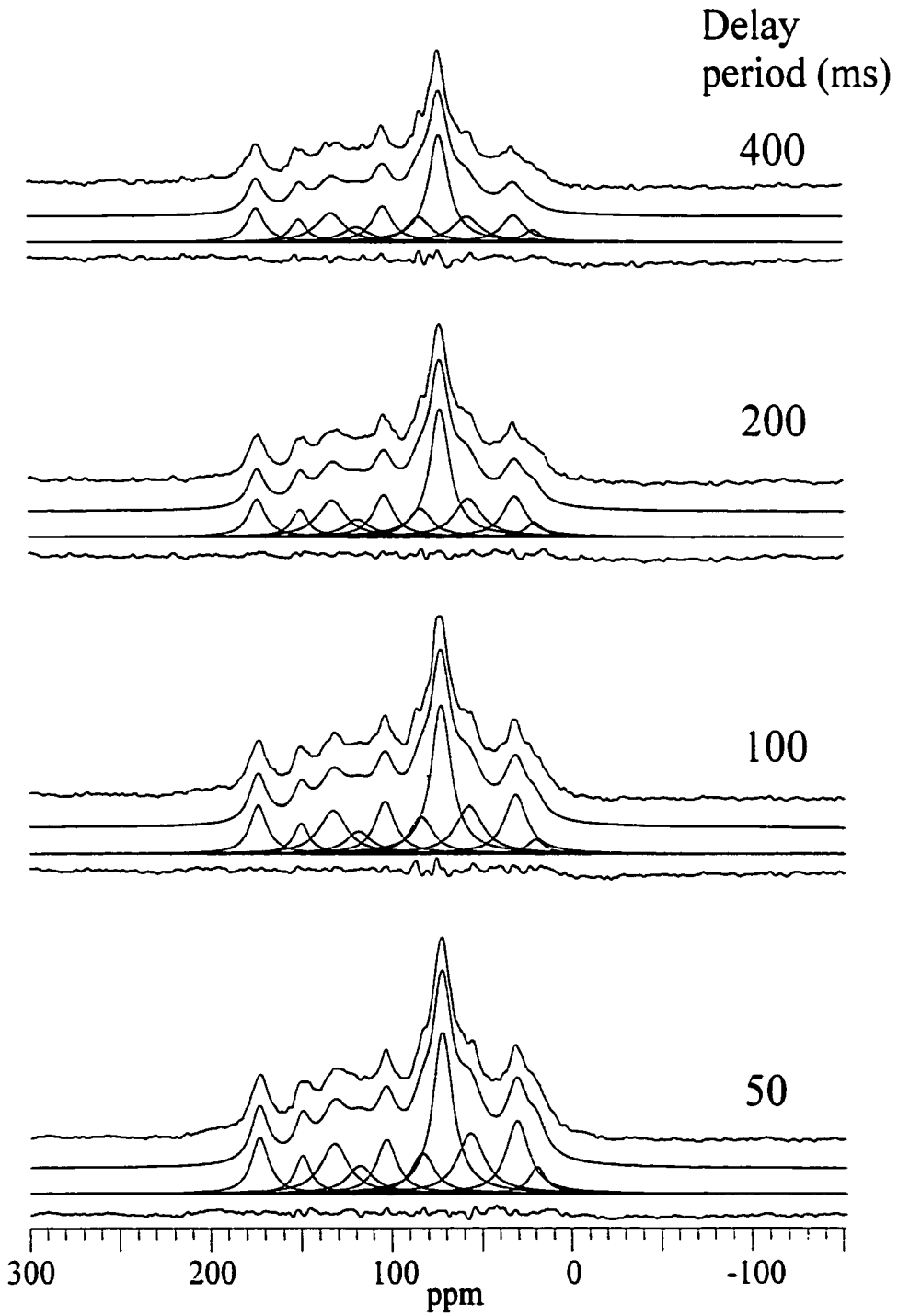

Figure A2-4 (Continued).

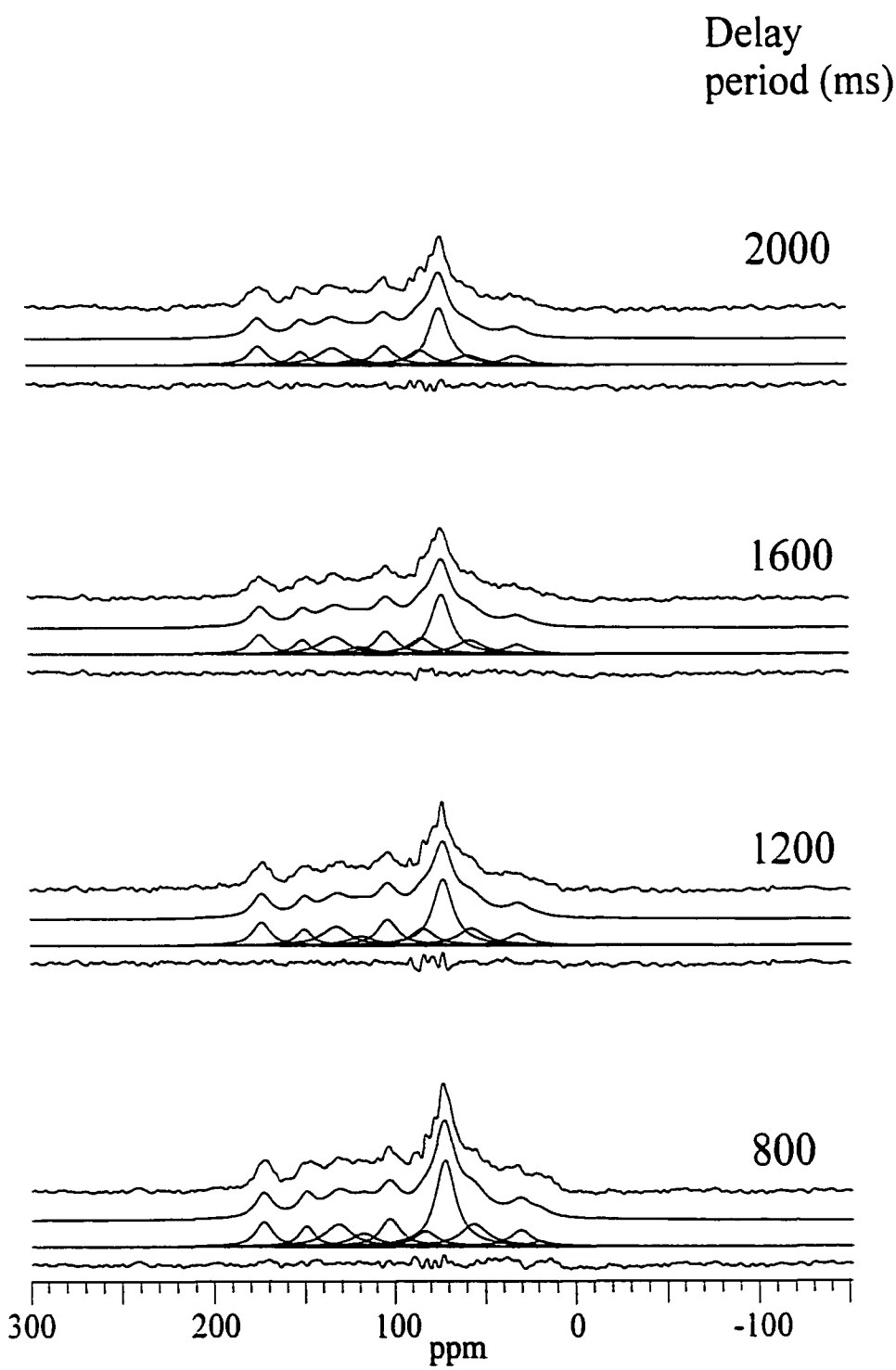

Figure A2-4 (Continued).

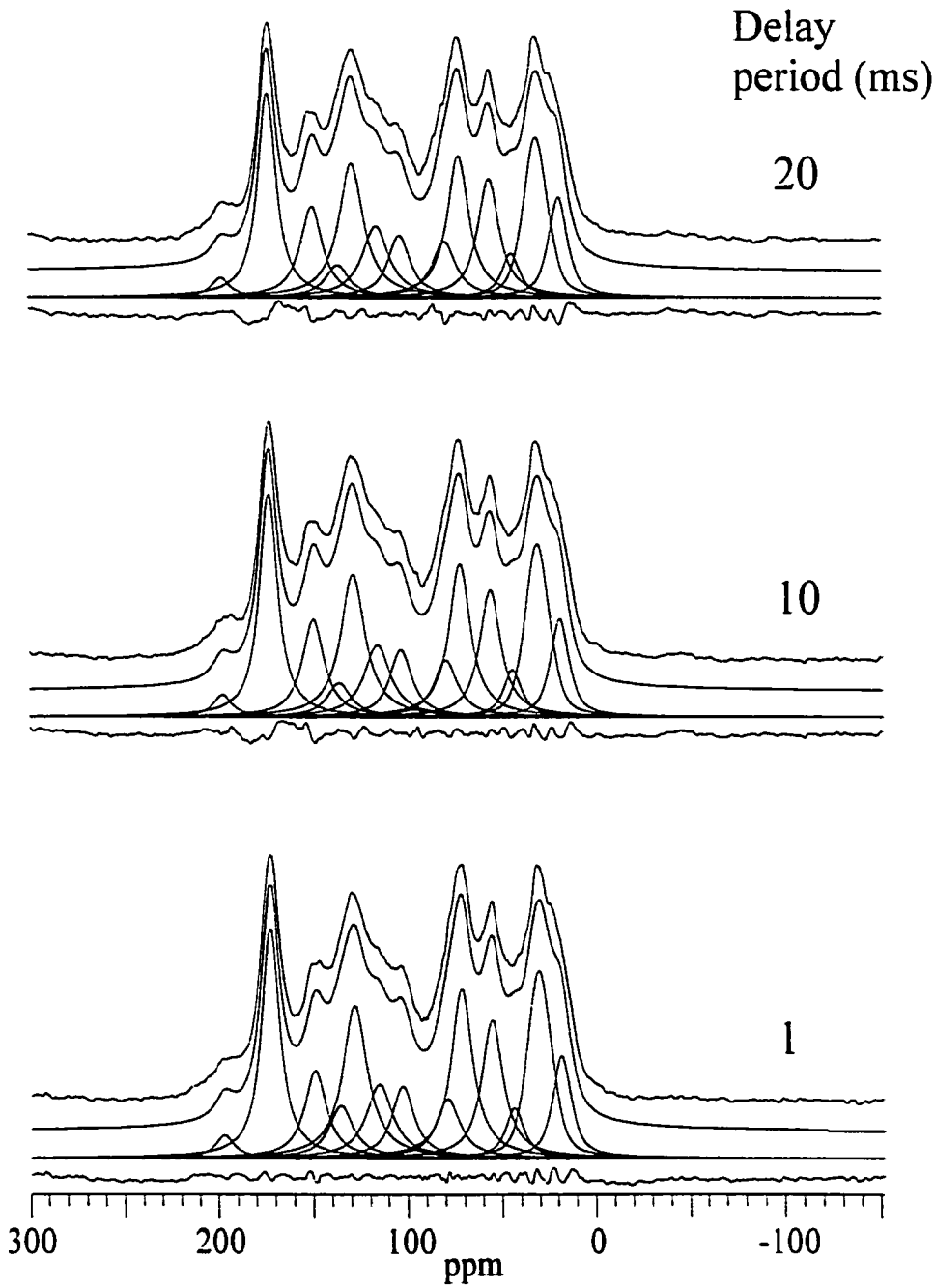

Figure A2-5 Deconvolutions of the ^{13}C T_1 relaxation spectra of the humic acid fraction data found in Figure 2.5(a). The delay period for each spectrum is written above and to the left of each spectrum. For each delay period, the uppermost spectrum is the experimental spectrum, the next lower trace is the "synthetic" spectrum, the next lower are the individual deconvoluted peaks, and the lowermost spectrum is the "difference spectrum". The synthetic spectrum was generated by adding the peak areas of the deconvoluted peaks (third trace from top). The difference spectrum is generated by subtracting the experimental spectrum from the synthetic spectrum and gives an indication of the success of the deconvolution procedure.

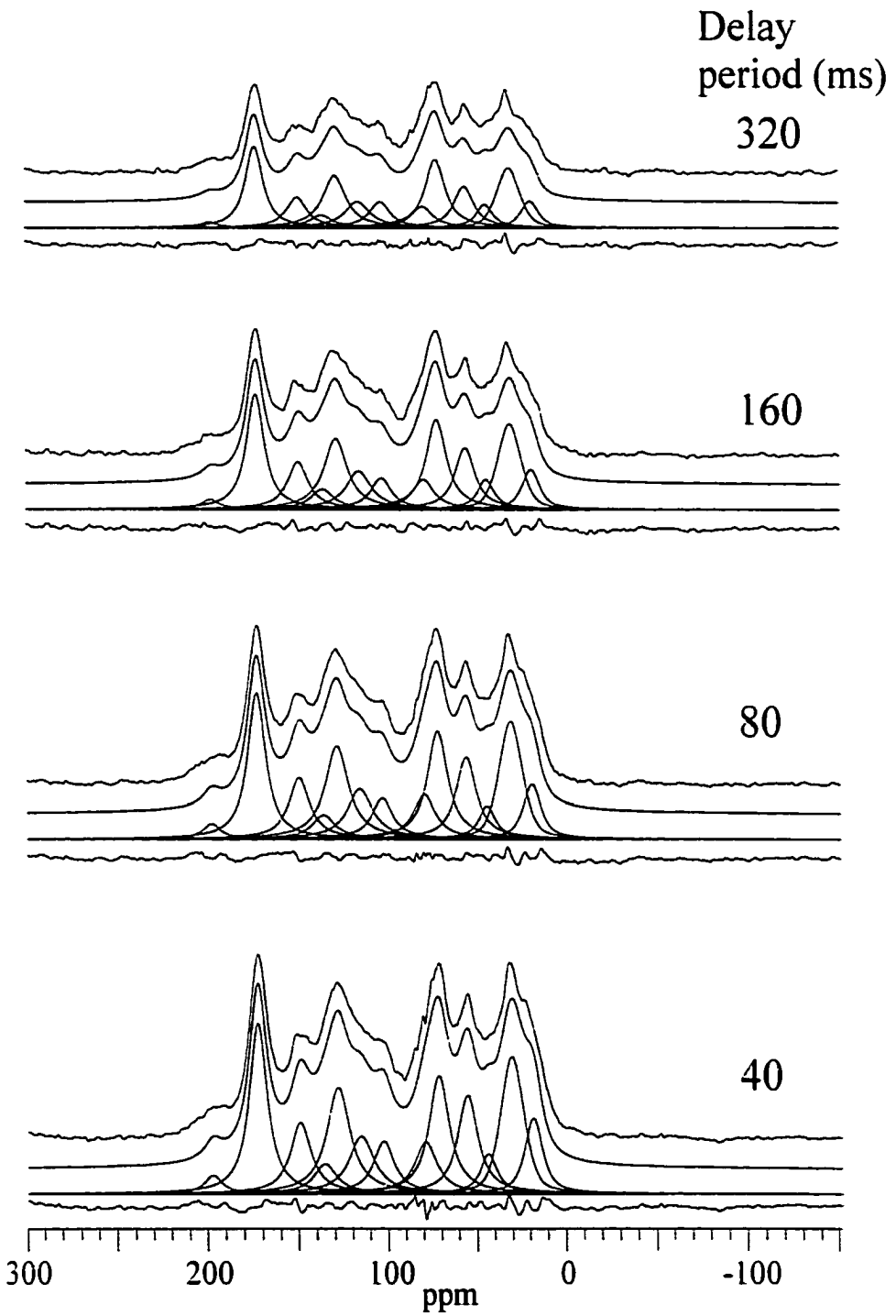

Figure A2-5 (Continued).

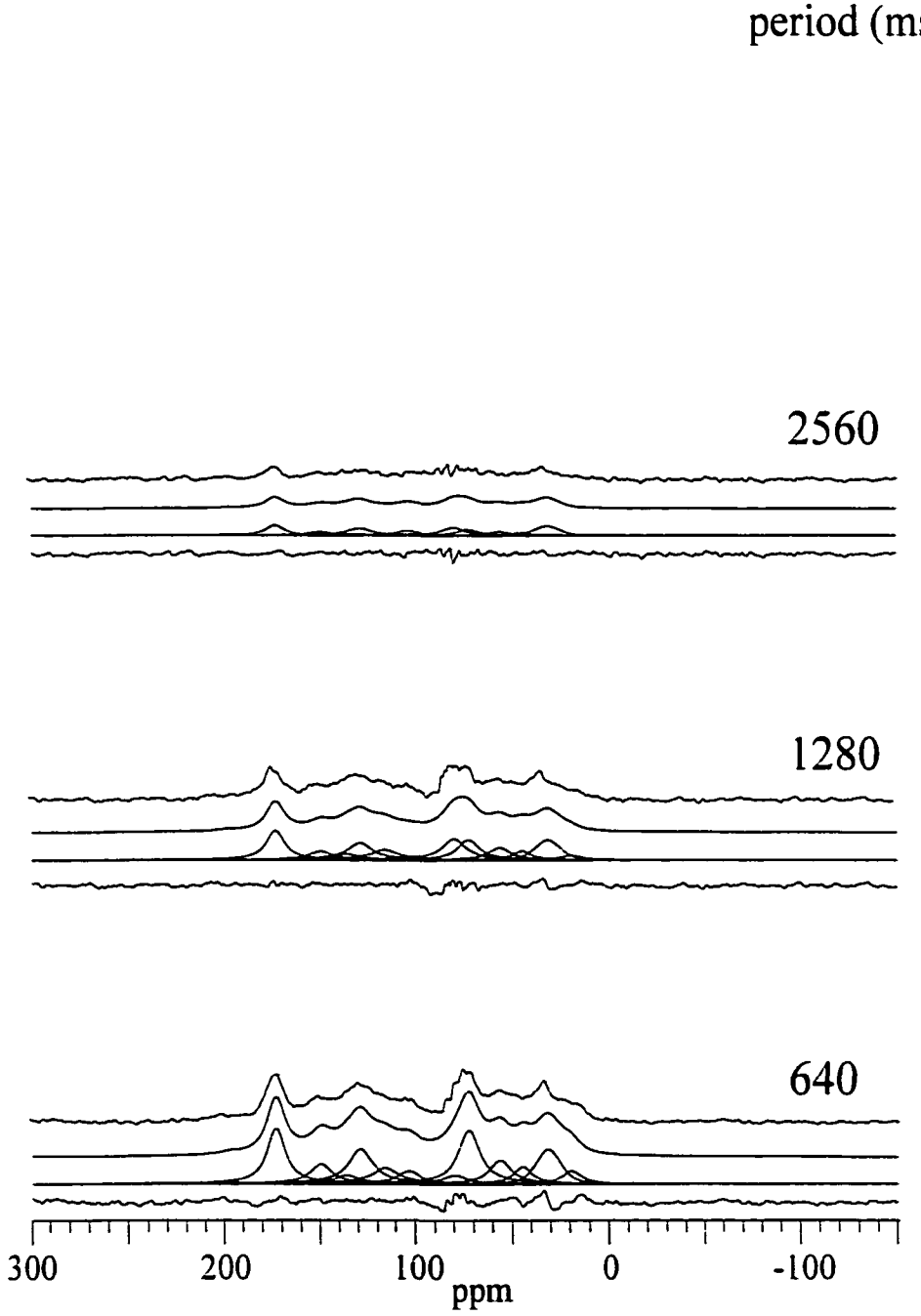

Figure A2-5 (Continued).

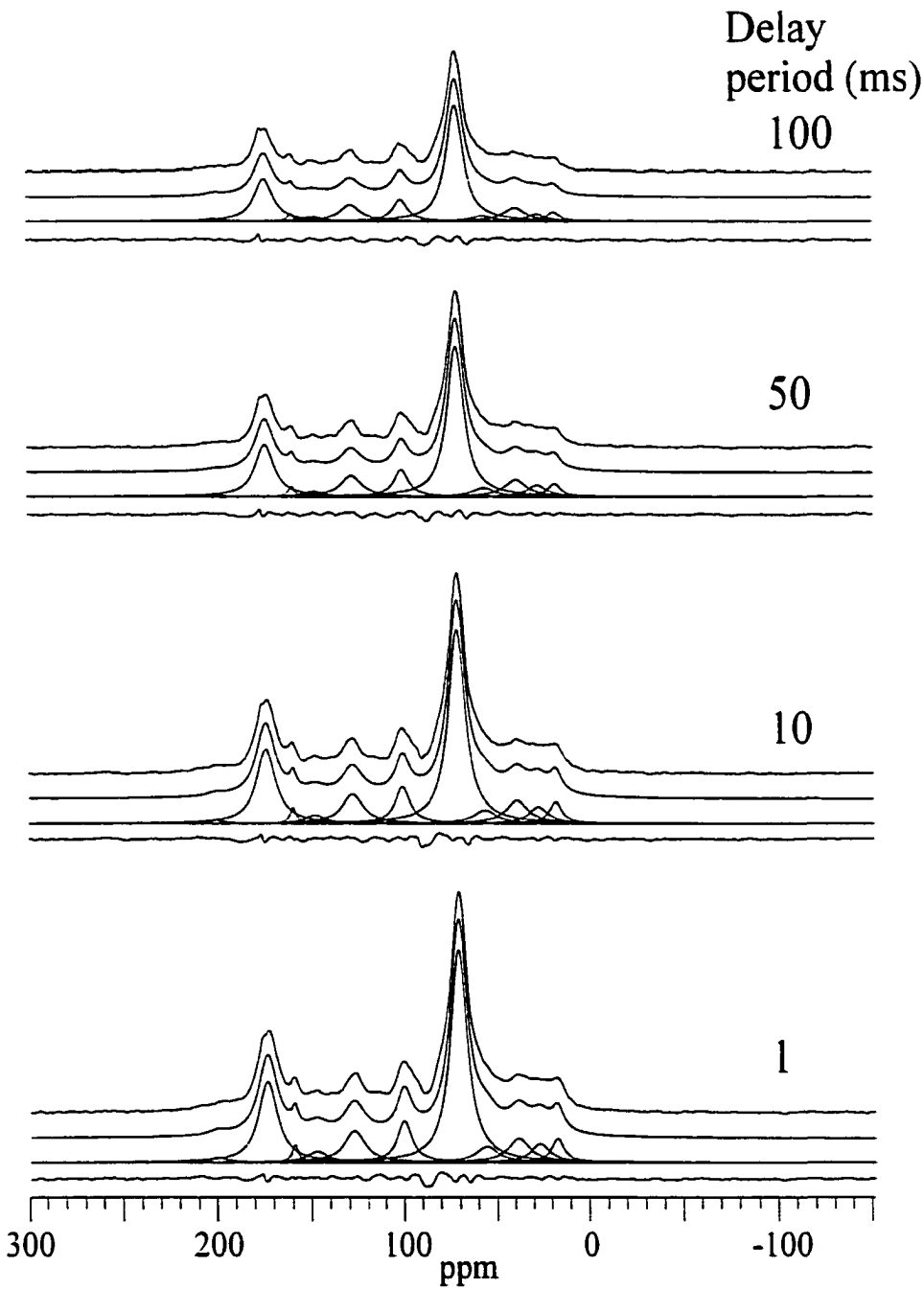

Figure A2-6 Deconvolutions of the ^{13}C T_1 relaxation spectra of the fulvic acid fraction data found in Figure 2.6(a). The delay period for each spectrum is written above and to the left of each spectrum. For each delay period, the uppermost spectrum is the experimental spectrum, the next lower trace is the "synthetic" spectrum, the next lower are the individual deconvoluted peaks, and the lowermost spectrum is the "difference spectrum". The synthetic spectrum was generated by adding the peak areas of the deconvoluted peaks (third trace from top). The difference spectrum is generated by subtracting the experimental spectrum from the synthetic spectrum and gives an indication of the success of the deconvolution procedure.

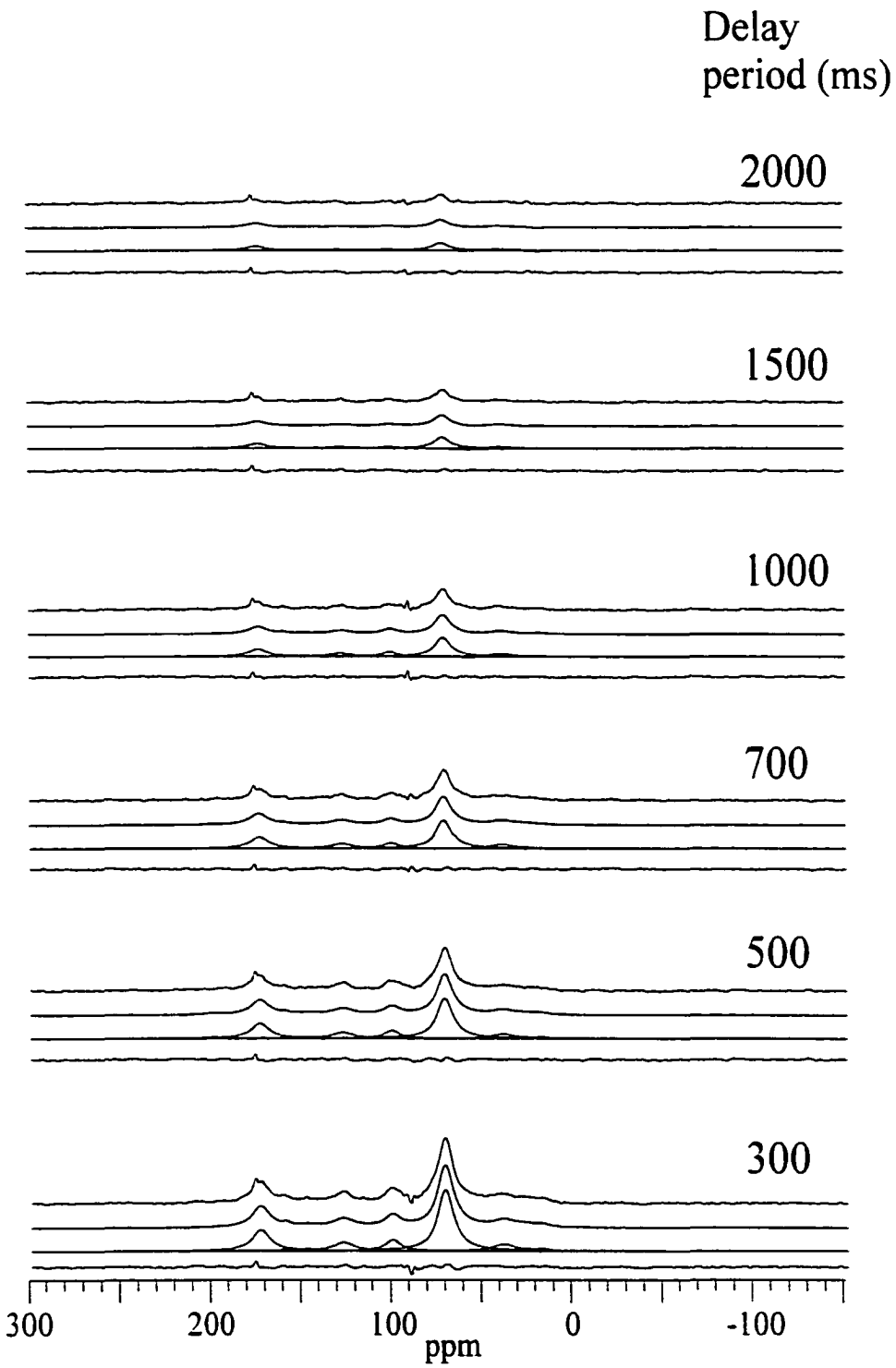

Figure A2-6 (Continued).

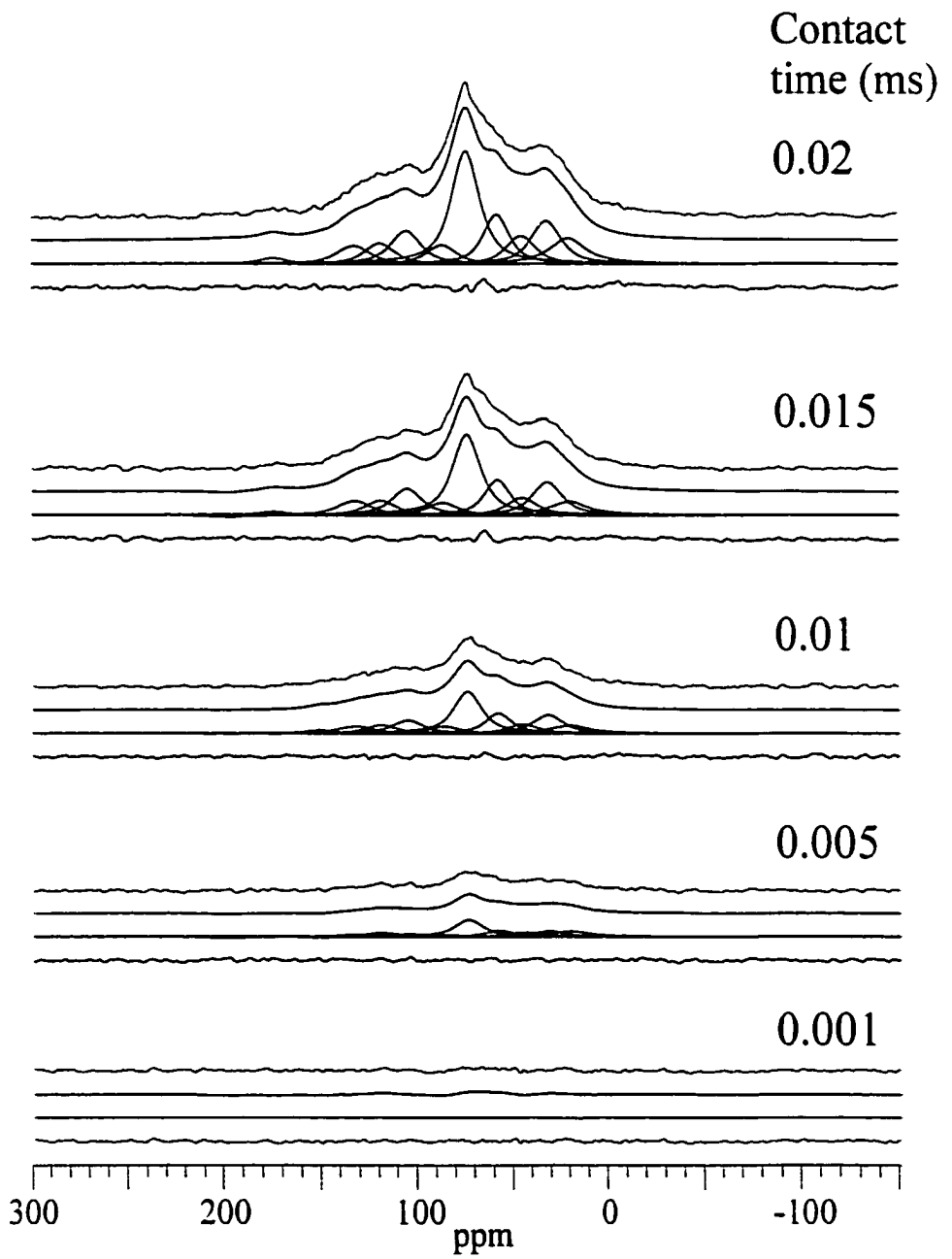

Figure A3-6 Deconvolutions of the variable contact time spectra of the Uncompahgre whole soil data found in Figure 3.6(a). The contact time for each spectrum is written above and to the left of each spectrum. For each contact time, the uppermost spectrum is the experimental spectrum, the next lower trace is the "synthetic" spectrum, the next lower are the individual deconvoluted peaks, and the lowermost spectrum is the "difference spectrum". The synthetic spectrum was generated by adding the peak areas of the deconvoluted peaks (third trace from top). The difference spectrum is generated by subtracting the experimental spectrum from the synthetic spectrum and gives an indication of the success of the deconvolution procedure.

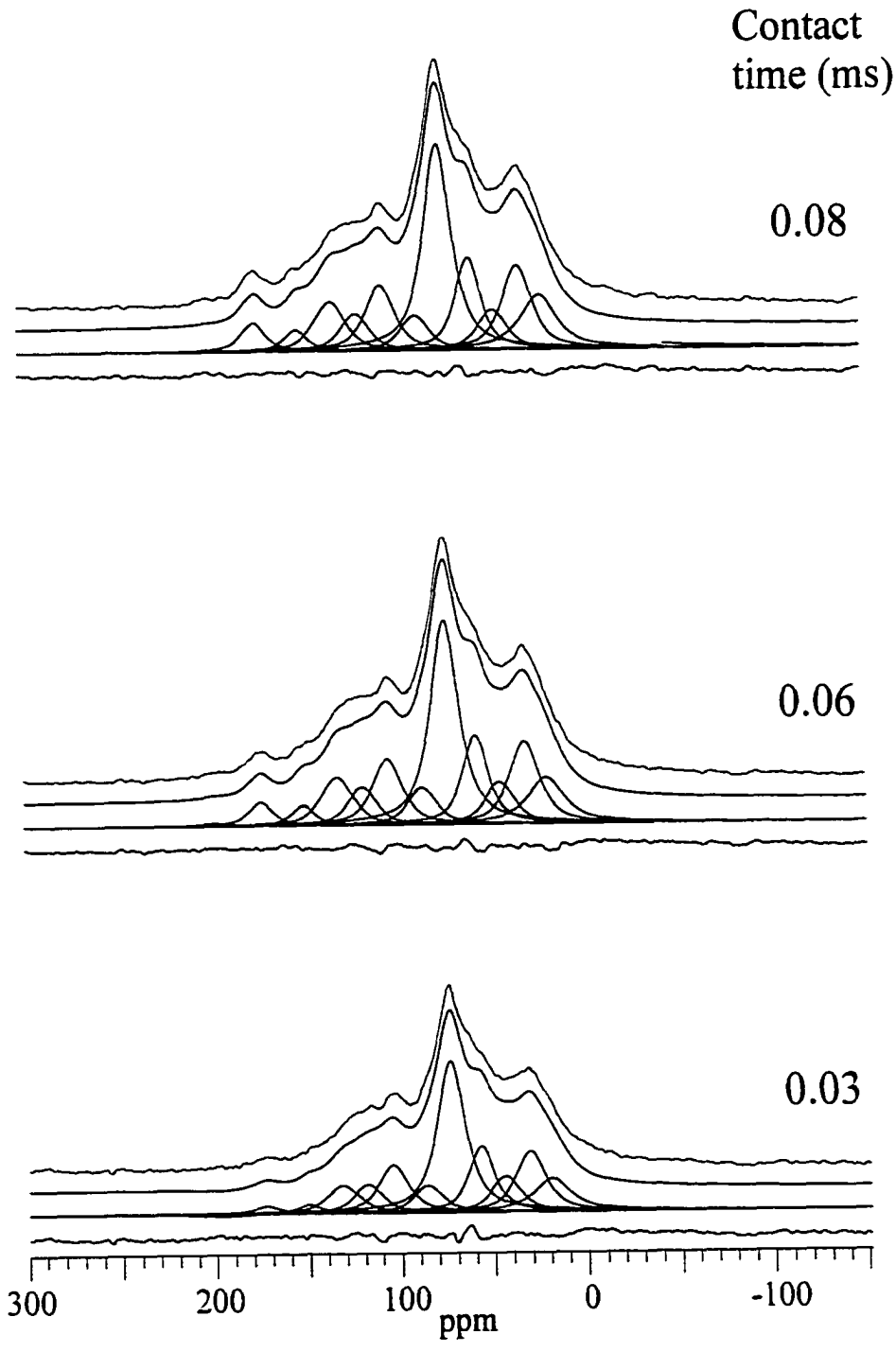

Figure A3-6 (Continued).

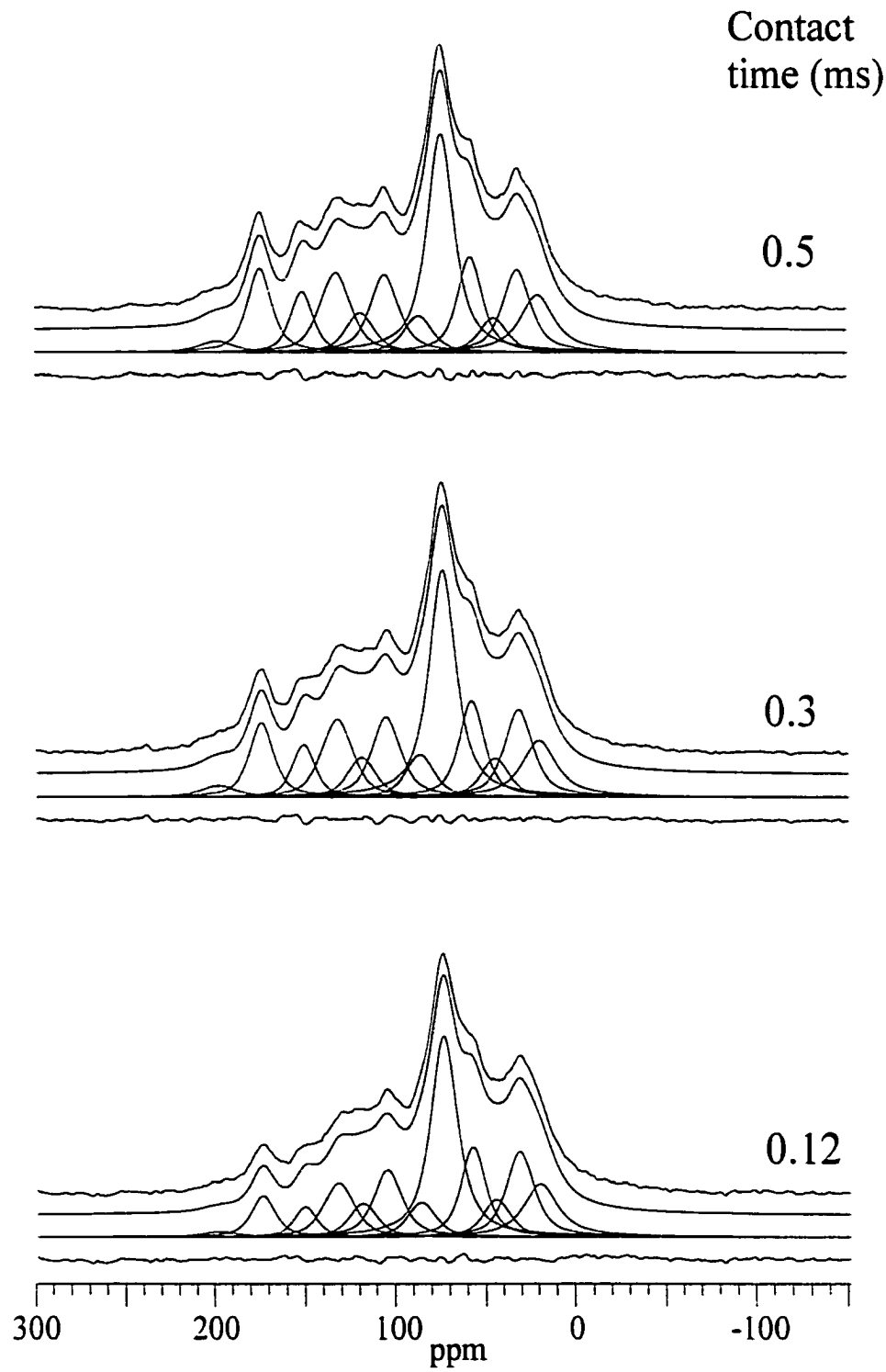

Figure A3-6 (continued).

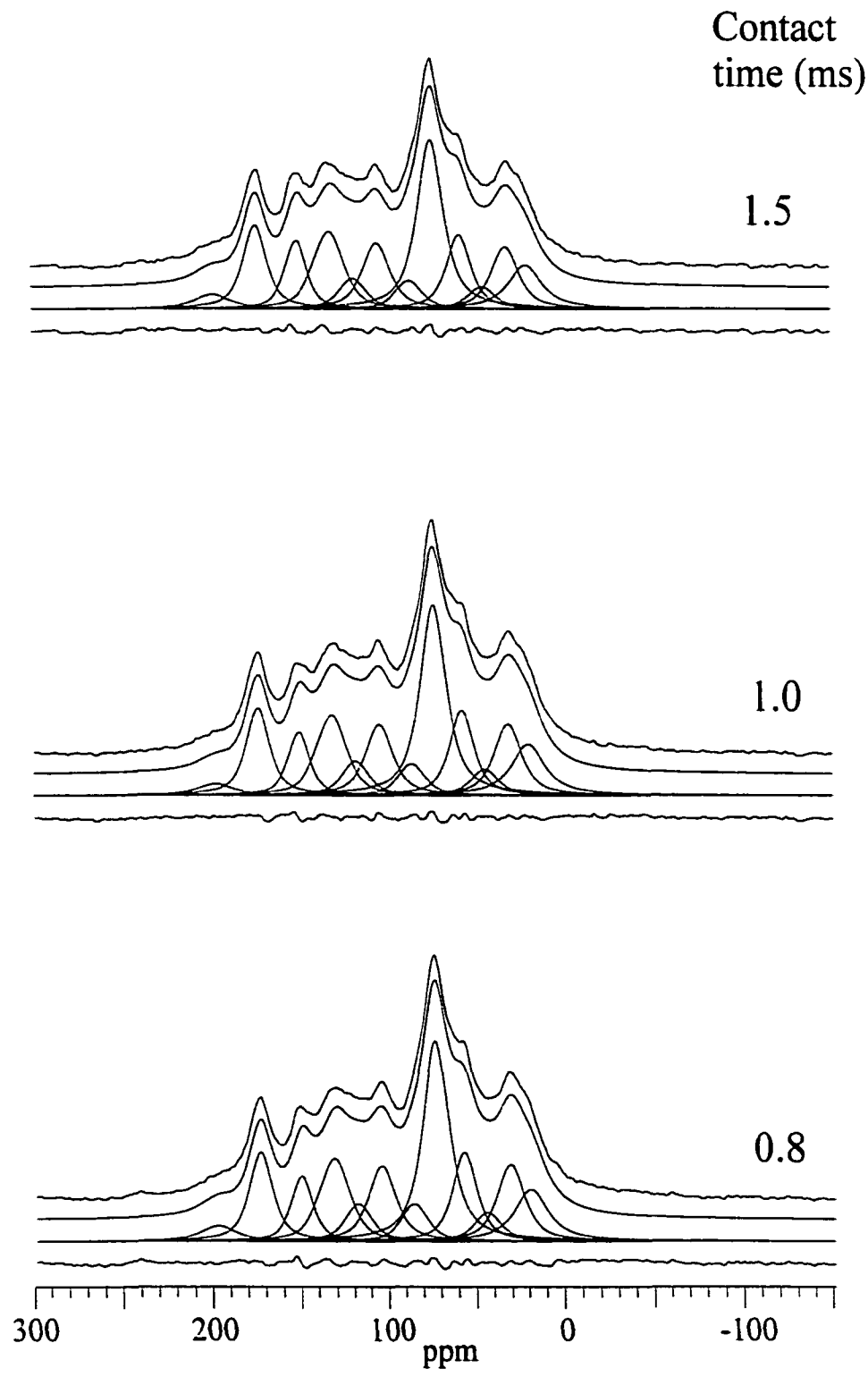

Figure A3-6 (Continued).

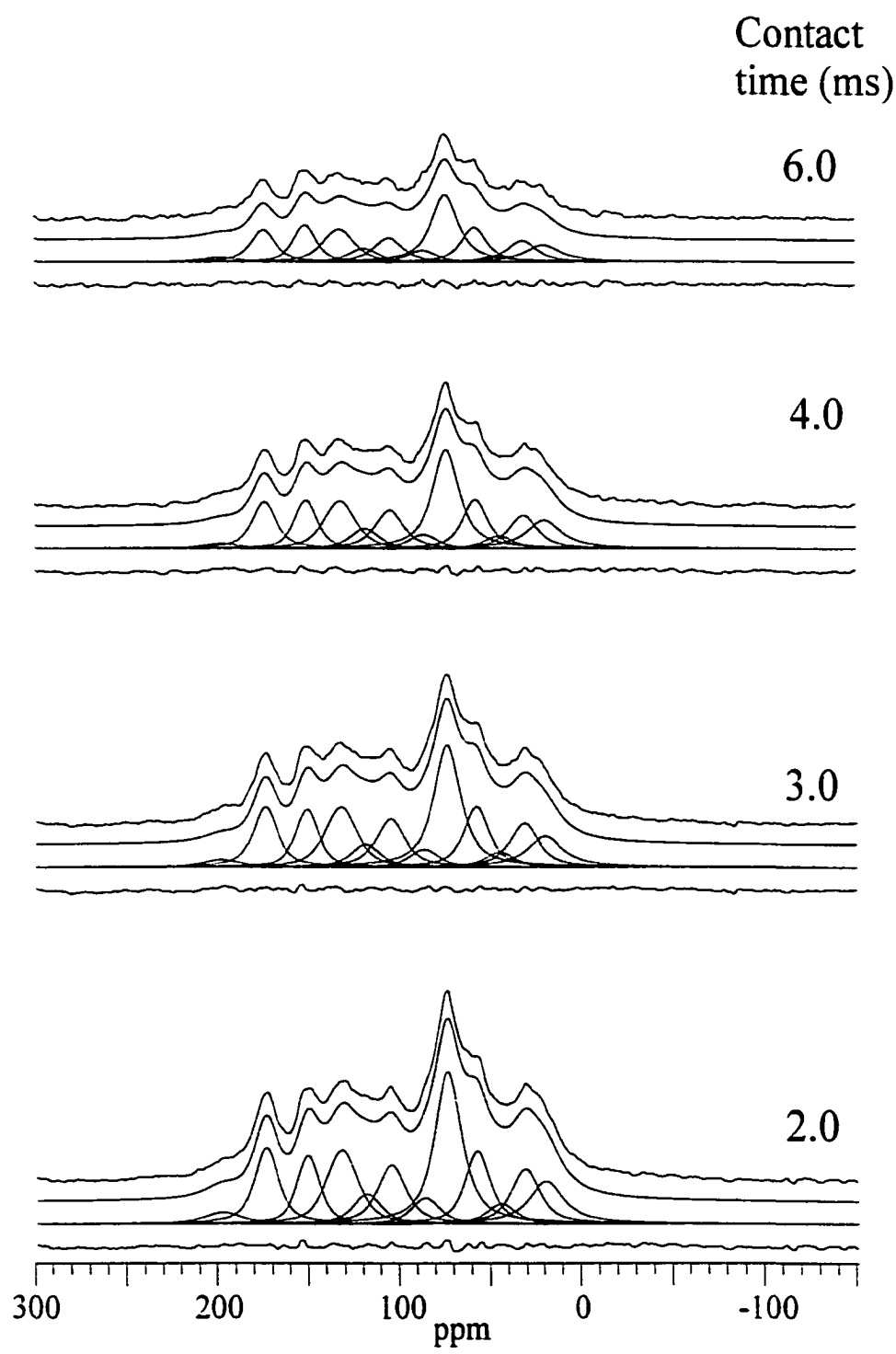

Figure A3-6 (Continued).

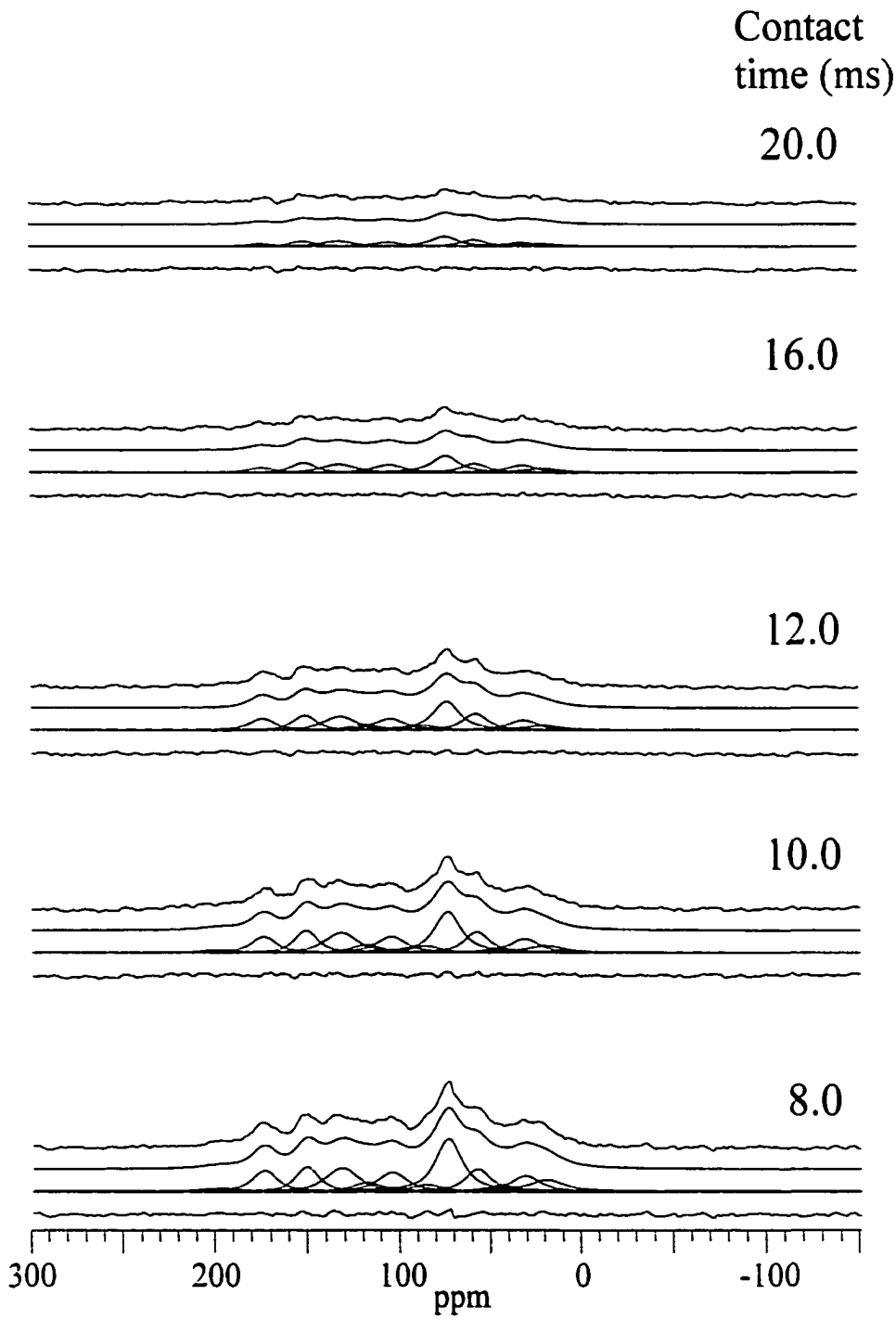

Figure A3-6 (continued).

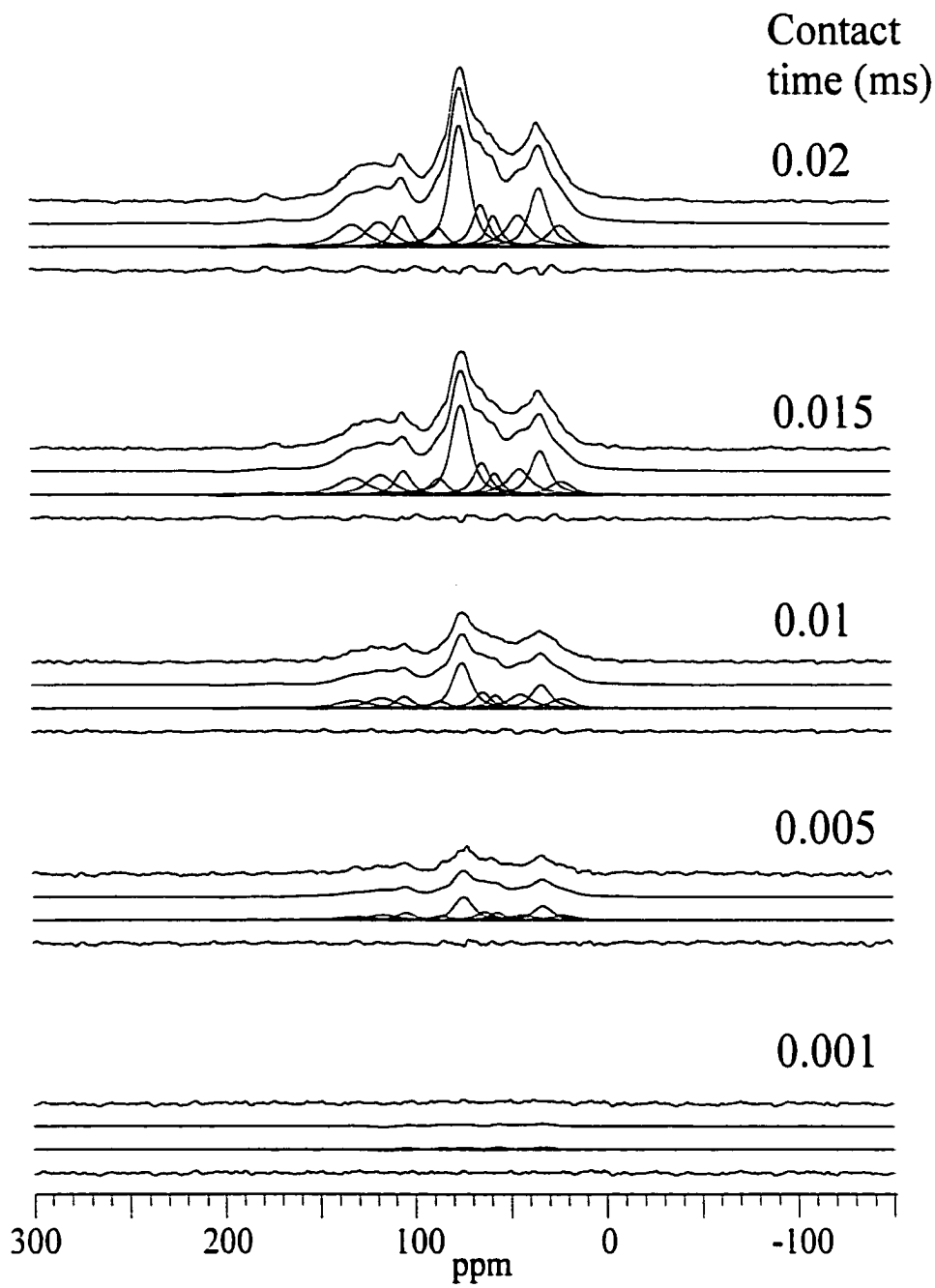

Figure A3-7 Deconvolutions of the variable contact time spectra of the HF-treated Uncompahgre whole soil data found in Figure 3.7(a). The contact time for each spectrum is written above and to the left of each spectrum. For each contact time, the uppermost spectrum is the experimental spectrum, the next lower trace is the "synthetic" spectrum, the next lower are the individual deconvoluted peaks, and the lowermost spectrum is the "difference spectrum". The synthetic spectrum was generated by adding the peak areas of the deconvoluted peaks (third trace from top). The difference spectrum is generated by subtracting the experimental spectrum from the synthetic spectrum and gives an indication of the success of the deconvolution procedure.

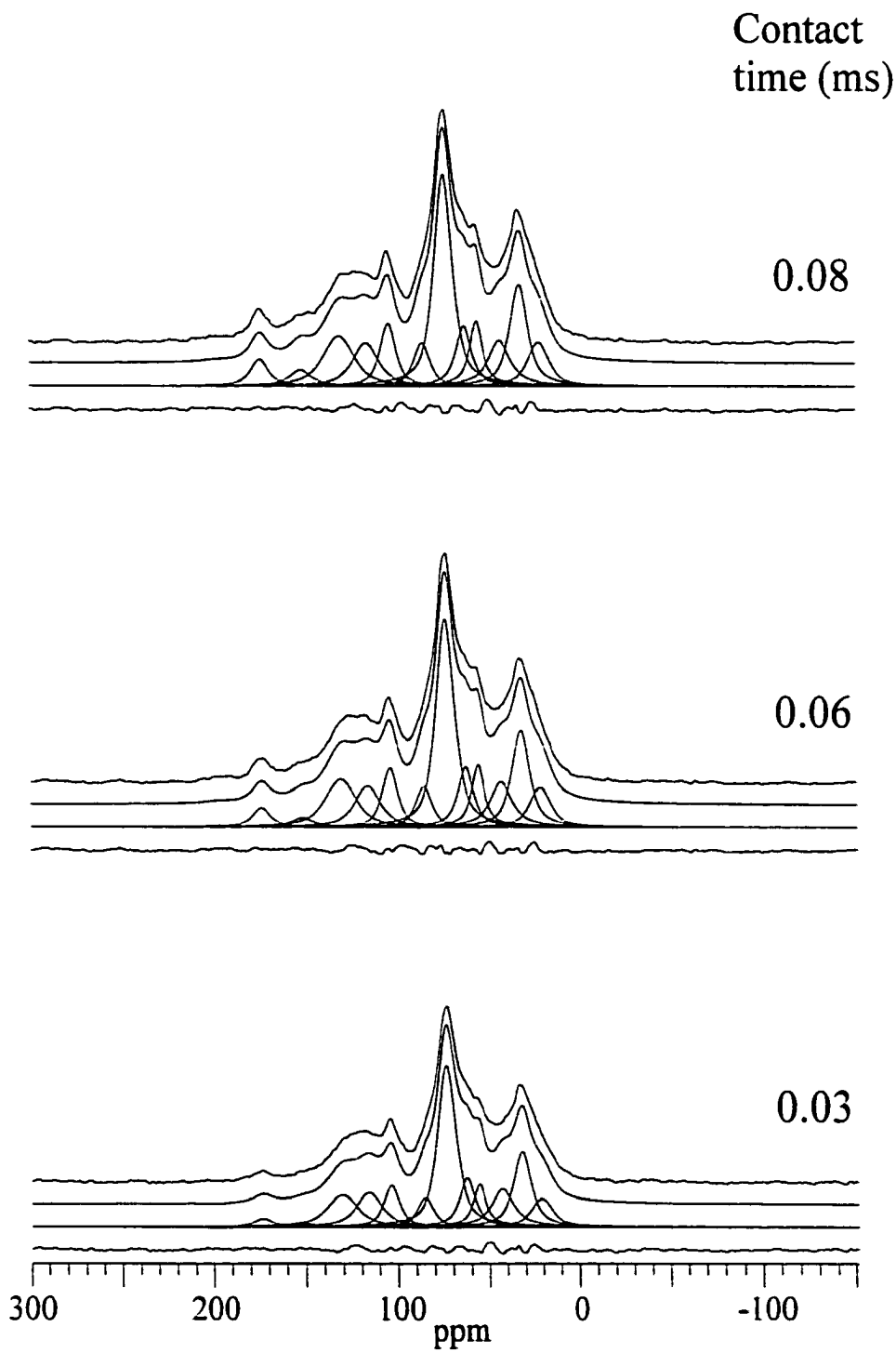

Figure A3-7 (Continued).

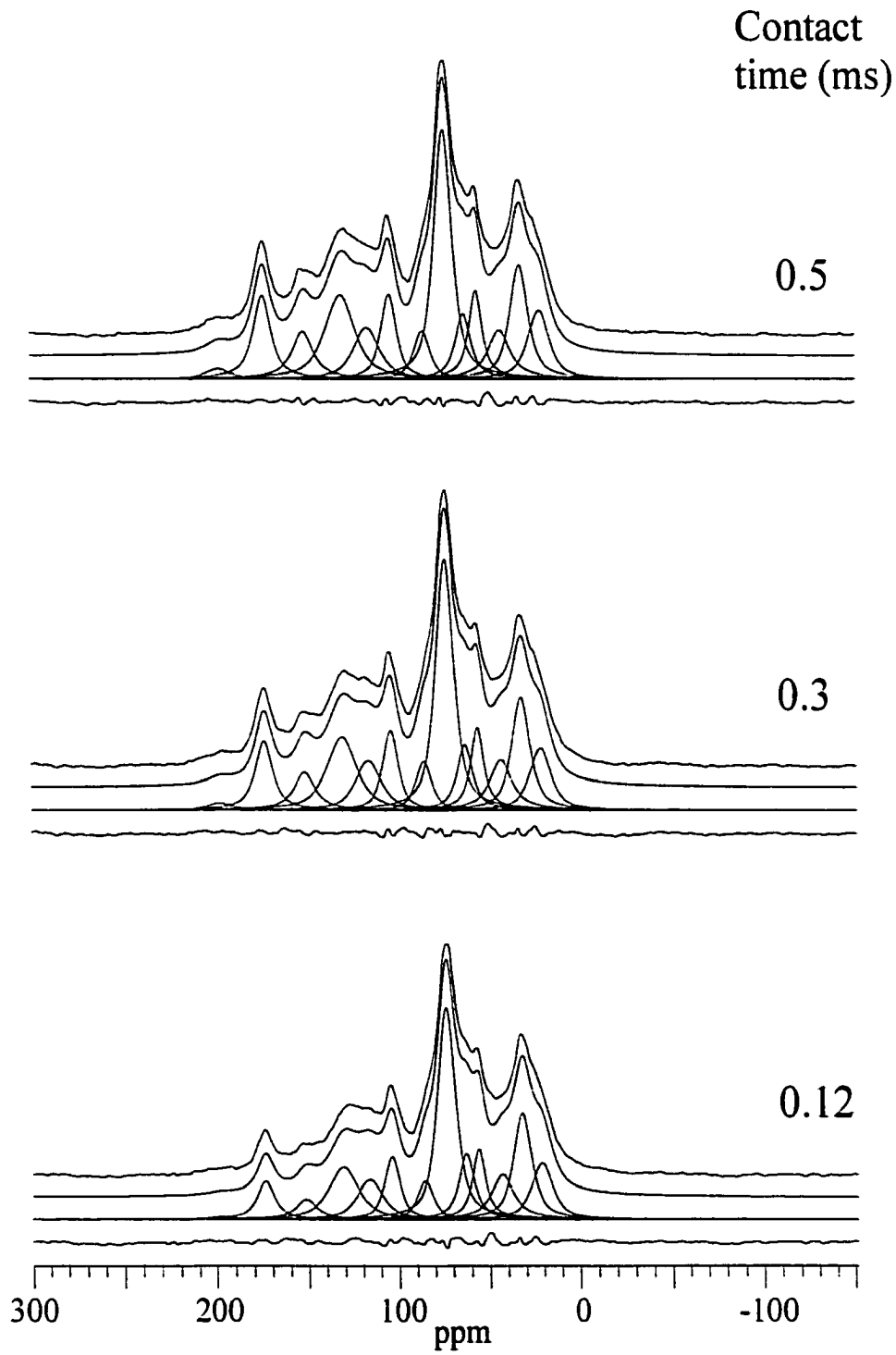

Figure A3-7 (Continued).

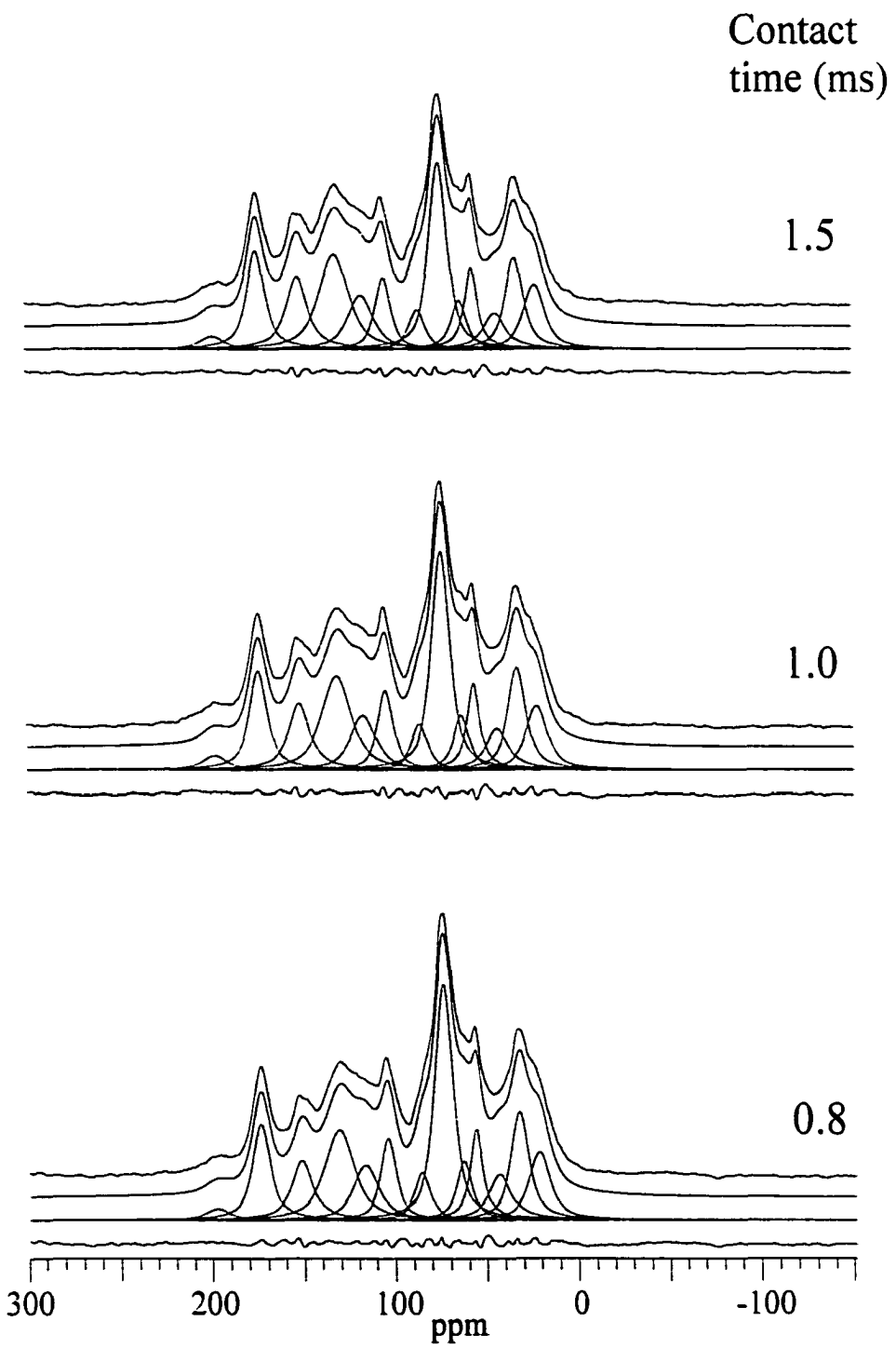

Figure A3-7 (Continued).

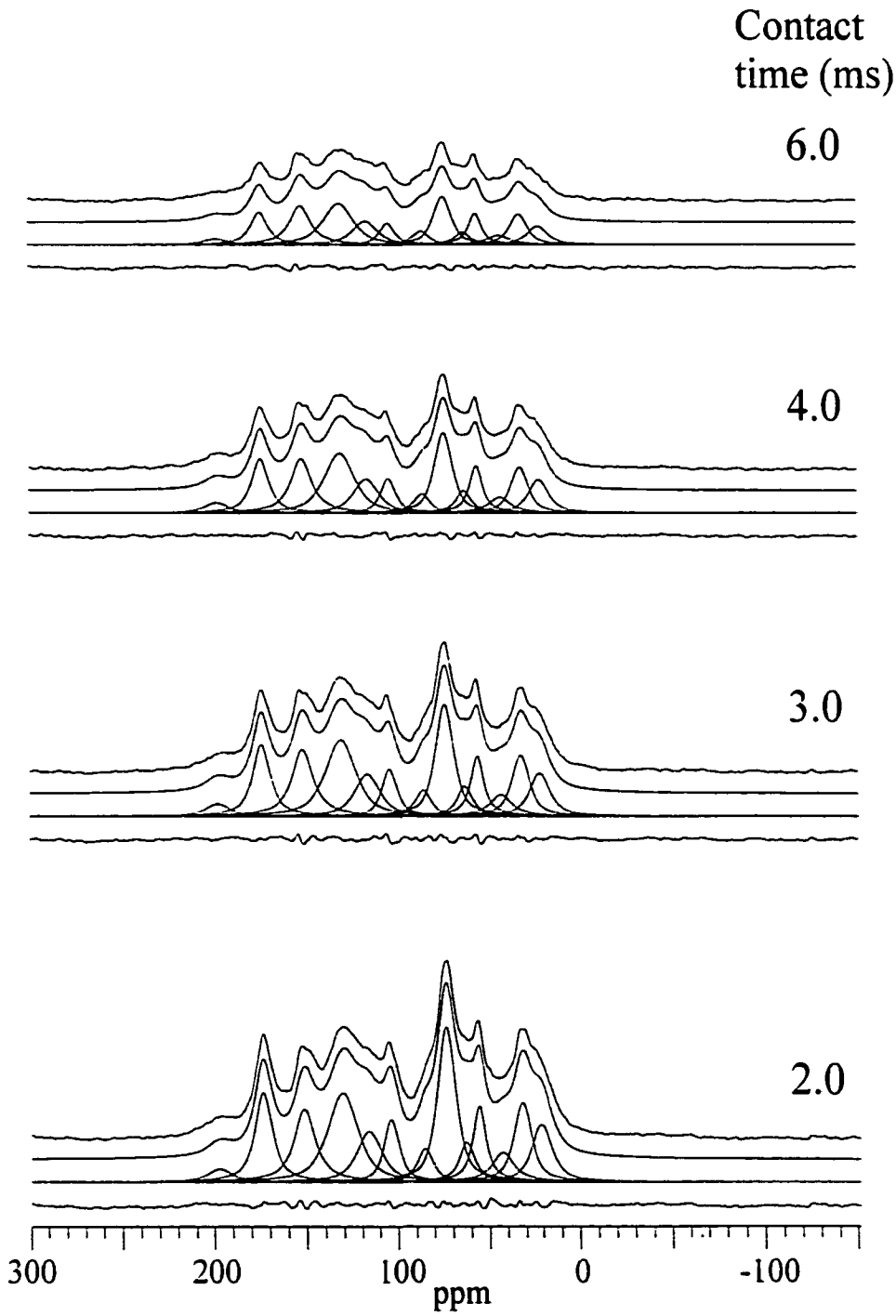

Figure A3-7 (Continued).

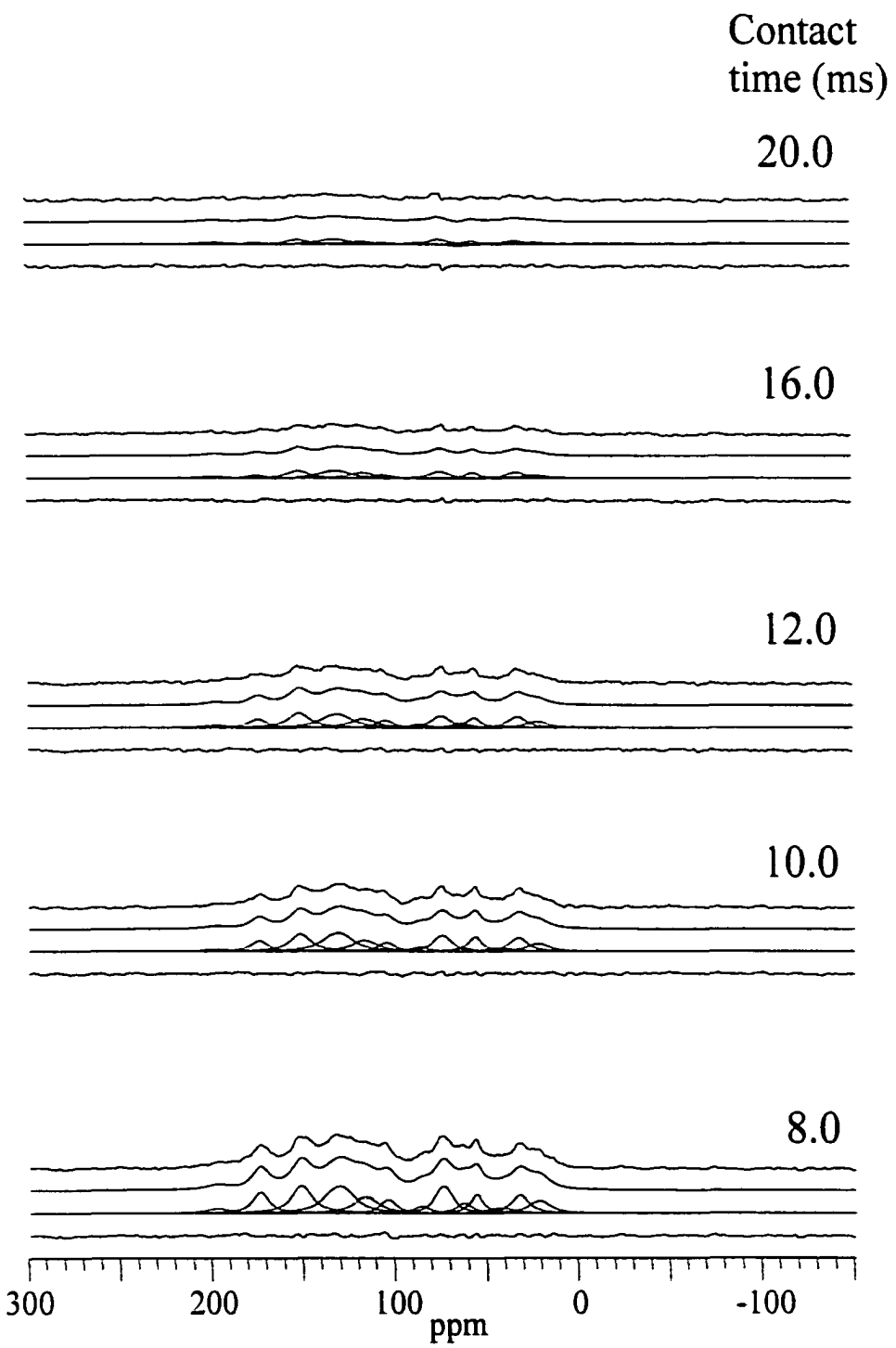

Figure A3-7 (Continued).

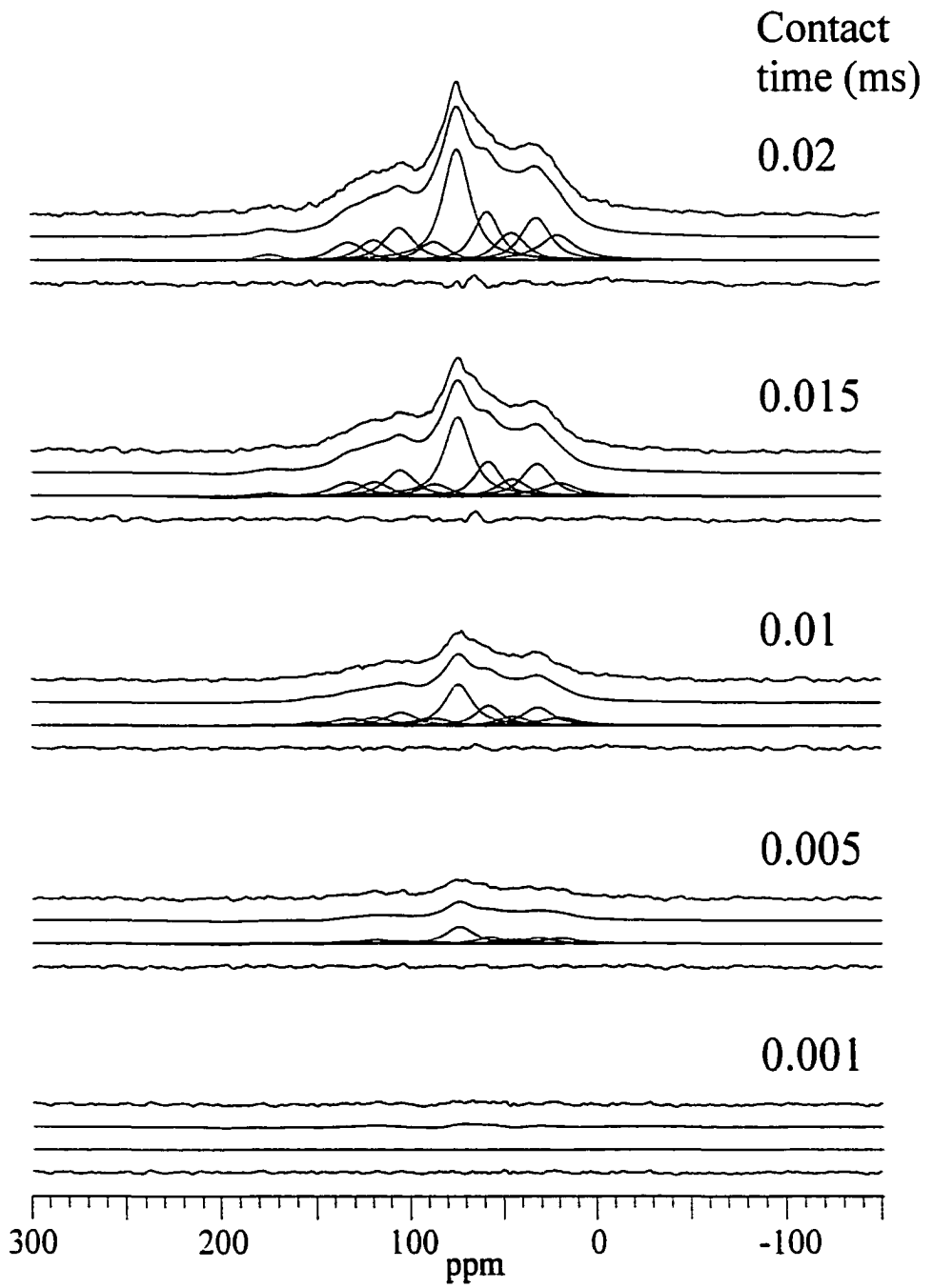

Figure A3-8 Deconvolutions of the variable contact time spectra of the humin fraction data found in Figure 3.8(a). The contact time for each spectrum is written above and to the left of each spectrum. For each contact time, the uppermost spectrum is the experimental spectrum, the next lower trace is the "synthetic" spectrum, the next lower are the individual deconvoluted peaks, and the lowermost spectrum is the "difference spectrum". The synthetic spectrum was generated by adding the peak areas of the deconvoluted peaks (third trace from top). The difference spectrum is generated by subtracting the experimental spectrum from the synthetic spectrum and gives an indication of the success of the deconvolution procedure.

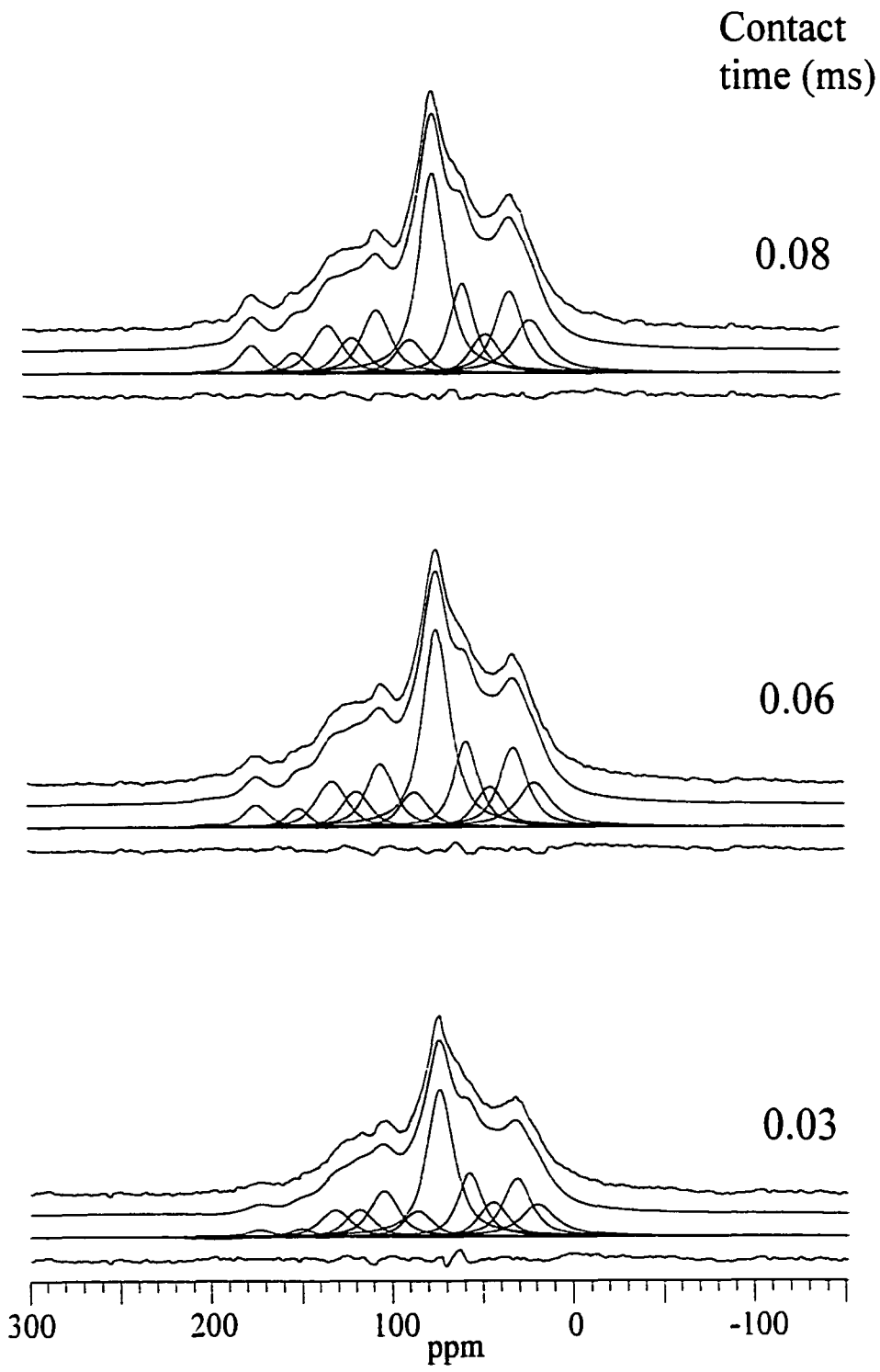

Figure A3-8 (Continued).

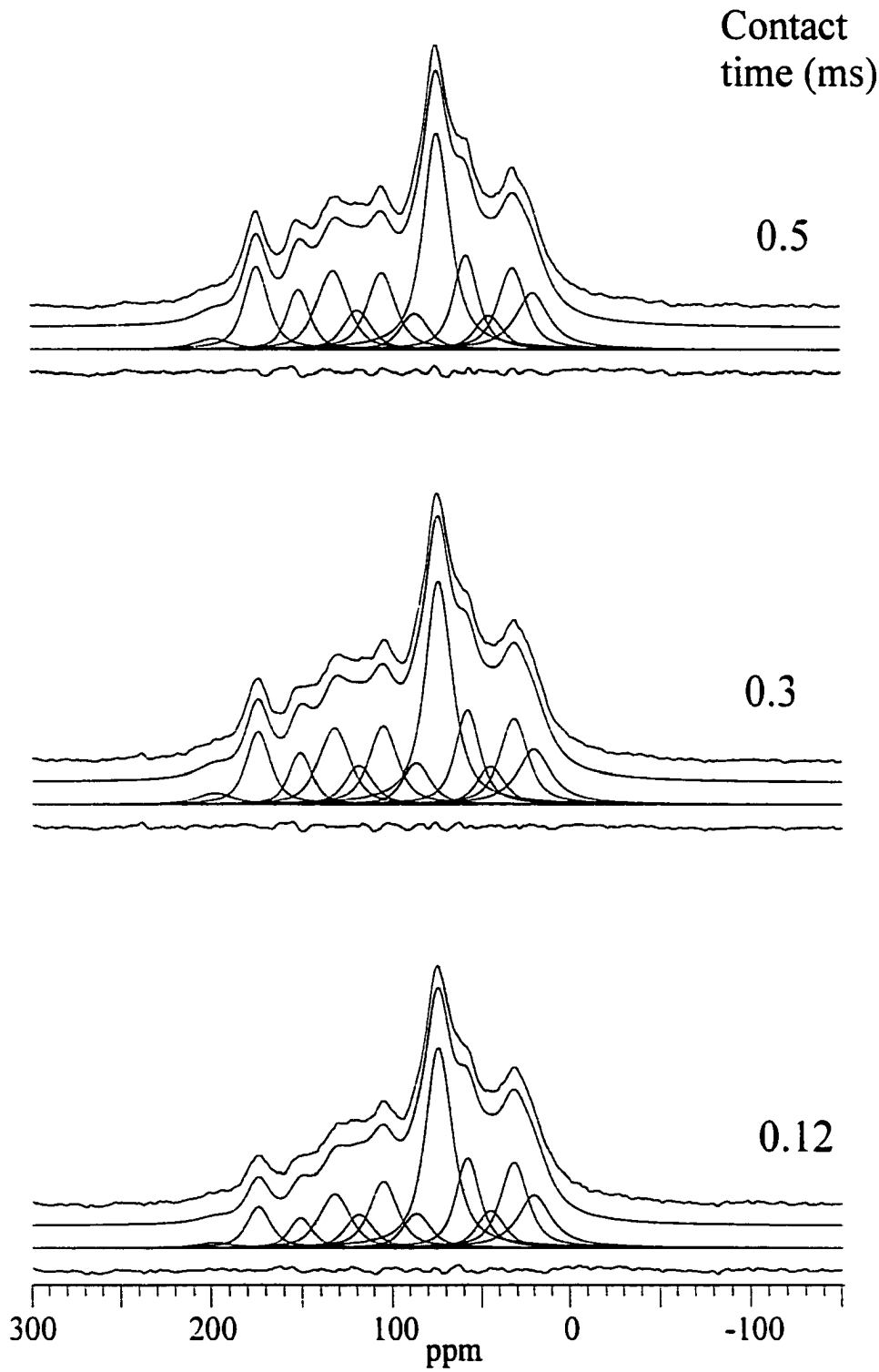

Figure A3-8 (Continued).

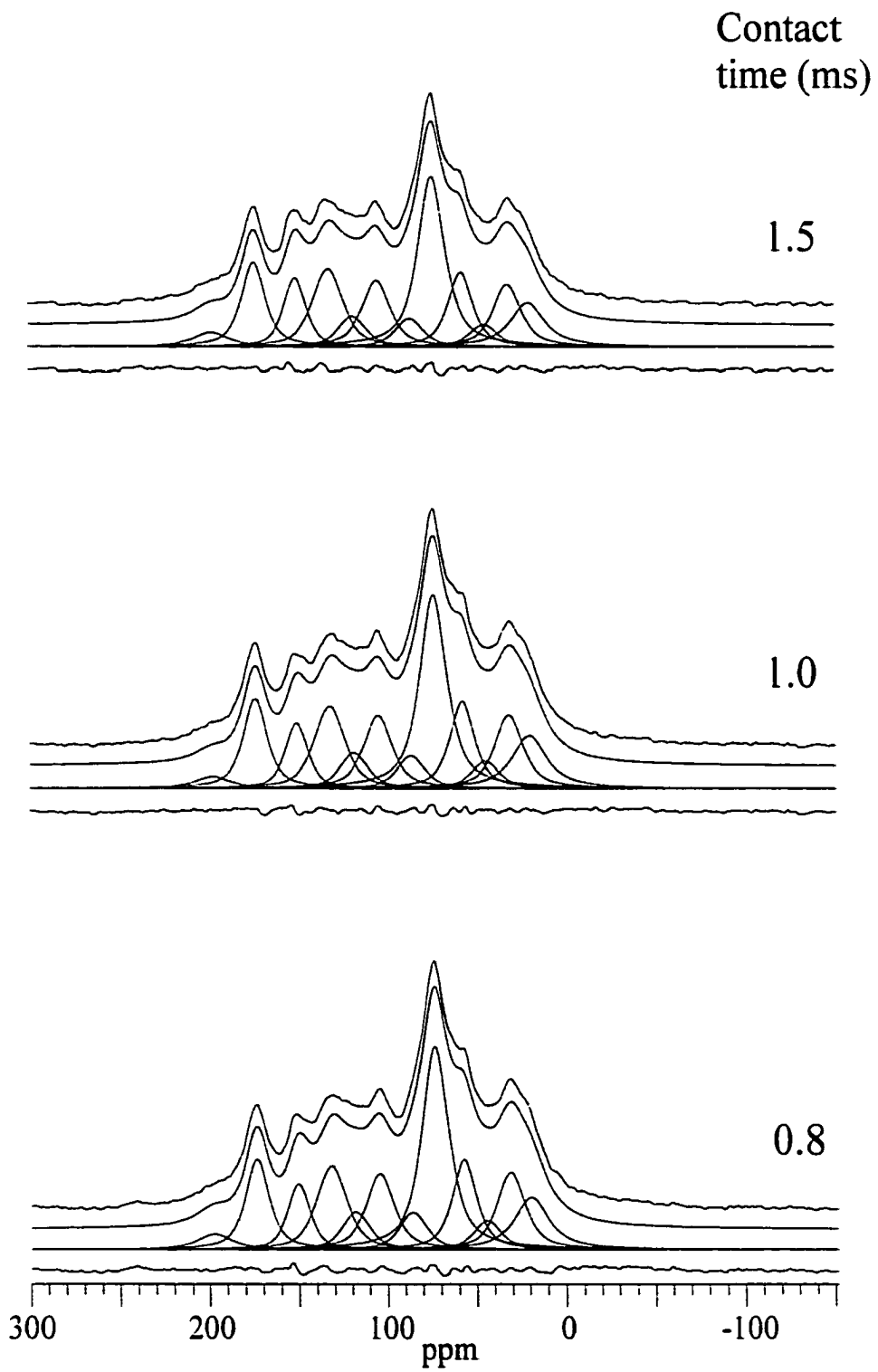

Figure A3-8 (Continued).

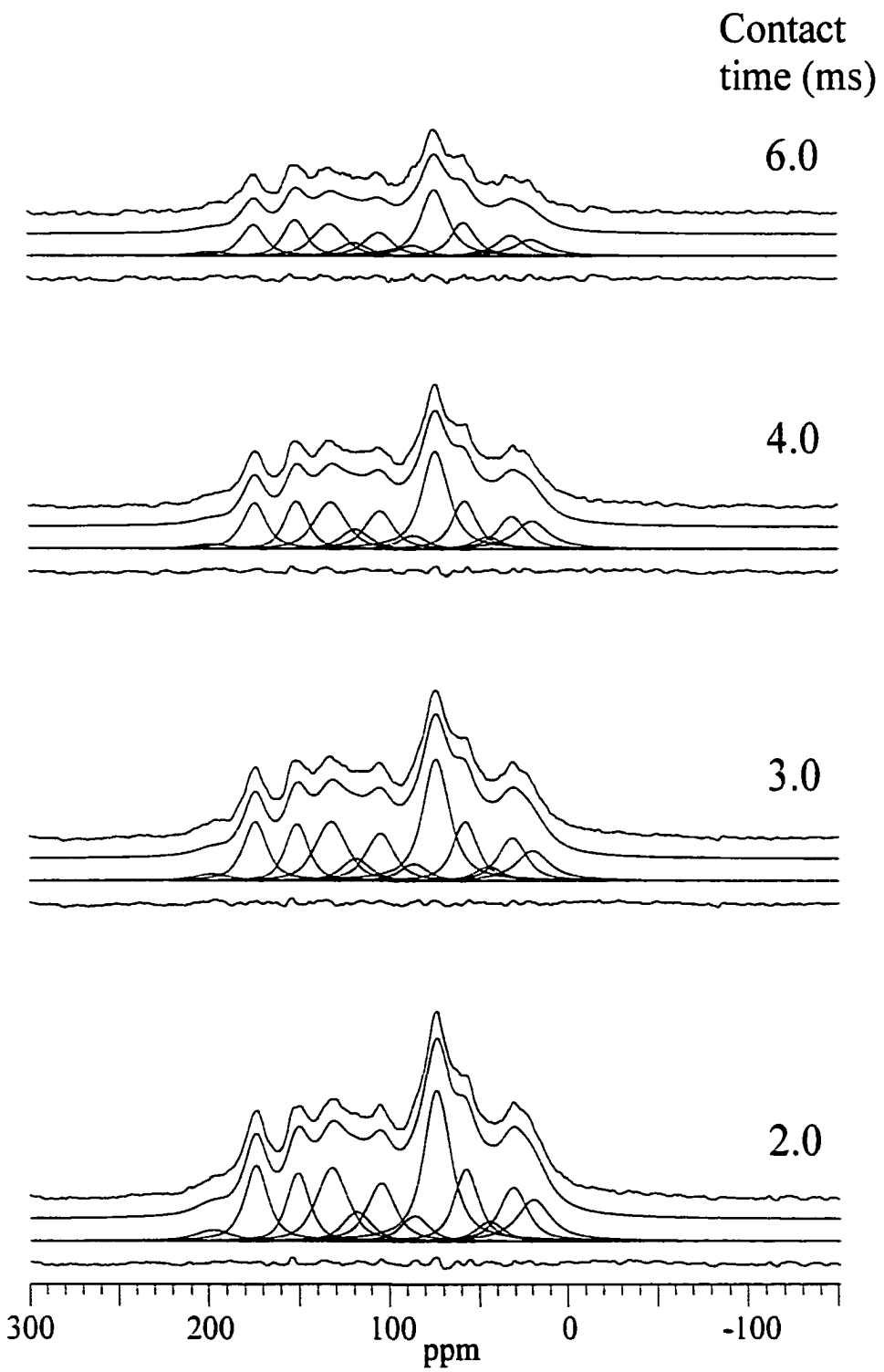

Figure A3-8 (Continued).

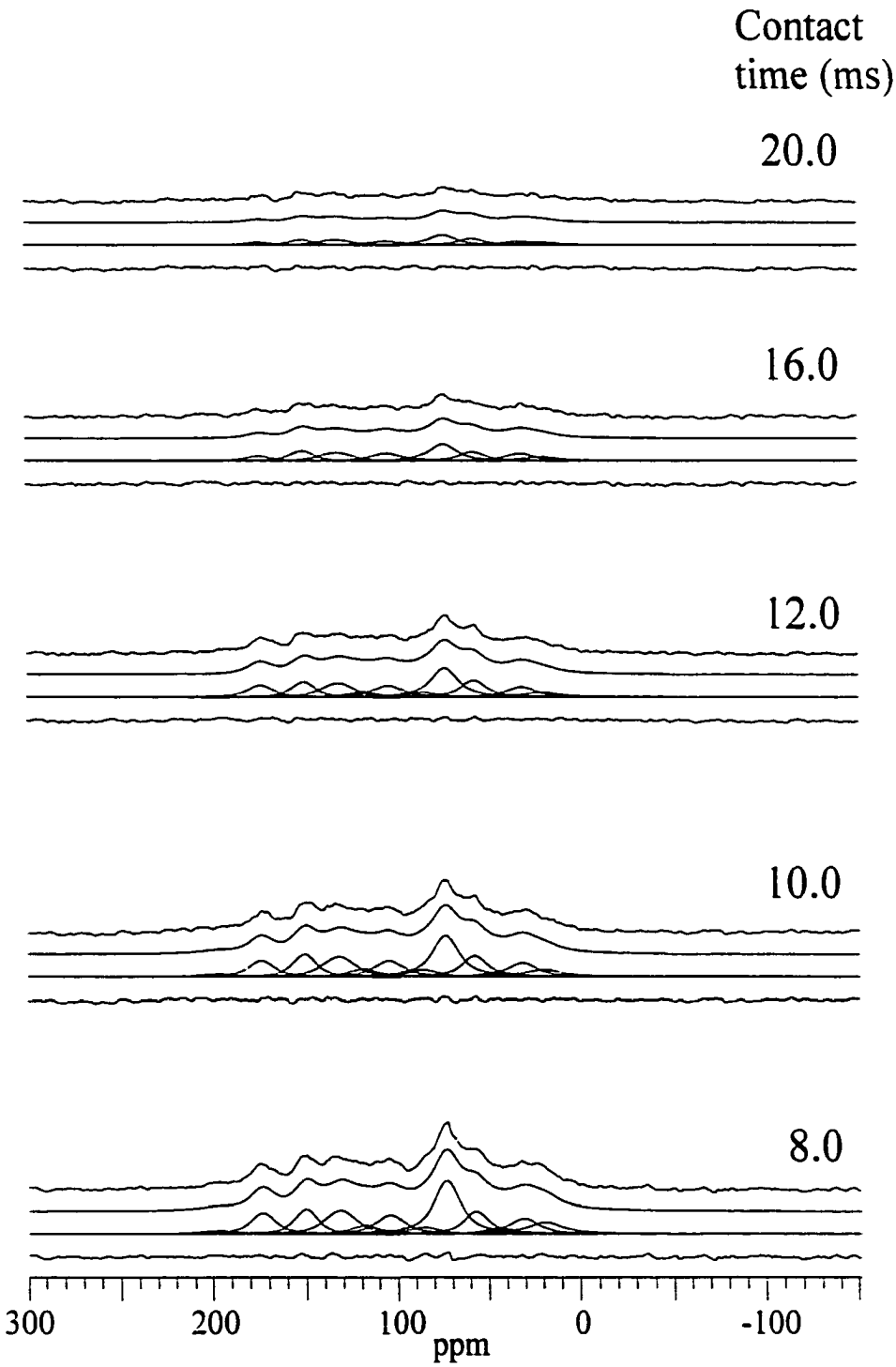

Figure A3-8 (Continued).

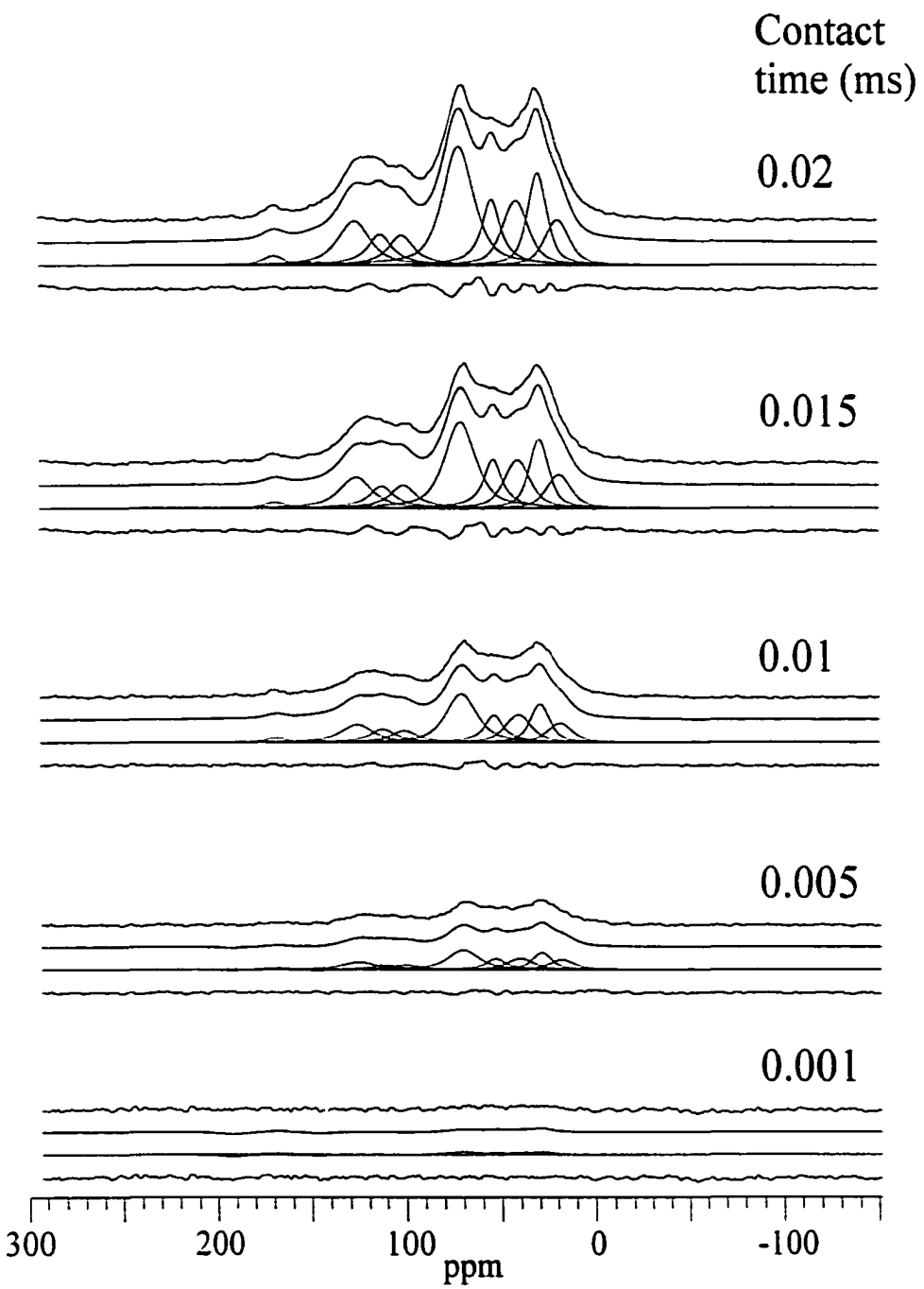

Figure A3-9 Deconvolutions of the variable contact time spectra of the humic acid data found in Figure 3.9(a). The contact time for each spectrum is written above and to the left of each spectrum. For each contact time, the uppermost spectrum is the experimental spectrum, the next lower trace is the "synthetic" spectrum, the next lower are the individual deconvoluted peaks, and the lowermost spectrum is the "difference spectrum". The synthetic spectrum was generated by adding the peak areas of the deconvoluted peaks (third trace from top). The difference spectrum is generated by subtracting the experimental spectrum from the synthetic spectrum and gives an indication of the success of the deconvolution procedure.

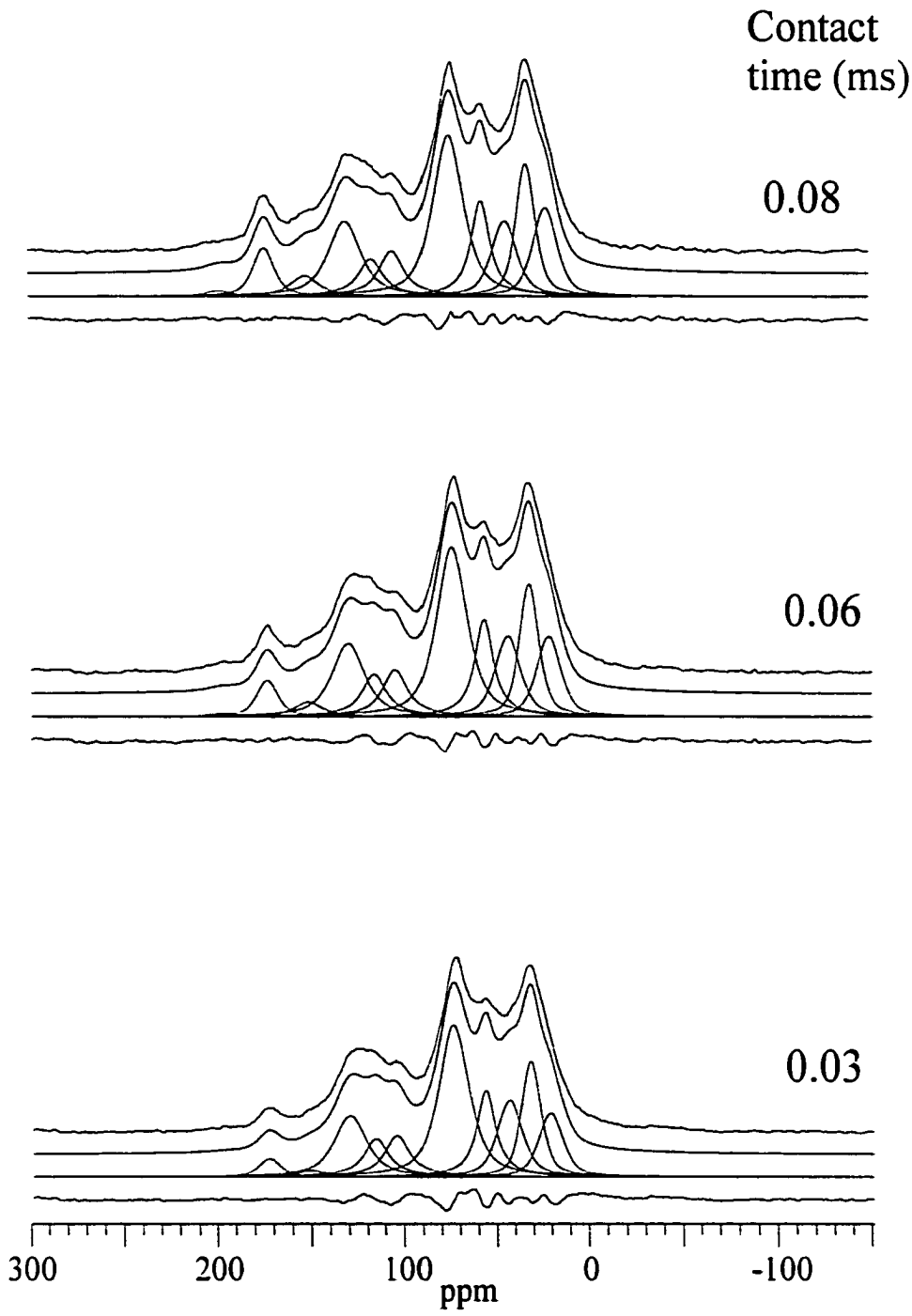

Figure A3-9 (Continued).

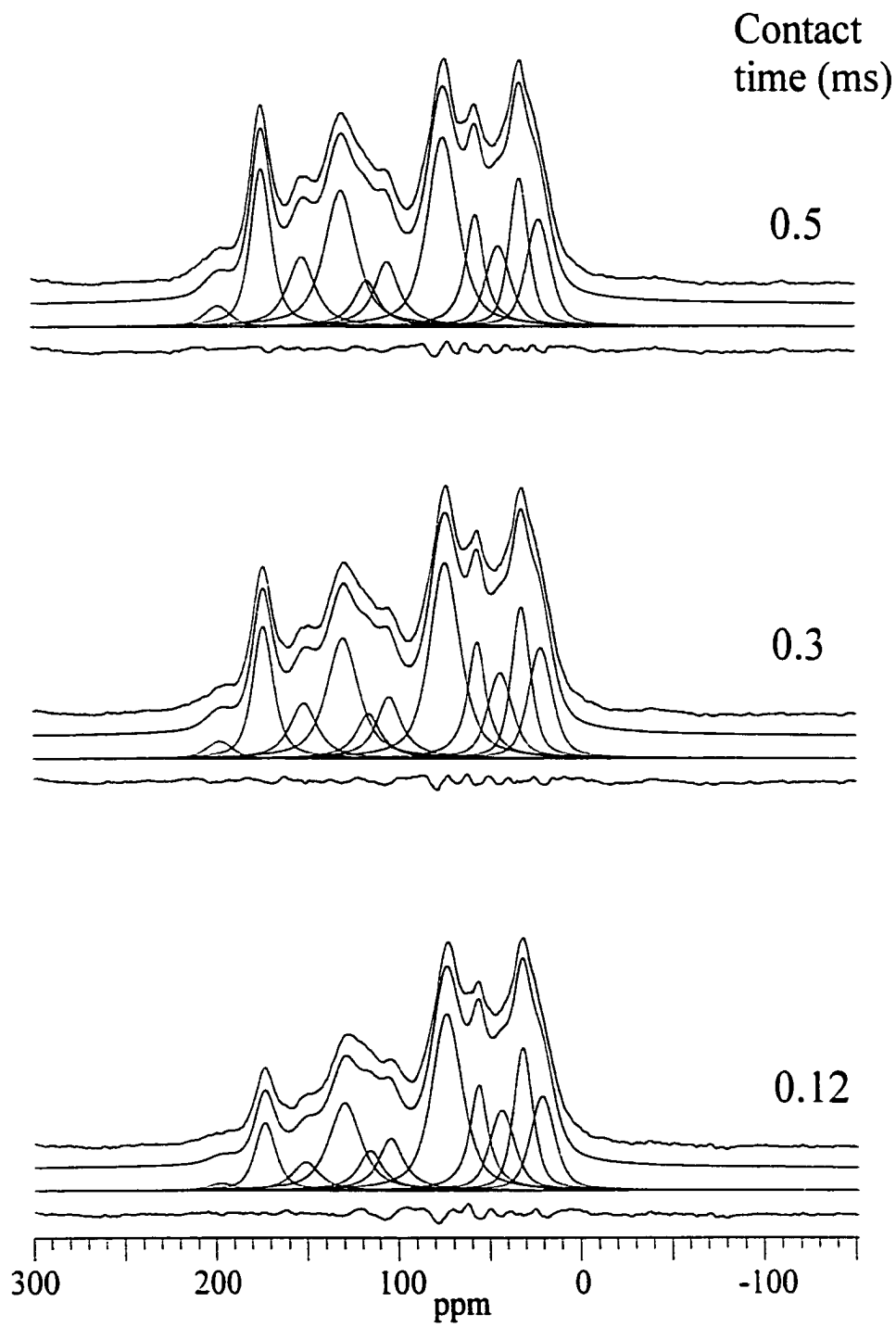

Figure A3-9 (Continued).

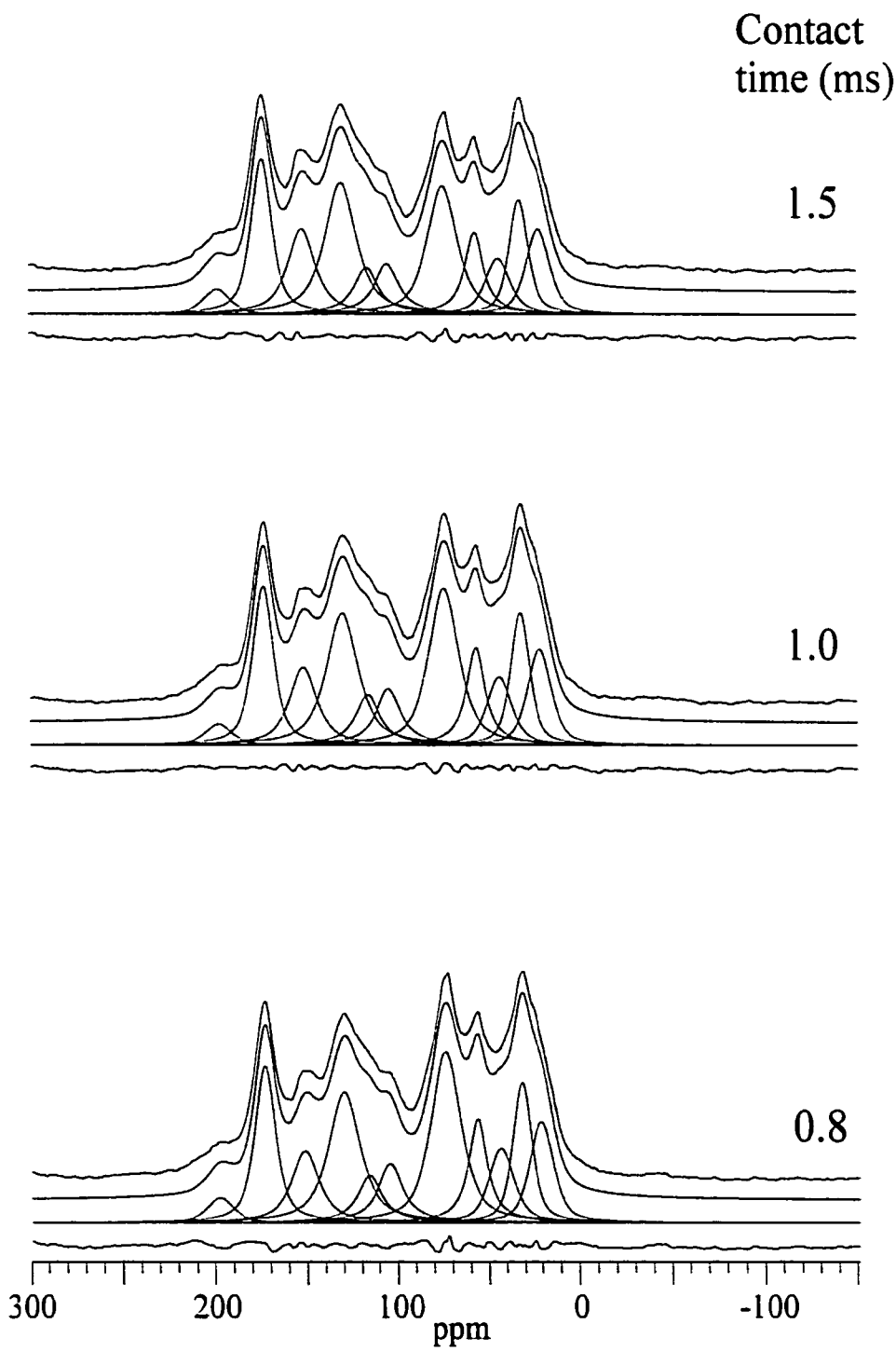

Figure A3-9 (Continued).

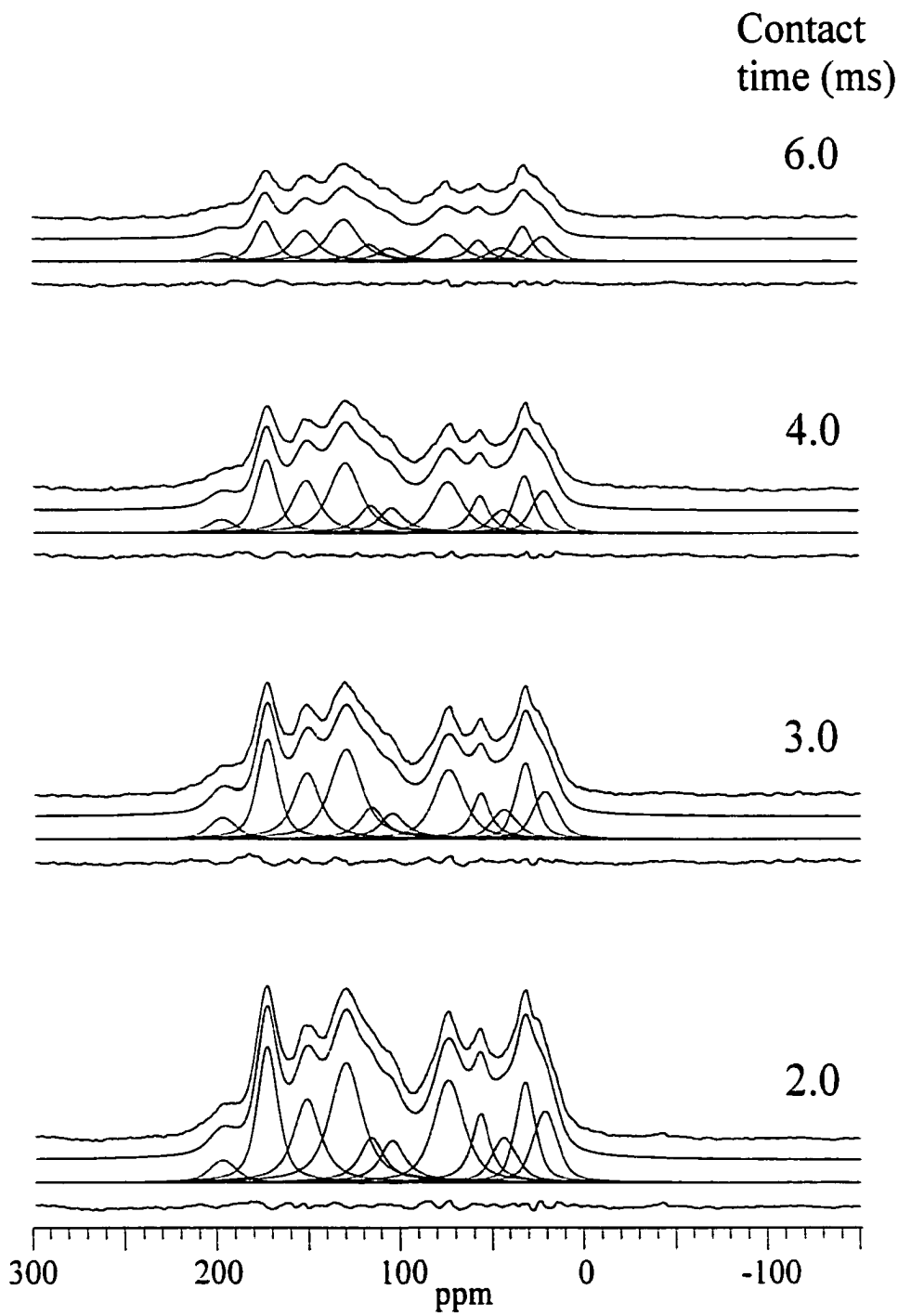

Figure A3-9 (Continued).

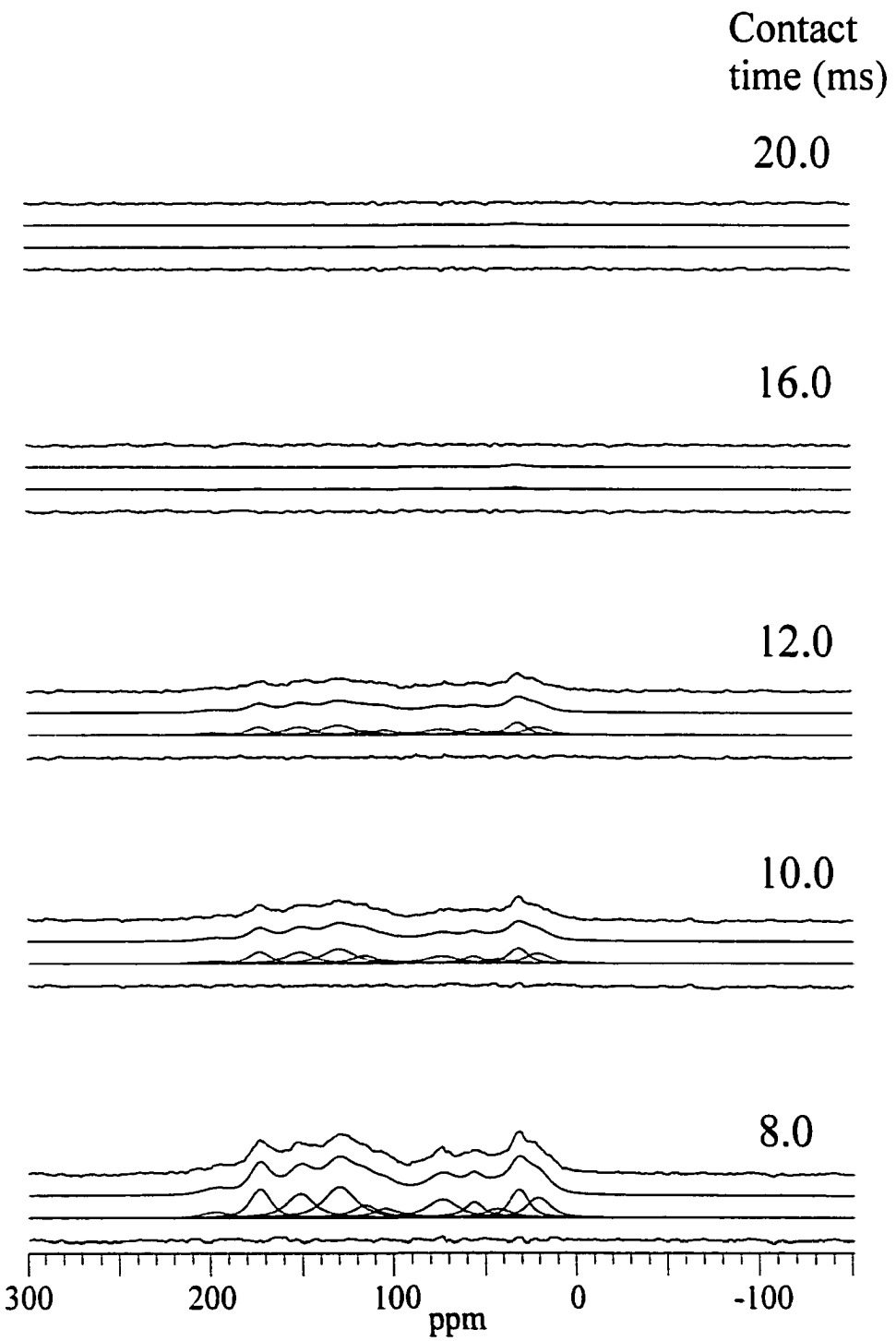

Figure A3-9 (Continued).

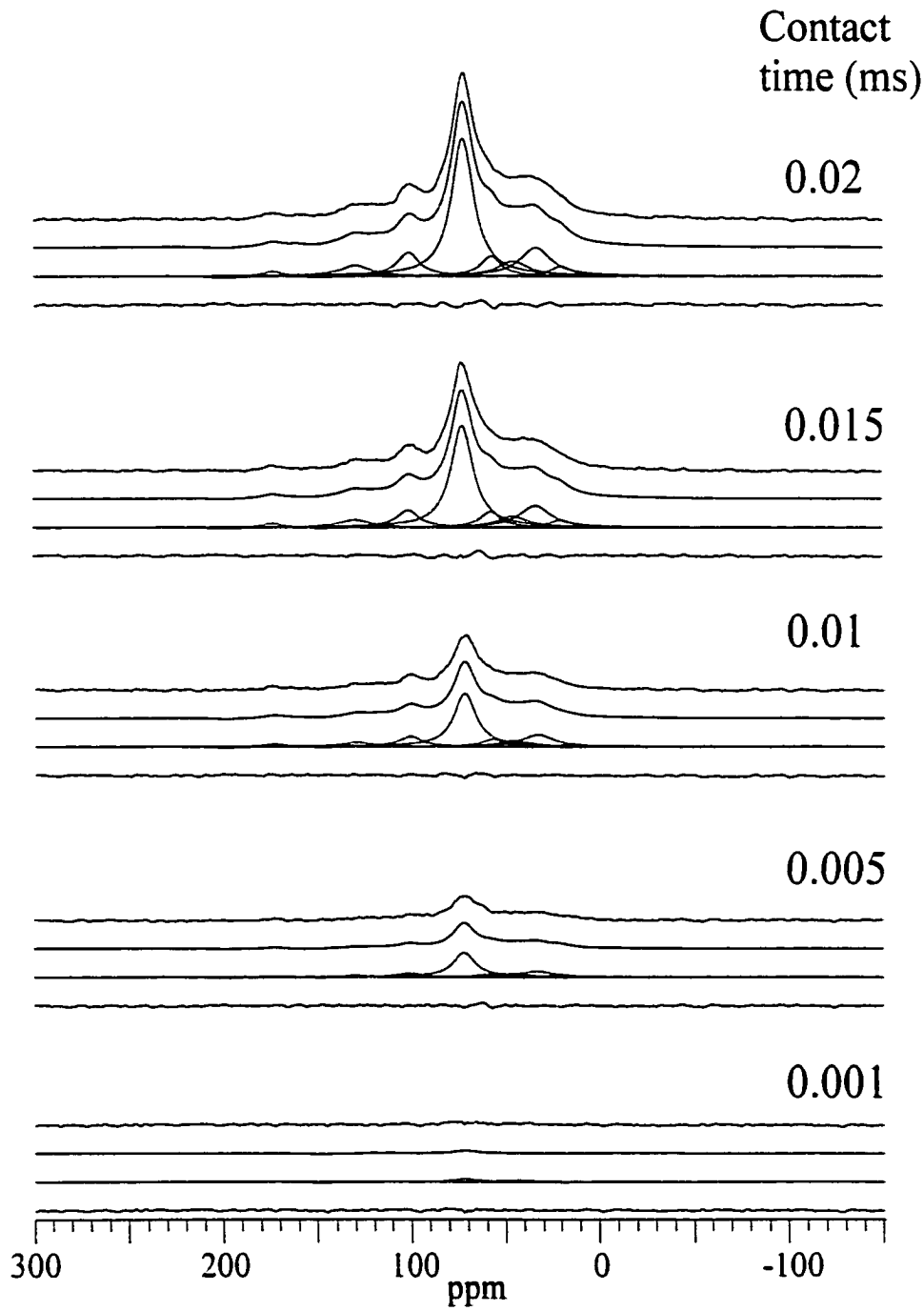

Figure A3-10 Deconvolutions of the variable contact time spectra of the fulvic acid data found in Figure 3.10(a). The contact time for each spectrum is written above and to the left of each spectrum. For each contact time, the uppermost spectrum is the experimental spectrum, the next lower trace is the "synthetic" spectrum, the next lower are the individual deconvoluted peaks, and the lowermost spectrum is the "difference spectrum". The synthetic spectrum was generated by adding the peak areas of the deconvoluted peaks (third trace from top). The difference spectrum is generated by subtracting the experimental spectrum from the synthetic spectrum and gives an indication of the success of the deconvolution procedure.

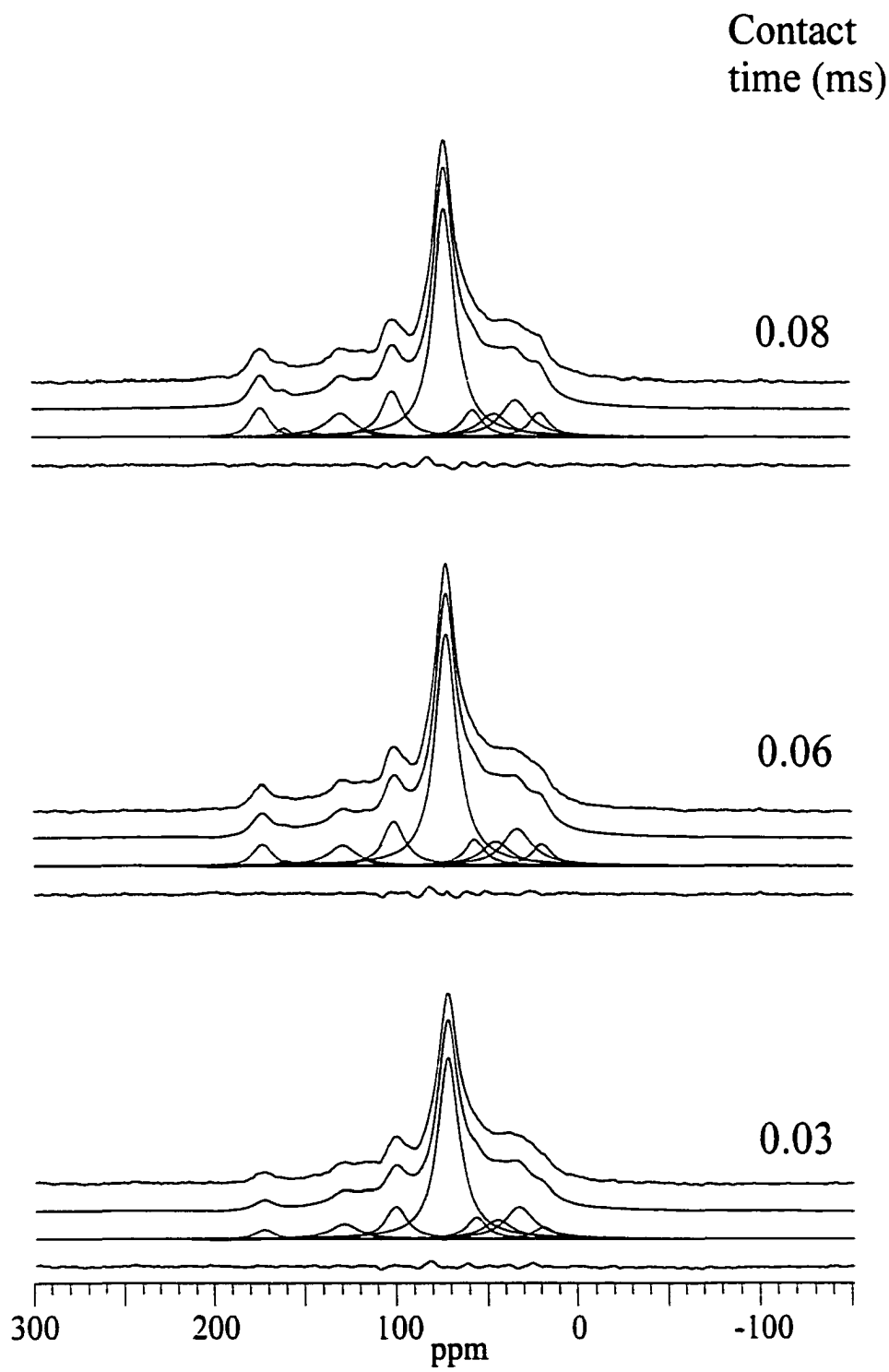

Figure A3-10 (Continued).

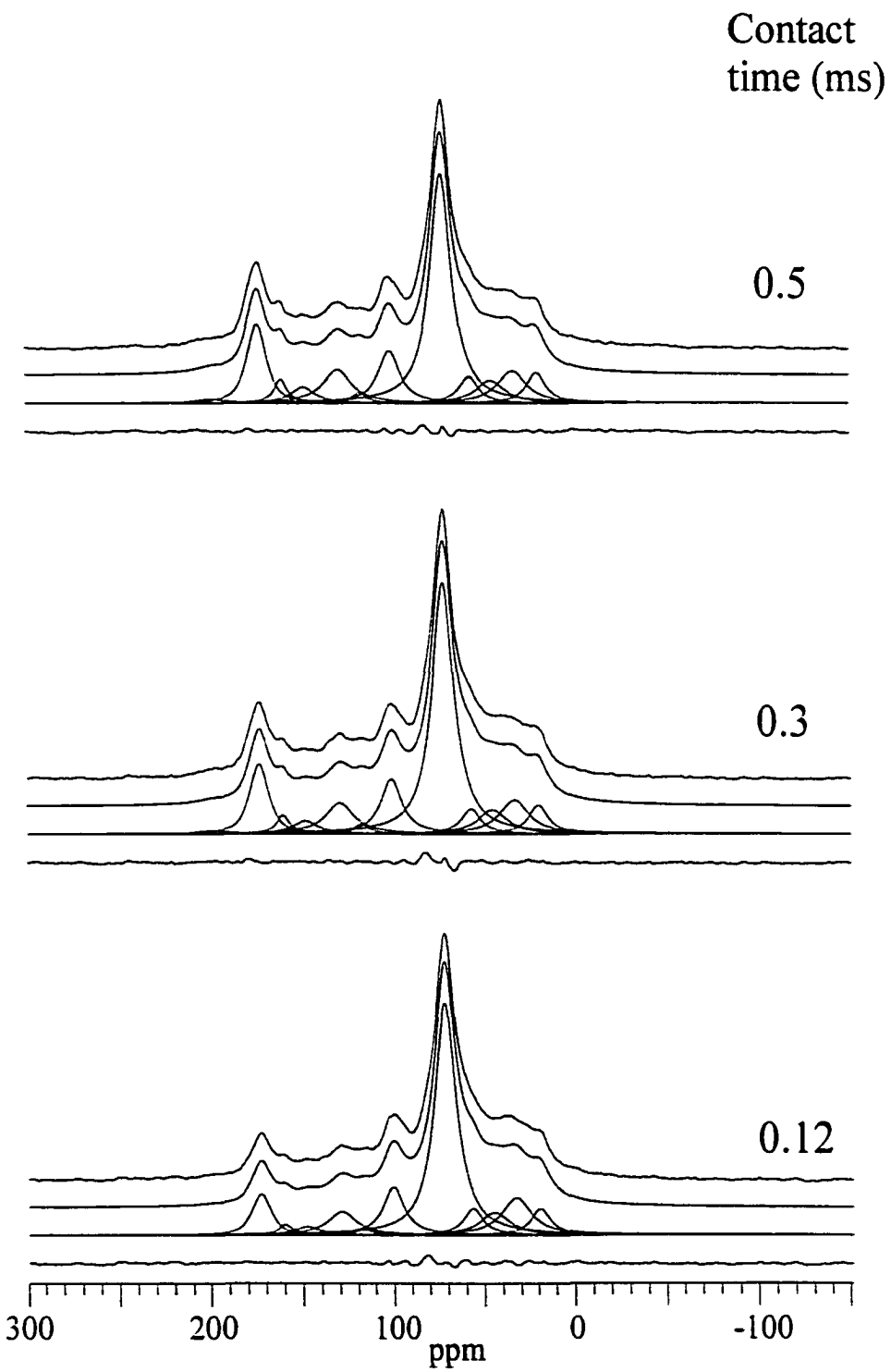

Figure A3-10 (Continued).

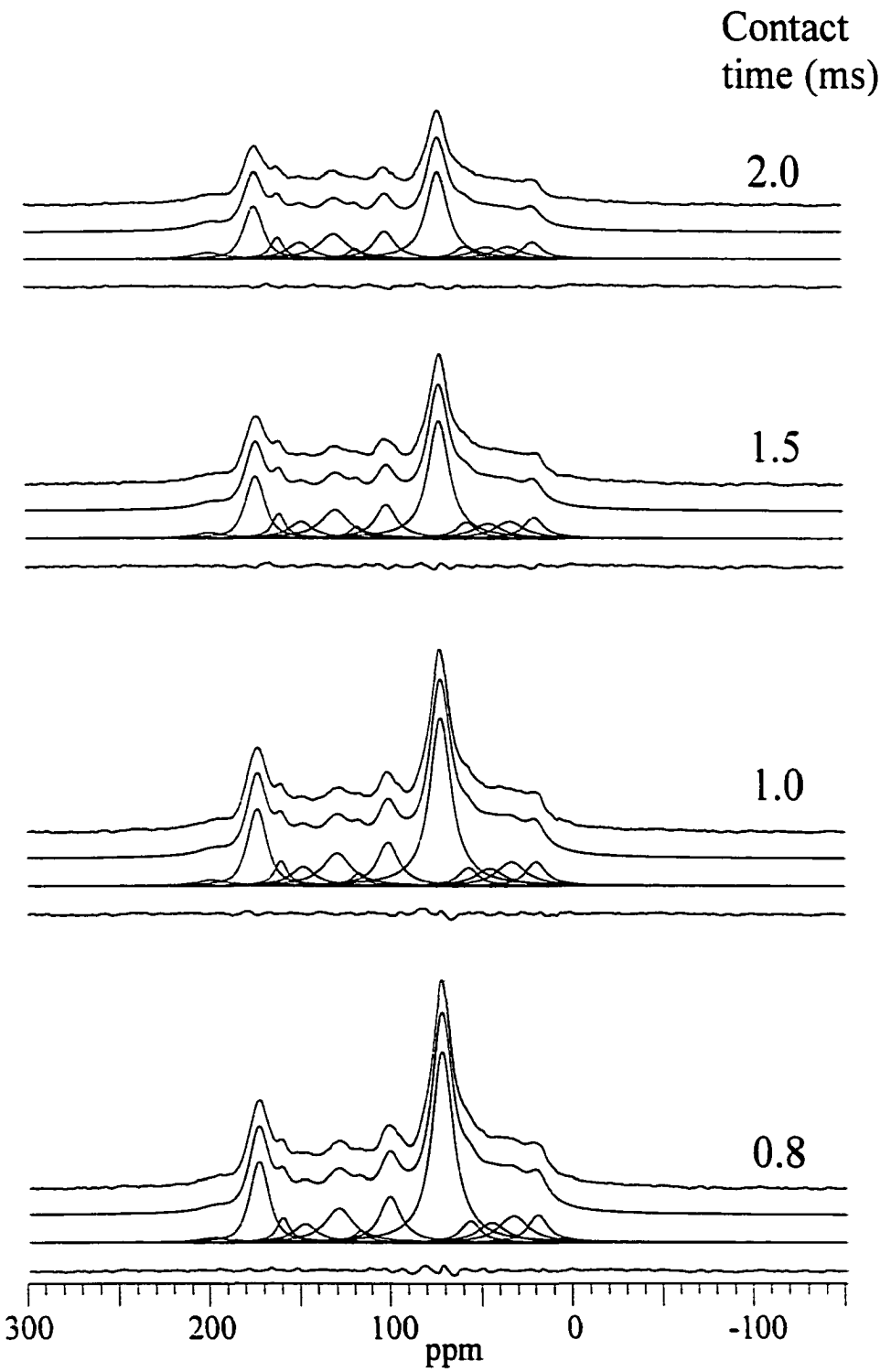

Figure A3-10 (Continued).

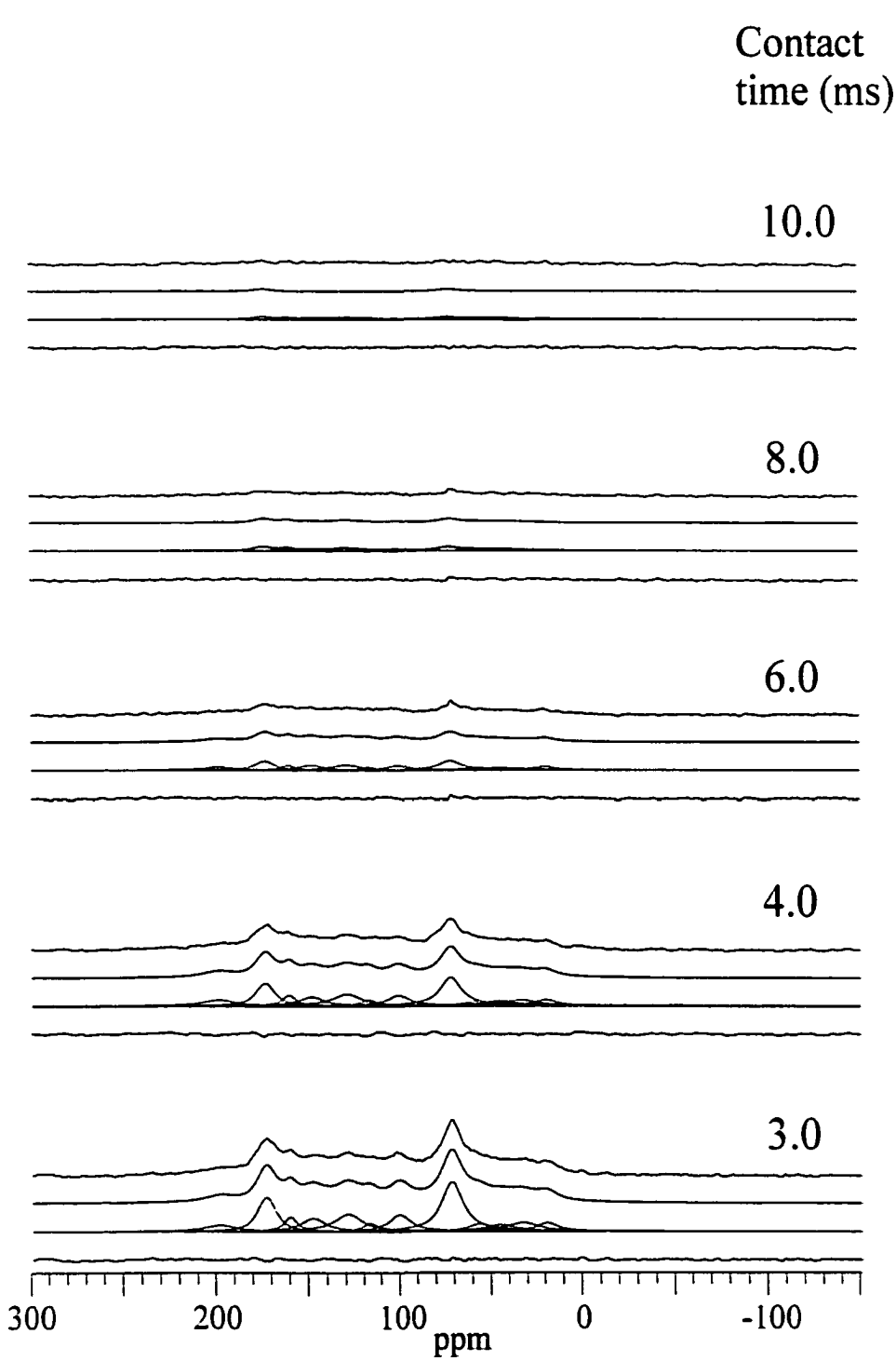

Figure A3-10 (Continued).